uOttawa

L'Université canadienne
Canada's university

FACULTÉ DES ÉTUDES SUPÉRIEURES ET POSTOCTORALES

uOttawa

L'Université canadienne
Canada's university

FACULTY OF GRADUATE AND POSDOCTORAL STUDIES

Majid Sadoughi Yarandi
AUTEUR DE LA THÈSE / AUTHOR OF THESIS

Ph.D. (Civil Engineering)
GRADE / DEGREE

Department of Civil Engineering
FACULTÉ, ÉCOLE, DÉPARTEMENT / FACULTY, SCHOOL, DEPARTMENT

Seismic Retrofit and Repair of Existing Reinforced Concrete Bridge Columns by Transverse Prestressing

TITRE DE LA THÈSE / TITLE OF THESIS

Murat Saatcioglu
DIRECTEUR (DIRECTRICE) DE LA THÈSE / THESIS SUPERVISOR

CO-DIRECTEUR (CO-DIRECTRICE) DE LA THÈSE / THESIS CO-SUPERVISOR

EXAMINATEURS (EXAMINATRICES) DE LA THÈSE / THESIS EXAMINERS

K. Elwood (teleconference)	D. Palermo
B. Isgor (absent)	
B. Martin-Perez	

Gary W. Slater
Le Doyen de la Faculté des études supérieures et postdoctorales / Dean of the Faculty of Graduate and Postdoctoral Studies

Seismic Retrofit and Repair of Existing Reinforced Concrete Bridge Columns by Transverse Prestressing

by

Majid Sadoughi Yarandi

A thesis submitted to the Faculty of Graduate Studies and Research
in partial fulfillment of the requirements for the degree of
DOCTORATE OF PHILOSOPHY
in Civil Engineering*

* The Doctorate of Philosophy Program in Civil Engineering
is a joint program with the Carleton University,
administered by The Ottawa-Carleton Institute for Civil Engineering

Department of Civil Engineering
University of Ottawa
Ottawa, Ontario, Canada

Your file Votre référence
ISBN: 978-0-494-32425-7
Our file Notre référence
ISBN: 978-0-494-32425-7

IN THE NAME OF GOD
THE COMPASSIONATE THE MERCIFUL

To...

All the people around the world who suffered from devastating earthquakes especially those in my beloved country Iran

ABSTRACT

Performance of bridges during recent earthquakes has revealed inadequacies of pre-1970's designs, especially in concrete columns. The 1989 Loma Prieta and 1994 Northridge earthquakes in California, and the 1995 Kobe earthquake in Japan, after the 1971 San Fernando earthquake, have demonstrated seismic deficiencies and resulting damage to a considerable number of major bridges. The deficiencies in bridge columns essentially stem from lack of properly designed transverse reinforcement, increasing their vulnerability to shear, confinement and reinforcement splice failures.

The Structures Laboratory of the University of Ottawa has been active in developing new and effective seismic retrofit techniques. One such technique involves the transverse prestressing of concrete columns to improve concrete confinement, diagonal tension capacity and bond between steel and concrete in reinforcement splice regions. The technique, named as Retro-belt, has been verified through extensive experimental and analytical research on circular and square columns. However, questions remain in terms of its applicability to rectangular columns with a significantly different aspect ratio than square sections as well as its use as a repair technique. The objective of the current research effort is to extend the applicability of the Retro-belt technique to rectangular columns as well as explore the possibility of using it as a repair methodology.

The research presented in this thesis consists of experimental and analytical phases. The experimental phase includes the tests of nine full-size bridge columns under simulated seismic loading. Three pairs of rectangular columns were designed, built and tested to extend the retrofit technique to rectangular columns. Three additional columns with circular, square and rectangular cross sections were designed and built as shear dominant columns to be damaged and repaired. They were damaged by initial loading, repaired by transverse prestressing and then retested to develop a repair methodology involving the Retro-belt technique. The analytical research was carried out to verify the applicability of existing design principles to columns that are transversely prestressed. Strength and deformability of columns computed by analytical means and recorded experimentally were compared to verify the analysis techniques. Design procedures were

developed for retrofitting rectangular columns with shear, confinement and splice deficiencies. A repair design method was also proposed based on limited test data, to be further developed. The results indicate that pre-1970's columns suffer from lack of strength and deformability. Shear- and splice-deficient columns showed limited deformability of about 1% drift ratio. Columns that lacked confinement and behaved predominantly in the flexure mode developed approximately 2% lateral drift before they failed in a brittle manner. Those retrofitted by transverse prestressing showed improved deformability of approximately 4% lateral drift, indicating the effectiveness of the Retro-belt techniques as a seismic retrofit methodology for rectangular columns. The application of transverse prestressing as shear repair techniques was explored through testing. The test results showed that the Retro-belt technique was effective in restoring shear strength of a damaged column and improving its deformability from 1% to 4% lateral drift. However, the technique, as applied in the current investigation, demonstrated only a limited improvement when used for repairing a splice-deficient column. Further research is needed to develop the column repair technology.

ACKNOWLEDGEMENT

I am most grateful to my thesis supervisor Dr.Murat Saatcioglu for his guidance, help and support. Many thanks to Muslim Majeed, the technical officer at the structural laboratory, for his assistance and technical support during the construction and testing of specimens. I would also like to thank my fellow graduate students specially Dr. Mohammad Shooshtari, Mansour Navidpour and Sattar Dolatyar for their assistance in the lab and during the progress of my research.

I gratefully acknowledge Dr.Ameir Altaee and Urkkada Technology Ltd. for the financial support of my research. I would also like to thank the following organizations for their financial support throughout my Ph.D degree at the University of Ottawa: the National Sciences and Engineering Research Council (NSERC) of Canada, Ministry of Training, Colleges and Universities (Ontario Graduate Scholarship) and the University of Ottawa.

A debt of love and gratitude is due to my wife son and daughter, for the long hours spent on my studies and research rather than spending time with them. Their patience and understanding was essential to the successful completion of my studies.

Finally, I would like to thank my parents and brother for their encouragement, prayers and support.

CONTENTS

LIST OF TABLES

LIST OF FIGURES

NOTATIONS

A_b Cross sectional area of longitudinal steel

A_c Area of core concrete

A_g Gross area of cross section

A_{ps} Nominal area of prestressing strands

A_s Area of one reinforcing steel bar

A_{st} Area of one leg of transverse reinforcement

A_{str} Area of one leg of prestressing strand

A_{sx} Area of one leg of transverse reinforcement in x direction

A_{sy} Area of one leg of transverse reinforcement in y direction

A_v Area of shear reinforcement within a distance s

b_c Core dimension measured center to center of perimeter hoop

b_{cx} Core dimension measured center to center of perimeter hoop in x direction

b_{cy} Core dimension measured center to center of perimeter hoop in y direction

b_w Minimum effective web width within depth d

c Neutral axis depth (distance from the extreme compression fibre to neutral axis)

d Effective depth of the cross section (distance from the extreme compression fibre to the centroid of the tension steel)

d_b Longitudinal bar diameter

d_p Diameter of prestressing strands

D_b Diameter of the pulley used at the corner of columns for Retro-belt system

e Maximum tendon eccentricity

e_1, e_2 Raiser disk diameters of Retro-belt system

E_c Modulus of elasticity of plain concrete

E_p Modulus of elasticity of prestressing strands

E_{sec} Secant modulus of elasticity

f_c Stress in concrete

f_c' Cylinder compressive strength of concrete specimens

f_{cc}' Confined concrete compressive strength in member

f_{co}' Unconfined concrete strength in member

f_l Average confinement pressure

f_{le} Equivalent lateral pressure that produces the same effect as uniformly applied pressure

f_{lex} Equivalent lateral pressure perpendicular to b_{cx}

f_{ley} Equivalent lateral pressure perpendicular to b_{cy}

f_{pe} Effective stress in prestressing strands

f_{pi} Initial stress in strands

f_{ps} Recorded stress in strands by strain gauges

f_{pu} Ultimate stress in strands

f_{py} Yield stress in strands

f_s Maximum steel stress in the elastic range

f_{st} Tensile stress in transverse reinforcement at peak concrete stress

f_y Yield strength of reinforcing steel

f_{yh} Yield strength of transverse hoop reinforcement

f_{ys} Yield strength of prestressing strands

f_{yt} Yield strength of transverse reinforcement

F Effective prestressing force in strands

h Average od cross sectional dimensions in two orthogonal directions

H_L Height of the lugs (deformations) on the longitudinal reinforcing bar

k_c Confinement efficiency parameter

K Coefficient used in Eq.4.7

K' Coefficient used in Eq.4.19

k Strength enhancement coefficient

k_1 Coefficient that relates confinement pressure to strength enhancement

k_2 Coefficient that reflects efficiency of confinement reinforcement

k_3 Coefficient to reflect effect of concrete strength

k_4 Coefficient to reflect effect of transverse steel strength

l Length of parabolic segment

l_d Development length of longitudinal reinforcing steel

l_e Elastic length of longitudinal reinforcing steel

l_p Plastic hinge length

L_{pc} Pull out length of longitudinal reinforcing steel

L_{sh} Strain hardening length of longitudinal reinforcing steel

L_{yp} Yield length of longitudinal reinforcing steel

L Shear span of column (column height)

M_u Factored moment at section

N_u Factored axial load normal to cross section occurring simultaneously with V_u

P Axial force on column, maximum axial compressive force on column for design

P_f Factored axial force on column

P_h Hook force

P_{hu} Ultimate hook force

P_0 Axial capacity under pure compression

q Equivalent uniform force per unit length

r Modular ratio

s Spacing of transverse reinforcement

s_l Spacing of longitudinal reinforcement, laterally supported by corner of hoop or hook crosstie

s_p Spacing of prestresing strands along column height

s_{st} Spacing of external prestressing strands along column height

S_L Spacing of the lugs (deformations) on the longitudinal reinforcing bar

u_{ACI} Average bond stress proposed by ACI Committee 408

u_e Elastic bond stress

u_f Frictional bond stress

V_c Nominal shear strength provided by concrete

V_e Seismic shear force

V_p Total shear resistance provided by external prestressing

V_{pi} Shear contribution of initial prestressing force to nominal shear strength

V_{ps} Total shear contribution of prestressing strands to nominal shear strength

V_s Shear provided by transvers reinorcement

V_u Factored shear force at section

Z Distance between the critical section and point of inflection (zero moment point)

ε_c Concrete strain

ε_1 Strain corresponding to peak stress of confined concrete

ε_{01} Strain corresponding to peak stress of unconfined concrete

ε_{085} Strain at 85% of peak unconfined stress

ε_c Strain in concrete

ε_s Strain in reinforcing steel

ε_{sh} Strain hardening strain of reinforcing steel

ε_y Yield strain of reinforcing steel

Δ_{horz} Horizontal deflection at the tip of the column

Δf_s Incremental longitudinal steel stress within the yield region

δ Design Drift Ratio

δ_{ext} Total extension of longitudinal steel due to loading

δ_h Total extension of longitudinal steel due to hook force (slippage of reinforcement)

δ_T Total extension of longitudinal steel

θ_e Rotation due to extension of reinforcing steel

λ Factor to account for low density concrete

φ Capacity reduction factor for axial compression

φ_c Resistance factor for concrete

ρ_c Total transverse steel area in two orthogonal directions divided by corresponding concrete area

ρ_w $A_s / b_w d$

Chapter 1

Introduction

1.1 General

Bridge infrastructure in North America, designed and built prior to the enactment of seismic design provisions of 1970's, may be seismically deficient. It was reported that approximately 50% of all bridges in the United States were built before 1940 and 42% of these bridges suffer some form of structural deficiency (Klaibar et al. 1987). The 1971 San Fernando earthquake, resulting in the collapse of five apparently well-designed modern concrete freeway bridges, while seriously damaging another 37 similar bridges (Jennings, P. C. 1971), was the first to alarm bridge engineers in North America. During the Loma Prieta earthquake of 1989 in San Francisco, more than 80 bridges were damaged, resulting in 40 deaths, $1.8 billion in damage, and severe economic disruptions due to the loss of major transportation routes (Cooper et al. 1994). In the aftermath of an earthquake, the demand on the transportation network and other lifelines increases. Emergency vehicles move into the area, the injured and homeless seek medical care or shelter, and people outside the area try to

find family members and loved ones. Other lifelines such as electricity, water and phone lines that may be on bridges require repairs, and this may be difficult if the supporting bridge is damaged and the required access can not be ensured. Damage to critical bridge infrastructure that forms an integral part of a transportation network disrupts traffic for an extended period with immediate and prolonged social and economic consequences. This was very much evident in the recent devastating earthquakes of Kobe and San Fernando.

Original seismic design criterion for bridges focused on the level of earthquake forces induced by the ground shaking. This resulted in the increase in lateral strength of bridges. However, this increase was found to be self-defeating, because strengthened members attracted larger forces that severely damaged other elements along their lateral load paths. Currently, a capacity-based approach is used that allows controlled yielding of specially designed elements. This limits the force demand to protect bridges. According to this design philosophy, bridges are designed to resist small-to-moderate earthquakes with little damage, but may receive considerable damage to predetermined elements during a large earthquake.

Today's challenge is to design bridges for a variety of hazards that can occur during an earthquake. Particularly problematic are near-fault effects that may cause very large demands and challenge the traditional methods of seismic analysis and design.

Following the 1971 San Fernando earthquake and the consequent collapse of several freeway structures, major changes were introduced to the North American seismic design practice. Bridges built after 1971 have generally performed well in recent earthquakes. However, the vulnerability of older, pre-1971 bridges was evident in the 1989 Loma Prieta, and the 1994 Northridge earthquakes. Following that earthquake, there was an upsurge in research interest into the seismic performance of concrete bridge structures worldwide.

Performance of concrete structures during recent earthquakes has demonstrated the vulnerability of columns to structural damage. In particular, it was observed that bridge columns erected prior to 1970's lacked proper seismic design and detailing practices, leading to complete structural collapses. Because it is not feasible to remove and rebuild previously built bridge infrastructure, the only viable approach remains retrofitting and repairing these structures for improved strength and ductility. A number of different techniques are currently utilized to improve seismic performance of concrete columns. These include steel

jacketing, reinforced concrete jacketing, FRP wrapping and a recently developed technique of transverse prestressing, known as "Retro-Belt".

1.2 Review of Previous Research

Literature review on seismic performance of bridge columns was conducted in two parts to be in line with the scope of current research. In the first part, "seismic retrofit techniques" were reviewed and in the second part "seismic repair of bridge columns" was reviewed. The previous literature on these two primary topics is reviewed in the following sections.

1.2.1 Literature Review on Retrofit of Concrete Columns

Column Retrofit strategies may remedy one or more deficiencies in bridge columns. These deficiencies often occur in the form of inadequate shear and/or flexural capacity, insufficient longitudinal reinforcement lap splice or insufficient confinement of compression concrete. According to the field reports on recent devastating earthquakes, columns are vulnerable structural elements, particularly if they attract high seismic shear forces (Mahin et al. 1976, Selna et al. 1973) and columns with span to depth ratios of less than 2.5 demonstrate a shear dominated behavior (Maruyama et al. 1984, Umehara et al. 1984). The cause of failures of six of the seven bridge structures that failed in 1994 Northridge Earthquake was attributed to column shear failure (Priestly et al. 1994). Inadequate shear design was evident in pre 1971 designs, which resulted in poor column performance during the 1971 San Fernando Earthquake. It was common at that time to design bridge columns with very little transverse reinforcement, consisting of No. 3 (9.5 mm diameter) or No.4 (12.7mm diameter) hoops at 12 in. (305mm) spacing regardless of cross-sectional dimensions or shear forces. Furthermore, the hoops had short extensions and were anchored only by lapping the ends in the cover concrete while intermediate ties were rarely used. This detailing made many older columns susceptible to shear failures. The current design practice requires up to approximately eight times the transverse steel reinforcement present in most pre-1971 designs (Roberts, J. E. 1991). Furthermore, longitudinal bars were commonly lap spliced at the bottom of the columns in older bridges. Lap-splice lengths as short as 20 bar diameter were commonly used although this length could not be sufficient to transfer

stresses from one bar to the other. Bond failure is also triggered once the cover concrete spalls off. The splice length regions in most existing bridges continue to be deficient, unless retrofitted.

Inadequate concrete confinement due to low levels of transverse reinforcement was another widespread problem in older bridge columns, resulting in brittle flexural crushing of compression concrete. The typical detailing of # 3 (9.5 mm diameter) and # 4 (12.5 mm diameter) ties at 12 in (305 mm) spacing with 90-degree hooks hardly provided any confinement beyond the spalling of cover concrete. Many concrete bridge columns suffered failures associated with insufficient concrete confinement.

Recognizing the above deficiencies, a significant amount of research has been conducted during the last three decades on the development of seismic retrofit and repair methodologies for concrete bridge columns. These activities have resulted in the development of different techniques for repair and retrofit of structural components.

1.2.1.1 Steel and Concrete Jacketing

Column jacketing is one of the widely used retrofit techniques for bridge columns. Two of the common types of jacketing with conventional construction materials are; i) steel and ii) concrete jacketing.

Chai et al. (1991) investigated retrofitting circular columns by enclosing plastic hinge regions with bonded steel jackets. They drew attention to the deficiencies of pre 1971 designs and the importance of upgrading older bridge columns. They further indicated that structural inadequacies in many older bridge columns were due to insufficient flexural strength caused by low lateral seismic force coefficients specified in pre 1971 design codes. This also resulted in higher ductility demands and inadequate flexural ductility capacities. Furthermore, bridges constructed before 1971 contained insufficient transverse reinforcement where columns had #4 (12.5 mm diameter) ties at 12 in. (305 mm) regardless of the column sectional dimension. Many bridges were spliced by a development length of 20 times the bar diameter with footing dowels. This lap length was found to be insufficient for developing the yield strength of reinforcement, especially when large diameter bars are involved. Bridge footings were identified as other elements with inadequate performance. Pile caps and footings in older bridges were often provided with only a bottom mat of

reinforcement, assuming that only the gravity load was resting on the footing and the lateral seismic force would cause no disturbance. Other problems included shear strength and inadequate anchorage of transverse reinforcement which resulted in brittle shear failures. Short columns exhibited low ductility and poor energy dissipation characteristics. Joint regions, either at column footing interface or column bent cap beam connections were also identified as potentially critical regions due to the high shear stresses expected during strong earthquakes. However, these regions in old bridges were not designed to resist such stresses. Tests of rectangular columns with oval steel shells, used for shear strength enhancement showed similar performance as circular columns. Column tests conducted by the authors showed that closely spaced lateral confinement increased the ultimate compressive strain from 0.005 to 0.030 and higher, with displacement ductility factors of more than 6. Footing designs that were common in pre 1970's may be shear deficient directly under the column-footing interface. They concluded that steel jacketing increased the column stiffness by about 10 to 15 percent.

Yoshimura et al. (1991) tested a total of nine square columns with a 7 in. (178 mm) cross-sectional dimension. Three columns were tested as control columns with different amounts of longitudinal and transverse reinforcement. Three other columns were tested after strengthening with 1/4 in (6 mm) thick steel plates, while the control columns were tested again after repairing. The aspect ratio (span-to –depth) was 1.0. Two L shaped steel panels were installed on the sides of column and were held together by means of welding two opposite corners. The 5-mm gap between the steel jackets and the column was filled with epoxy based polymer cement. All specimens were tested under a constant axial load, equivalent to 0.1 $A_g f'_c$, and reversed cyclic lateral forces. Test results demonstrated that strengthened short columns by a welded steel square tube, prevented brittle shear failure and the columns could develop their ultimate flexural moment capacities. It was also shown by additional tests that the proposed strengthening method using steel plates was applicable to repair and rehabilitation of damaged short columns that failed in brittle shear mode. Finally, an application example of the proposed strengthening method to an actual existing short column was presented.

Unjoh et al. (1992) performed tests on 500 mm square columns subjected to cyclic loading to study the effect of splicing and the effect of strengthening by using 1.0 mm

(0.04") thick steel jackets. Every column was reinforced with 46 No.3 (9.5 mm diameter) longitudinal bars which were cut at 900 mm above the column-footing interface. The columns were transversely reinforced by No.2 (6.3 mm diameter) bars at 250 mm spacing. A total of three columns were tested, R_1 was the control column, R_2 and R_3 were strengthened by steel jackets with a height of 1.0 and 1.5 times the depth of column cross section, respectively. Flexural hinging, accompanied by shear failure, was observed at the cutoff location of R_1. The strengthened columns exhibited flexural behavior with complete elimination of shear cracks near the bar cutoff section for R_3.

Priestly et al. (1994) conducted theoretical and experimental investigation to study the shear failure mode of concrete bridge columns designed before 1971. The experimental phase included eight circular columns and six rectangular columns. Circular and rectangular columns were strengthened using circular and elliptical steel jackets, respectively. The effectiveness of full height steel jacketing, to improve the seismic shear strength, was explored. Shear failure of squat bridge columns has been one of the major problems of reinforced concrete bridges under earthquake excitations. Lack of proper shear strength provisions before 1970s resulted in greatly smaller shear capacity than that corresponding to flexural yielding. Since the transverse reinforcement had short extensions with 90-degree lapped ends in the cover concrete, which was expected to spall off under cyclic loading, the problem was very complex. This detail resulted in such columns being susceptible to shear failures, followed by quick strength and stiffness decay. The approach used in this research was based on the principles of capacity design which explicitly considered the problem of determining the failure mechanism of members. The basic idea was to force the member to fail in a ductile manner by making the capacity of the member higher in other possible failure modes. This was assured by setting the shear strength above the maximum possible shear force that could be developed at the formation of plastic hinge due to flexure. They suggested that, unlike the flexural retrofit, the full height jacket would normally be required for shear retrofit of squat columns. Design equations for finding the steel jacket thickness and elliptical radius were developed. Strengthening of shear deficient circular and rectangular columns resulted in enhanced shear strength and flexural ductility at high levels of displacement ductility while the unretrofitted columns suffered shear failures.

Aboutaha et al. (1999) tested concrete columns constructed prior to 1970's with shear deficiencies before and after strengthening. Short columns with inadequate shear reinforcement demonstrated a rapid strength and stiffness degradation. Total of eleven rectangular columns, with 36" x 18" (900 mm x 457 mm) were tested, eight in the weak direction and the remaining three in the strong direction of column section. Columns were laterally loaded (without axial load) with two full cycles at every load/drift-ratio level. The transverse reinforcement was of Grade 40 (275 MPa) No.3 (9.5 mm diameter) ties at every 16 in (400 mm) and the longitudinal reinforcement was No.8 (25.4 mm diameter) Grade 60 (400 MPa) steel. The specimens had a height of 4' - 9" (1448 mm). Three types of steel jackets were used; i) solid steel jackets, ii) partial steel jackets and iii) steel collars made of channel sections. At displacements immediately following 2 % drift ratios, as-built columns demonstrated dramatic loss in strength and displacement. Diagonal shear failure mechanism was observed to take place and caused the loss of lateral strength. The development of shear cracks was not prevented by the jackets, but they did prevent widening of diagonal cracks. It was mentioned that the increase in the flexural capacity of the retrofitted columns were due to: i) the strain hardening of longitudinal steel reinforcement, and ii) due to the confinement provided by the steel jacket which increased the concrete compressive strength. Since the steel jackets provided high shear resistance, the resulting increase in shear demand was not critical. The conclusion was that thin rectangular steel jackets are very effective in retrofitting concrete columns with an aspect ratio of 1.33 and cross-sectional width of up to 36 in (900 mm), with insufficient shear strength.

Saiidi et al. (2001) performed an experimental and analytical study on four 40% scale columns. They evaluated the seismic performance and shear retrofit of flared reinforced concrete bridge columns under seismic attack. All of the specimens were tested in the strong direction, under a constant axial load and quasi-static cyclic lateral loading. The objective was to increase the shear capacity without a significant increase in flexural strength due to jacketing. Two columns (HS, HL) represented the as built conditions and the other two (R-HS, R-HL) were retrofitted using the same steel jacket thickness and elliptical shape. Grout was used to fill the gap between the steel jacket and the column. A 25 mm space was implemented to avoid the jacket from bearing against the two ends. A 6.4 mm thick layer of polystyrene sheet was used in R-HS, between the column surface and the grout, to prevent

composite action, while the void was fully grouted in R-HS. A 38 mm wide gap was provided in R-HS, at 762 mm above the footing, to represent a plastic hinge and a weaker section compared to other jacketed areas to minimize the increase in flexural strength due to jacketing. The jacket in R-HS did not improve the displacement ductility of column, but it did prevent the shear failure and longitudinal bar buckling. It was concluded that, unlike the prismatic columns, the location of plastic hinge in reinforced concrete columns with flares could occur away from the two ends. Therefore this should be considered in any retrofit design to prevent any shift in plastic hinge to more critical locations. In flared columns, the maximum bending moment is not necessarily the plastic hinge location, but it can be predicted by moment-curvature analysis at different cross sections. Finally, using a gap within the height of retrofitted column could result in the control of the plastic hinge location, ductility capacity and shear demand.

Sugano et al. (1981) conducted an experimental study on the seismic retrofit of short reinforced concrete columns using welded wire fabric wrapping and mortar. Square columns with a 250 x 250 mm cross section and an aspect ratio of 1.0 were tested under both cyclic lateral and constant axial loading. Retrofitted columns compared to the control columns showed a significant increase in both stiffness and strength with improved ductility.

Bett et al. (1988) conducted tests of two-third scale short reinforced concrete columns. The researchers studied the behavior of repaired and retrofitted 12-in square cross section columns under constant axial and cyclic lateral loading. Eight No.6 (19.05 mm diameter) longitudinal bars, No.2 (6.35 mm) ties spaced at 8 in. (200 mm) and 1.0 in. (25 mm) cover was used. Two specimens were jacketed prior to testing (1-2, 1-3) and one specimen was first tested, repaired by jacketing, and then re-tested. Specimen 1-2 and 1-3 were both strengthened with a shotcrete jacket and 1-3 had an additional No. 6 (19.05 mm diameter) longitudinal bar at each mid-face, connected by No.3 (9.5 mm diameter) supplementary crossties at 9 in. (225 mm), inserted through drilled holes in the column and cemented with epoxy adhesive. Specimens were first roughened by sandblasting, jacket steel reinforcement cages were placed on the columns and they were shotcreted and float-finished. The same steps were taken for the repaired column, but after the removal of loose concrete. As built specimens showed a brittle and shear dominated failure. Both the

strengthened and the repaired columns were laterally stiffer and stronger than the original column. The repaired column performed almost as well as the strengthened columns.

Ersoy et al. (1993) studied the behavior of jacketed columns. Two series of tests were conducted. The first series consisted of reinforced concrete jacketed columns tested under uniaxial loading and the second series were subjected to combined axial load and monotonic or reversed cyclic loading. A total of four columns representing the as-built conditions were tested in the first series under uniaxial load, and were re-tested after jacketing. Two of the specimens were jacketed while under load and the other two after unloading. The second series consisted of five columns, three jacketed and subjected to a constant axial load and reverse cyclic loading, and two monotonic reference specimens. After jacketing, if the reference specimens were loaded up to the damage level they were marked as "repaired jacket" otherwise as "strengthening jacket". All columns had a square (650x 650mm) cross section and four 10 mm-diameter longitudinal bars with 4mm ties spaced at 50 mm. Jacket reinforcement was the same as the original column reinforcement. Test results showed that under uniaxial loading, the repaired and strengthened columns reached 80 to 90 percent of the strength of reference monotonic specimen. Columns strengthened under load performed well; however, the repaired jacketing under load could only carry 50 percent of the axial load of that carried by the reference column. Repaired and strengthened specimens under axial and transverse cyclic loading showed 90 % of the reference specimen's capacity.

Rodriguez et al. (1994) reported the results of an experimental study of the improvement in seismic behavior of strengthened/repaired reinforced concrete columns by concrete jacketing. A total of four square (350x350mm) columns were tested. Two of the control columns were repaired after unloading and retested. The other two were strengthened. The columns contained 8-20 mm diameter plain round longitudinal bars with 6 mm hoops located at 256 mm centers and were tested under axial and reverse cyclic loading. A low ductility factor of approximately 2 and bond degradation of longitudinal bars were found in control columns. The column surface was roughened and new longitudinal reinforcement was either bundled on the four corners of the jacket at 438 mm apart with single square hoops as transverse reinforcement or distributed around the jacket at 198 mm spacing with square and octagonal hoops as transverse reinforcement. The results showed that the nominal displacement ductility factors increased up to 6, while increase in energy

dissipation and a small reduction in strength was observed. Previous damage and two different reinforcing details used in the jacketed columns had no major influence on the overall seismic behavior of jacketed columns. Significant improvement was observed in strength and ductility, accompanied with significantly reduced strength degradation. This technique was found to be labor intensive.

1.2.1.2 FRP Wrap

The use of composite materials in the construction industry and infrastructure related applications have increased significantly in recent years. The majority of these applications have been in corrosive environments to take advantage of the corrosion resistance of composites (Chambers R.E. 1992). Jackets made of advanced fiber-reinforced composite materials have also been investigated for seismic strengthening of reinforced concrete columns.

Katsumata et al. (1988) researched and developed a method of winding carbon fibers of HP grade to increase the seismic capacity of existing reinforced concrete columns. Continuous type carbon fiber strands were used to wind the existing columns in order to increase transverse reinforcement. A total of ten ¼ scale square columns with 200 x 200 mm cross sections were tested. To reduce the stress concentration on carbon fibers the corners of the columns were rounded with a radius of 30mm. Two sets of specimens with different interface between the carbon fibers and concrete were tested. Isolating film was provided between the fiber and the concrete in the first set while fibers were epoxy bonded on to the concrete substrate in the second set. It was established that the winding of carbon fibers around the columns had an ample effect on increasing the capacity. The quantity of applied carbon fiber had an approximate linear relationship with increase in ultimate displacement and energy dissipation. The earthquake-resistance capacity of columns retrofitted with carbon fibers could be approximately correlated with the original column having only the hoop reinforcement. The amount of carbon fibers and steel hoops were mutually convertible. There was no significant difference in ultimate displacement of the two sets of specimens when the plies of carbon fibers were the same.

Priestly et al. (1990) performed tests on circular columns with inadequate shear resistance by using fiberglass/epoxy composite wraps as a means of strengthening them.

Eight feet high (2438 mm), 24in. (610 mm) diameter columns were tested under a 592 kN (133 kips) constant axial load and reversed cyclic loading. Twenty six No. 6 (19.05 mm) grade 60 (400 MPa) deformed bars were used as longitudinal reinforcement and were transversely reinforced with No. 2 (6.35 mm) hoops at every 5 in. (127 mm). Shear span to depth ratio was 2.0 and the fibers were wrapped over the height of the column. Fiber reinforced polymer (FRP) jacketed columns showed improvement in shear strength and ductility.

Saadatmanesh et al. (1996) experimentally investigated the use of FRP composite straps to overcome the poor performance of concrete columns due to inadequate lateral reinforcement and insufficient lap length of starter bars. A total of five circular columns were constructed with a scale factor of 1/5. The columns were tested under constant axial load and reversed cyclic loading. Test columns were designed to model pre-1971 bridge columns. Unidirectional FRP straps were impregnated with polyester resin and wrapped around potential plastic hinge regions. Three columns had longitudinal reinforcement and the other two were lap spliced. One lap spliced (C-1) and one continuous column (C-4) were tested as control while the two spliced columns (C-2, C-3) and the remaining continuous column (C-5) were retrofitted with FRP straps. Columns C-2 and C-5 were strengthened using a passive retrofit scheme while C-3 had a grout filled jacket and hence had an active retrofit scheme. C-1 degraded rapidly after the first cycle to a displacement ductility ratio μ=1.5 with a maximum lateral load of 58.3 kN (13.1 kips) due to the failure of the lapped reinforcement. C-2 and C-3, strengthened with six plies of composite straps, showed a significant improvement of up to ductility levels of $\mu = \pm 6$. No sign of structural degradation associated with bond failure of lap spliced bars were observed. Maximum strength of 81.4 kN (18.3 kips) was noted for C-2 which is approximately 40 percent more than that of the reference column. Due to active confinement pressure, C-3 had a higher lateral load resistance. Column C-4 showed lateral strength decay at a displacement ductility level of $\mu = 4$ with a maximum lateral load of 71.6 kN (16.1 kips) at $\mu = 3$. However, due to concrete failure and longitudinal bar buckling, the specimen showed rapid deterioration in its strength at $\mu = 5$. Significant improvement was observed in C-5 in terms of energy absorption and dissipation characteristics with an increase in strength. It was concluded that reinforced concrete columns, especially those with lap spliced reinforcement in their plastic

hinge regions, needed to be retrofitted. Test results showed that the composite straps are very effective in the seismic strengthening of circular concrete columns with inadequate seismic resistance.

Crawford et al. (1997) investigated analytically the effectiveness of jacketing the existing reinforced concrete structures to resist blast effects. Different standoff distances, charge sizes and composite jacketing systems were considered. Two building designs were modeled by a three dimensional Lagrangian finite element code DYNA3D (Whirley et al. 1993), using a concrete material model which was designed to predict nonlinear concrete response to explosive loads. Two types of building designs were analyzed. One building was designed based on UBC (Uniform Building Code 1993) seismic zone 1, mainly based on gravity loads, and the other was based on UBC seismic zone 4, in which the members were designed to resist seismic loads. The authors made reference to earlier research and indicated that increase in strength and ductility is the main benefit of steel jacketing while FRP wraps have shown to increase the ductility from 1.5 to 10 (Priestly et al.1994). It was concluded that structural collapse is a result of the shearing of the first and second floor perimeter columns and retrofitting would prevent most of the shear failures studied. The authors recommended more research to develop new retrofit techniques to enhance the floors against blast effect and reduce debris production.

Saadatmanesh et al. (1997) tested a total of five 1/5 scale rectangular columns subjected to lateral cyclic and constant axial loading with substandard design and different reinforcement details. Two of the columns were tested as control columns so that their hysteresis response could be compared with the other three retrofitted columns. Epoxy resin was brushed on high-strength fiber reinforced plastic (FRP) composite straps for interlaminar bonding of the layers of the straps, while they were wrapped around a potential plastic hinge region or along the height of column, as desired. To further improve concrete confinement, an active retrofit strategy was suggested, involving the application of lateral pressure to the column. Gaps produced by placing spacers between the straps and the column were suggested to be filled by expansive grout or by pressure injecting epoxy resin in the gap. Design variables studied included, reinforcement splicing and cross-sectional shape (rectangular vs. oval shaped). Two types of prefabricated strap configurations, oval and rectangle, were designed to investigate their effects on confinement. The straps were

applied only at estimated potential hinge regions with a length equal to twice the effective depth (635mm). E-glass, 152mm wide unidirectional tapes were used in the production of straps. The authors acknowledged the absence of seismic resistance in rectangular concrete bridge columns designed before the new seismic design provisions were in place. Due to the insufficient development length and lack of transverse reinforcement, columns with lapped splice starter bars appeared to have failed in a brittle manner at low displacement ductility ratios of about 1.5. In rectangular columns with continuous rebars and high longitudinal reinforcement ratio of 0.05, a brittle shear failure occurred due to the minimal transverse reinforcement used. FRP strap retrofitted columns improved significantly in strength and demonstrated a high displacement ductility level of $\mu = \pm 6$. Considering the limited range of the retrofit design parameters of this study and by comparing the test results, no major difference was observed between the oval and rectangular shaped straps.

Saatcioglu et al. (2001), based on experimental research, described the common deficiencies that exist among reinforced concrete columns, such as the insufficient amount of transverse reinforcement resulting in poor confinement and inadequate development length of starter bars. Total of 4 full scale circular (508mm diameter) and square (500mm) columns with spliced longitudinal reinforcement were tested. Tests were carried out by using three MTS hydraulic actuators, two of them applying 15% of column concentric capacity as axial load and the third actuator simulating cyclic earthquake loading. Four plies of CFRP Jackets were applied to the circular columns and five plies to the square specimens. Although retrofitted square columns showed limited improvement and the technique was found to be ineffective as a retrofit methodology, retrofitted circular columns were able to sustain in excess of 6% lateral drift ratio without significant strength decay.

Satoh et al. (2001) developed a new active confining seismic retrofit technique, in which aramid fiber belts are prestressed and used as external transverse reinforcement. Five shear critical columns with shear span to depth ratio of 1.0 and poor steel hoops were retrofitted and tested under reversed cyclic lateral and constant axial loads. Although the as-built columns exhibited shear failure, retrofitted columns developed ductile flexural response. They indicated that the proposed technique was effective for RC columns with inadequate shear resistance or poor bond strength. The retrofitted column developed ductile

flexural response. Since there was a 20mm gap between the aramid fibers used and the column surface, fiber belts could not prevent the spalling of cover concrete.

Haroun et al. (2003) conducted an experimental study on a total of fourteen half-scale circular and rectangular reinforced concrete bridge columns repaired and retrofitted with composite-material jackets. Half-scale squat concrete bridge columns were tested under fully reversed cyclic shear in a double-curvature configuration. Columns consisted of three as-built columns, ten columns retrofitted with different composite-jacket systems and one circular as-built column repaired after damage. Experimental results showed that all as-built columns developed unstable behavior and failed in a brittle shear mode. The common failure mode for all retrofitted samples was flexure, but with significant improvements attained in ductility. In the second phase, a total of thirteen half-scale circular and square column models were constructed with short lap-splice details at the base, and were tested in flexure under lateral cyclic loading. Three as-built columns were tested and a total of ten columns were tested after being retrofitted with different composite-jacket systems. In general, the common mode of failure for as-built samples was brittle failure due to bond deterioration of lap-spliced longitudinal reinforcement. The jacketed circular columns demonstrated a significant improvement in their cyclic performance. However, tests conducted on square jacketed columns showed very limited improvement in developing sufficient clamping forces in the lap splice region for ductility enhancement.

1.2.1.3 Retro-belt

Experimental research has been underway at the University of Ottawa since 1995 to develop a rational and economical retrofit technique to strengthen concrete bridge columns with seismic deficiencies (Saatcioglu and Yalcin 2003, Saatcioglu et al. 2002a, Saatcioglu et al. 2002b). The technique consists of external transverse prestressing columns to improve concrete confinement, diagonal tension resistance, as well as bond in the lap splice region. A detailed summary of previous research, that forms the earlier three phases of the current investigation, is provided below.

Yalcin, as part of his PhD research (1998), experimentally investigated the effectiveness of external prestressing as a retrofit technique on columns with circular (D = 510 mm) and square (550 mm) cross sections. A total of seven seismically shear deficient

columns were tested using either prestressing strands or high strength steel straps. All specimens had twelve No.25 grade 400 MPa, longitudinal reinforcement and No.10 ties placed at 300 mm spacing with the first tie placed at 75 mm from the column-footing interface simulating pre-1971 bridge columns. Columns had a height of 1200 mm and were subjected to a constant axial load equivalent to 15% of the axial capacity of columns under pure compression and incrementally increasing reversed cyclic lateral loading in the displacement control mode. One square and one circular column were tested as control specimens without retrofitting, while the five other columns were retrofitted by transverse prestressing of 7-wire strands or steel straps. Details of the test parameters are given in Table 1.1. The retrofit technique involved external prestressing of circular and square columns with individual hoops that consisted of the prestressed tendons and specially designed anchors. In the case of circular columns, the hoops were placed directly on the concrete surface, providing uniform lateral pressure generated by hoop tension. Additional hardware was used for square columns in the form of steel spreader frames and raiser discs to enable the development of perpendicular force components on all faces, bringing lateral pressure to near uniform distribution. Column tests were conducted to verify the parameters involved in the technology. The results indicate improvements in lateral drift capacity from 1% in shear-critical columns to up to 5% in retrofitted columns.

Mes, as part of his M.A.Sc. research (1999), designed, built and tested six full-size reinforced concrete columns under simulated seismic loading and constant axial load. The experimental program concentrated on pre-1970s columns as well as a recently designed column, all with flexure dominant behaviour. It included columns with a circular and a square cross-section and two different aspect ratios built in pairs to compare the results of as-built and retrofitted columns. The columns were labelled BR-C6 and BR-C7 for circular tied columns, BR-S3 and BR-S4 for square tied columns and BR-SP1 and BR-SP2 for spirally reinforced circular columns. The test specimens represented a portion of a bridge column between the footing and the point of inflection.

Columns BR-C6 and BR-C7 had a 508 mm circular cross-section and a 1725 mm specimen height with a shear span of 2000 mm measured to the point of application of the horizontal force. The reinforcing steel was of grade 400 MPa, and consisted of twelve #20 (19.5 mm diameter) longitudinal bars and #10 (11.3 mm diameter) hoops with overlapping

ends. The hoop spacing was 300 mm starting at 125 mm from the column base. The out-to-out dimension of the hoops was 410 mm, leaving a clear cover of 50 mm. The hoop spacing reflects the common design practice used prior to 1970s. The longitudinal reinforcement and column aspect ratio were selected to produce flexure dominant behaviour. Both columns had identical material and geometric properties, but column BR-C7 was retrofitted by external circular prestressing.

Columns BR-S3 and BR-S4 had a 500 mm square cross-section and the same height as the previous two columns. The reinforcement consisted of twelve #20 (19.5 mm diameter) longitudinal bars and #10 (11.3 mm diameter) hoops with 135° hooks at the ends. The spacing of hoops was 300 mm starting at 150 mm above the column base. The out-to-out dimension of the hoops was 410 mm leaving a clear cover of 45 mm. The longitudinal reinforcement and column aspect ratio were selected to produce flexure dominant behavior. Column BR-S4 was retrofitted by external prestressing.

Columns BR-SP1 and BR-SP2 were spirally reinforced columns with a 610 mm circular cross-section and a 1270 mm height. They had a reduced shear span of 1550 mm measured to the point of application of the horizontal force to increase shear stresses. The reinforcement consisted of twelve #20 (19.5 mm diameter) longitudinal bars and a #10 (11.3 mm diameter) spiral with a 75 mm pitch. These columns represented properly confined columns conforming to the current design practice (ACI 318, 2002). Out-to-out dimension of the spiral was 500 mm leaving a clear cover of 55 mm. Column BR-SP2 was retrofitted by external prestressing. Details of test parameters are given in Table 1.2.

Mes concluded that existing flexure dominant columns designed on the basis of pre 1970's practice are seismically deficient and need to be retrofitted. The proposed technique was found to be very effective in increasing concrete confinement and improving the inelastic behavior of columns.

Beausejour, as part of his M.A.Sc. research (2000), conducted tests on columns with splice deficiencies within the plastic hinge region. Six columns were tested by using three MTS actuators applying constant axial load and simulated seismic transverse loading. Three columns were tested as control columns and the other three were tested after being retrofitted with external prestressing. The first pair was long shear-span circular (D = 508mm) columns, labeled BR-C8 and BR-C9. The second pair consisted of two square (500 mm)

columns with similarly long shear spans, marked as BR-S5 and BR-S6. The third pair was built with a short shear span to amplify the effects of shear stresses reversals, labeled as BR-C10 and BR-C11, and had a circular cross-section (D = 610 mm). Retrofit details of columns are summarized in Table 1.3 No.20 longitudinal and starter bars were used with No.10 hoops. The control columns, which were built based on pre-1970's design practice with spliced longitudinal bars within the potential plastic hinge region, had a limited drift capacity of 1% and showed a sudden brittle failure. The lap splice length was 20 times the bar diameter and was found to provide inadequate development length, resulting in the slippage of bars and eventually failure of columns. Although the initial level of prestressing, at 25% f_{pu} with strands at every 150 mm, did improve the drift capacity from 1% to 2%, it was observed that a higher lateral pressure had to be applied for further improvement. It was found that the prestress of 50% f_{pu} with strands placed at every 100 mm within the splice region was found to be an effective retrofit strategy, increasing column drift capacity to 4%. Major improvements were achieved in regard to inelastic deformability and energy dissipation capacity by the application of Retro-belt technology.

1.2.2 Literature Review on Repair of Concrete Elements

Following an earthquake, the operation of life lines is hindered with negative consequences on relief and response efforts, as well as on the economy in general. Very little information is available in the literature on the seismic performance of repaired bridge columns and therefore seismic repair techniques are desperately needed to salvage damaged bridge infrastructure. The following provides a summary of research on repairing concrete elements.

Chung (1981) carried out tests to investigate the effectiveness of epoxy injection in repairing bond between steel and concrete. These tests were conducted on pullout specimens and reinforced concrete beams. A total of nine concrete cubes with 150mm cover over a single high strength deformed bar were tested with each cube having a different diameter bar embedded along the centroidal axis. To further investigate the pullout tests, a pair of 2 m long rectangular beams, with a 200 mm x 300 mm cross section and 25 mm diameter deformed bars, were built and tested. The beams were tested over a span of 1850 mm with two concentrated loads applied at 300 mm from the supports. The damaged specimens were

repaired by epoxy injection of the cracks and left for 7 days period. The control beams failed in shear with substantial slip of reinforcing bars. Although it was not possible to access all fine and discontinuous cracks through pressurized epoxy injection, the bond strength of the repaired specimens was observed to be the same as that of the original ones. It was also concluded that the repaired concrete could resist the same bond stress with more reduced slippage than the original (uncracked) concrete.

French et al. (1990) looked into the effectiveness of two different epoxy techniques to repair moderate earthquake damages to concrete structures. Two repair techniques known as pressure injection (RPI) and vacuum impregnation (RVI) were applied to interior beam-column joint specimens because such joints are subjected to severe conditions under lateral load reversals. Large size reinforcement was used so that it would develop severe anchorage requirements through the joint region. The damaged specimens were repaired by using epoxy, cured for four weeks and subjected to simulated seismic loading. Subsequently, the measured response histories for the control and retrofitted columns were compared and evaluated. They concluded that both repair techniques worked well and the repaired structures gained over 85% of the initial stiffness of the undamaged structures.

Yoshimura et al. (1991) investigated the effectiveness of steel jackets to repair damaged concrete columns that had inadequate shear strength and ductility. A total of nine square columns (178 x 178mm) were tested under axial load and cyclic lateral displacements simulating earthquake loading. An aspect ratio of 1.0 was selected to attain shear dominant columns. The transverse reinforcement ratio varied between 0.33% and 1.64% and the longitudinal reinforcement ratio varied between 2.5% and 6.64%. Three groups of columns were tested; I) reference columns, II) retrofitted columns and III) repaired columns. The focus of the review presented in this section is on the latter part. The reference columns were damaged and retested after being repaired by two L-shaped 6 mm (¼ in.) thick steel plates. The damaged concrete cover was replaced and the voids between the aggregates were filled by epoxy–based polymer cement. The jackets covered the full height of columns leaving a 6 mm gap at column ends. The reference columns that were designed based on pre-1970s design provisions exhibited dramatic shear failures. The repaired columns appeared to have higher strength and displacement ductility. The steel jacketing was found to be an effective

means of repairing damaged concrete columns which had insufficient shear strength and ductility.

Xiao et al. (1995) investigated the effectiveness of prefabricated glass fiber polymer composite jackets to repair circular concrete columns with splice deficiencies. The as-built columns represented prototype bridge columns on the I-10 Santa Monica Freeway in California with a 1:2 scale. The columns were reinforced with 20 No. 6 (19.05 mm) Grade 60 (400 MPa) longitudinal bars, had a 24 in. (610 mm) diameter cross-section and had No.2 (6.35 mm) smooth steel transverse reinforcement hoops spaced at every 5 in. (127 mm). All of the column reinforcements were spliced close to the footing with an overlap length of 15 in. (381 mm). The tested reference column that failed as a result of inadequate splice length was repaired by the use of four layers of prefabricated composite wrapping which were made of unidirectional glass fiber sheets and two part epoxy. The fibers were applied over the lower 4 ft. (1219 mm) of the column with a ¾ in. (19.05 mm) gap at the top of footing. Although the reference columns failed dramatically as a result of splice deficiency, the repaired column demonstrated a ductile behavior with a lateral drift ratio of up to 6%, and a slightly improved lateral strength. This research concluded that prefabricated glass fiber jacketing is an effective seismic repair strategy for circular columns with insufficient lap splices.

Saadatmanesh et al. (1997) used prefabricated fiber reinforced plastic (FRP) wraps to repair earthquake damaged reinforced concrete columns. A total of four 1/5 scale prototype bridge columns were damaged to the point of failure and were retested using hydraulic rams at the base of the specimens to apply a constant axial load of 445 kN, simulating dead load, and a horizontal actuator at the top of the specimen, simulating lateral earthquake loading. The design details replicated the existing seismic deficiencies, such as inadequate starter bar lap lengths and insufficient transverse reinforcement. Circular and rectangular cross sections were used to show the effectiveness of the technique employed. Columns C-1 and R-1, having a lap length of twenty times the bar diameter starter bars in the potential hinging region with No.4 (13mm diameter) and No.5 (16mm diameter) longitudinal reinforcement respectively, were used to examine bond failure mechanisms. Specimens C-2 and R-2 had continuous reinforcement consisting of No.4 and No. 5 bars respectively, with 9-gage steel wires (3.5 mm diameter) used as transverse reinforcement. Load control was used up to the

yielding of longitudinal bars and the tests then continued with loading applied in a displacement control mode. The as-built columns experienced severe damage, such as spalling and crushing of concrete in the compression zone. C-1 and R-1 failed as a result of de-bonding of starter bars. Column C-2 failed due to the local buckling of longitudinal reinforcement. Column R-2 failed in shear because of high longitudinal reinforcement ratio.

The columns to be repaired were pushed back to their original positions and loose concrete was removed and replaced. An active retrofit technique was applied by prestressing the straps. Either six or eight plies of straps were applied, depending on the required amount of lateral confinement pressure in circular and rectangular columns respectively. Each strap was 151 mm wide and was placed as close to the others as possible along the height. In general all repaired columns performed well and showed that FRP composite wraps are effective in restoring the flexural strength and ductility capacity of earthquake damaged columns. Repaired columns with lapped starter bars developed stable hysteresis loops up to a lateral drift ratio of 4%, while the columns with continuous bars showed stable hysteretic relationships up to 6% drift ratio.

Aboutaha et al. (1999) studied the effectiveness of various types of steel jackets for seismic rehabilitation of damaged rectangular reinforced concrete columns with splice deficiencies. Two specimens were tested as control columns with different numbers of crossties provided in transverse reinforcement. The reference columns were designed based on the provisions of ACI 318-56 (ACI Committee 318, 1956), and ACI 318-63(ACI Committee 318, 1963) building codes. In all of the six specimens tested (where four were repaired columns), longitudinal steel consisted of 16 No. 8 (25.4 mm) Grade 60 (400 MPa) deformed bars. No.3 (9.5 mm) Grade 40 (275 MPa) ties were used with a spacing of 16 in (406 mm). The splice length was 24 in. (610 mm) above the footing surface and the columns were tested without axial load. Three different types of retrofit schemes were used I) solid rectangular steel jackets, II) steel jackets with anchor bolts, and III) steel jackets with through rods and welded lap splices. Experiments showed that existing columns with inadequate lap splices are seismically deficient and have very low strength and ductility. All of the repair techniques employed provided some improvement when compared with reference columns. The most effective technique was found to be the steel jacket with

through rods which confined the splice region resulting in a large increase in flexural strength and ductility.

Lehman et al. (2001) evaluated the possibility of using currently available repair techniques to rehabilitate spirally reinforced concrete columns to meet the current seismic requirements. Four different repair techniques were applied to four companion concrete columns with identical properties except for the longitudinal reinforcement ratio. Three of the columns were severely damaged and the forth one was moderately damaged. Each column consisted of No.5 (16 mm) longitudinal reinforcement with a diameter of 2 ft (610mm) and a height of 8 ft (3.8m). Spiral reinforcement was 1/4 in. (6 mm) diameter with a pitch of 1- 1/4 in. (32 mm). Columns were tested under axial load by means of a spreader beam which was placed on top of the column and the load was applied by using two post tensioned rods that were attached to the floor. The simulated cyclic load was applied by using a displacement controlled hydraulic actuator. The columns 407S, 415S, 415M, and 430S had 0.75, 1.5, 1.5, and 3% steel ratios respectively. The letter S and M in the specimen labels represents "severe" and "moderate" damage. Severe damage is defined by 20% or higher strength decay and moderate damage is defined as damage prior to strength decay. An appropriate repair scheme was introduced on the basis of the level and severity of damage. Lehman stated that the type of damage observed and the characteristics of original column design dictated the repair technique required. They suggested a repair strategy for severely damaged columns involving replacement of the damaged region and jacketing the damaged area to promote subsequent hinging outside the jacketed region while enabling this region to develop further plastic hinging during subsequent loading. Repairing moderately damaged columns by cover concrete patching and epoxy injection was suggested. Repaired column 407SR showed comparable results to that of the companion non-retrofitted column. Columns 415SR and 430SR had the same properties as 407SR except for shorter effective column length and reduced longitudinal reinforcement ratio near the base respectively, hence exhibiting reduced deformability. In the case of column 415MR which initially suffered moderate damage, considerable decrease in stiffness was observed although strength and deformation capacities remained about the same.

Haroun et al. (2003) conducted a comprehensive experimental study on half-scale bridge columns repaired and retrofitted with composite-material jackets. A total of fourteen

half-scale, squat, circular and rectangular reinforced concrete columns were tested under fully reversed cyclic shear in a double bending configuration. Columns consisted of three as-built columns, ten columns retrofitted with different composite-jacket systems and one circular as-built column repaired after failure. The repair process involved crack injection followed by carbon/epoxy composite jacketing. The repaired column demonstrated ductility enhancement, as compared to the as-built sample.

Yamakawa et al. (2003) used the technique developed by Satoh et al. (Satoh, et al. 2001) to rehabilitate damaged shear deficient columns. In this method, 17 mm wide and 0.612 mm thick aramid fiber belts were cut in desired lengths and impregnated with epoxy resin. Cross bars (a piece of threaded bar) are passed through the eye-hook ends. Fiber belts are prestressed by manually screwing the bolts of crossbars using a wrench. Corners of columns are protected by steel angles and a frictionless film. This repair technique is intended for situations where the repair time is the major factor in facilitating immediate relief and response efforts. Six shear critical square columns with a 250 x 250 mm cross section were constructed. Specimens had a shear span to a depth ratio of 1.5 and a scale ratio of 1 to 2.4. Columns were tested under reversed cyclic lateral loading and a constant axial load. Test results indicate that the proposed technique is effective in overcoming the brittle shear failure and in promoting ductile flexural response. As an emergency rehabilitation procedure it can restore the lateral strength of partially earthquake-damaged RC columns and in the case of severe damage, some repair operations such as replacing spalled and damaged concrete with new concrete, are necessary before applying the repair technique. The researchers also used epoxy injection as a repair technique for damaged beam-column joints. Epoxy repaired joints sustained over 85 percent of the initial stiffness of the original undamaged structures. The strength and energy dissipation capacities were restored and new cracks developed adjacent to epoxy repaired cracks in the repaired structures.

1.2.3 Conclusions from Previous Studies

The following conclusions can be drawn from the review of previous research presented in the preceding section.

- Bridge infrastructure in North America, designed and built prior to the enactment of seismic design provisions of 1970's, may be seismically deficient. It was reported

(Stallings et al. 2000), that approximately 50% of all bridges in the United States were built before 1940 and 42% of these bridges have some form of structural deficiency (Klaibar et al. 1987). As a result of bridge damage from past earthquakes such as the San Fernando Earthquake and more recently, the 1994 Northridge and the 1995 Kobe Earthquakes, it has been demonstrated that bridges are one of the most vulnerable structures. The inadequacies of the pre-1971 designs of bridge structures have been recognized and the need for seismic retrofit and repair has been well accepted.

- Among the most popular retrofitting techniques, concrete and steel jacketing is more common. Since concrete jacketing reduces the aspect ratio, steel jacketing appears to satisfy most of the requirements. However, this technique has some disadvantages such as, difficulty in handling the plates, deterioration of bond at the steel and concrete interface and the need for massive scaffolding or heavy lifting equipment during installation. Therefore more practical and economical alternative solutions would be to investigate the application of newly developed techniques.
- One of the new retrofit and repair techniques that has gained acceptance in recent years is the use of FRP as externally bonded or wrapped elements. FRP jacketing was shown to be effective in improving inelastic deformability of shear and confinement deficient columns, especially for columns with circular geometry. However, the effectiveness of the technique for splice deficient columns remains controversial, with experimental evidence indicating limited or negligible improvements in such columns.
- A new technique, consisting of external transverse prestressing concrete columns and known as Retro-belt, is emerging as an economical and structurally effective technology for seismic retrofitting. The technique was shown to produce significant improvements in column strength and deformability in shear, flexure and splice deficient columns.
- All of the research done so far on Retro-belt technique has been on columns with circular and square sections. There is no research done on the applicability of this technique to rectangular columns. The technique has not been researched for potential application to repairing damaged columns either.

1.3 Research Needs

Considering the large number of concrete columns that require seismic strengthening and repair, and the need for economical techniques for upgrading these structures, it is obvious that more research is needed in the area. The following topics need to be researched, relative to the Retro-belt technology which was developed at the University of Ottawa:

- Capacities of existing bridge columns in terms of strength and inelastic deformability.
- Applicability of the Retro-belt technique to rectangular columns.
- Repair of seismically damaged columns using the Retro-belt technique. Since it is not feasible to rebuild all damaged columns after an earthquake, repairing remains to be a viable option. In the aftermath of an earthquake, with loss of operation of life line structures, repair effort must be made in a timely manner to prevent further economic or functional losses. Experimental research is needed to investigate the applicability of the Retro-belt technique to repair severely and moderately damaged columns with different types of deficiencies, i.e., shear, flexure and reinforcement splice length.

1.4 Objectives and Scope

The objective of this research project is to extend the use of the external prestressing system of seismic retrofitting concrete columns (the Retro-belt system) to rectangular columns while also investigating the use of the same technique for repairing damaged columns with different cross sections. This objective is attained through experimental and analytical research. The following tasks form the scope of the project:

Retrofit Phase:

- Design and construction of 6 concrete columns with a rectangular cross-section and two different shear-spans, with and without the splicing of longitudinal reinforcement.
- Retrofitting 3 of the columns with external prestressing.
- Instrumentation of all 6 columns.

- Testing under constant axial compression simulating gravity loads, and incrementally increasing lateral load reversals simulating seismic loading.
- Data acquisition and processing of test data.
- Analyses of columns and the verification of current analytical approaches in establishing flexural and shear strengths of columns.
- Development of design and construction methodologies for the Retro-belt system for rectangular columns.

Repair Phase:

- Design and construction of 3 shear-deficient concrete columns with rectangular, square and circular cross-sections.
- Instrumentation of all 3 columns.
- Testing under constant axial compression simulating gravity loads, and incrementally increasing lateral load reversals simulating seismic loading to induce moderate seismic damage in diagonal tension.
- Repair of all 3 columns. Retrofitting of the columns with external prestressing and instrumenting them for further data acquisition.
- Testing under constant axial compression simulating gravity loads, and incrementally increasing lateral load reversals simulating seismic loading to assess the effectiveness of the Retro-belt repair technique.
- Data acquisition and processing of test data.
- Development of design and construction methodologies for the Retro-belt system to repair damaged columns.

Table 1.1 Test parameters for Columns Tested by Yalcin (1998)

Test Column	Type	Cross-Section	Retrobelt Hoops		
			Hoop Steel	Hoop Spacing	Initial Prestress
BR-S1	Short	550 mm Square	N/A		
BR-S2	Short	550 mm Square	7-Wire	150 mm	300 MPa
BR-C1	Short	610 mm Circular	N/A		
BR-C2	Short	610 mm Circular	7-Wire	150 mm	300 MPa
BR-C3	Short	610 mm Circular	7-Wire	150 mm	50 MPa
BR-C4	Short	610 mm Circular	7-Wire	300 mm	300 MPa
BR-C5	Short	610 mm Circular	Steel Strap	150 mm	50 MPa

Table 1.2 Test parameters for columns tested by Mes (1999)

Test Column	Type	Cross-Section	Retrobelt Hoops		
			Hoop Steel	Hoop Spacing	Initial Prestress
BR-S3	Long	500 mm Square	N/A		
BR-S4	Long	500 mm Square	7-Wire	150 mm	$25\%f_{pu}$
BR-C6	Long	508 mm Circular	N/A		
BR-C7	Long	508mm Circular	7-Wire	150 mm	$25\%f_{pu}$
BR-SP1*	Short	610 mm Circular	N/A		
BR-SP2*	Short	610 mm Circular	7-Wire	300 mm	$25\%f_{pu}$

*Transverse reinforcement of No.10 spiral with a 75 mm pitch was used.

Table 1.3. Test parameters for columns tested by Beausejour (2000)

Test Column	Type	Cross-Section	Retrofitting by external hoops		
			Hoop Steel	Hoop Spacing	Initial Prestress
BR-C8	Long	508 mm Circular	N/A		
BR-C9	Long	508 mm Circular	7-Wire	150 mm	25% f_{pu}
BR-S5	Long	500 mm Square	N/A		
BR-S6*	Long	500 mm Square	7-Wire	100 mm	50% f_{pu}
BR-C10	Short	610 mm Circular	N/A		
BR-C11*	Short	610 mm Circular	7-Wire	100 mm	50% f_{pu}

*Initial prestress within the splice region (390 mm) was 50% f_{pu} @ 100 mm, beyond this point it was 25% f_{pu} @ 150mm.

Chapter 2

Experimental Research

2.1 General

Experimental research was conducted to investigate the application of the Retro-belt technique to rectangular columns and to explore the possibility of repairing reinforced concrete columns that have already been damaged by an earthquake, through the use of the same technique. A total of nine full-scale specimens were tested under simulated seismic loading. Six of the specimens had a 350 mm by 700 mm rectangular cross-section, and were included in Phase I of the test program for retrofitting. A circular column with a diameter of 600mm, a square column with a 500mm x 500mm cross section and a rectangular column with a 350mm x 700mm cross section were tested as part of Phase II of the experimental program on repair. The specimens represented a segment of a bridge column between the footing and point of inflection. The columns were designed to represent pre-1971 designs with 11.3 mm diameter (#10) transverse reinforcement at 300 mm spacing.

In Phase I of the test program, two different specimen heights were considered to create shear-critical and flexure-critical columns. The aspect ratio (the ratio of column shear

span to the cross-sectional dimension in the direction of loading) was 2.16 and 2.87 for shear and flexure dominant columns, respectively. The columns were built in pairs with one column in each pair representing as-built conditions to investigate inelastic deformability and failure modes of existing bridge columns, while the other column was retrofitted by external prestressing to investigate improvements resulting from the retrofit. One pair of the flexure-dominant columns had spliced longitudinal reinforcement within the potential plastic hinge region near the base, simulating the practice in most existing bridge columns.

Phase II columns were designed to be critical in shear, with aspect ratios of 2.5, 3.0, and 2.14 for circular, square and rectangular columns, respectively. Columns were subjected to a constant axial load corresponding to 15% of concentric column capacity, and subsequent application of incrementally increasing lateral deformation reversals. The columns were loaded to induce significant diagonal tension (shear) cracking, simulating a moderate level of damage prior to strength decay. Then the columns were repaired and retested.

The specimen details, material properties, instrumentation and test setup are presented in the following sections. Table 2.1 provides a summary of the column specimens tested in the current investigation.

2.2 Construction of Column Specimens

Full scale test specimens were constructed at the structures laboratory of the University of Ottawa. The Structures Laboratory has a 13 x 22 m strong test floor and a 10-ton overhead crane, providing facilities for full-scale testing of structural components. Concrete used for casting test specimens and pre-bent steel reinforcement was supplied by local companies.

2.2.1 Footings and Formwork

Steel cages were built after installing strain gauges on the reinforcement at designated locations. Column footings were over-reinforced making them very rigid and strong to provide full fixity. Footings of control columns were cast first followed by the columns. Then, the footings of the columns to be retrofitted were cast followed by the columns. All column footings in the repair stage were cast at the same time. This was followed by the casting of the columns of the same specimens. The formwork was built by

using sheets of two-inch thick plywood. Figure 2.1(a) and (b) illustrates the steps followed for constructing the steel cages and footing formwork.

2.2.2 Columns

Once the footings gained strength and hardened, column formwork was installed on top of the footings. Sona tubes (for columns with circular cross section) or plywood pieces (for columns with rectangular and square sections) were used for column formwork. Column formwork was restrained against lateral concrete pressure during casting and potential opening of formwork, by means of ropes tied in the transverse direction. Pieces of wood kept the formwork in an upright position after the formworks were vertically leveled with a plumb bob. The footing surface to form column-footing interface was roughened and wetted before the column concrete was cast. The formwork was removed forty eight hours after casting, and the columns were subjected to a wet cure for two weeks. They were painted white to make the cracks more visible during testing. The reinforcement locations were marked with black lines on the columns. The column formwork and concrete casting are shown in Figure 2.1(c) for columns with different cross-sectional geometry.

2.2.3 Retrofit and Repair through External Prestressing

One column in each pair of the specimens tested under the Retrofit Phase and two of the columns in the Repair Phase were externally prestressed in the transverse direction to retrofit or repair the columns, respectively, using the Retro-belt technology. The transverse prestressing was done by means of standard 7-wire strands. Each strand had a 9.53 mm nominal diameter and 55 mm^2 steel area. While the strands were directly applied on circular columns, to take advantage of uniform hoop tension that develops in a circular geometry, they were applied through raiser frames on rectangular and square columns to produce a parabolic tendon profile and activate hoop tension. The raiser frames were manufactured from hollow steel sections (HSS 31.8x31.8x6.35mm) with three semi-circular disks welded on each side to raise the level of strand. This ensured reasonably uniform application of confinement forces on each face of column. Figure 2.10 shows the details of the raiser frames. A specially manufactured anchor was used to perform the prestressing of each strand. This anchor was placed on one of the steel hollow sections replacing one of the semi-

circular disks while enabling the anchoring of stressed strands. A small piece of greased steel strip was placed around each corner to prevent damage to the corners and to allow the strands to slide freely during prestressing.

The locations of hollow sections were first marked on columns. The hollow sections were then nailed to the column concrete to ensure proper positioning during prestressing. The strands were wrapped around the raiser frames or directly on columns (for circular columns), and were locked in the anchors by means of two pairs of wedges. Two jacks were used to prestress the strands. The first jack applied the prestressing force while a load cell was placed between the jacks and the anchor for readings the applied force. Upon developing the required level of prestressing, the second jack was used to push and lock the wedges into the anchor to eliminate anchorage loss of prestress. The jacks were removed and the excess strands were cut. The application of Retrobelt and the hardware used are illustrated in Figures 2.2 and 2.3. The strands were stressed using Dywidge twisted ring anchors.

2.3 Description of Test Specimens in the "Retrofit Phase"

Three pairs of rectangular columns with the same cross section but different heights and longitudinal reinforcement details were built and tested. The column cross-section was 350 x 700 mm. One column in each pair represented as built conditions while the other column was retrofitted and tested.

The specimens were cast using ready mixed concrete. Standard concrete cylinders were tested (152mm diameter and 305mm height) to establish the strength of concrete. Average concrete strengths on the day of column tests were 42 MPa and 38 MPa for unretrofitted and retrofitted columns respectively. Tension coupon tests were performed on steel re-bars to establish the stress-strain relationships for reinforcing steel bars used as longitudinal and transverse reinforcement. The yield strength for #10 and #20 bars were established as 550 and 460MPa, respectively. Seven-wire prestressing strands used to retrofit columns had a nominal diameter of 9.53 mm and ultimate strength of 2096 MPa.

2.3.1 Shear Dominant Rectangular Columns (SR-C, SR-R)

A pair of short rectangular columns, with a height of 1220 mm (shear span of 1500 mm, measured to the point of application of the horizontal actuator) was built and tested to investigate column performance under relatively high shear stress reversals. These columns had shorter lengths, relative to others to amplify shear stresses, and are characterized as "Short Columns." The columns were labeled SR-C and SR-R for short control and retrofitted columns, respectively. The reinforcing steel was of grade 400 MPa, and consisted of twelve #20 (19.5 mm diameter) longitudinal bars. The column transverse reinforcement was provided by using # 10 (11.3 mm diameter) hoops with 135° hooks at a spacing of 300 mm. The spacing of ties was reduced near the top, outside the test region, to avoid the possibility of premature damage due to stress concentration that might be caused by the loading beam. The clear concrete cover over the ties was 45 mm. The column geometry and reinforcement details are illustrated in Figure 2.4.

The retrofitting consisted of prestressing strands placed at 150 mm spacing, with the first strand placed at 75 mm from the column base. The strands were prestressed up to approximately 25% f_{pu} (524 MPa). The transverse prestressing was intended to overcome diagonal tension caused by shear and also to provide additional shear reinforcement, and to enhance concrete confinement thus improving the flexural deformability of column. The details of retrofitting are illustrated in Figure 2.5.

2.3.2 Flexure Dominant Columns (LR-C, LR-R)

Two companion columns with 1720 mm height were built and tested. The columns had an effective cantilever height (shear span) of 2000 mm when measured to the point of application of the horizontal actuator. The reinforcement consisted of twelve #20 (19.5 mm diameter) longitudinal bars and #10 (11.3 mm diameter) hoops with 135° hooks at both ends. The spacing of hoops was 300 mm, starting at 75 mm above the column base. The spacing of ties was reduced near the top, outside the test region, to avoid the possibility of a premature damage due to stress concentration that might be caused by the loading beam. The clear concrete cover over the ties was 45 mm. Figure 2.6 illustrates the geometric details of column specimens tested.

The retrofitting consisted of prestressing strands placed at 150 mm spacing, with the first strand placed at 75 mm from the column base. The strands were prestressed up to approximately 25% f_{pu} (524 MPa). The transverse prestressing was intended to enhance concrete confinement, improving the flexural deformability of the column. The details of retrofitting are illustrated in Figure 2.7.

2.3.3 Flexure Dominant Columns with Splice Deficiencies (LS-C, LS-R)

Two rectangular columns, labeled as LS-C and LS-R, with the same height as those tested for flexure (LR-C and LR-R) were prepared and tested to investigate the effect of lap splice on column behaviour. The reinforcement consisted of twelve #20 (19.5 mm diameter) longitudinal bars and #10 (11.3 mm diameter) hoops with 135° hooks at both ends. The longitudinal reinforcement was spliced near the footing, with a splice length equal to 20 times the bar diameter (20 x 19.5 = 390 mm). The spacing of hoops was 300 mm, starting at 75 mm above the column base. The spacing of ties was reduced near the top, outside the test region, to avoid the possibility of premature damage due to stress concentration that might be caused by the loading beam. The clear concrete cover over the ties was 45 mm. Figure 2.8 shows the steel detailing for spliced rectangular columns.

Column LS-C was tested without retrofitting while the companion column, LS-R, was retrofitted with prestressing strands placed at every 100 mm in the splicing region, starting at 75 mm from the column base. The initial prestress level was 50% of the ultimate strand strength, f_{pu} (1048MPa). This was felt necessary because of the increased lateral clamping stress needed to increase bond between spliced reinforcement and concrete, as evidenced by earlier tests (Beausejour, P. 2000). Other strands above the potential hinging region were installed at every 150 mm up to the top of the column, and prestressed to 25% f_{pu} (524 MPa). Figure 2.9 shows the retrofitting details of Column LS-R.

2.4 Description of Test Specimens in the "Repair Phase"

Three shear dominant columns with square, circular and rectangular cross sections were designed, built and tested. The lateral loading was first applied to create sufficiently high shear distress. The columns were then repaired and re-tested to study the effectiveness of the technique used earlier for retrofitting as a repair methodology, except for the circular

column which had developed a sudden failure before the test could be stopped for subsequent repair work.

2.4.1 Shear Dominant Circular Column (CR-C)

A short circular column, with a sectional diameter of 600 mm and a height of 1220 mm (with a shear span of 1500 mm measured to the point of application of the horizontal force) was designed and built to simulate pre-1970's practice. It was labeled CR-C. The column reinforcement consisted of twelve #20 (19.5 mm diameter) longitudinal bars and #2 (6.35 mm diameter) hoops with 135° hooks at both ends. The spacing of hoops was 300 mm, starting at 75 mm above the column base up to the fifth hoop. The hoops above this level (above the test region) were placed to over-reinforce the column at its end to prevent a premature failure resulting from possible stress concentration caused by the top loading beam; consisting of #10 (11.3 mm diameter) hoops at every 100 mm. The clear cover was 45 mm. Column geometry and reinforcement details are illustrated in Figure 2.11.

The specimen was cast using ready mixed concrete. Standard concrete cylinders were tested to establish the strength of concrete. The concrete strength on the day of column test was 35 MPa. Tension coupon tests were performed on steel re-bars to establish their stress-strain relationships.

The column was first loaded by two vertical MTS actuators to apply a constant axial load of about 15% of column compressive capacity. It was then subjected to three cycles of elastic deformations at about ½% drift ratio, followed by incrementally increasing lateral drift until a significantly wide diagonal crack was observed implying the yielding of the hoop steel. The deformation level was increased to 1% and cycled three times. Longitudinal reinforcement and hoops were observed to yield at the first cycle of this drift level. This level of deformation was sufficient to cause visible diagonal tension cracks. It was felt that the cracks were not wide enough to suggest moderate damage. Hence, it was decided to increase the level of deformation to 1.5%. However, the column failed beyond repair in a brittle manner before developing the expected crack pattern. Therefore, while this column provided insight into the shear capacity of existing shear deficient bridge columns, it could not be repaired and retested.

2.4.2 Shear Dominant Square Columns with Splice Deficiencies (SSR-C, SSR-R)

A shear-dominant square column, labeled as SSR-C, with a 500 mm cross-sectional dimension and 1220 mm height as the previous shear dominant column was built and tested. The column had an effective cantilever height of 1500 mm, measured to the point of application of the horizontal force. The reinforcement consisted of twelve #20 (19.5 mm diameter) longitudinal bars and #2 (6.35 mm diameter) hoops with 135° hooks at both ends. The spacing of hoops was 300 mm, starting at 75 mm above the column base. In order to avoid a premature failure at the top of the specimen, outside the test region, due to the anticipated stress concentration caused by the loading beam, transverse reinforcement spacing was reduced to 40 mm near the tip of the columns. The lap splice length was 390 mm, corresponding to 20 times the bar diameter, and the clear cover was 35 mm. Figure 2.12 shows the steel detailing for spliced square column.

Column SSR-C was loaded initially to induce shear distress and then repaired and re-tested. It was first loaded by two vertical MTS actuators to apply a constant axial load of about 15% of column compressive capacity. It was then subjected to three cycles of elastic deformations at about ½% drift ratio, followed by incrementally increasing lateral drift ratios until a significantly wide diagonal crack was observed to imply the yielding of hoop steel. The deformation level was increased to 1% and cycled three times. This level of deformation was sufficient to cause visible diagonal tension cracks that indicated possible yielding of the hoops. Therefore the test was stopped, the actuators were removed, including the vertical actuators that applied gravity loading, and then the specimen was repaired using external transverse prestressing. The prestressing strands were placed at every 100 mm in the splice region, starting at 75 mm from the column base. They were stressed to about 50% of the ultimate strand strength, f_{pu} (1048 MPa). Other strands above the potential hinging region were placed at every 150 mm up to the top of the column, and prestressed to 50% f_{pu} (1048 MPa). The repaired column was labeled as SSR-R. Figure 2.13 shows a schematic view of the repair details used. The hardware used for the repair was exactly identical to those used for retrofitting, with the exception of the greased circular pieces that had wedges cut to fit into the corners to help improve the prestressing operation without damaging the corners and to reduce friction at sharp corners. Figure 2.10 illustrates the details of the hardware used to retrofit and repair the rectangular and square columns.

2.4.3 Shear Dominant Rectangular Column (RR-C, RR-R)

A shear dominant rectangular column with cross sectional dimensions of 350 x 700 mm and a height of 1220 mm was prepared for testing. It was labeled RR-C when it was loaded to induce shear cracking, and RR-R after it was repaired and re-tested. The total effective height of the column (shear span) was 1500 mm measured to the point of application of the horizontal actuator. The reinforcing steel was of grade 400 MPa, and consisted of twelve #20 longitudinal bars which were lap spliced near the column base with a lap length of 390 mm. The column transverse reinforcement was provided using #2 (6.3 mm diameter) hoops with 135° bends at the ends starting at 75 mm from the column base and 300 mm thereafter. In order to avoid premature failure at the top of the specimen due to anticipated stress concentration caused by the top loading beam, the top four hoops were made from #10 (11.3 mm diameter) bars and were spaced at 44 mm. The clear concrete cover used was 45 mm. The column geometry and reinforcement details are illustrated in Figure 2.14.

The column was loaded initially to induce shear distress and then repaired and re-tested. It was first loaded by two vertical MTS actuators to apply a constant axial load of about 15% of column compressive capacity. It was then subjected to three cycles of elastic deformations at about ½% drift ratio followed by incrementally increasing lateral drift until a significantly wide diagonal crack was observed to indicate the yielding of hoop steel. The deformation level was increased to 1% drift ratio and the column was cycled three times. This level of deformation was sufficient to cause visible diagonal tension cracks that indicated possible yielding of the hoops. Therefore, the test was stopped, the actuators were removed including the vertical actuators that applied gravity loading and then the specimen was repaired using external transverse prestressing. The prestressing strands were placed at every 100 mm in the splice region, starting at 75 mm from the column base. The strtands were stressed to about 50% of the ultimate strength, f_{pu} (1048 MPa). Other strands above the hinging region were placed at every 150 mm up to the top of the column, and prestressed to 50% f_{pu} (1048 MPa). The repaired column was labeled as RR-R. Figure 2.15 shows a schematic view of the repair details used. The hardware used for the repair was identical to those used for retrofitting rectangular columns in the earlier phase, except for the greased

circular pieces that had wedges cut to fit into the corners to help improve the prestressing operation without damaging the corners and to reduce friction at sharp corners.

2.5 Material Properties

The material properties were established through standard tests. Concrete cylinders and steel coupon tests were conducted three times for each material in order to establish their stress-strain relationships.

2.5.1 Concrete

Standard concrete cylinders with 152 x 305 mm dimensions were cast to establish the stress-strain relationship of concrete, and to monitor strength gain with time. The cylinders were tested using a Fourney testing machine with 2225 kN capacity as shown in Figure 2.16. Strain data was obtained by using two LVDT's installed on the opposite sides of concrete cylinders and a data acquisition system. Figure 2.16 (a) shows the data acquisition system and the LVDT's on concrete cylinders. For the retrofit phase of the experimental program, concrete casting was done on three different dates. The cylinders were capped with a sulfur compound to ensure uniform loading. The ends of the cylinders for concrete used in the repair phase were ground before testing. Figures 2.17, 2.18 & 2.19 illustrate the stress strain relationships obtained from the cylinder tests for control, retrofitted and repaired columns respectively. The strain values for Figure 2.17 are not reliable due to the slippage of LVDTs. Therefore, only the strength values are used.

2.5.2 Reinforcing Steel

Tension coupon tests were conducted on #10 and #20 deformed reinforcement as well as 6.3 mm smooth wire to establish stress-strain relationships. The # 20 bars with a nominal diameter of 19.5 mm were used as the longitudinal reinforcement in all columns while # 10 with a nominal diameter of 11.3mm, and 6.3mm bars were used as the transverse reinforcement for columns in Retrofit and Repair Phases of experiments, respectively. The coupon tests were done using a 600 kN capacity Galdabini Universal testing machine illustrated in Figure 2.20. The same figure also shows the deformed shape of tested reinforcement. The three different size bars yielded at different stress levels. The # 20 bar

yielded at 465 MPa while # 10 and the 6.35mm bars yielded at 570 MPa and 491 MPa, respectively. Test data is plotted in Figures 2.21, 2.22 & 2.23.

2.5.3 Prestressing Strands

Size 9, Grade 1860 MPa seven-wire strands were used to retrofit and repair columns. The nominal strand diameter was 9.53 mm with 55 mm^2 cross sectional area. Three prestressing strands were tested using a Tinius Olsen universal testing machine of 1500 kN capacity and the results were recorded with a data acquisition system. Figure 2.24 shows the machine used as well as the coupons before and after testing. Although the ultimate tensile strength was specified by the supplier to be 1860 MPa, the coupon tests indicated the ultimate rupturing strength to be 2195 MPa. Therefore the prestressing values of 25% f_{pu} and 50% f_{pu} corresponded to 465 MPa and 930 MPa respectively. Figure 2.25 illustrates the stress-strain relationships for the strands.

2.6 Test Setup

The columns were fixed to the laboratory strong floor and subjected to axial compression by means of two 1000 kN capacity MTS-Hydraulic actuators. A third MTS actuator was positioned horizontally to apply incrementally increasing lateral deformation reversals. The test setup is shown in Figure 2.26. It was oriented in the North-South direction, which was the direction of lateral loading. The same setup was used for both long and short columns in both the Retrofit and Repair Phases of research except that the position of the horizontal actuator was adjusted as needed. A reinforced concrete spacer block, with a height of 965 mm, was used for short columns and a height of 460 mm was used for long columns. Figure 2.27 shows the two different spacer blocks used.

2.7 Loading Program

A constant axial load of 15% P_o was applied to the specimens during testing, representing the effect of the gravity load, were (P_o) was computed based on ACI code using Eq. 2.1. The level of axial load applied on each column is presented in Table 2.2.

$$P_O = 0.85 f_c^{'} (A_g - A_s) + A_s f_y \qquad (2.1)$$

The horizontal load was applied in the deformation control mode imposing incrementally increasing lateral displacements. Column drift ratio was used as the basis for deformation increments. Each column was first loaded by the vertical actuators and the axial load was then kept constant during testing. The horizontal deformations were applied in three cycles at each level. Following the three cycles at the first drift level simulating post-cracking elastic response, the drift ratio was increased incrementally until a significant drop in load resistance was recorded.

2.8 Instrumentation

The columns were instrumented with the following:

- LVDTs (Linear Variable Displacement Transducer) of 50 mm stroke.
- Temposonic LVDTs.
- Electrical-resistance strain gauges on reinforcing bars and prestressing strands.
- Calibrated load cells of actuators.
- Plumb bob (For vertical leveling of repaired columns and column formwork).

A total of eight electric resistant strain gauges (14 in columns with lap splices) were used to measure the strains in longitudinal reinforcement. An additional four strain gauges were placed on transverse reinforcement (6 in shear dominant rectangular columns) on the second and third column ties. Figures 2.28 to 2.33 illustrate the positions of strain gauges on reinforcing steel. Two strain gauges (one in some of the columns due to the limitation on the data acquisition system) were placed on each prestressing strand as shown in Figure 2.34. Total of four LVDTs were used to measure the flexural rotations within h (Θ_h) and h/2 ($\Theta_{h/2}$) distances from the footing (where h is the cross-sectional dimension of column parallel to loading). One Temposonic LVDT was used to measure the lateral displacement while another two were used to evaluate the anchorage slip rotation at column footing interface. All the data collected during testing was recorded by a data acquisition system. Figure 2.35 shows the locations of instrumentation.

Table 2.1 Test parameters

Test Column	Type	Cross-Section	Retrofitting by external hoops		
			Hoop steel	Hoop spacing	Initial prestress
SR-C	Short	350X700 Rectangular	N/A		
SR-R	Short	350X700 Rectangular	7-Wire	150 mm	25% f_{pu}
LR-C	Long	350X700 Rectangular	N/A		
LR-R	Long	350X700 Rectangular	7-Wire	150 mm	25% f_{pu}
LS-C	Long(Spliced)	350X700 Rectangular	N/A		
LS-R*	Long(Spliced)	350X700 Rectangular	7-Wire	100 mm	50% f_{pu}
C-C	Short	500 mm Circular	N/A		
SSR-C	Short(Spliced)	500X500 mm Square	N/A		
SSR-R**	Short(Spliced)	500X500 mm Square	7-Wire	100 mm	50% f_{pu}
RR-C	Short	350X700 Rectangular	N/A		
RR-R	Short	350X700 Rectangular	7-Wire	150 mm	50% f_{pu}

* Initial prestress within the splicing region (390 mm) was 50% f_{pu} @ 100 mm, beyond this point it was 25% f_{pu} @ 150mm.

** Initial prestress within the splicing region (390 mm) was 50% f_{pu} @ 100 mm, beyond this point it was 50% f_{pu} @ 150mm.

Table 2.2 Constant axial load applied to the columns

Column			Compressive Load Applied	
Label	**Description**	**f'_c**	**Value(kN)**	**Load/P_o**
SR-C	Short Rectangular Column-Control	42	1508	15%
SR-R	Short Rectangular Column-Retrofitted	38	1386	15%
LR-C	Long Rectangular Column-Control	42	1508	15%
LR-R	Long Rectangular Column-Retrofitted	38	1386	15%
LS-C	Spliced Long Rectangular Column-Control	42	1508	15%
LS-R	Spliced Long Rectangular Column-Retrofitted	38	1386	15%
C-C	Circular Short Column-Control	35	1436	15%
SSR-C	Spliced Square Short Column-Control	35	1294	15%
SSR-R	Spliced Square Short Column-Repaired	35	1294	15%
RR-C	Rectangular Short Column-Control	35	1294	15%
RR-R	Rectangular Short Column-Repaired	35	1294	15%

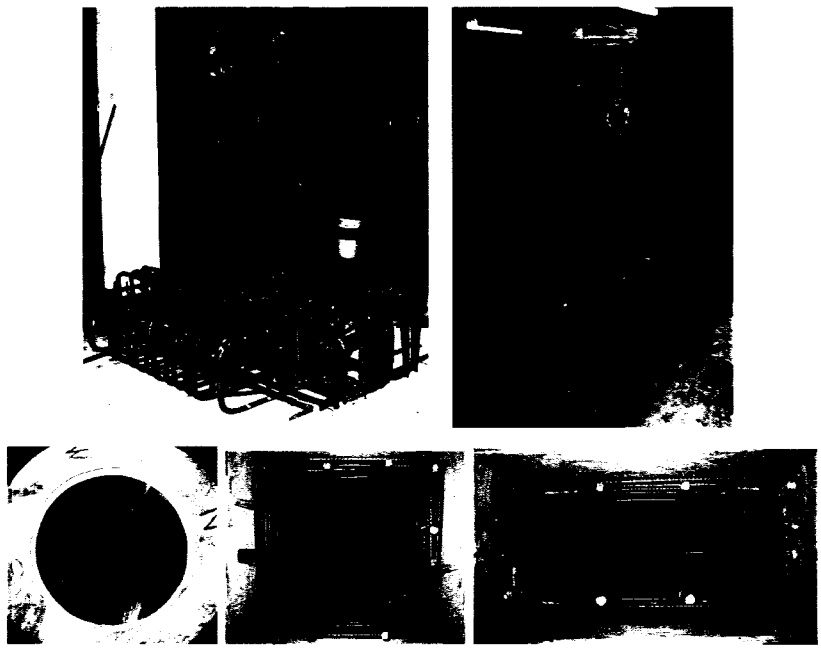

a) Steel cages

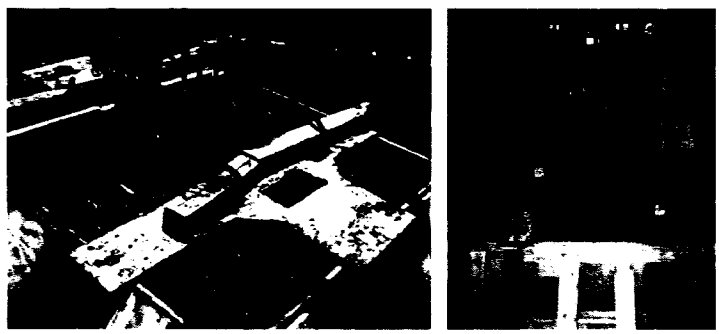

b) Footing Formwork

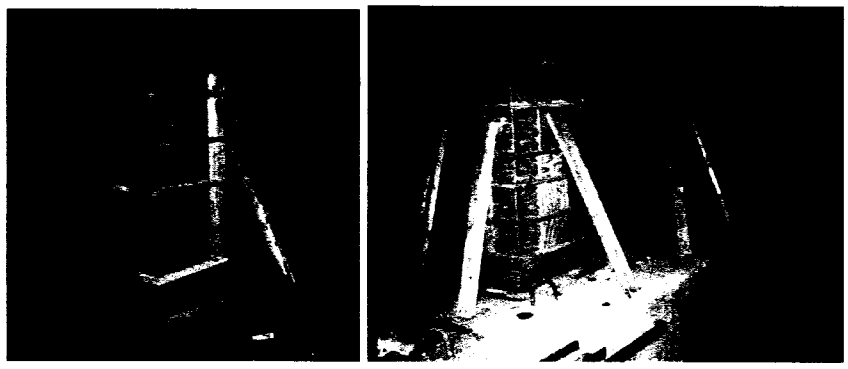

(c) Column Formwork

Figure 2.1 Construction of column specimens

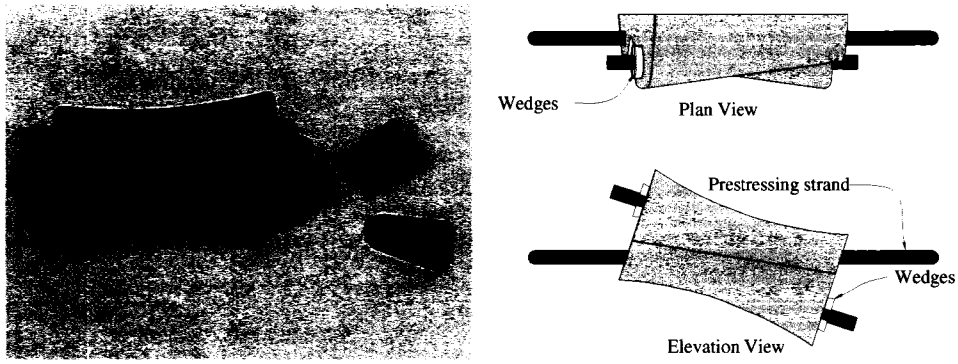

a) **Retro-belt anchors**

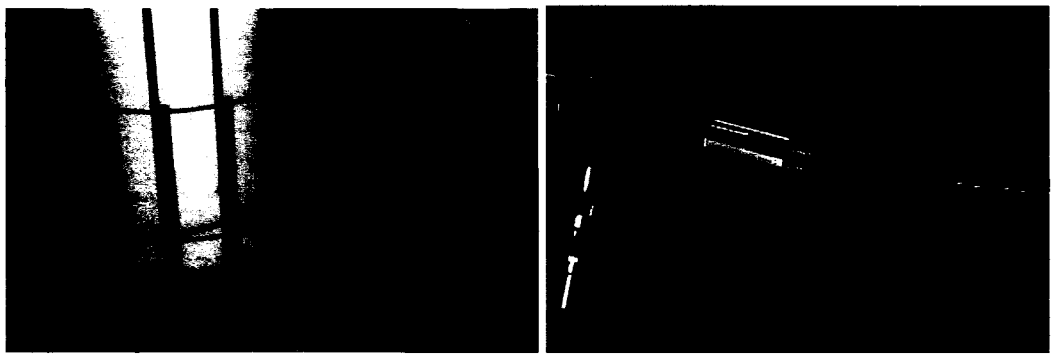

b) **Installation of strands on circular columns**

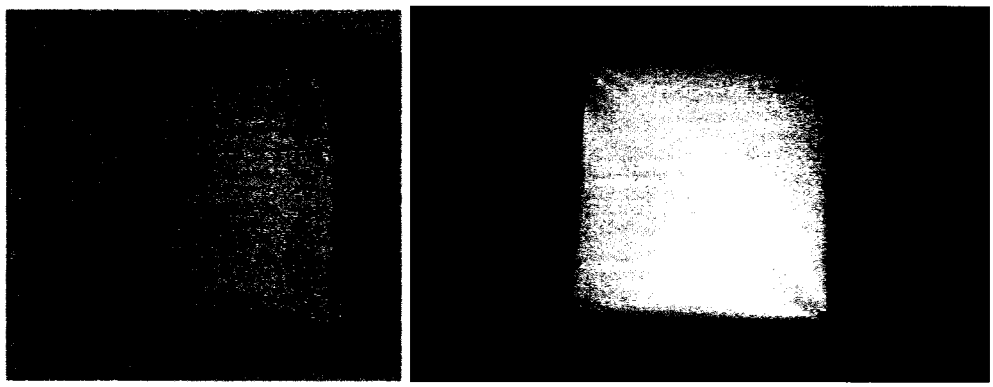

c) **Raiser frames and installation of strands on square columns**

Figure 2.2 Hardware required for the installation of prestressing strands

a) Retrofitting a rectangular column

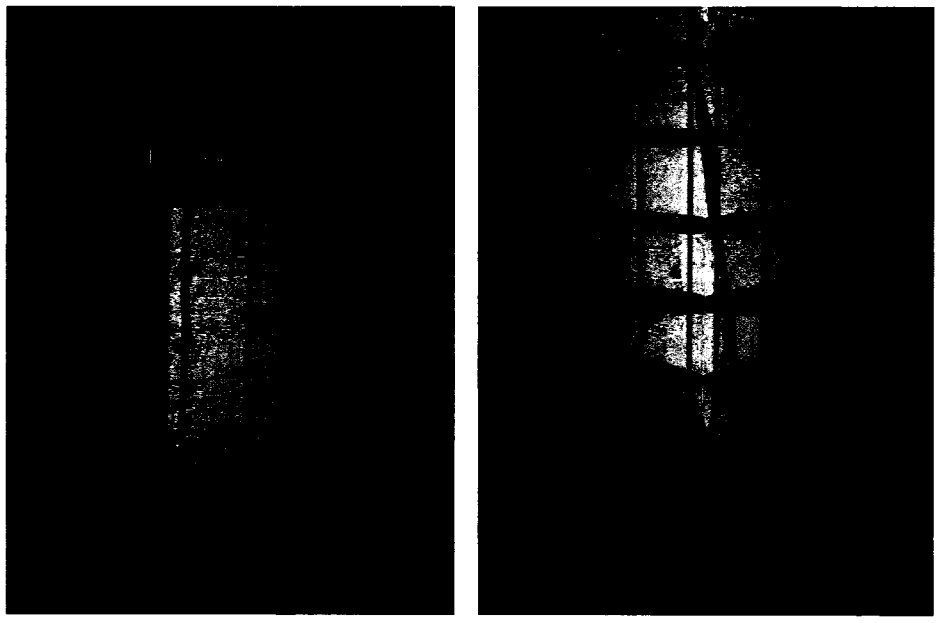

b) Repairing a square column

Figure 2.3 Installation of Retro-belt on rectangular and square columns

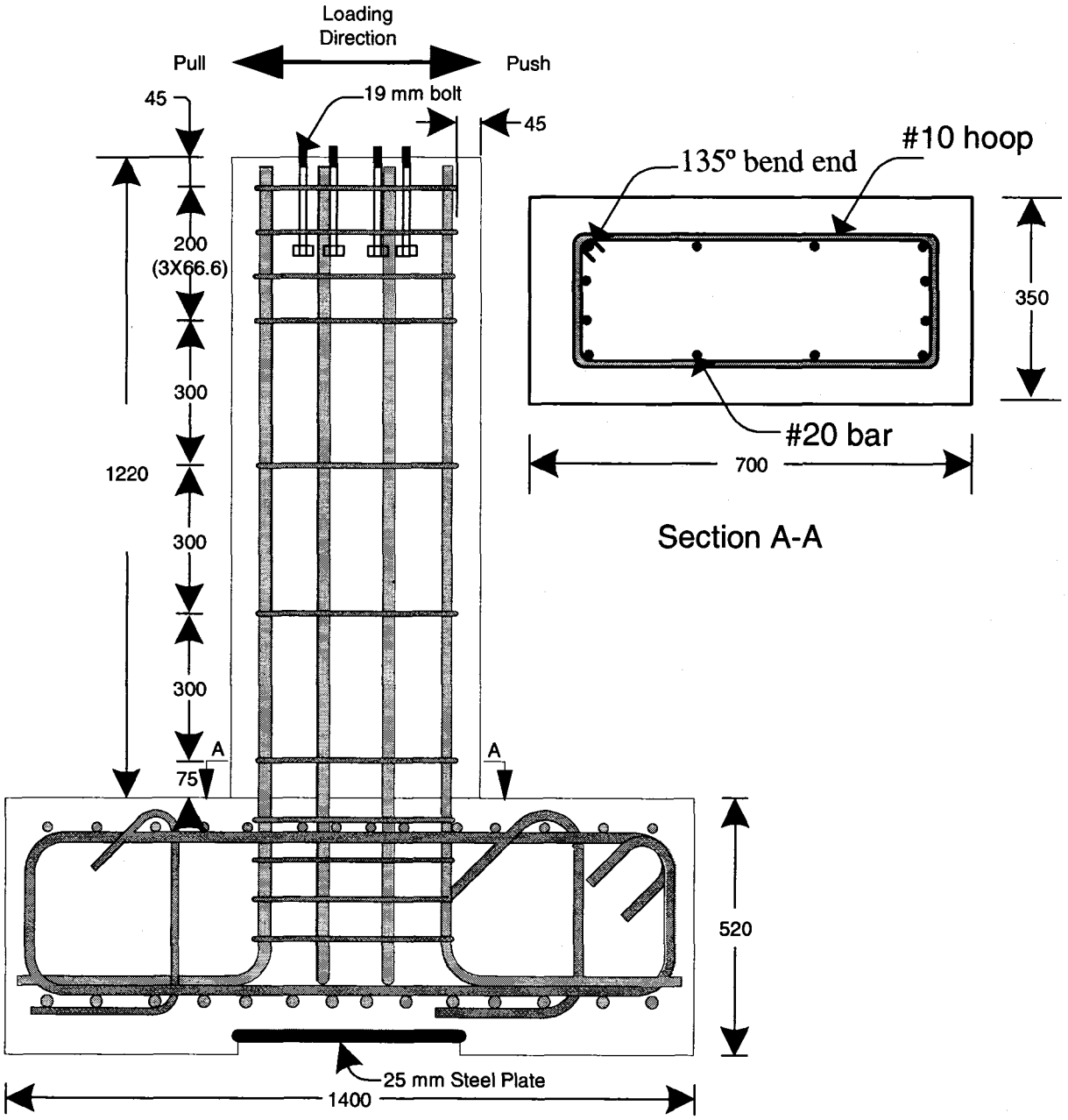

Figure 2.4 Geometry and reinforcement details for Columns SR-C and SR-R

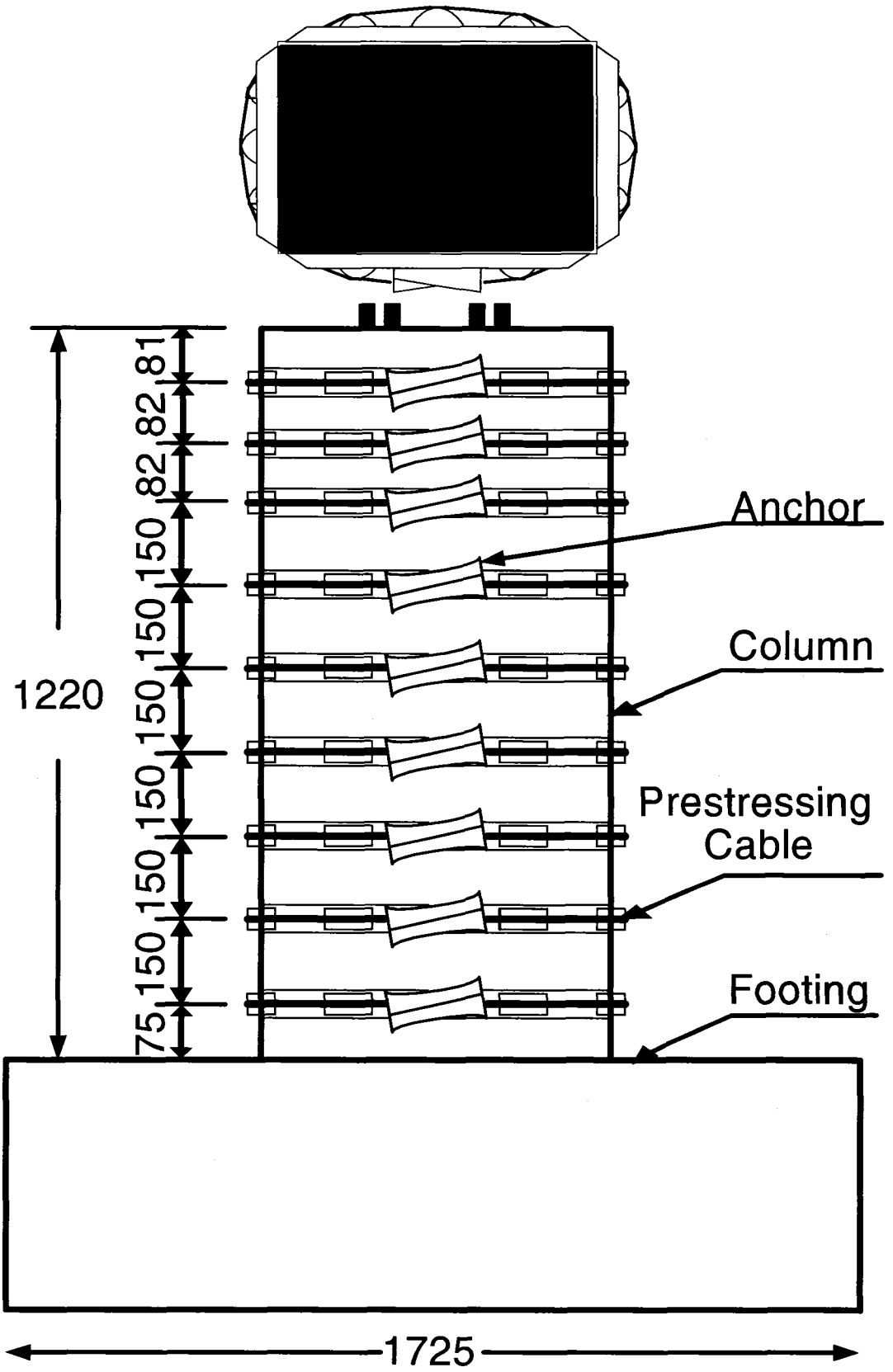

Figure 2.5 Retrofitting details for Column SR-R

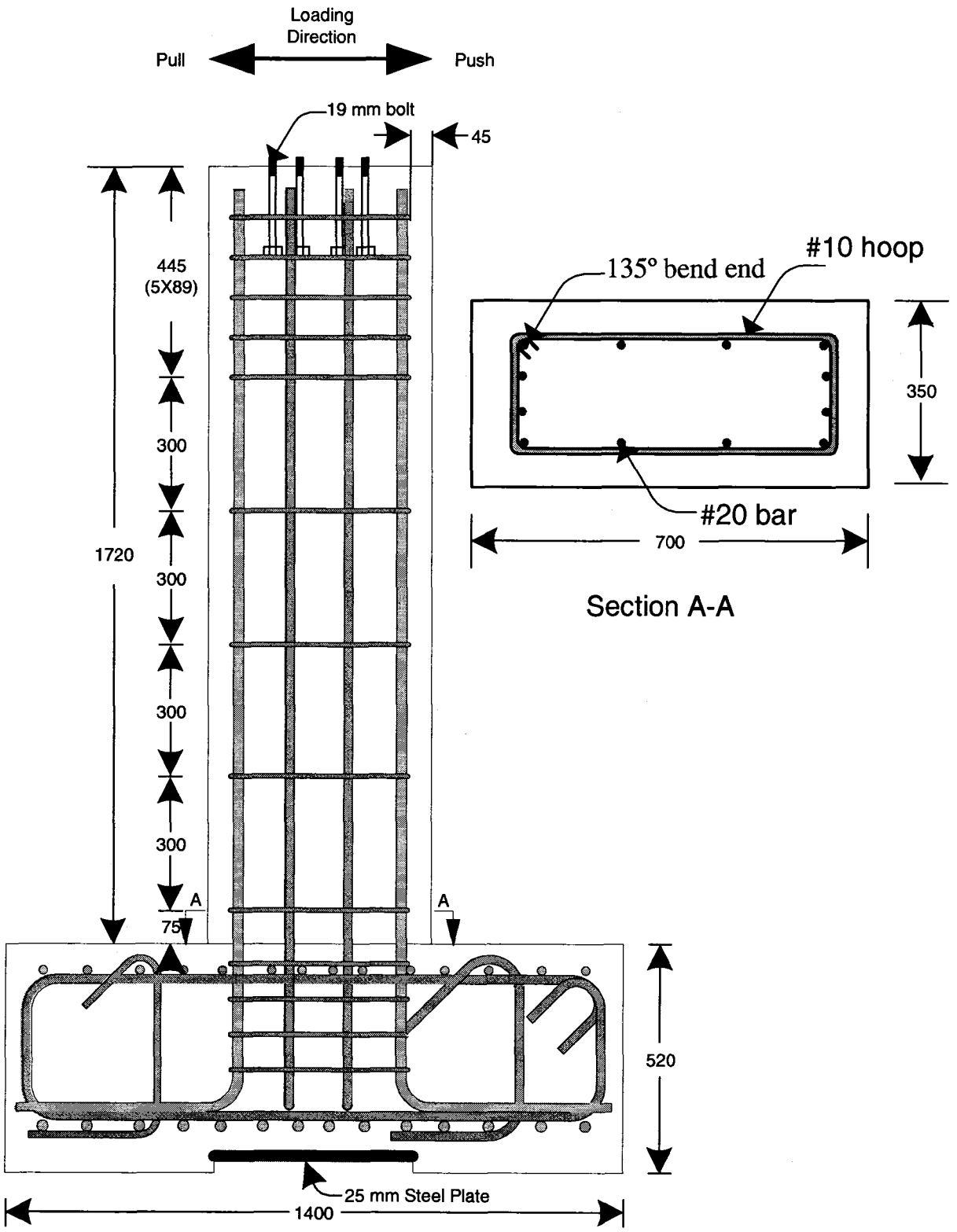

Figure 2.6 Geometry and reinforcement details for Columns LC-C and LC-R

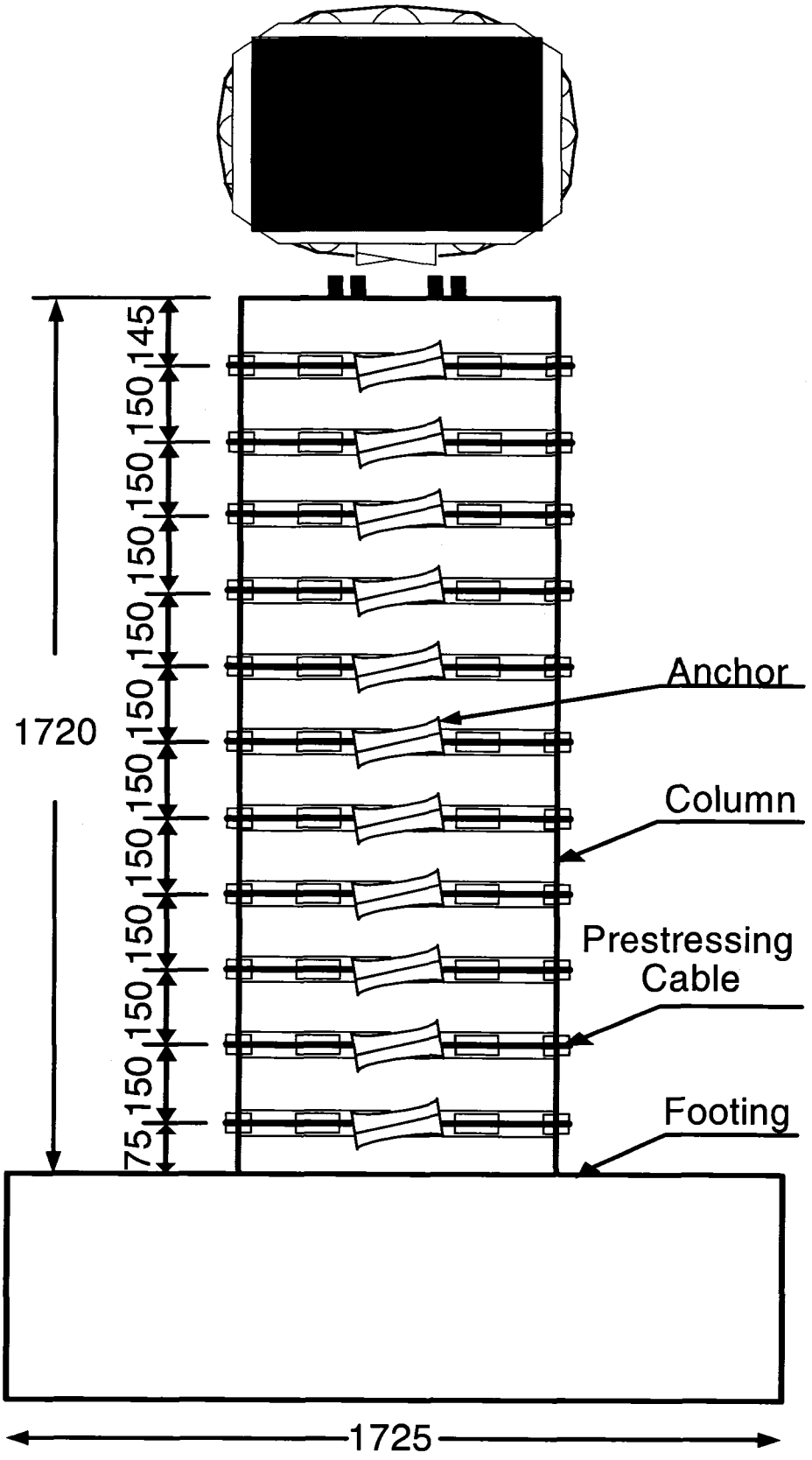

Figure 2.7 Retrofitting details for Column LC-R

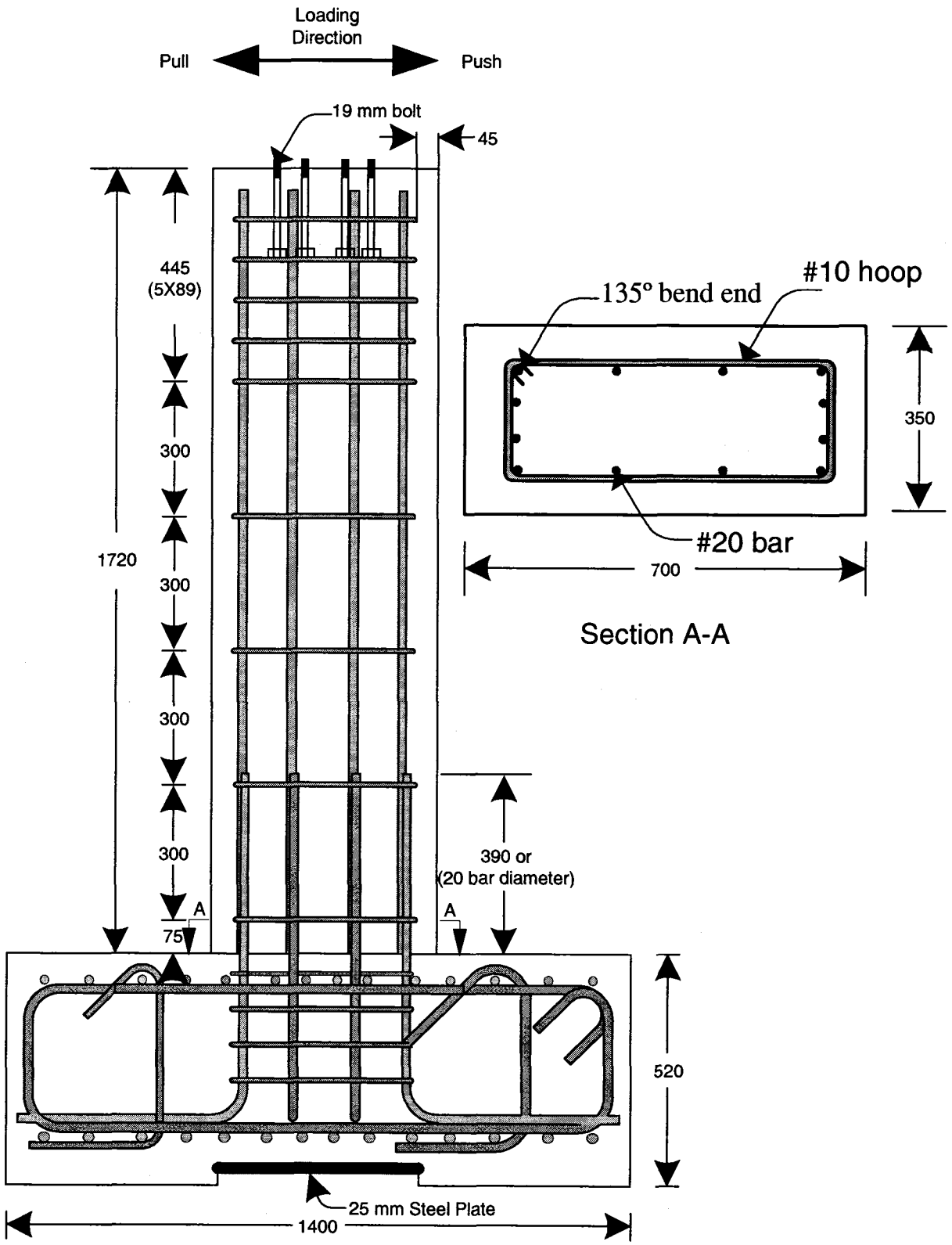

Figure 2.8 Geometry and reinforcement details for Columns LS-C and LS-R

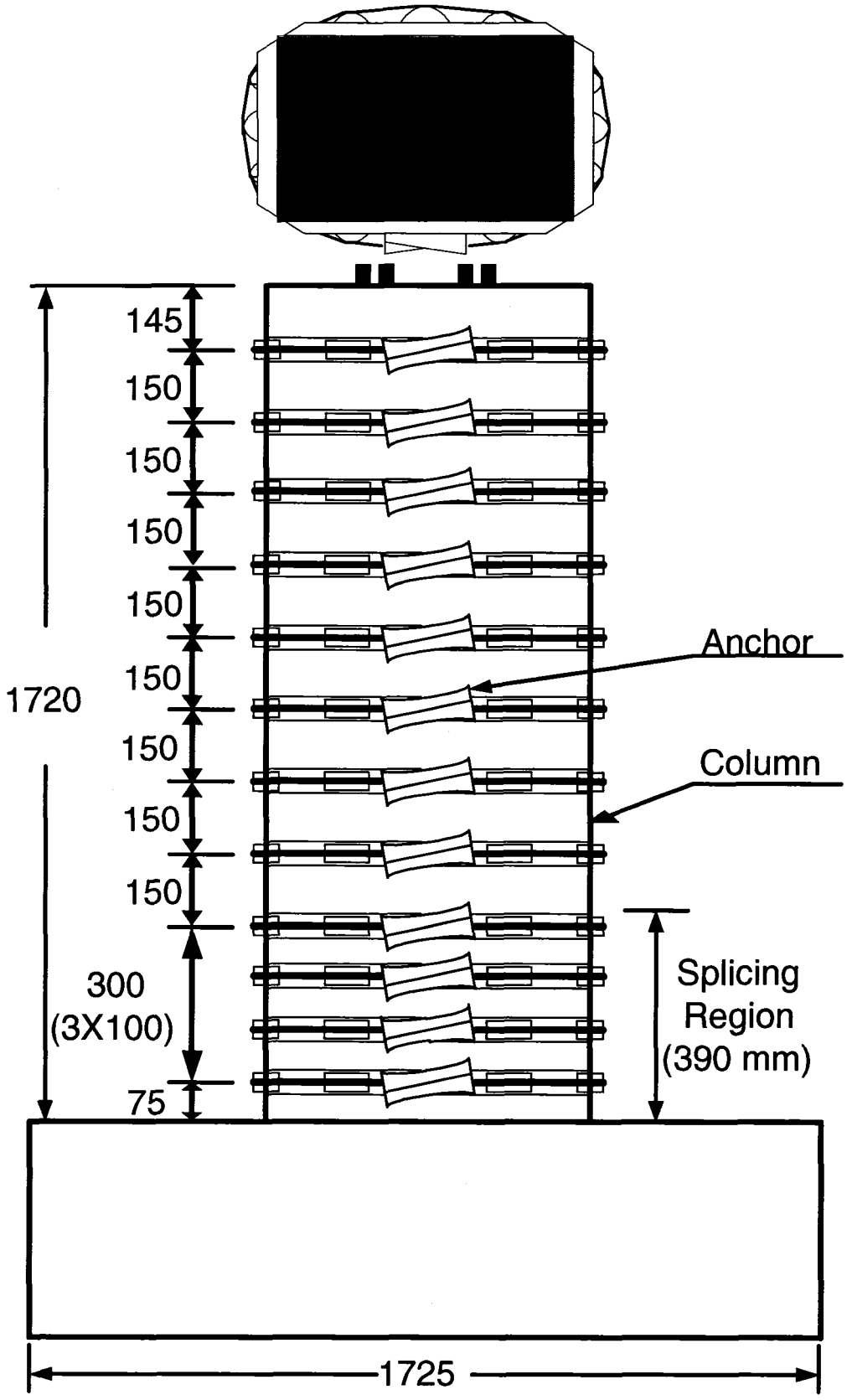

Figure 2.9 Retrofitting details for Column LS-R

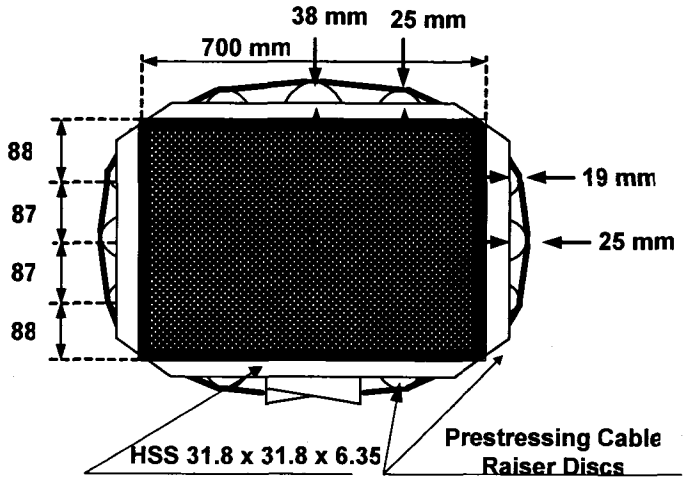

a) Retrofit columns

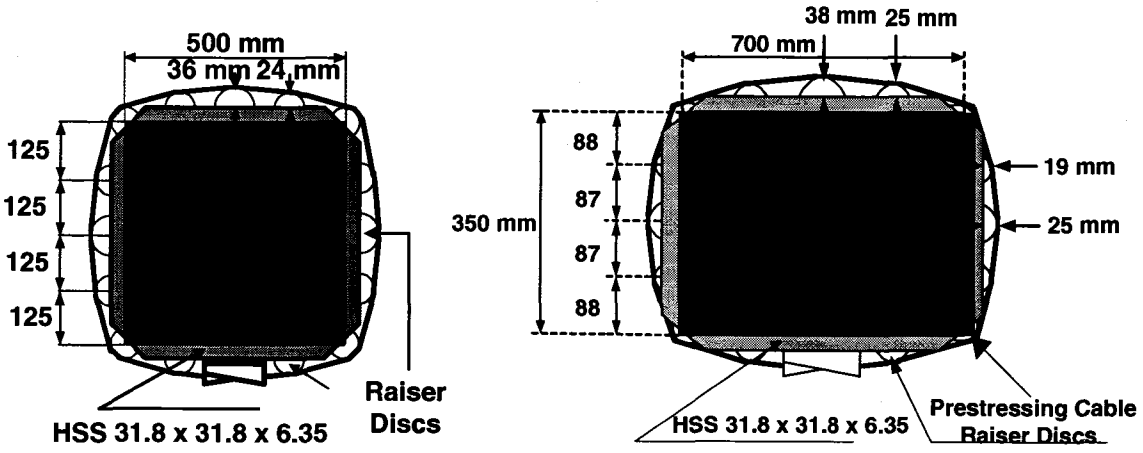

b) Repair columns

Figure 2.10 Details of raiser frames

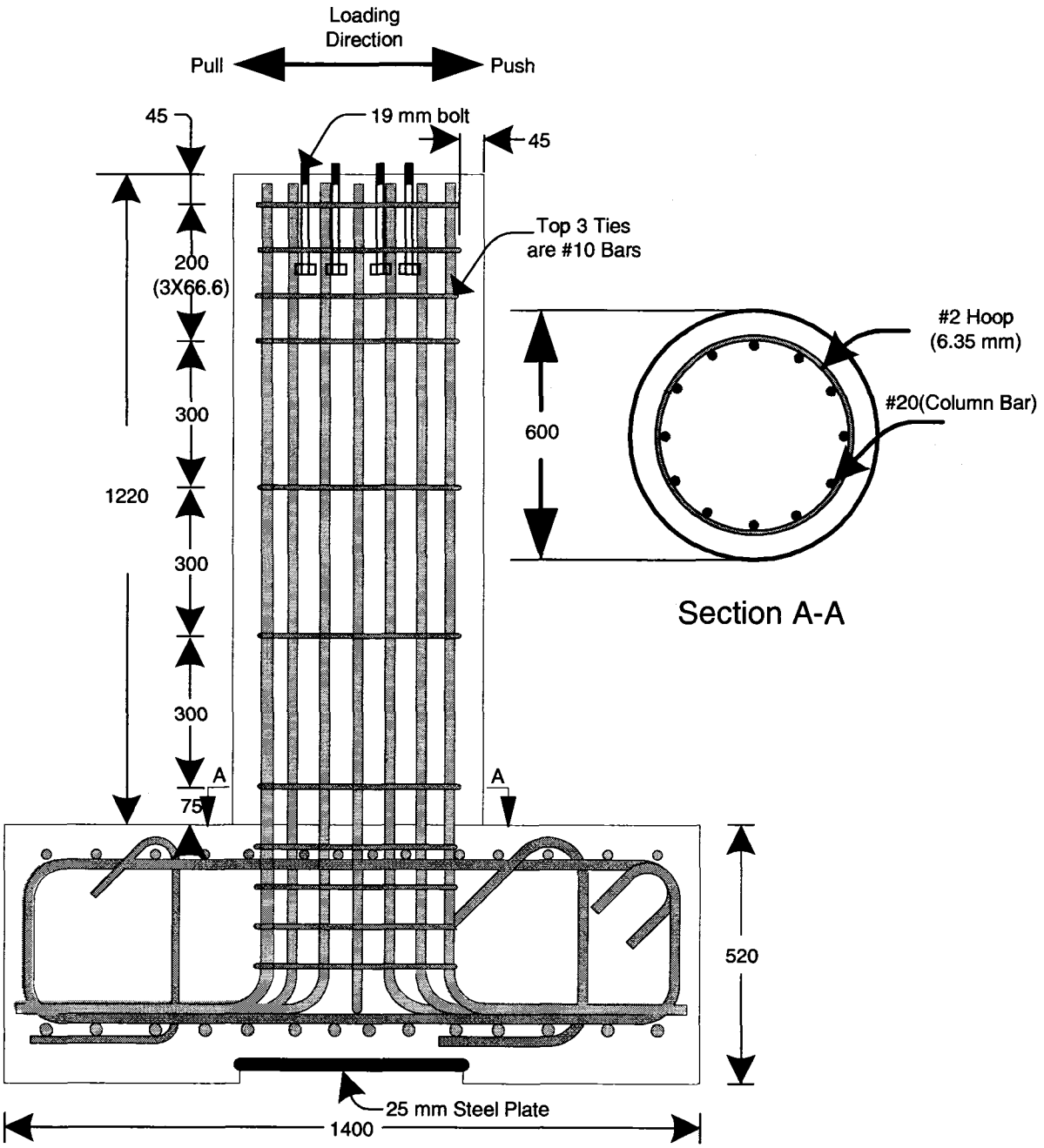

Figure 2.11 Geometry and reinforcement details for Column CR-C

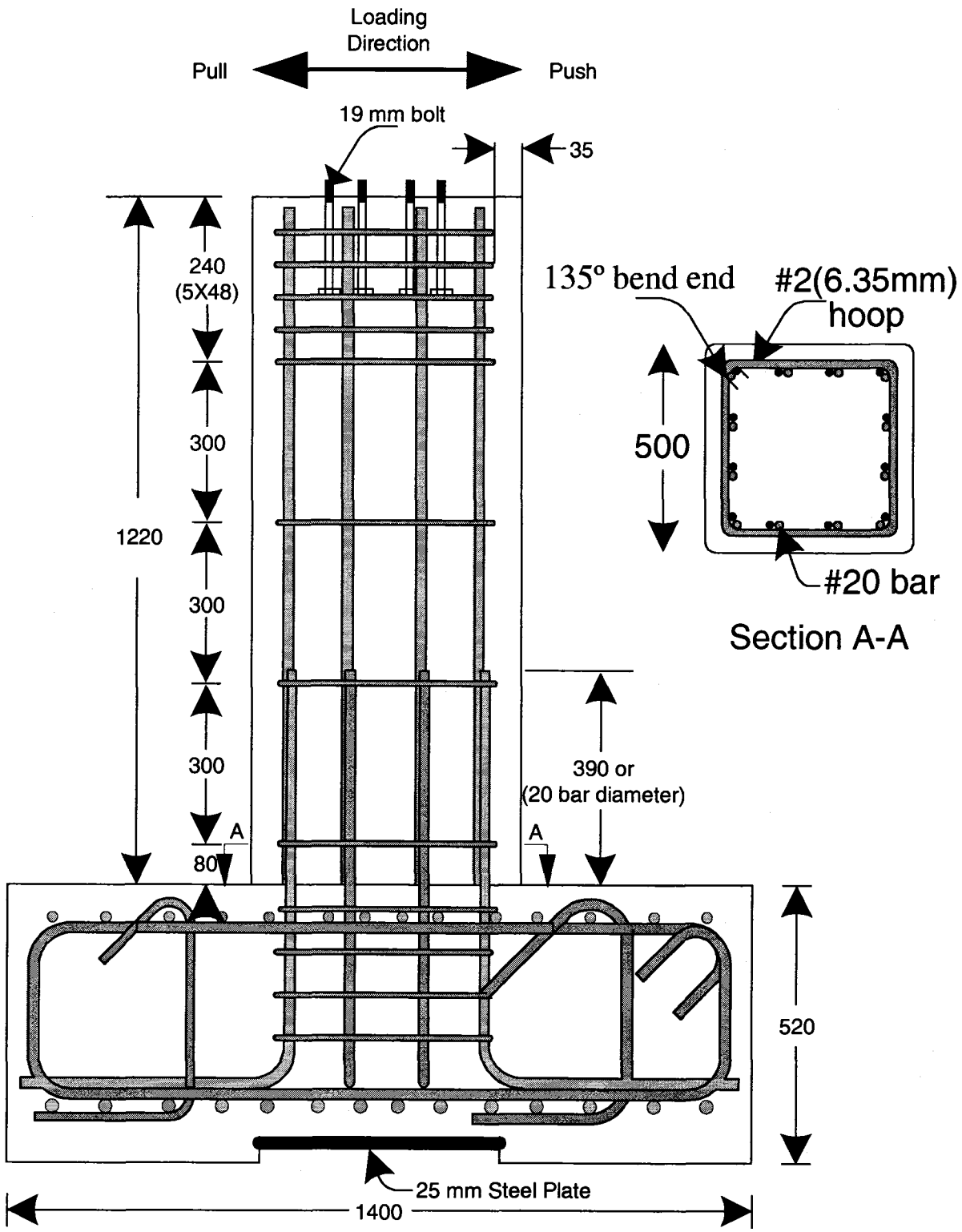

Figure 2.12 Geometry and reinforcement details for Columns SSR-C and SSR-R

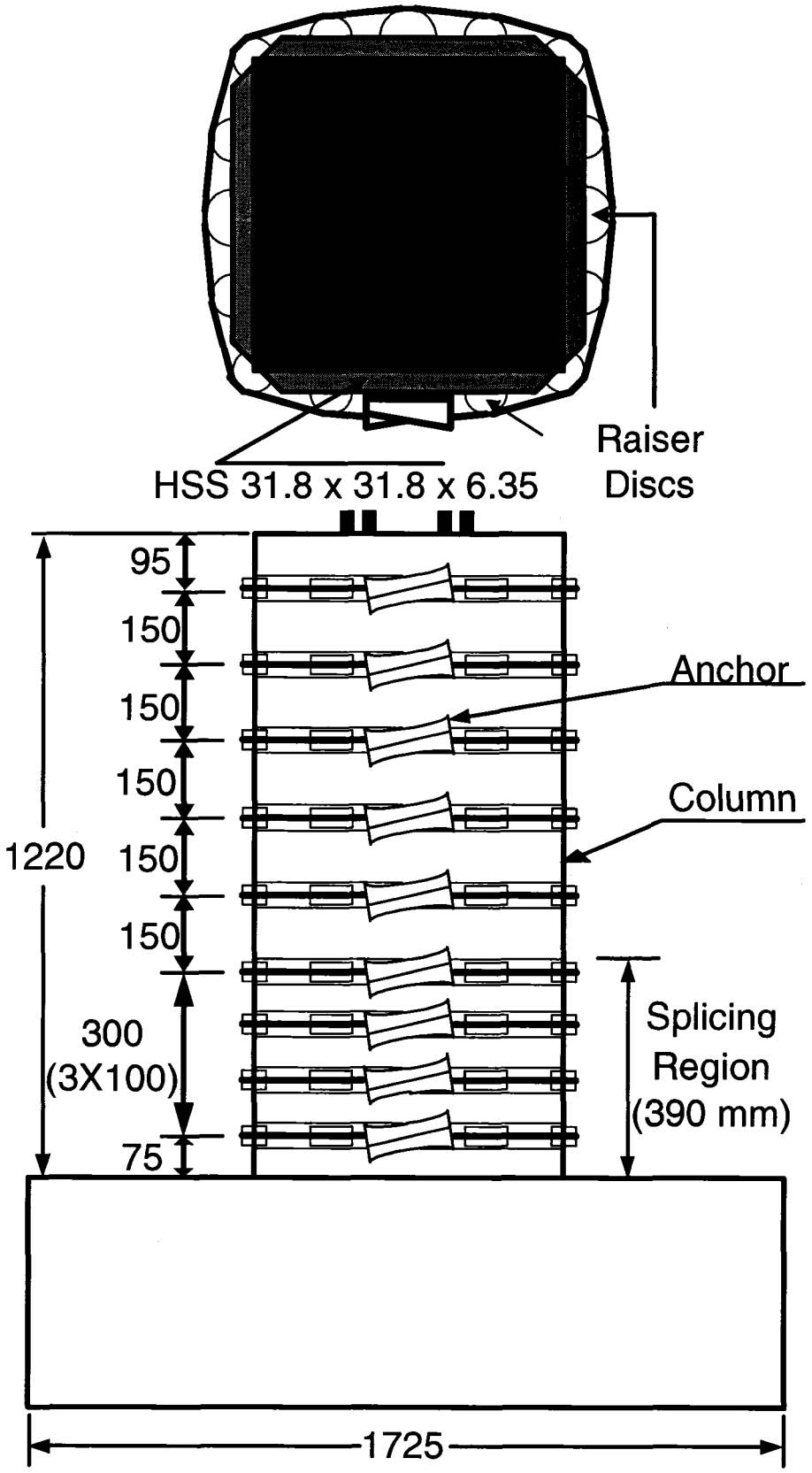

Figure 2.13 Repairing details for Column SSR-R

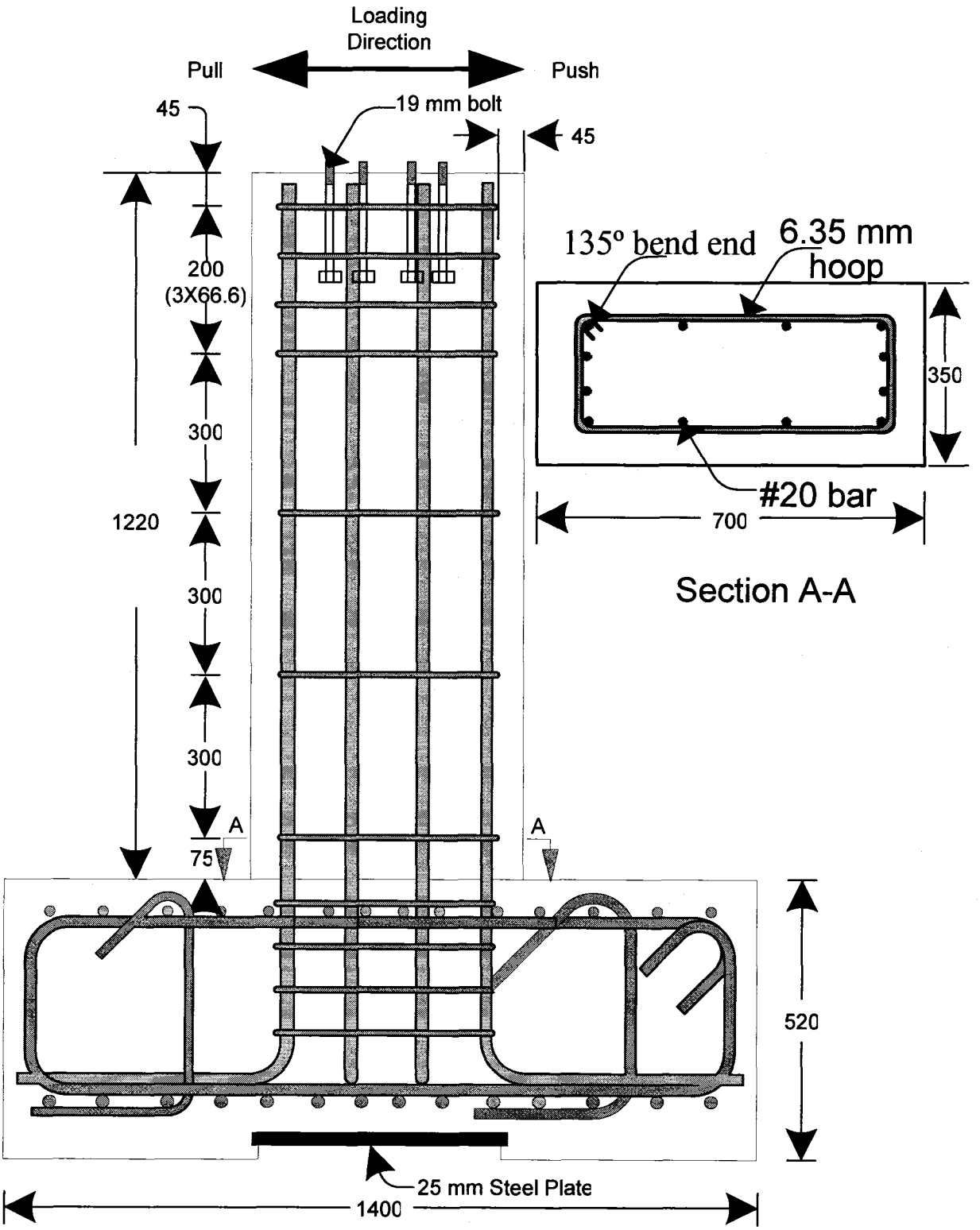

Figure 2.14 Geometry and reinforcement details for Columns RR-C and RR-R

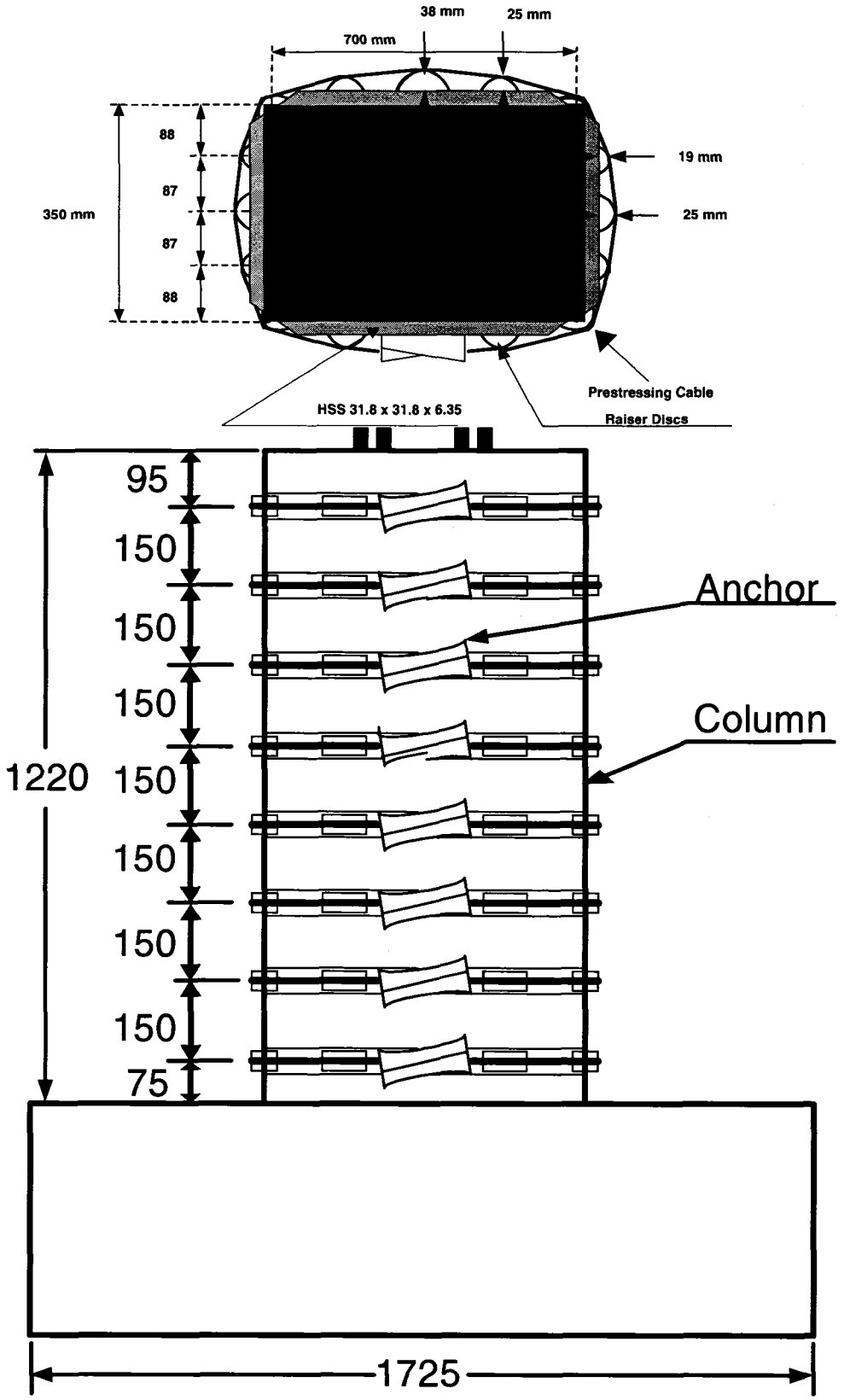

Figure 2.15 Repairing details for Column RR-R

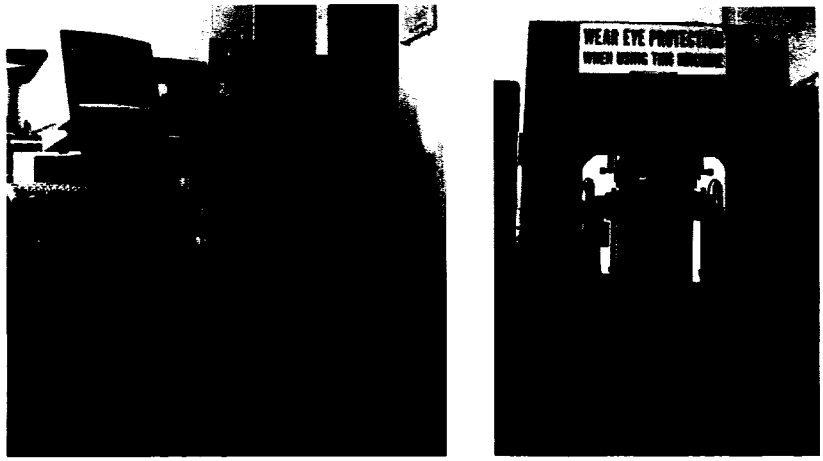

a) Fourney testing machine

b) Before testing

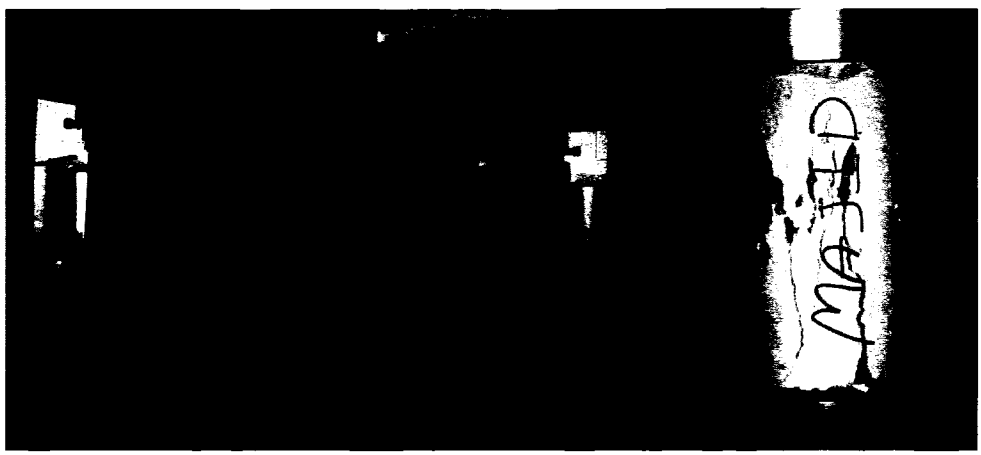

c) After testing

Figure 2.16 Testing of standard concrete cylinders

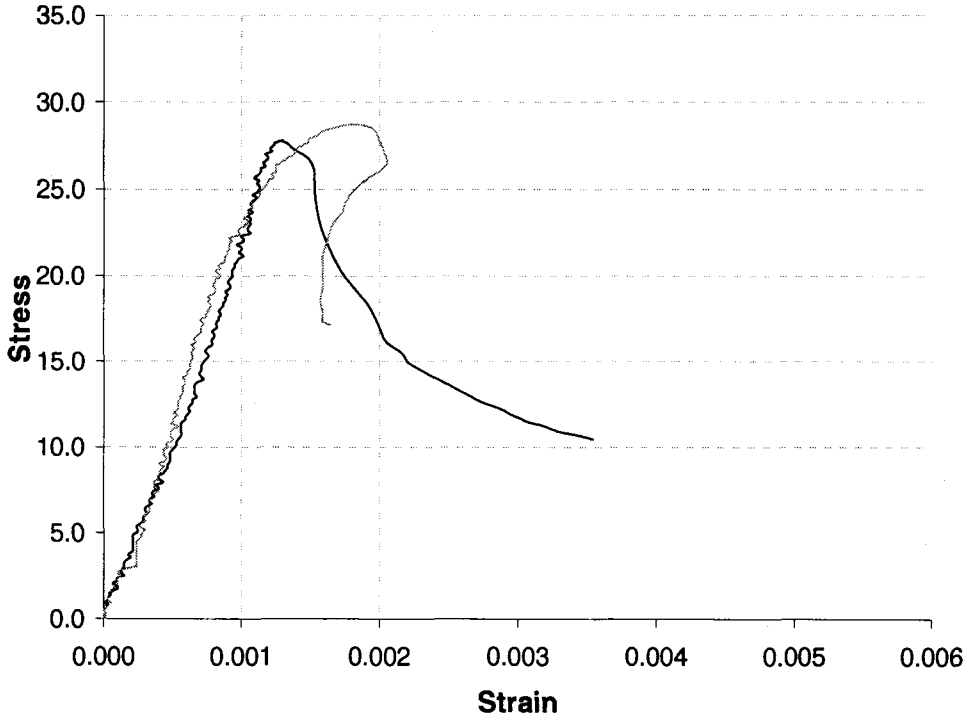

Figure 2.17 Cylinder test results for control columns in the Retrofit Phase (28 days)

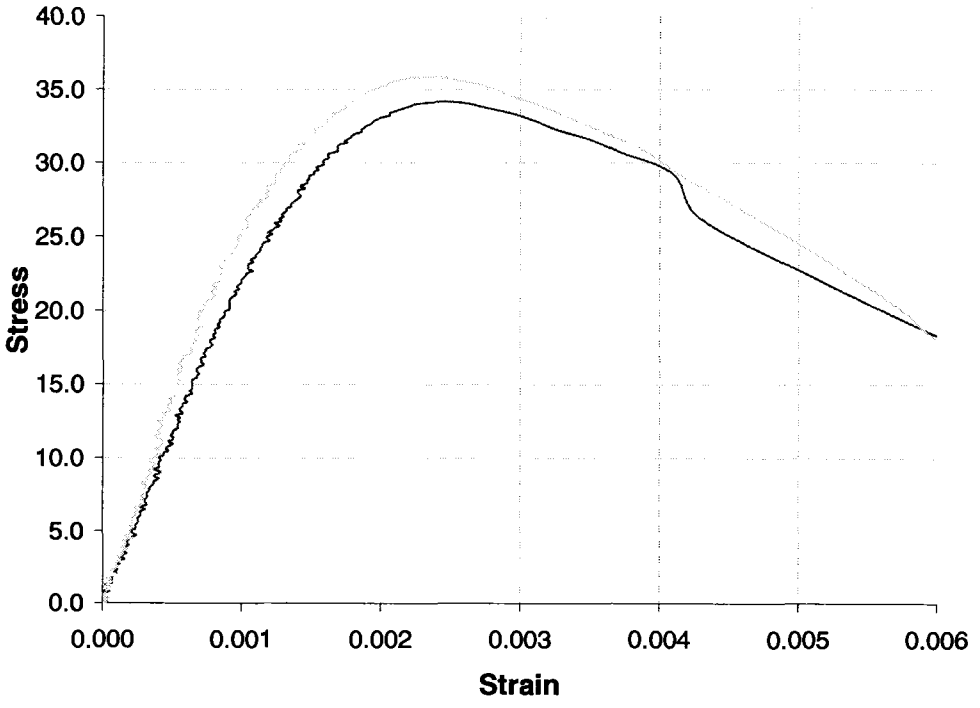

Figure 2.18 Cylinder test results for retrofitted columns (28 days)

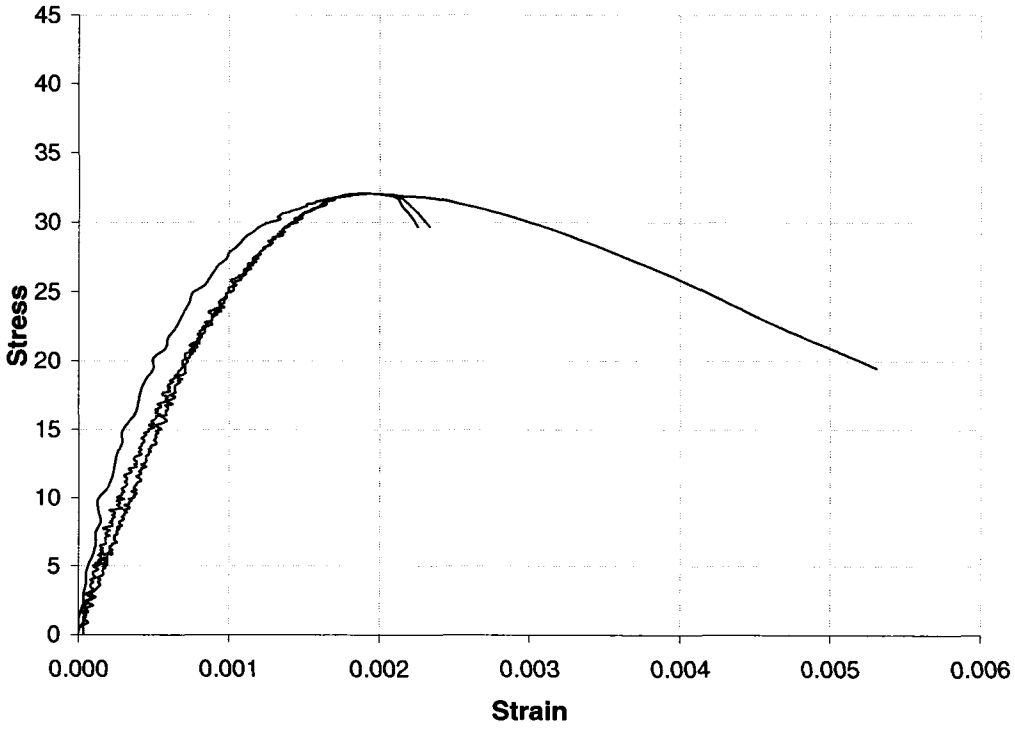

Figure 2.19 Cylinder test results for repaired columns (28 days)

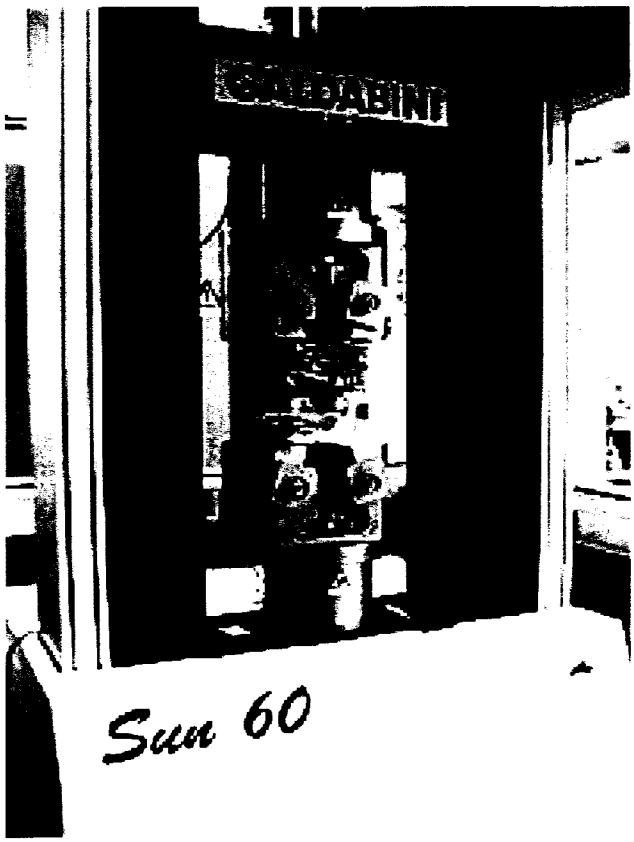

a) Galdabini universal testing machine

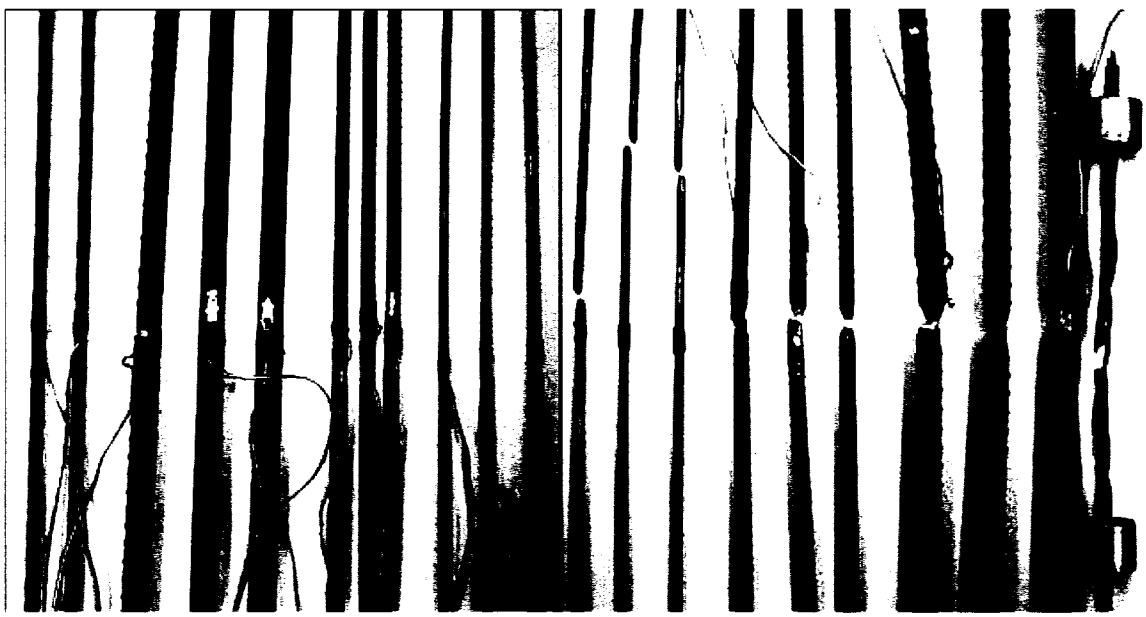

b) Steel coupons prior to testing c) Steel coupons after testing

Figure 2.20 Standard coupon tests for longitudinal and transverse reinforcement

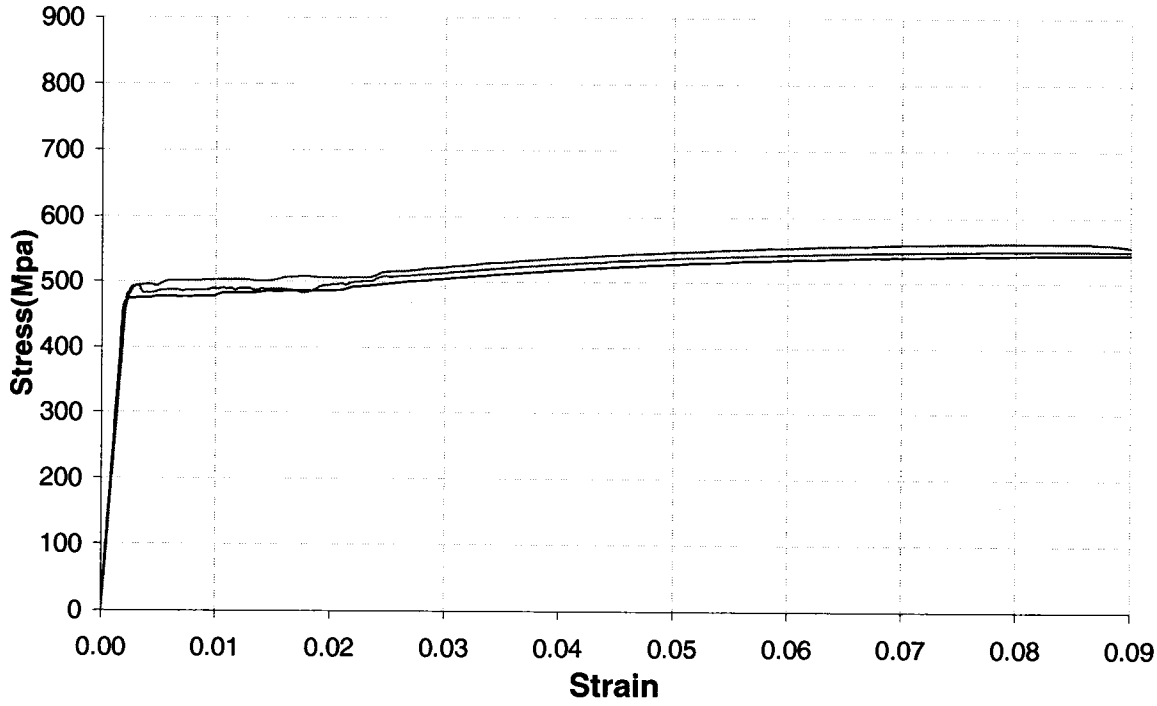

Figure 2.21 Stress-strain relationships for 6.3 mm steel wire

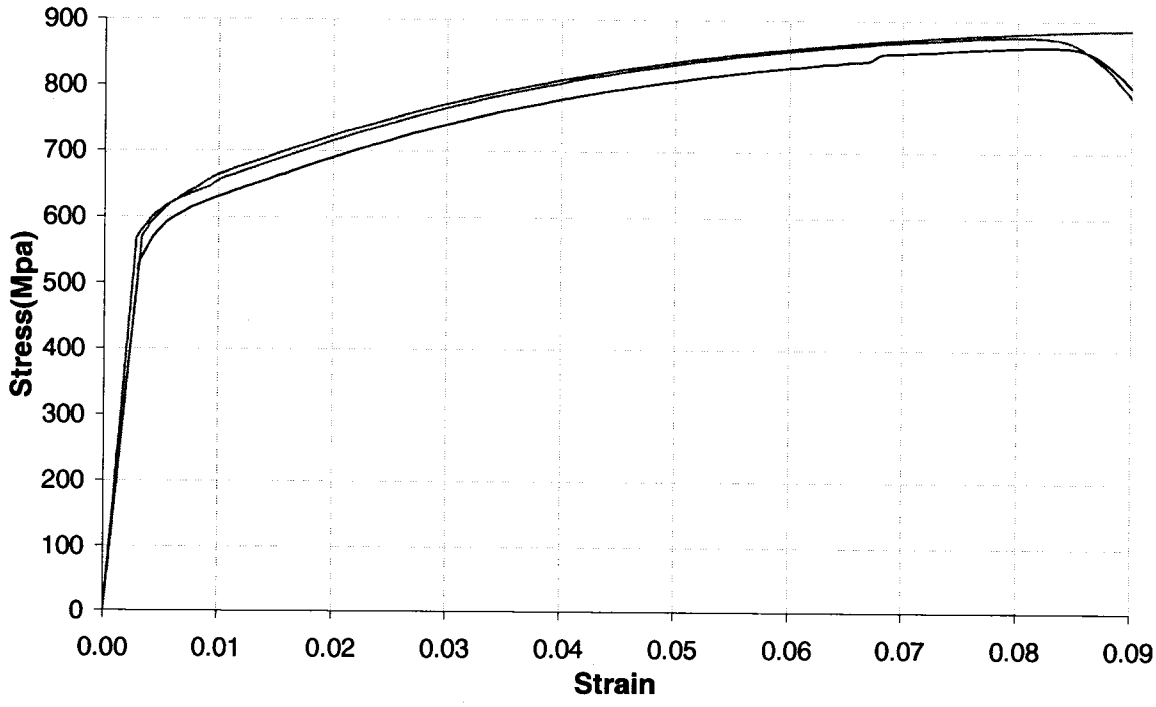

Figure 2.22 Stress-strain relationships for #10 steel ties

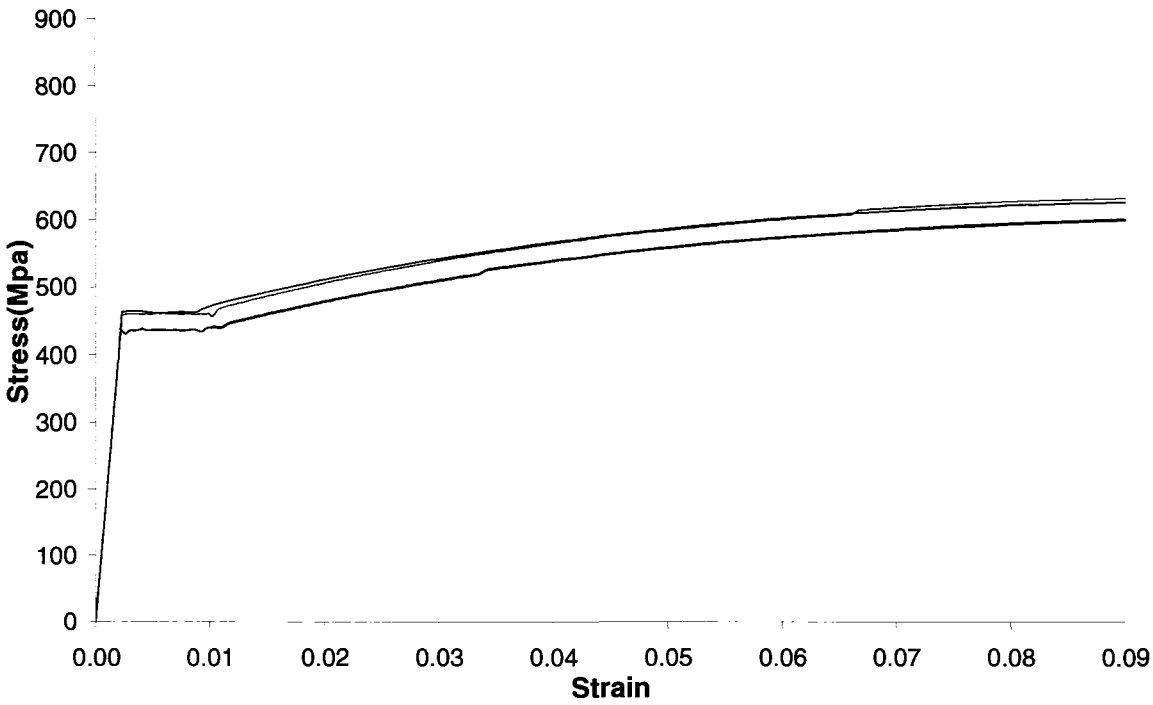

Figure 2.23 Stress-strain relationships for #20 steel rebar

Figure 2.24 Coupon test of size9 seven wire strands; before and after the test

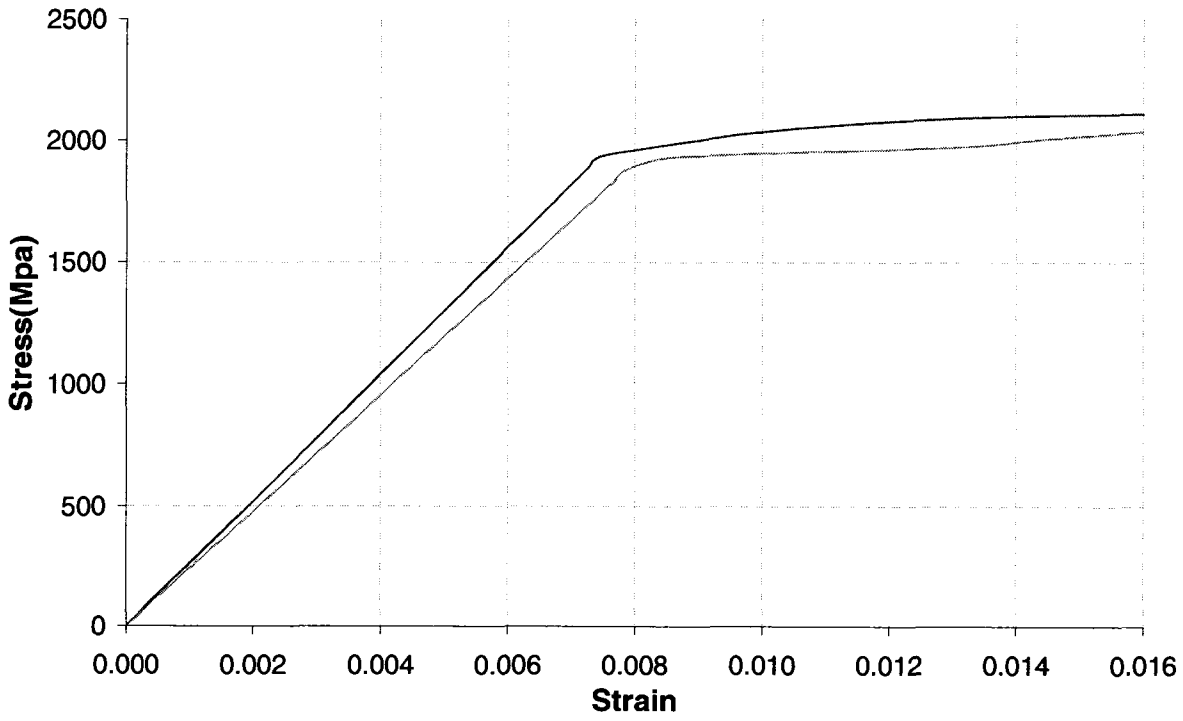

Figure 2.25 Stress-strain relationships of size9 seven wire strands

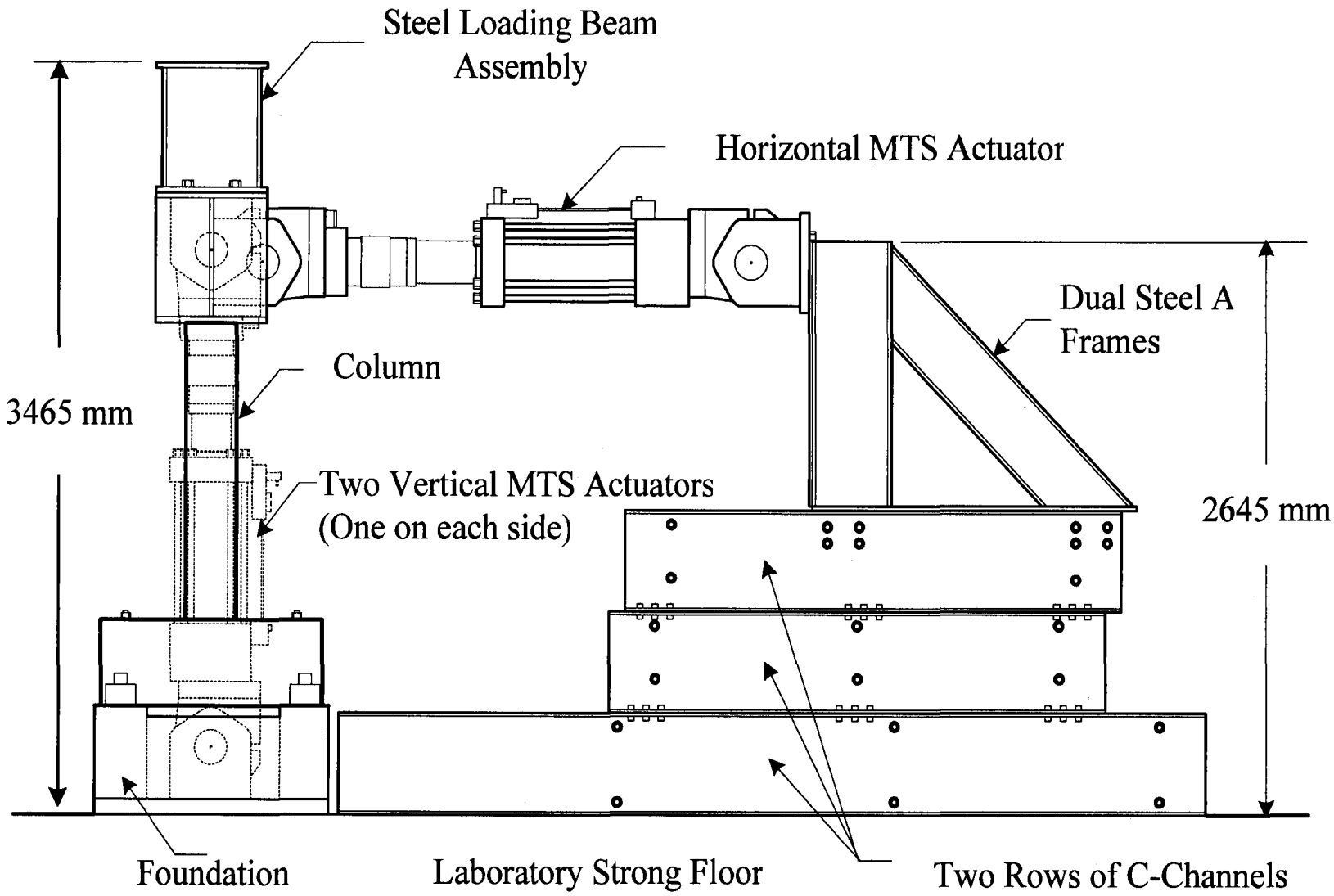

Figure 2.26 Test setup configuration

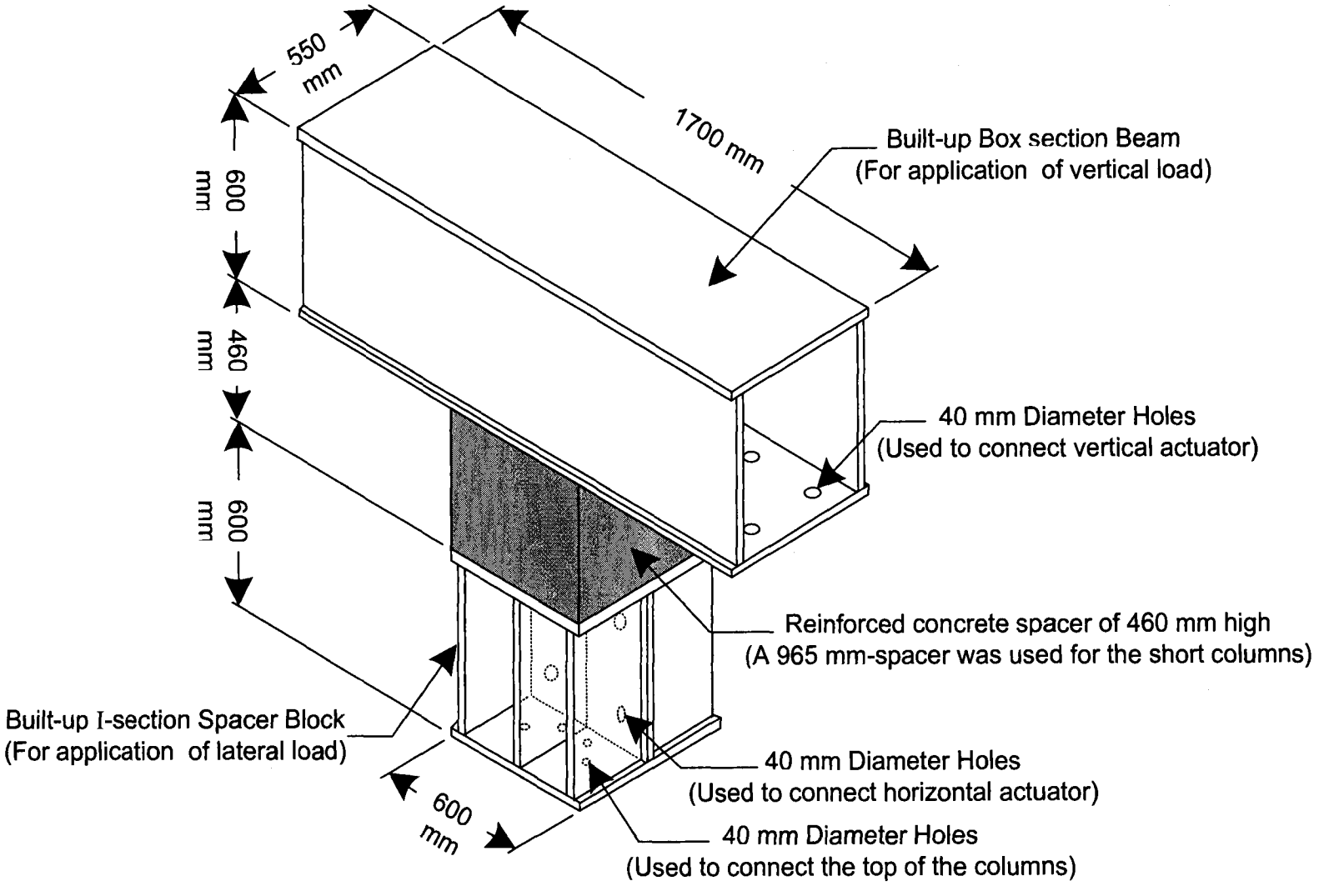

Figure 2.27 Details of loading beam assembly

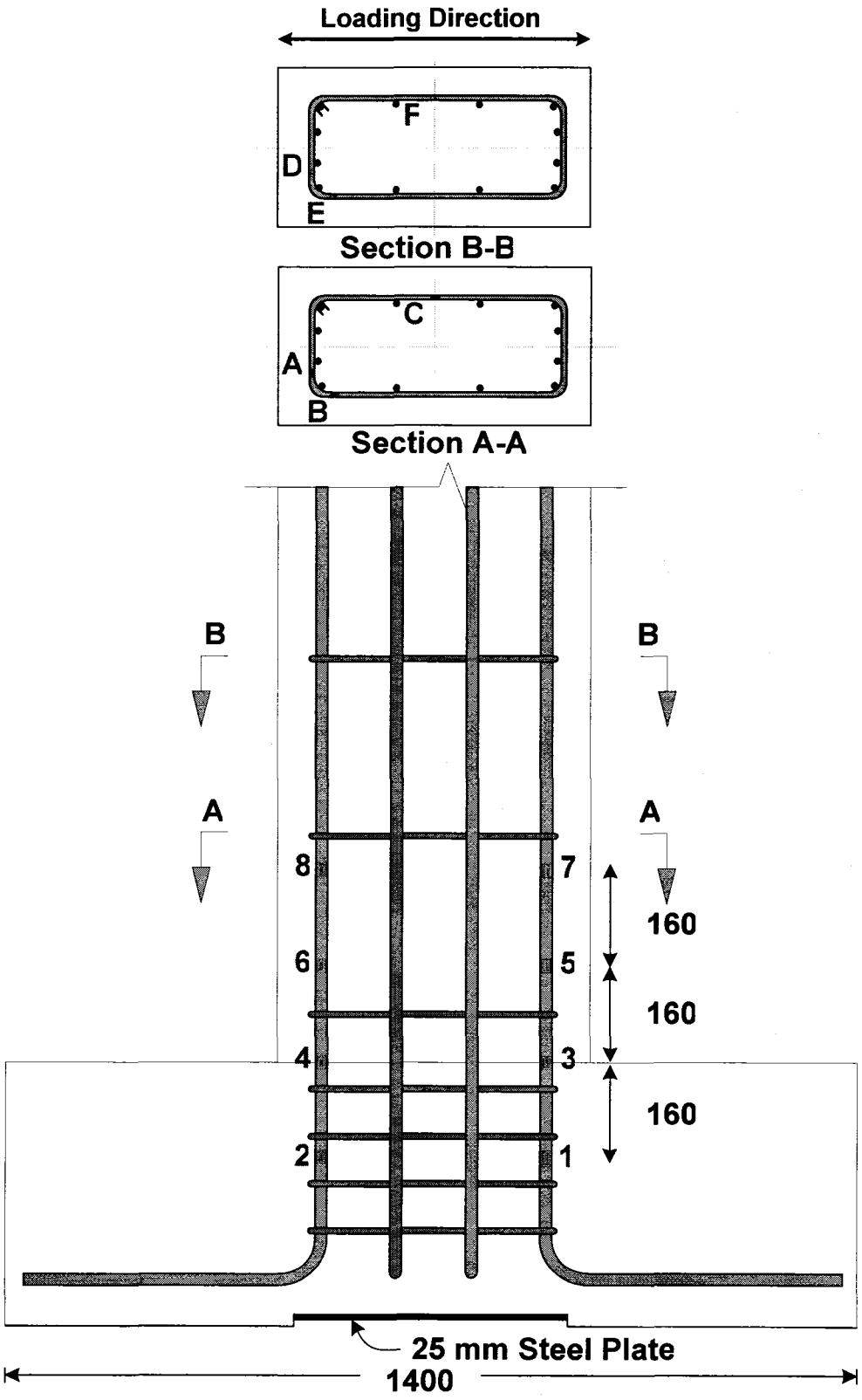

Figure 2.288 Strain gauge location on reinforcing steel for Columns SR-C and SR-R

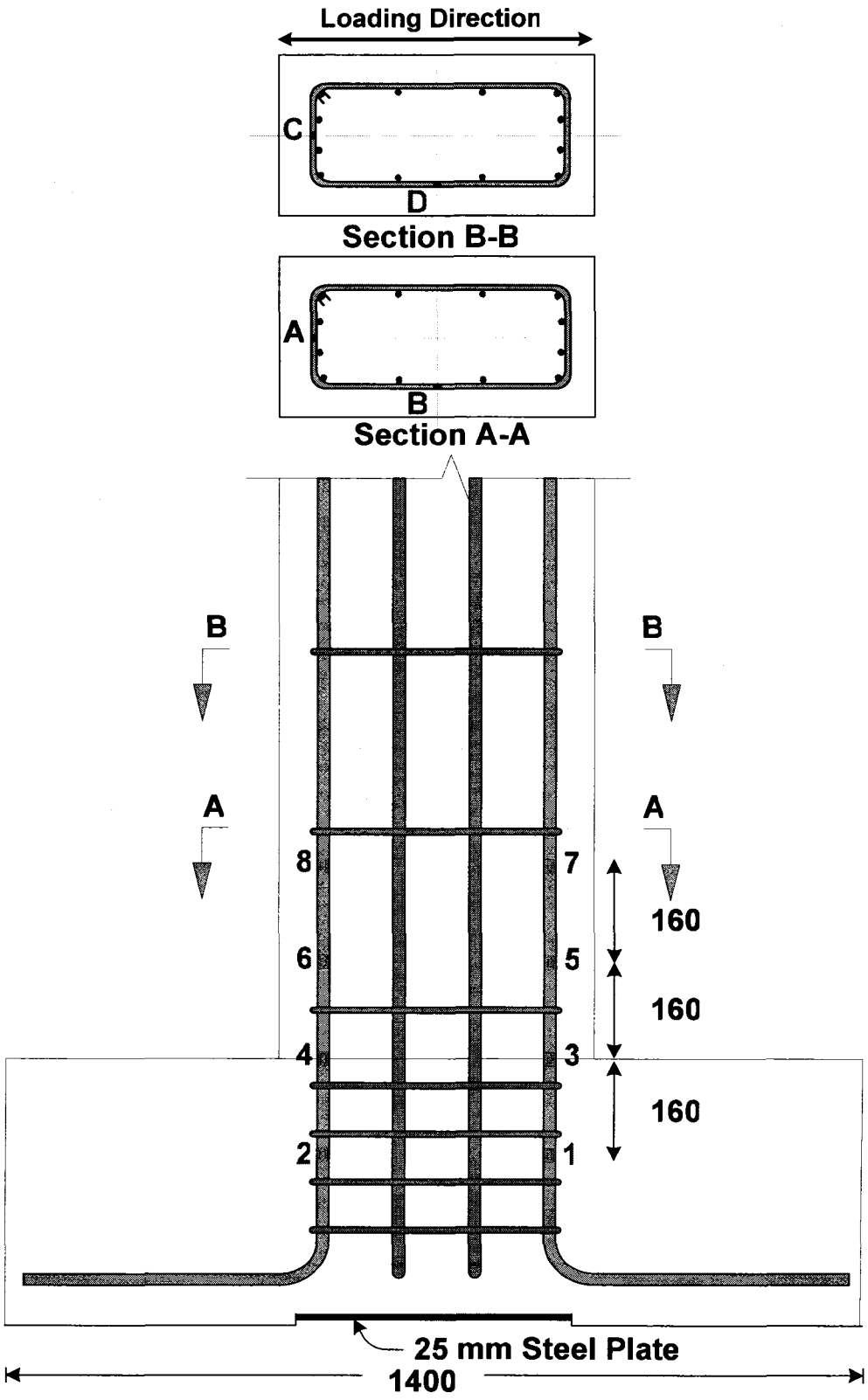

Figure 2.29 Strain gauge location on reinforcing steel for Columns LR-C and LR-R

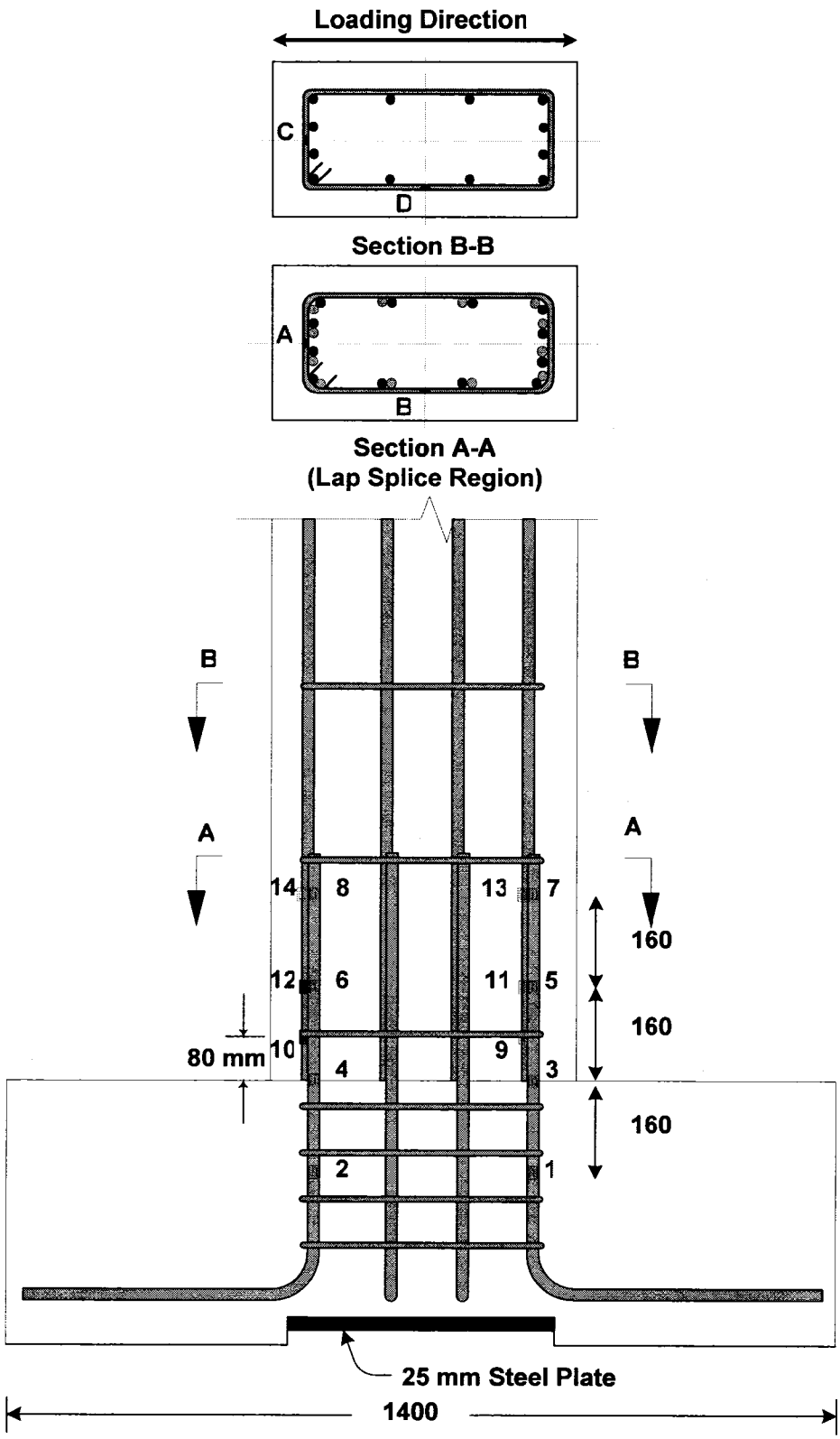

Figure 2.30 Strain gauge location on reinforcing steel for Columns LS-C and LS-R

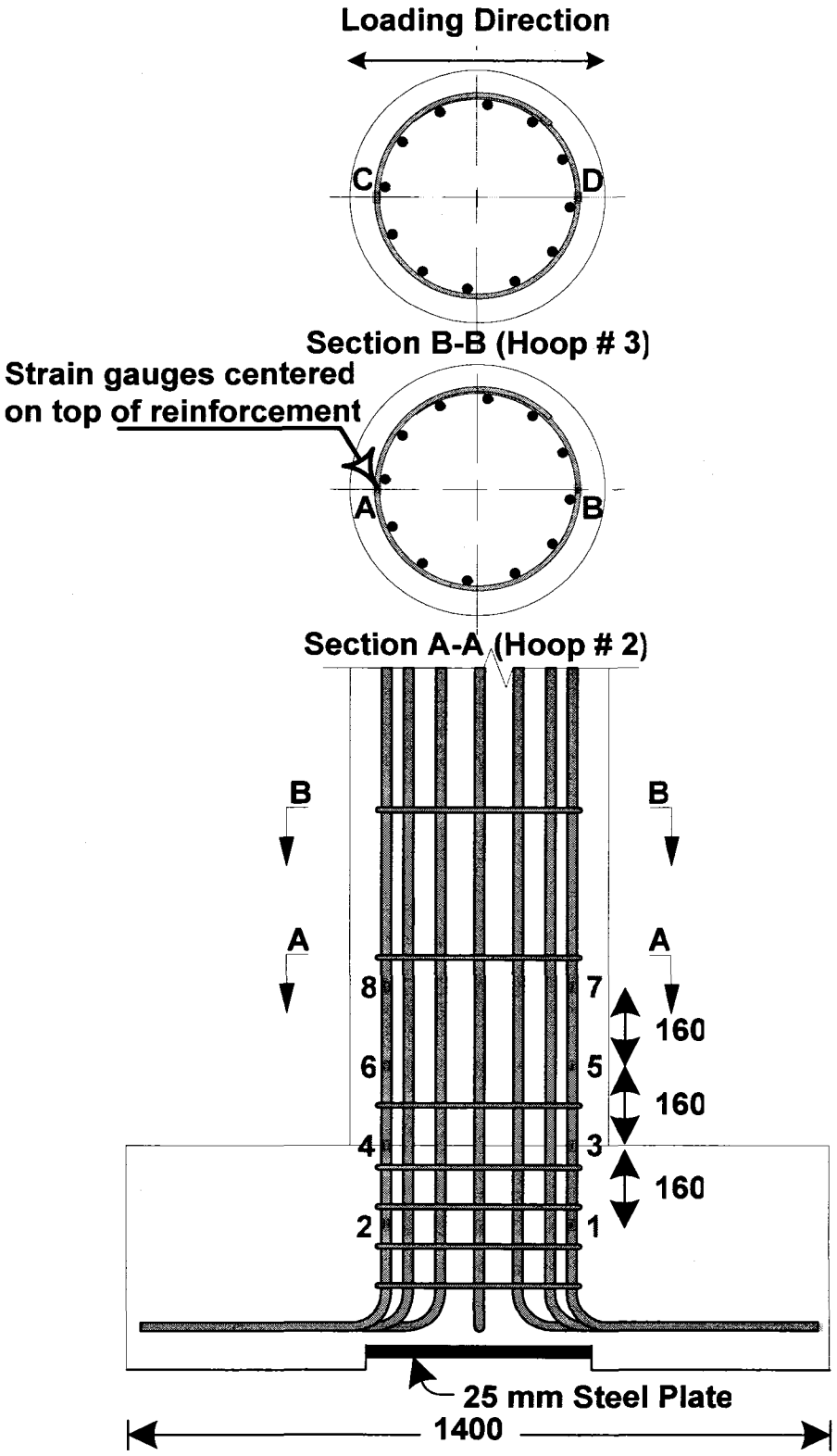

Figure 2.31 Strain gauge location on reinforcing steel for Column CR-C

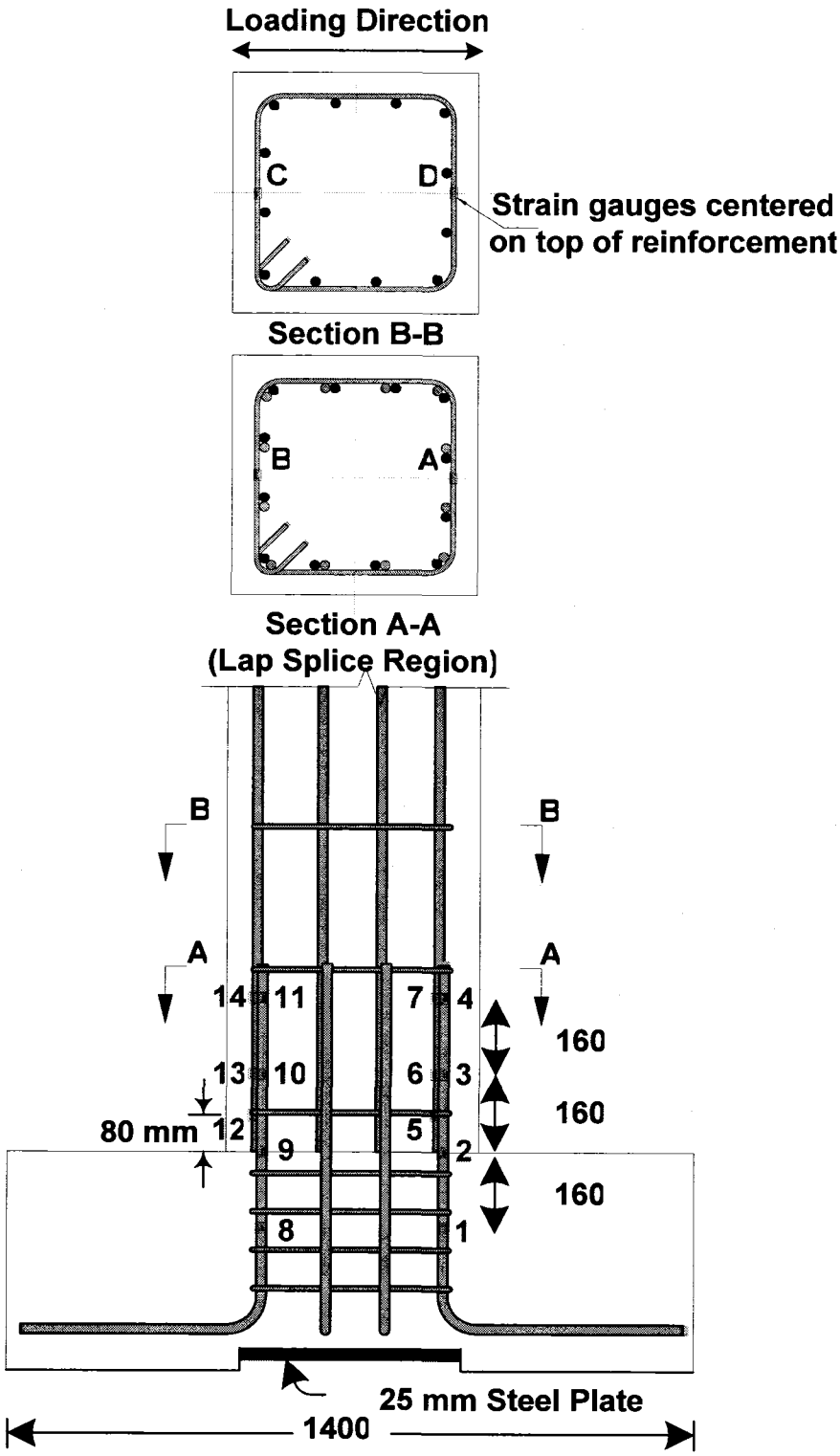

Figure 2.32 Strain gauge location on reinforcing steel for Columns SSR-C and SSR-R

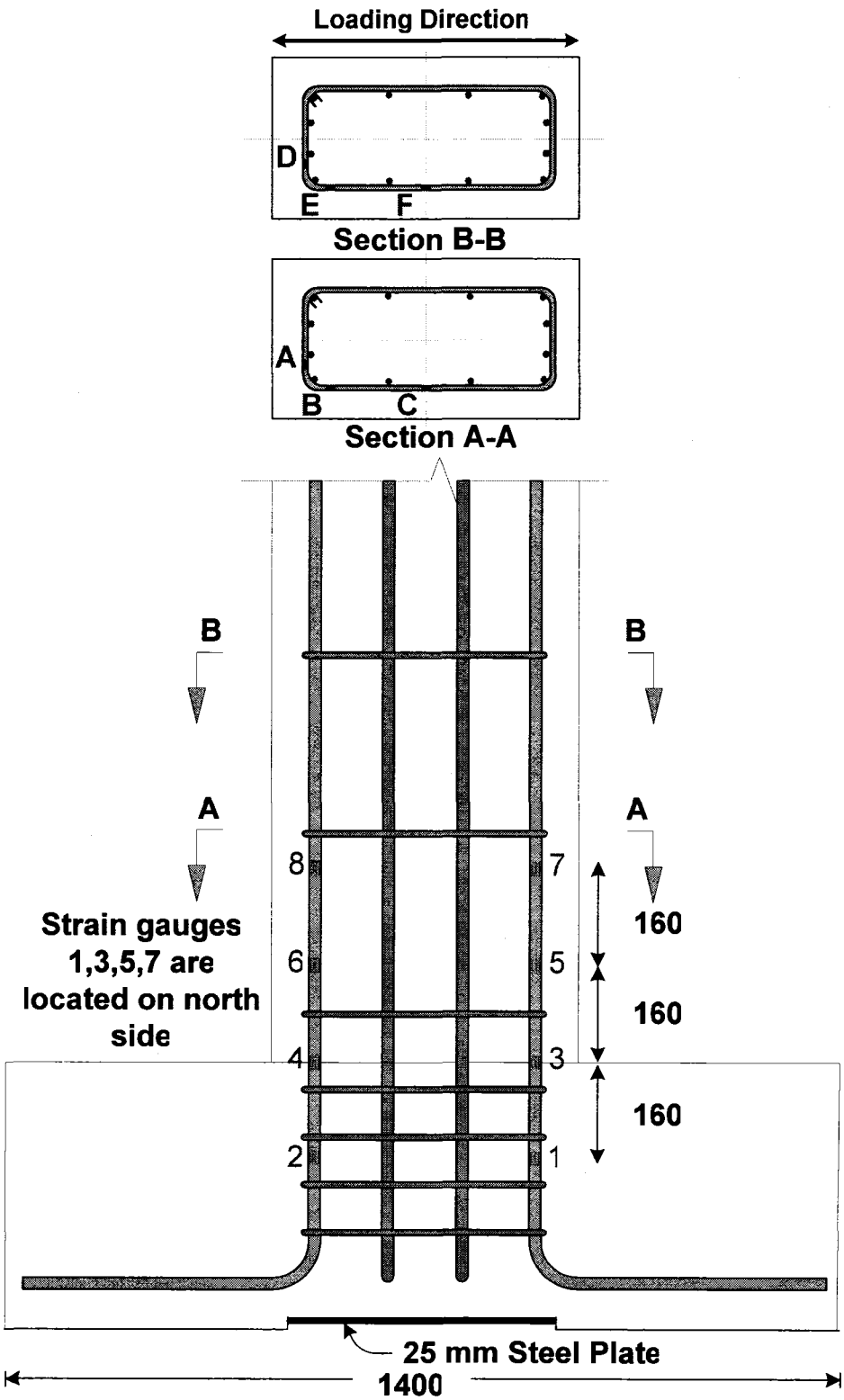

Figure 2.33 Strain gauge location on reinforcing steel for Columns RR-C and RR-R

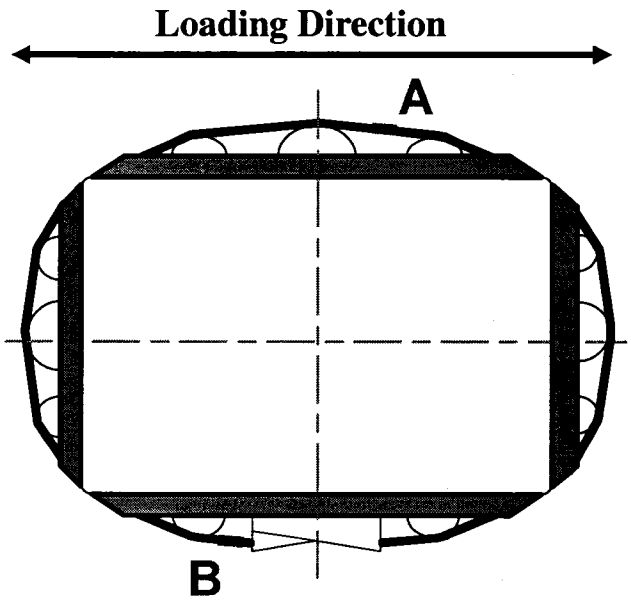

a) Retrofitted columns

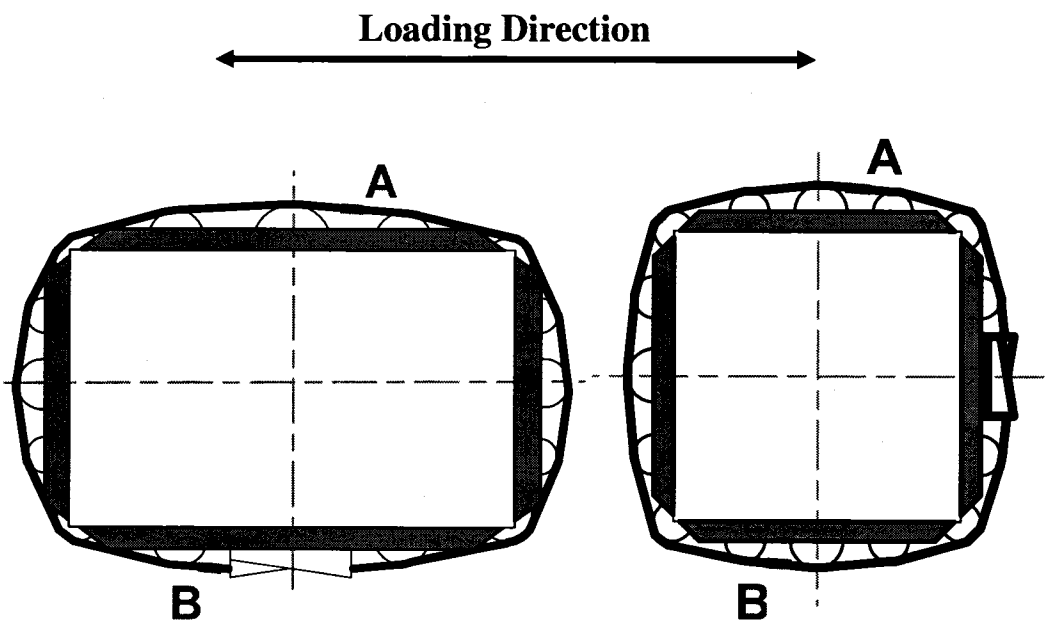

b) Repaired Columns

Figure 2.34 Strain gauge locations on prestressing strands

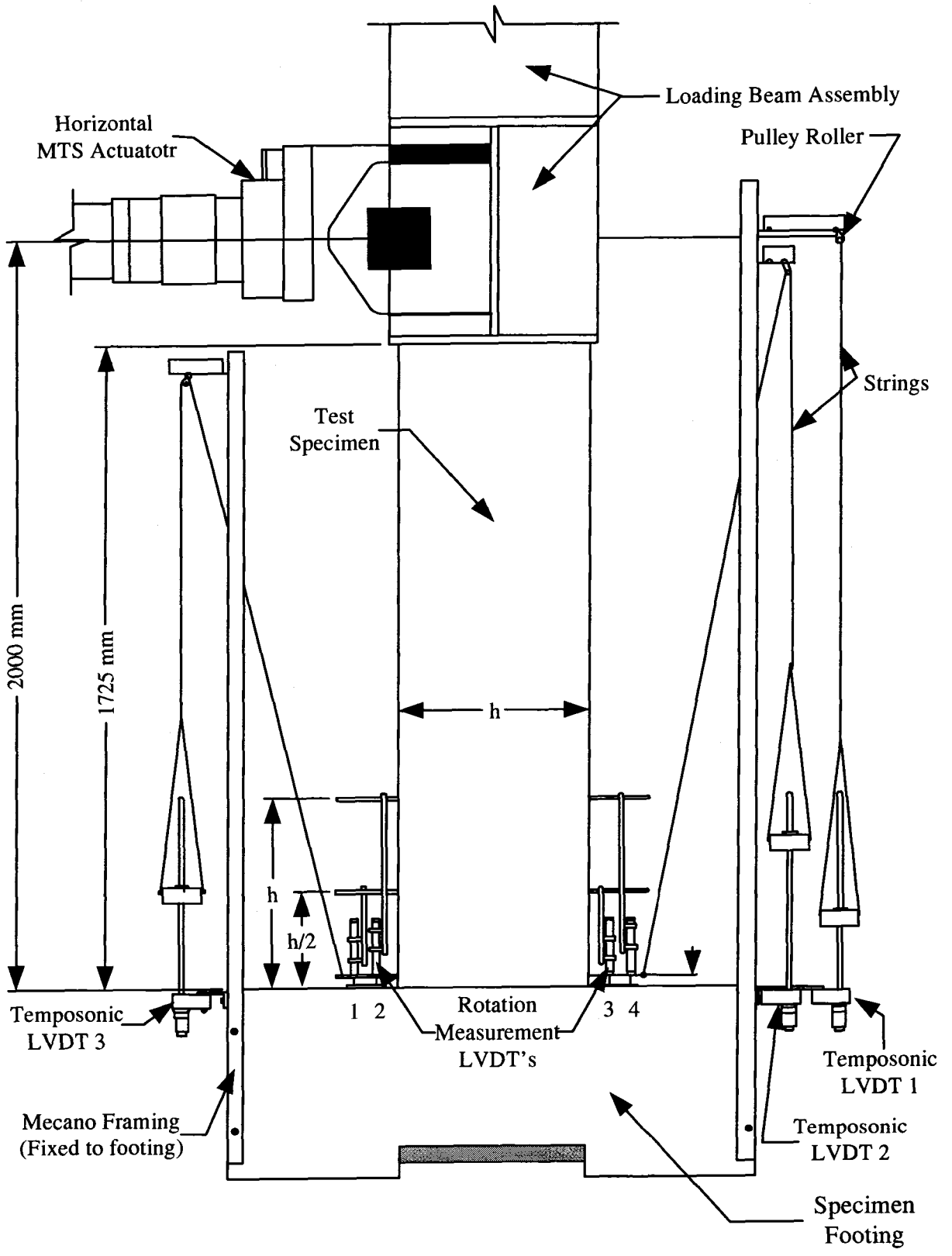

Figure 2.35 Column Instrumentation

Chapter 3

Experimental Results

3.1 General

Observations made and data recorded during column tests are presented and discussed in this Chapter. The observations include overall specimen behaviour, crack patterns and damage to concrete and steel at different stages of loading. The first part of the chapter summarizes the results of column tests conducted to assess the effectiveness of Retro-belt technique for rectangular columns (Retrofit Pahase). The second part includes column tests conducted to investigate the effectiveness of the same technology as a repair technique (Repair Phase). The tests continued until a minimum of 20% drop was recorded in the load carrying capacity. The overall specimen behaviour is presented in the form of force-lateral drift and moment-lateral drift hysteretic relationships, displaying overall strength, stiffness and deformability of columns. These relationships also illustrate the effects of the P-Δ effect.

The failure mechanism and the results obtained from column tests are presented and discussed for each specimen separately. Some of the data could not be recorded reliably

beyond certain stage of loading either due to the damage to the specimen or the stroke limit of the LVDT's. For these cases the data is presented up to the level beyond which the recorded data was questionable. The right-hand side of each hysteretic relationship (positive side of horizontal axis) shows the column behaviour during pushing, generating positive deformations, and the left-hand side shows the behaviour during pulling, generating negative deformations. All the columns were first pushed to a certain desired drift level and then pulled back to the same level in the opposite direction. These cycles were repeated three times at each deformation level and then the drift level was increased to the next level.

3.2 Column Tests for the Verification of Retrofit Methodology

The first three pairs of columns were tested to investigate the applicability of external transverse prestressing to rectangular columns as a seismic retrofit methodology. The three pairs consisted of: I) shear critical, II) flexure critical and III) splice deficient columns. One column in each pair was tested to simulate as-built conditions of existing bridge columns, and the other was retrofitted and tested to investigate the effectiveness of the technology that was being researched.

3.2.1 Short Rectangular Columns

This section presents the performance of two shear dominant rectangular columns, labeled as SR-C and SR-R, where the first specimen represents the as-built conditions without the retrofit and the second column represents a rectangular column retrofitted by transverse prestressing. The shear span-to-depth ratio of the columns was 2.14.

3.2.1.1 Non-Retrofitted Column SR-C

Column SR-C was representative of a typical shear deficient bridge column with No.10 (11.3 mm diameter) ties placed at 300 mm spacing. This was the control column without the retrofit. Figure 3.1 demonstrates the observed behavior at various stages of testing.

The initial loading was applied at 0.5% drift level, during which stage the reinforcement remained elastic. Flexural cracks were observed after the first cycle on the North and South faces of column perpendicular to the direction of lateral loading. These

cracks propagated into the sides, in the form of inclined shear cracks, during the third cycle of 0.5% drift ratio. When the load was increased to 1% lateral drift ratio, the spalling and crushing of cover concrete was observed near the base within the bottom 75 mm segment of column. The previous shear cracks propagated further towards the sides as new diagonal cracks formed. The strains recorded in the first two hoops and longitudinal bars showed that they yielded (exceeded 0.2% or 2000 $\mu\varepsilon$) at the first cycle of 1% drift ratio. The strain gauge data is presented in Appendix A. Figures A.1 and A.2 illustrate the strains in longitudinal and transverse reinforcement, respectively.

The column reached its peak resistance during the first cycle of 1.5% drift ratio, and further cycling resulted in gradual strength decay. Moment resistance in the direction of first load excursion (loading towards North) dropped by approximately 25% at the end of the third cycle. This level of strength drop was considered to be significant enough to label the drift capacity to be 1.0 %, since the column could not sustain three cycles at 1.5% drift level without experiencing less than 20% strength decay (the failure criterion used). During subsequent deformation cycles, the diagonal cracks as well as flexural cracks within the lower 350 mm segment widened. The crack at the column-footing interface also widened as yield penetration occurred into the footing and the longitudinal bars continued extending within the footing.

The experimentally recorded force-lateral drift and moment-lateral drift hysteretic relationships are shown in Figure 3.2. The force and moment values plotted were computed from recorded horizontal forces and the horizontal and vertical components of axial load including the P-Δ effects. It is clear from the hysteretic relationship shown in Figure 3.2 that the column experienced severe strength degradation immediately after the cycles at 1% lateral drift. The moment resistance dropped below 50% of the maximum recorded value when cycled at 2% drift level, and the test was terminated. The hysteresis loops show some pinching signifying shear dominant response. This failure was triggered by insufficient transverse reinforcement against diagonal tension.

The rotation of the hinging region at h (700mm) and h/2 (350mm) distances above the column base, and the anchorage slip rotation at the column footing interface were recorded by means of 4 LVDT's and two temposonic LVDT's and are shown in Figures 3.3 and 3.4. The graphs in Figure 3.3 illustrate that much of the rotation was caused by flexure

within the first 350 mm segment. The difference between total rotation of the hinging region relative to the footing and the anchorage slip rotation gave the amount of rotation caused by flexure alone.

3.2.1.2 Retrofitted Column SR-R

Column SR-R was the companion column to SR-C, with identical geometric and material properties. However, this column was retrofitted by external prestressing as explained earlier. The same loading scheme was used for testing the column.

The first flexural hairline crack was observed during 0.5% drift cycles. The number of flexural cracks increased during subsequent cycles at 1% drift. A crack was observed at the column-footing interface on the south side during the third cycle at 1% drift ratio. The first set of shear cracks was observed on both side faces during the 2nd cycle of 1.5% drift ratio when the lateral force was at 590 kN. The first cycle at 2% drift resulted in additional hairline flexural cracks on the north and south faces. The crack at the column-footing interface widened and became longer during the 2nd cycle at 2% drift ratio. Some crushing of cover concrete was observed near the base during the third cycle of the same deformation level. Increased diagonal shear cracks were observed during 3% drift cycles with widening of one of the cracks. However the crack was well under control due to the external prestressing. The column maintained its strength until 4% lateral drift ratio and experienced some strength decay beyond this level.

The strain data is presented in Appendix A. There was no yielding in the first two hoops that were instrumented, while the longitudinal reinforcement started yielding at 0.5% drift ratio, as demonstrated in Figures.A.3(c) and(f). Figure A.3 illustrates the longitudinal reinforcement strains for column SR-R.

Figure 3.5 illustrates the column behavior with photographs taken during various stages of loading. It also shows the column at the end of 3% drift cycles with virtually no damage. The hysteretic force and moment-lateral drift relationships are plotted in Figure 3.6 showing stable loops until after 4% lateral drift ratio.

Total rotations of the column critical region were measured at 350 mm (h/2) and 700 mm (h) form the column footing interface. The hysteretic relationships of measured rotations are shown in Figure 3.7. The comparison of data indicates that a large portion of flexural

rotations took place within the bottom 350 mm segment. It should be noted that the rotation data recorded at "h" location is only valid up to 3% drift ratio, since the stroke limit of one of the LVDT's was exceeded beyond this level. The anchorage slip rotation was also measured and is plotted in Figure 3.8.

The strains in prestressing strands were measured along the height. The data recorded throughout the test is presented in Figure A.5 of Appendix A. All of the strands were initially prestressed up to 25% f_{pu} (or up to the strain level of approximately 1900 $\mu\varepsilon$). The increase in strains during testing is attributed to the shear stress resisted by each strand in controlling diagonal tension cracks.

3.2.1.3 Comparison of Columns SR-C and SR-R

When the moment-deformation hysteretic relationships of Columns SR-C and SR-R are compared, it can be seen that the retrofitted column (SR-R) was able to sustain about 4 times the lateral drift sustained by the control column (SR-C). This is attributed to the improvement in shear resistance. Transverse prestressing counteracted diagonal tension and improved concrete shear resistance by delaying the formation of diagonal cracks. Beyond diagonal cracking, the prestressing continued to control cracking, improving aggregate interlock at higher inelastic deformations and providing additional transverse shear reinforcement. This resulted in a significant overall increase in column shear resistance, changing the mode of response from shear to flexure. The column then behaved in a ductile flexural mode exhibiting improved deformability. Further improvement in deformability was achieved due to the confinement of concrete, which delayed the crushing of compression concrete in flexure. The damage was much less in the retrofitted column, compared to the unretrofitted specimen at each level of deformation. This is shown in Figure 3.9. Once the peak resistance was attained in as-built column (1.5% drift ratio), the strength decay and degradation was rapid and the capacity dropped quickly. Retrofitting the column increased its flexural capacity by about 10% because of the confinement of concrete. Furthermore, the energy dissipation capacity was enhanced substantially.

3.2.2 Long Rectangular Columns

This section reports on the performance of two flexure-dominant rectangular columns, labeled LR-C and LR-R, where the former represents an as-built column without the retrofit and the latter represents a retrofitted column through external prestressing. The objective of these two tests was to study the effectiveness of external prestressing on confinement of compression concrete in rectangular columns and the resulting increase in column deformability. The columns had a shear-span to depth ratio of 2.86 with longitudinal bars continuous into the footing, without lap splicing.

3.2.2.1 Non-Retrofitted Column LR-C

The performance of Column LR-C during various stages of loading is demonstrated in Figure 3.10. Initial flexural cracks perpendicular to the loading direction and shear cracks on the side faces formed as early as the second cycle of 0.5% drift ratio mainly in the lower half of the column. The longitudinal reinforcement started yielding at this drift level while the hoops did not yield until 2% drift ratio. Lateral load resistance at this stage of loading was 319 kN, which was increased to 415 kN during the first cycle at 1% drift ratio. During this cycle, the strains in longitudinal reinforcement increased well beyond the yield strain(ε_y), as the number of flexural cracks increased and widened. The number of shear cracks also increased during this level of deformation on the side faces. The lateral load resistance was 402 kN during the first cycle at 1.5 % drift ratio. Visible signs of cover crushing and spalling were observed on the compression side near the base. During the third cycle of the same drift level, vertical cracks were noticed along the longitudinal reinforcement. These cracks propagated towards the top, within the lower half of the column, signifying the onset of further cover spalling. The flexural cracks also propagated further towards the compression zone as the column was deformed to 2% lateral drift. The cover spalled off completely at the second hoop level, 375 mm above the column-footing interface, exposing the reinforcement cage. Strength decay was observed as the column was deformed to 2.5% drift ratio. The load resistance dropped from 388 kN during the first cycle to 287 kN during the third cycle. Finally, the longitudinal reinforcement buckled in compression and the test was discontinued. Figure 3.10(c) shows a picture taken after the test, illustrating the buckling of all the bars between the first and second ties. One of the

shear cracks on the side of the column opened up by 20 mm. The experimentally recorded hysteretic force and moment-lateral drift relationships are plotted in Figure 3.11.

Column rotations at h (700 mm) and h/2 (350 mm) above the footing (assumed hinging region) were recorded by LVDT's and are plotted in Figure 3.12. The anchorage slip of longitudinal reinforcement within footing is plotted in Figure 3.13. This data exhibits significant asymmetry, probably because of potential instrumentation problems.

The strain gauge data is presented in Appendix A (Figures A.6 and A.7). Accordingly, the strains in lateral reinforcement started yielding at 2% lateral drift, just before the column experienced strength decay. Yielding of longitudinal reinforcement was generally reached during the cycles at 0.5% drift ratio. The yield plateau in both tension and compression are clear in data recorded by gauges No. 1, 2, 4 and 8.

3.2.2.2 Retrofitted Column LR-R

Column LR-R was companion to LR-C and was retrofitted by employing the Retro-belt technology. It was externally prestressed by hoops at every 150 mm. Figure 3.14 shows the observed damage during various stages of loading.

Initial damage at 0.5% drift was limited to two hairline flexural cracks when the column lateral force resistance was 323 kN. The load resistance subsequently increased to 418 kN at 1% lateral drift ratio. More flexural cracks were observed during the cycles at this deformation level. The longitudinal reinforcement developed yield strains during the first cycle at 1% drift. The 2nd hoop from the base started yielding at this deformation level as well. As the column was deformed to 1.5% lateral drift, a flexural crack started initiating at the column-footing interface, indicating yield penetration into the footing and the extension of longitudinal reinforcement in the footing, resulting in anchorage slip. Widening of the previously formed flexural cracks was observed. Shear cracks started to appear on the side faces between the lower five strands. The crushing of concrete started at the column-footing interface as the number of cycles at 1.5% drift ratio increased. This also resulted in the widening of the flexural crack at the interface. The lateral load resistance reached to 428 kN. However, unlike the control column (LR-C) this was not the peak resistance. A few more flexural and shear cracks occurred during 2% drift cycles. Some spalling of concrete was observed in the lower 200 mm segment of column. The width of flexural cracks widened to

6 mm during 3% drift cycles, which propagated towards the sides in the form of shear cracks. Spalling of concrete continued within the bottom region of column. The peak resistance of 430 kN was reached at 4% drift ratio and it dropped to 419 kN (96 % of peak) in the subsequent cycles of 4% drift level. The damage observed did not change during the deformation cycles at this level of drift except for widening of flexural cracks, some developing a width of 8 mm. During the first cycle at 5% drift ratio the lateral resistance dropped to 378 kN (88% of peak). The resistance further dropped to 206 kN (48% of peak) during subsequent cycles. Eventually, the concrete at the interface was destroyed. The cover concrete spalled off between the first two strands and the width of the flexural cracks increased up to 9 mm in the lower 225 mm segment. The middle two longitudinal bars ruptured on the north side of column during the third cycle of 5 % drift ratio. At 6% drift ratio, the lateral load resistance dropped to 187 kN (44% of peak). All four longitudinal bars on the south side and one of the remaining bars on the north side (perpendicular to the loading direction) ruptured. The experimentally recorded Force-Drift and Moment-Drift hysteretic relationships are illustrated in Figure 3.15, showing significantly improved inelastic deformability when compared with the companion control column.

Steel strains and column rotations were measured up to 1% drift only due to an instrumentation error. Figure 3.16 shows the rotation readings and Appendix A presents the strain readings in Figures A.8 to A.10, including the strains in prestressing strands.

3.2.2.3 Comparison of Columns LR-C and LR-R

The comparison of Force and Moment-Drift hysteretic relationships for Columns LR-C and LR-R in Figures 3.11 & Figure 3.15 shows a substantial improvement in column deformability resulting from the retrofit technique employed. The as–built column (LR-C) had a limited capacity of 2% drift ratio. The retrofitted column (LR-R) was able to develop a drift capacity of up to 4% and lost its lateral load resistance during 5% drift cycles gradually, exhibiting ductile response (Figure. 3.15). Furthermore, it was damaged less than the companion column as illustrated in Figure 3.17. Although retrofitting considerably enhanced the drift capacity, it did not change the moment capacity significantly.

3.2.3 Long Rectangular Columns with Splice Deficiencies

Two companion columns (LS-C and LS-R) with the same shear span (2000 mm) as the flexure dominant columns discussed earlier were built with spliced longitudinal reinforcement. They were tested to investigate the performance of columns with splice deficiencies and the effectiveness of external prestressing in improving the clamping force and resulting bond between concrete and spliced reinforcement. The results are discussed and compared in this section.

3.2.3.1 Non-Retrofitted Column LS-C

Column LS-C was representative of a flexural dominant rectangular column with lap splices in the potential hinging region. It was the control column which reflected non-seismic design practices utilized in existing bridge columns. The shear span was long enough to promote flexure dominant response with spliced reinforcement subjected to critical flexural tension near the column base. The observed damage during testing is illustrated in Figure 3.18, showing the slippage of reinforcement as the failure mode.

Flexural cracks were observed after the first cycle of loading at 0.5% drift ratio on the north and south faces within the lower 1.0 m segment of column. Further cycling at this deformation level caused the propagation of cracks. The maximum lateral load resistance at this level was 360 kN. Flexural cracks propagated towards the sides, in the form of inclined shear cracks, when the load was increased to 1% lateral drift ratio. Spalling and crushing of concrete was observed near the base at this deformation level within the bottom 75 mm segment of column. The column had already reached its peak resistance during the first cycle of 1% drift ratio (392 kN), corresponding to peak moment resistance of 811 kN.m. Further cycling resulted in the decay of strength. Moment resistance in the direction of first load excursion (loading towards north) dropped by approximately 25% (showing moment resistance of 609 kN.m) at the end of the third cycle. This level of strength drop was considered to be significantly high to label the drift capacity to be 1%. During the subsequent deformation cycles, the cracks widened within the lower 350 mm segment as well as at the column-footing interface. Reinforcement slippage could be observed in the hysteretic relationship recorded in the form of significant pinching of hysteretic loops.

The force and moment-lateral drift hysteretic relationships for the column are shown

in Figure 3.19. The moment values plotted were computed from recorded horizontal forces and the horizontal and vertical components of accompanying axial load. The rotations of the hinging region are shown in Figure 3.20. Only a small portion of total column rotation within the base region can be attributed to anchorage slip at the column footing interface. Figure 3.21 demonstrates the anchorage slip rotations recorded. Longitudinal reinforcement did not show any indication of yielding, as demonstrated in Figure A.11 and the hoops did not seem to yield up to 2% lateral drift. The strain gauge "D" was the only strain gauge that exceeded 2000 με at this deformation level. This is illustrated in Figure A.12.

3.2.3.2 Retrofitted Column LS-R

Column LS-R was the companion column to LS-C with identical geometric and material properties. However, this column was retrofitted by external prestressing in transverse direction, as explained earlier. The same loading scheme that was used for the former column was also used for this column. Damage observed at various stages of testing is shown in Figure 3.22.

The first flexural hairline crack was observed during the third cycle of 0.5% drift. The number of flexural cracks increased during deformation cycles at 1% drift ratio. A crack formed at the column footing interface during the second cycle at 1% drift ratio. The first shear crack was also observed on one of the side faces during the same load stage, at the 2nd deformation cycle, when the lateral force was 460 kN. The third cycle at 1% drift ratio resulted in more hairline shear cracks on the side faces. Strain gauges located on dowels showed that they started yielding at the first cycle of 1% drift ratio. This is illustrated in Figure A.13. The crack at the column-footing interface widened and became longer during the 2nd cycle at 1.5% drift ratio. During the cycles of 2 % drift, more hairline shear cracks formed on the side faces while the previous cracks became longer. Flexural cracks widened up to 1 mm indicating an increase in the anchorage slip, as demonstrated in Figure 3.25. One of the LVDT's used to measure anchorage slip reached its stroke limit and could not record displacements beyond 20 mm, as shown in Fig. 3.25, resulting in error in data beyond this level of slippage. Some crushing of cover concrete was observed near the base at 3% lateral drift ratio and the longitudinal reinforcement started yielding at this drift ratio. Increased diagonal shear cracks were observed during the 4% drift cycles, with the widening of one

such crack. The column maintained its strength until 3% lateral drift towards south and developed approximately 20% strength decay in moment resistance during the first cycle at 4% drift ratio. However, it was able to maintain 4% drift cycles without significant strength decay in the other direction (loading towards north), and experienced noticeable strength decay during the second cycle of 5% lateral drift.

The starter bars ruptured at column footing interface during the third cycle of 5% drift and the column resistance dropped from 460 kN to 347 kN. This indicated the participation of starter bars to load resistance (rather than slipping) and the effectiveness of retrofit methodology. The load resistance continued to drop during subsequent deformation reversals and reached 129 kN at 6% drift ratio. Hysteretic Force and Moment-Drift relationships for the column are illustrated in Figure 3.23. The bond strength between the steel and concrete started to weaken under cyclic loading starting at 3% drift up to the first cycle of 4% drift, with total deterioration beyond this level. This is illustrated by the horizontal lines in Figure A.13. The strains recorded by gauge Nos.10, 11, 12, illustrated in Figure A.13, showed that at 4% drift the longitudinal bars started to strain harden in compression. Figure 3.24 shows the total rotation of the hinging region at the two measured locations (h, h/2). By comparing these recorded graphs it can be concluded that the main part of rotation took place at the lower 350 mm from the footing of column. Strain gauges A, B and C, D were placed on the second and third hoop at 380 mm and 680 mm from the base of the column, respectively. Figure A.14 shows the location and the strain gauge readings on these two hoops. The graphs indicate that these hoops did not experience yielding.

The strain data recorded on prestressing strands are plotted in Figure A.15. The first four strands within the splice region were prestressed up to 50% f_{pu} corresponding to a deformation of about 3800 $\mu\varepsilon$. The last eight strands were prestressed up to 25% f_{pu} corresponding to a deformation level of up to 1900 $\mu\varepsilon$. In most of the strands the maximum stress was reached at 5% column drift ratio. The manual readings that were done to record the strain gauge readings for the 6^{th} to 12^{th} strand from the base do not capture all the points during each cycle; they were only done at the end of each drift cycle.

3.2.3.3 Comparison of Columns LS-C and LS-R

The failure mechanisms of the two companion columns (LS-C and LS-R) were very different. The as-built column (LS-C) had a limited drift capacity of 1% and the failure was triggered by the slippage of spliced reinforcement. The failure of retrofitted specimen (LS-R) was ductile and much more gradual. Although the drift capacity of LS-R was much higher than the LS-C, the damage observed on the column after the test was less than that for the as-built column. This is illustrated in Figure 3.26. When the moment-deformation hysteretic relationships are compared, it can be seen that Column LS-R, with seismic retrofitting, was able to sustain 4 to 5 times the lateral drift ratio sustained by the control column LS-C. This is attributed to the improvement in bond characteristics of spliced longitudinal reinforcement as well as improved concrete confinement provided by transverse prestressing. Lateral prestressing also improved shear resistance and controlled diagonal tension cracks. This resulted in further improvements in column performance by eliminating the degradation of shear resistance mechanism. Furthermore, the flexural capacity increased by 18% and there was considerable increase in the energy dissipation of retrofitted column.

3.3 Tests for the Development of Column Repair Technique

In the aftermath of an earthquake, the operation of lifeline structures is critical and bridge columns need to be repaired in a timely manner. The retrofit technique may potentially offer a quick and effective solution to column repair problems. Research data is needed to develop the retrofit methodology as a repair technique. Therefore, the second phase of the experimental research program included design, construction and testing of three full-scale columns critical in shear, to investigate the applicability of the retrofit system as a column repair technique.

Three shear dominant columns, with different cross sectional shapes, were built as representatives of pre 1970's design. The columns were tested by following the same test procedure employed earlier in the previous phase. The following sections provide the observations made and data recorded during testing.

3.3.1 Short Circular Column

A full-scale circular bridge column with 600 mm diameter and 1220 mm height (effective shear span of 1500 mm) was designed, built and tested to induce some seismic damage. The column was critical in shear and the level of damage desired to be induced was similar to that of a column that would suffer significant diagonal tension cracking during a strong earthquake with wide enough cracking to signify the yielding of column ties. This indicated that a sufficiently wide diagonal tension crack was to be induced for subsequent repair.

The initial loading consisted of three cycles within 0.5% drift ratio. The first cracks occurred as flexural cracks near the first three hoops within the lower 700 mm segment of column. Some chipping and vertical cracking of concrete were observed close to the top of the column where the loading was applied. Maximum lateral load of 348 kN was recorded at 0.5% drift ratio.

Subsequently, the column was forced to deform 1% drift ratio. The maximum lateral load resistance of 425 kN was reached during the first cycle. Longitudinal reinforcement started yielding as shown in Figure A.16, developing the yield moment. The column experienced shear yielding during the same drift level because the strain gauges on hoops recorded deformations exceeding the yield strain, as indicated in Figure A.17. The subsequent cycles at 1% drift resulted in a few more flexural cracks on the north and south faces, with diagonal cracks that opened up about 2 mm on the side faces. As the column was cycled more at this deformation level the diagonal cracks widened and propagated towards the bottom and top ends of the column. At this stage, the maximum crack width was measured to be 4 mm. At this stage a critical decision had to be made as to whether this was a sufficient damage to be repaired or not. It was decided to induce further damage, and the specimen was forced to reach 1.5% drift. However, unexpectedly the column failed at 1.32% lateral drift ratio in a sudden and brittle manner.

The development of damage during the test is illustrated in Figure 3.27, including photographs taken at different stages of loading. The hysteretic behavior recorded is shown in Figure 3.28. The failure was due to diagonal tension as is clearly demonstrated by the wide diagonal crack shown in Figure 3.27. This sudden failure did not allow the repair of the column, and the data gathered was used in assessing the shear capacity of the column during

the subsequent analytical investigation. The flexural rotation of the hinging region and anchorage slip rotation at column-footing interface are shown in Figures 3.29 and 3.30, respectively. Two Temposonic LVDT's were used to evaluate total anchorage slip rotation at the base of the column but a technical problem was experienced with one of the Temposonic LVDTs during testing. Therefore the anchorage slip rotation was calculated using the data obtained from only one of the Temposonic LVDT, assuming similar behavior in the other. The data indicated that most of the rotations were developed within the first 300 mm segment of column from the base, and only a small portion of the total rotation was due to anchorage slip.

3.3.2 Short Square Column with Splice Deficiencies

Column SSR-C, with a 500 mm square cross-section and a 1220 mm height (with an effective shear span of 1500 mm) was tested, damaged, repaired and re-tested. The details of observed performance and test data are presented below.

The column had lap splices of longitudinal reinforcement in the potential hinging region. The ties consisted of 6.35 mm diameter (US #2 bar size) smooth reinforcement placed at 300 mm spacing. SSR-C was the control column which reflected non-seismic design practices utilized in existing older bridge columns. The column was subjected to the same loading history as the previous columns. The damage observed during testing is illustrated in Figure 3.31. Flexural cracks occurred after the first cycle of loading at 0.5% lateral drift ratio on north and south faces within the lower 700 mm segment of column. Further cycling at this deformation level increased the number of cracks and lengthened the cracks to the sides of column with a declining angle. The maximum lateral load resistance at this level was 320 kN. Flexural cracks propagated more into the sides in the form of inclined shear cracks when the load was increased to 1% lateral drift ratio and opened up to a crack width of 1.0 mm. The column reached its peak load resistance (370 kN) at this stage of loading, corresponding to peak flexural resistance of 575 kN.m. Pinching of hysteresis loops was observed, which was indicative of the combination of shear response and slippage of spliced reinforcement. Vertical cracks formed within the splice region. The strain data (shown in Figure A.18) indicated that most of the bars did not reach their yield capacity but instead slipped, except for one which had strain gauges 8, 9 and 10.

Because the width of diagonal crack was not indicative of significant shear damage, the deformation was increased to 1.5% drift level. Spalling and crushing of concrete was observed near the base at this deformation level within the bottom 75 mm segment of column. Further cycling resulted in the decay of strength. Moment resistance in the direction of first load excursion (loading towards north) dropped by approximately 30% (down to 383 kN.m) at the end of the second cycle at 1.5% drift. This level of strength drop was considered to be significant enough to label the column drift capacity to be 1%. During the 1.5% drift cycles the cracks widened within the lower 500 mm segment, as well as at the column-footing interface. Reinforcement slippage could be observed in the pictures taken which exhibit a number of vertical cracks on the north and south faces of column. This is also demonstrated in the strain data (Figure A.18).

Force and moment-lateral drift hysteretic relationships for the column are shown in Figure 3.32. The moment values plotted were computed from recorded horizontal forces and the horizontal and vertical components of axial loads, including the P-Δ effect. It is clear from the hysteretic relationship shown in Figure 3.32 that the column experienced severe strength degradation immediately after the cycles at 1% lateral drift. The hysteresis loops show some pinching signifying shear dominant response and slippage due to insufficient splice length. The reduction in load resistance was attributed essentially to insufficient transverse reinforcement against diagonal tension as evidenced by wide diagonal cracks that have formed, indicating the yielding of transverse reinforcement. Figure A.19 illustrates the recorded strain gauge readings on the transverse reinforcement. Although strain gauge B in this figure, which is located on the 2nd hoop at 380 mm above the column base, shows that the transverse reinforcement has yielded, the strain gauges on the third hoop at 680 mm above the base of the column do not indicate yielding.

Total rotations and anchorage slip rotations measured are shown in Figure 3.33 and Figure 3.34, respectively. The rotation measurements were taken at 275 mm (h/2) and 550 mm (h) above the column footing interface while the anchorage slip rotations were measured at the closest possible place to the column base. Figure 3.33 also illustrates that much of the total rotation that included flexural and anchorage slip rotations, was caused by flexure within the lower 275 mm segment. The difference between total rotations recorded and rotations caused by anchorage slip gives the rotations caused by flexure.

The damaged as-built column (SSR-C) was repaired by using external transverse prestressing. The repaired column was labeled as SSR-R. The transverse prestressing was applied by using the same hardware as that used for retrofitting columns in the earlier phase. A few small pieces of cover concrete that had become loose during previous loading were removed and the column was patched with fresh concrete in these areas, in an effort to prepare the surface for external prestressing. Raiser frames were nailed on the surface of the column for external prestressing as illustrated in Figure 3.47(a). Seven-wire strands with 9.53 mm diameter were placed on the raiser frames. The spacing of strands was 100 mm within the splice region and was increased to 150 mm above this region. The intended level of prestressing was 50% f_{pu} (1050 MPa) for each strand. Details of initial prestress are given in Table 5. This level of prestressing was found to be adequate to improve the performance of the splice region in earlier tests, and was used throughout the column to close diagonal tension cracks as much as possible. This level also allowed further stretching (stressing) during testing prior to developing the rupturing of strains. The same loading scheme that was used for the as-built column was also used for the repaired column.

No additional damage was observed during the 0.5% drift cycles. The chipping of the patched cover concrete at the column-footing interface was observed at 1% drift level. Additional flexural cracks formed and the existing crack between the first 2 strands started opening up to 2.0 mm. The column-footing interface crack became wider with a crack width of 4 mm at 1.5% drift ratio, indicating the slippage of column bars in the splice region. More chipping of the repaired cover concrete was observed at the column footing interface. The cycles at 2% drift ratio resulted in additional widening of the flexural cracks on north and south faces when the maximum lateral force was at 344 kN. New hairline diagonal shear cracks were observed during 3% drift cycles, however the cracks were well under control due to external prestressing. During 4% drift and subsequent drift levels, the interface crack kept on widening and the column maintained its strength until 10% lateral drift. The column showed a partial rocking mode about the base as the longitudinal bars continued slipping, however the external prestressing helped maintain a significant shear force resistance until the end of testing. The test was stopped at the end of this drift level due to the shortage of stroke in the horizontal actuator. Some strength decay was experienced up to 6% lateral drift

and a longitudinal bar rupture was observed at this deformation level while there was no concrete cover left below the first strand (75 mm from the column footing).

Figure 3.35 illustrates the column behaviour with photographs taken during various stages of testing. It also shows the column at the end of 10% drift cycles with virtually no damage except for the base. Hysteretic force and moment-lateral drift relationships are plotted in Figure 3.36, showing stable loops until 10% lateral drift. The column rotation measurements that were taken at 275 mm (h/2) and 550 mm above the column base of the column are plotted in Figure 3.37. By comparing these two graphs with their rotational similarity at different drift levels it can be concluded that most of the total rotation has taken place within the lower 275 mm (h/2) of the column. Figure 3.38 illustrates the anchorage slip of the longitudinal reinforcement and it is obvious that most of the total column rotation is attributed to the anchorage slip of the reinforcement rather than the flexural rotation. The recorded strains on the dowels as illustrated in Figure A.20 show yielding of reinforcement while the strain gauges on the spliced longitudinal reinforcement demonstrate the slippage of these bars. This also explains the rocking of the column about its base after 4% drift ratio. Based on the readings obtained from strain gauges located on the 2^{nd} and 3^{rd} hoop (and shown in Figure A.21), it can be concluded that the transverse reinforcement did not yield. The repair technique did provide sufficient lateral constraint against buckling of longitudinal reinforcement and prevented transverse reinforcement from yielding, but it was not adequate to control the slippage of spliced reinforcement beyond 4% lateral drift. Figure A.22 demonstrates the strains recorded on prestressing strands. The figure indicates a decrease in prestressing strand strains up to 4% drift. This signifies that by subjecting the column to incrementally increasing lateral deformation reversals, most of the lateral pressure is used to close the cracks and beyond this point the strands start expanding again. This behavior is more obvious in the first four strands from the base of the column within the splice region.

The failure mechanism for each column was very different. The as-built column (SSR-C) exhibited limited deformability with a maximum drift capacity of 1% followed by a drop in load resistance. The failure of the repaired/retrofitted specimen (SSR-R) was ductile and much more gradual. Although the strength of SSR-R did not improve over the capacity experienced prior to repair, it did maintain this capacity with a gradual reduction in strength, which never dropped below about 70% of the initial resistance. The eventual column

deformability, with some strength decay, was much higher than the control column. The damage observed on the repaired column after the test was almost the same as that for as-built column except for the column-footing interface which was damaged extensively due to the slippage of longitudinal reinforcement. This is shown in Figure 3.35. When the moment-deformation hysteretic relationships are compared it can be seen that column SSR-R with external prestressing was able to sustain more than 5 times the lateral drift sustained by the control column although it demonstrated up to 30% strength decay.

3.3.3 Short Rectangular Columns

This section reports on the behaviour and failure mechanisms of two full-scale rectangular concrete columns, RR-C and RR-R. A specimen representing as-built rectangular bridge columns (RR-C) with 1220 mm height was tested, damaged and then retested after being repaired (RR-R). The columns had a shear span of 1500 mm, measured to the point of application of the horizontal force. The failure mechanism, performance of columns and the effectiveness of external prestressing in repairing the column are discussed in the following paragraphs.

Column RR-C was the control column, with shear deficiency. This column was representative of a typical shear dominant bridge column with No.2 (6.3 mm diameter) perimeter ties at 300 mm spacing. The column was first subjected to a constant axial load of 15% of the column concentric capacity (1294 kN) to simulate typical gravity loading and was subsequently subjected to incrementally increasing lateral deformation reversals.

The initial cycles at 0.5% drift ratio produced up to four flexural cracks, propagating towards the sides of column, with an inclined shear angle. Increasing deformations to 1% drift ratio resulted in the further propagation of cracks towards the sides, with an increased width of 5 mm. One flexural crack, at 940 mm from the base on the north face extended towards the sides, with an inclination of 45°, joining to the interface crack. The column footing interface crack was about 5 mm wide at this stage of loading. Spalling and crushing of concrete was observed near the base within the bottom 75 mm segment of column. The previous shear cracks propagated further to column sides as new cracks formed although the amount of moment resistance in the direction of the first load excursion (loading towards north) dropped by approximately 16% at the end of the third cycle. The column was then

loaded to exceed 1% drift slightly (up to 1.2% drift ratio), but the test was stopped after one cycle at this deformation level since it was observed earlier in Phase I that a companion column could not sustain three cycles at 1.5% drift ratio. It was decided that the observed level of damage with a 16% drop in strength was sufficient for the next stage of testing after this column had been repaired through external prestressing.

The pictures taken during the test demonstrate the observed behavior of this specimen, as illustrated in Figure 3.39. Experimentally recorded Force-Lateral Drift and Moment-Lateral Drift hysteretic relationships for the column are shown in Figure 3.40. The force and moment values plotted were computed from recorded horizontal forces and the horizontal and vertical components of axial forces, including the P-Δ effect. It is clear from the hysteretic relationship shown in Figure 3.40 that the column experienced strength degradation immediately after the cycles at 1% lateral drift. The hysteresis loops showed some pinching, signifying shear dominant response. Column rotations, including anchorage slip rotations are shown in Figures 3.41 and 3.42. The rotation measurements were taken at 350 mm (h/2) and 700 mm (h). The graphs in Figure 3.41 indicate that much of the total rotation occurred within the lower 350 mm (h/2) from the base and Figure 3.42 shows how much of the total rotation was attributed to the anchorage slip. The strain gauge data recorded on column reinforcement are plotted in Figure A.23. The longitudinal bars generally reached their yield point during the first cycle at 0.5% drift and the cracks started widening indicating the yielding of transverse reinforcement. This yielding is also demonstrated by Figure A.24 which provides the recorded data obtained from strain gauges placed on transverse reinforcement (the second and third ties from the base). The failure was triggered by insufficient transverse reinforcement against diagonal tension.

The column was then repaired by external transverse prestressing and labeled as RR-R. The level of prestressing applied was 50 % f_{pu} (1050 MPa) and it was tested following the same loading scheme. New flexural cracks were observed during the second cycle at 1% lateral drift and their number increased during subsequent cycles. A crack formed at the column-footing interface on the south side during the third cycle at 1% drift ratio. The first set of new shear cracks were observed on both side faces, during the 2nd cycle of 1.5% drift ratio when the lateral force was at 590 kN. The first cycle at 2% drift resulted in additional hairline flexural cracks on north and south faces and the crack at column-footing interface

widened and became longer during the 2nd cycle at 2% drift level. Some crushing of cover concrete was observed near the base during the third cycle of 3% drift level while increased diagonal shear cracks were observed with widening of one of the cracks. However, the crack was well under control due to external prestressing. The column maintained its strength until 4% lateral drift and experienced some strength decay beyond 4% drift ratio. Figure 3.43 illustrates the behaviour of column with photographs taken at various stages of loading. It shows that the column exhibits virtually no damage at 3% lateral drift. The hysteretic force and moment-lateral drift relationships are plotted in Figure 3.44, showing stable loops until after 4% lateral drift ratio.

Recorded column rotations at 350 mm (h) and 700 mm (h) above the column base are shown in Figure 3.45. Rotations due to anchorage slip were measured close to the column base and are shown in Figure 3.46. The graphs shown in Figures 3.45 and 3.46 indicate that up to 4% drift much of the rotation occurred due to flexure at the lower 350 mm (h/2) segment of column and anchorage slip rotations are significantly lower than those caused by flexure. Longitudinal reinforcement strain readings are illustrated in Figure A.25. The strain recorded in the first two hoops is shown in Figure A.26. Due to external prestressing, the strain readings on these hoops show lower strain values than those recorded earlier, prior to repair. Strains were also measured in the prestressing strands as presented in Figure A.27. The maximum stress in each strand was reached between 4% and 6% drift. The second strand from the base of the column was the first to exceed 3000 με, which occurred at 5% drift ratio.

The comparison of repaired and as-built columns clearly demonstrates the improvement attained in column deformability by external prestressing. The prestressing controlled diagonal tension cracks and served as additional shear reinforcement. This resulted in a significant increase in the load capacity of damaged column, from approximately 500 kN to 600 kN. The column deformability also improved substantially, demonstrating the effectiveness of transverse prestressing as a column repair technique. However, considerable judgment needs to be exercised to assess whether the level of damage sustained by a column justifies its repair so that full reinstatement of strength is possible. Tests have indicated that spalling of cover concrete and yielding of either longitudinal or transverse reinforcement should not discourage repair. However, if

reinforcement has been fractured, buckled, or deformed significantly out of the straight, then column replacement should be considered as a serious option.

a) 0.5% Drift

b) 1% Drift

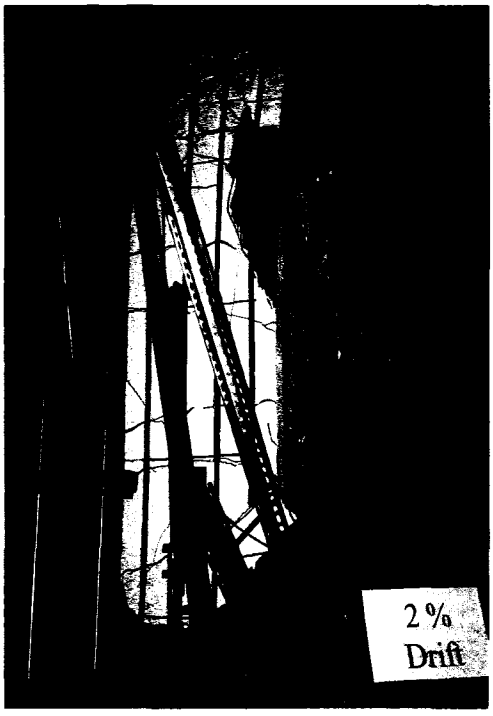

c) 2% Drift

d) After the test

Figure 3.1 Behaviour of Column SR-C

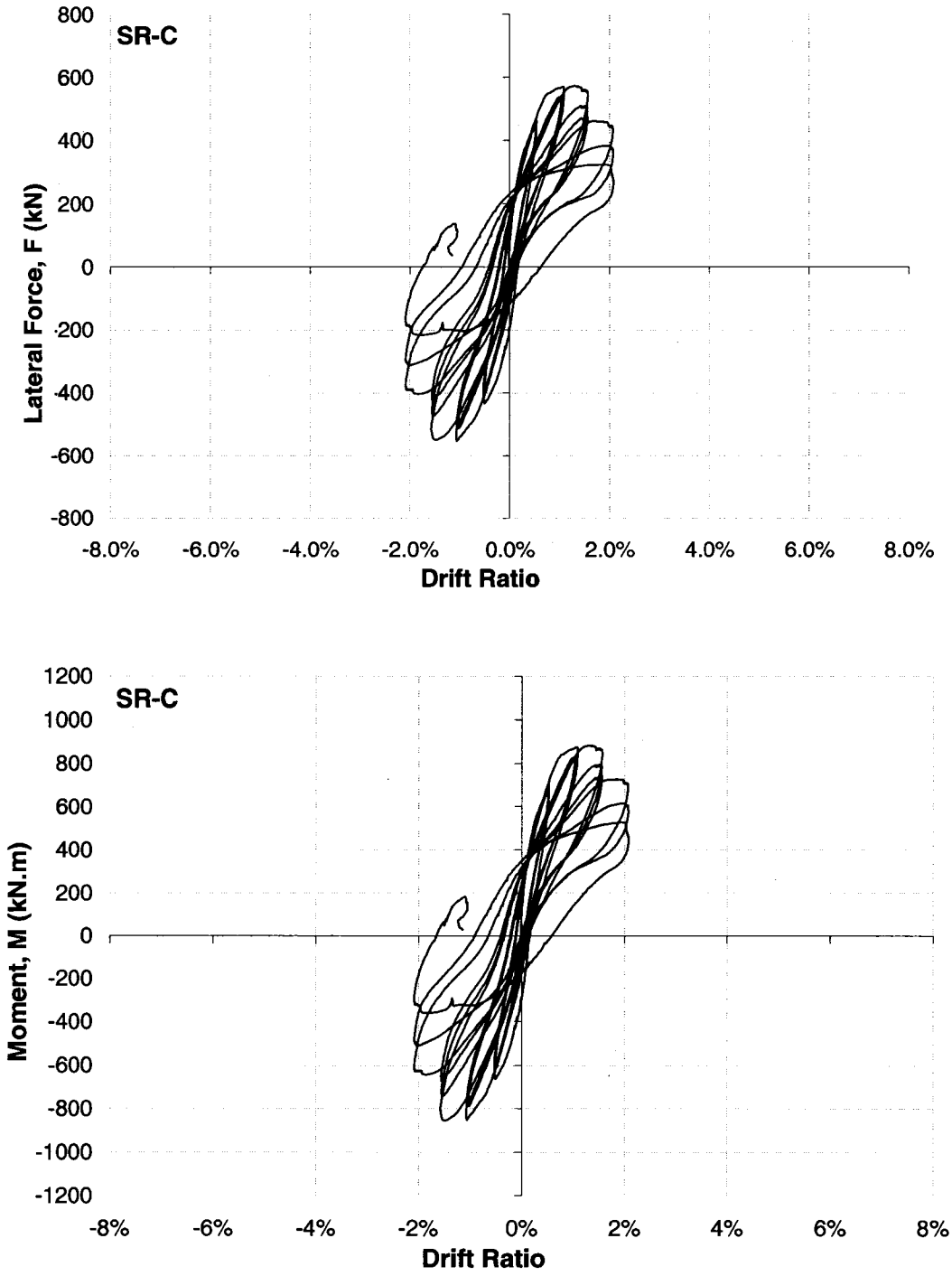

Figure 3.2 Hysteretic relationships for column SR-C (Force-drift &Moment-drift)

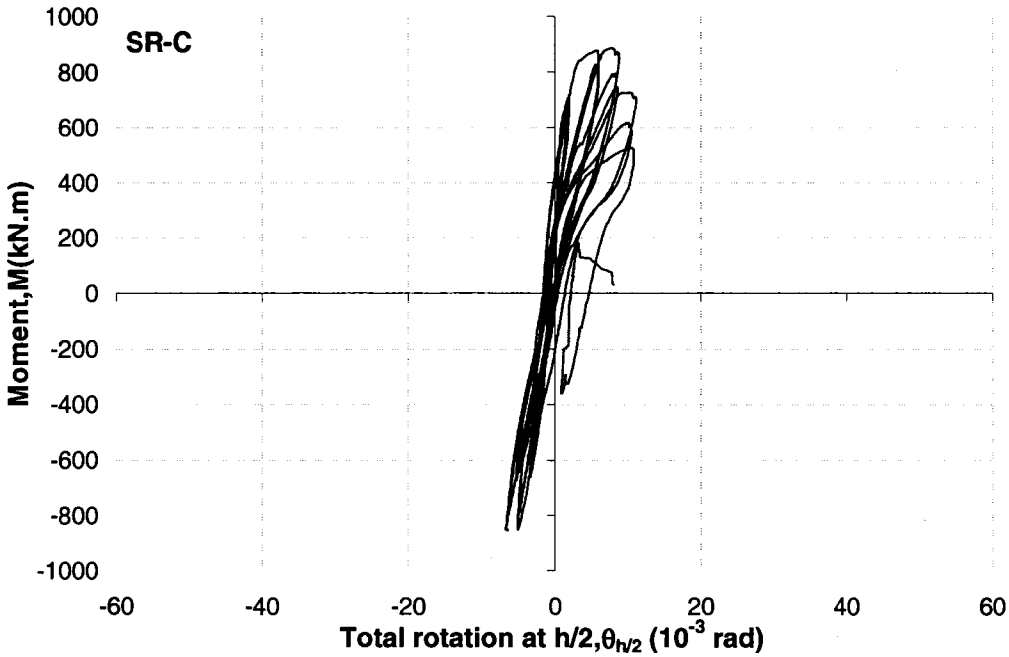

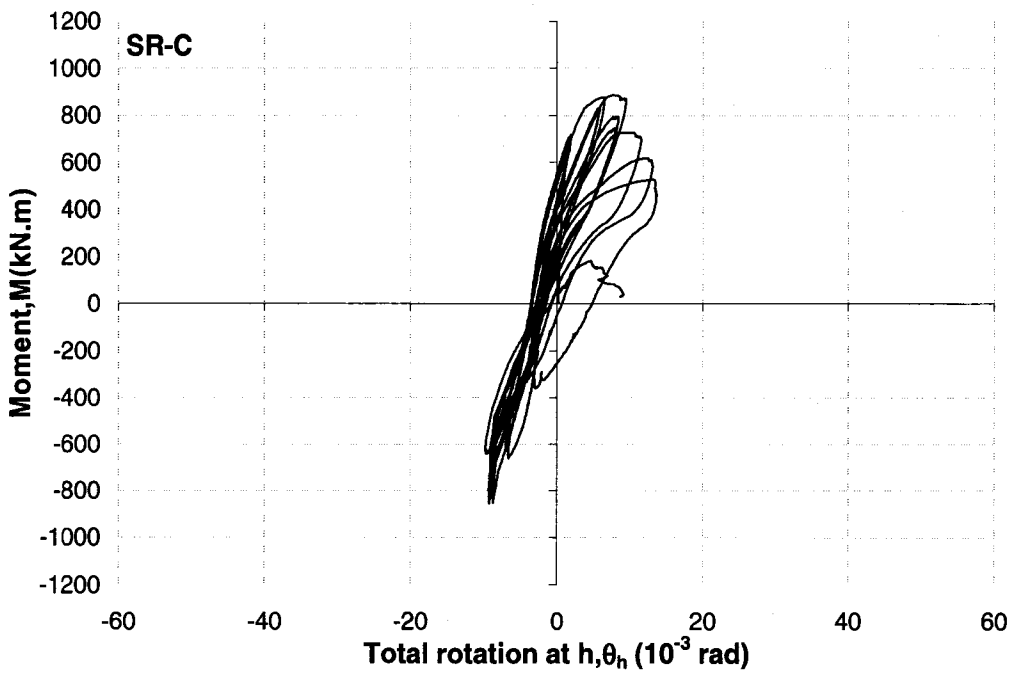

Figure 3.3 Rotation of the hinging region for column SR-C

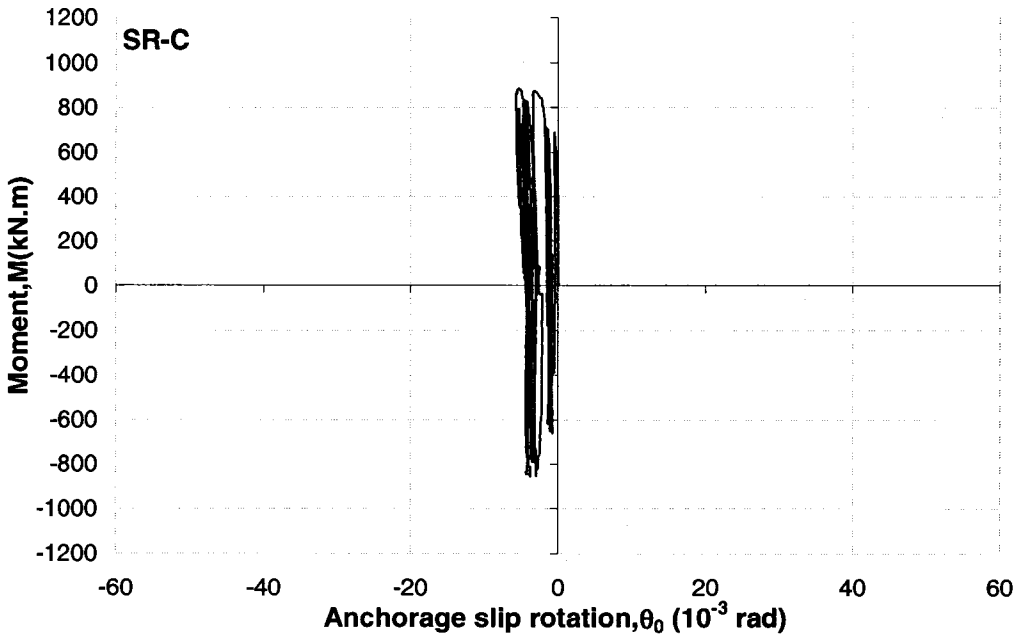

Figure 3.4 Anchorage slip at the column footing interface for column SR-C

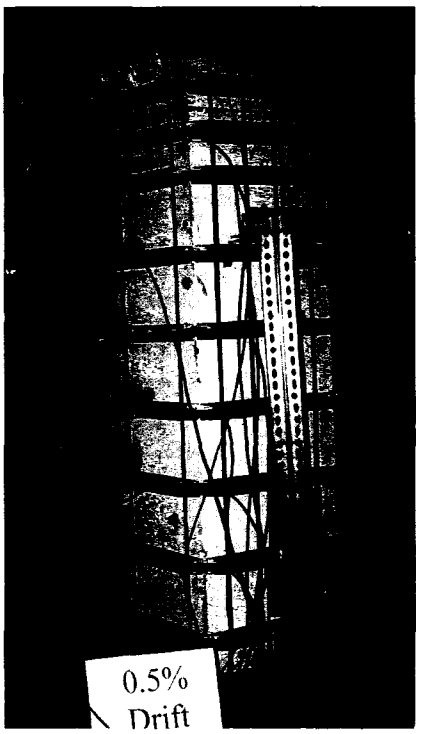

a) 0.5% drift

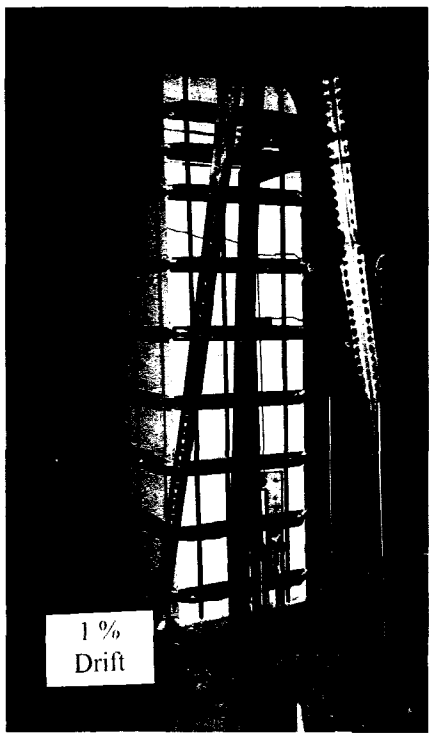

b) 1% drift

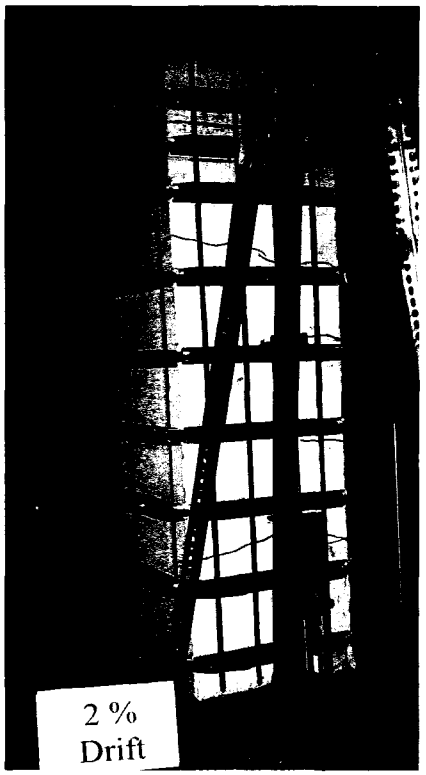

c) 2% drift

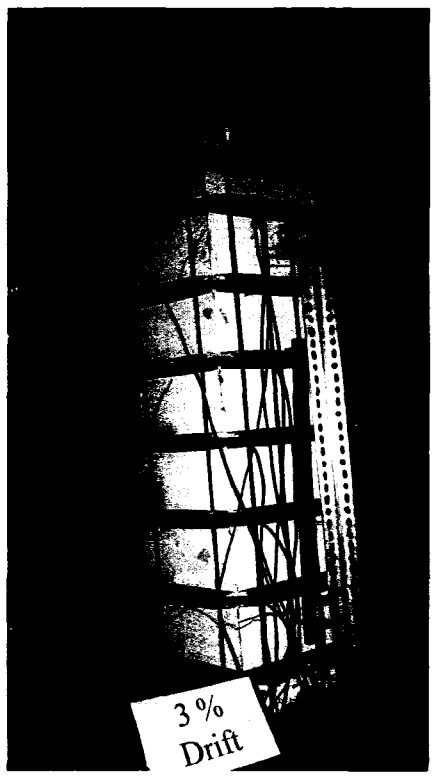

d) 3% drift

Figure 3.5 Behaviour of Column SR-R

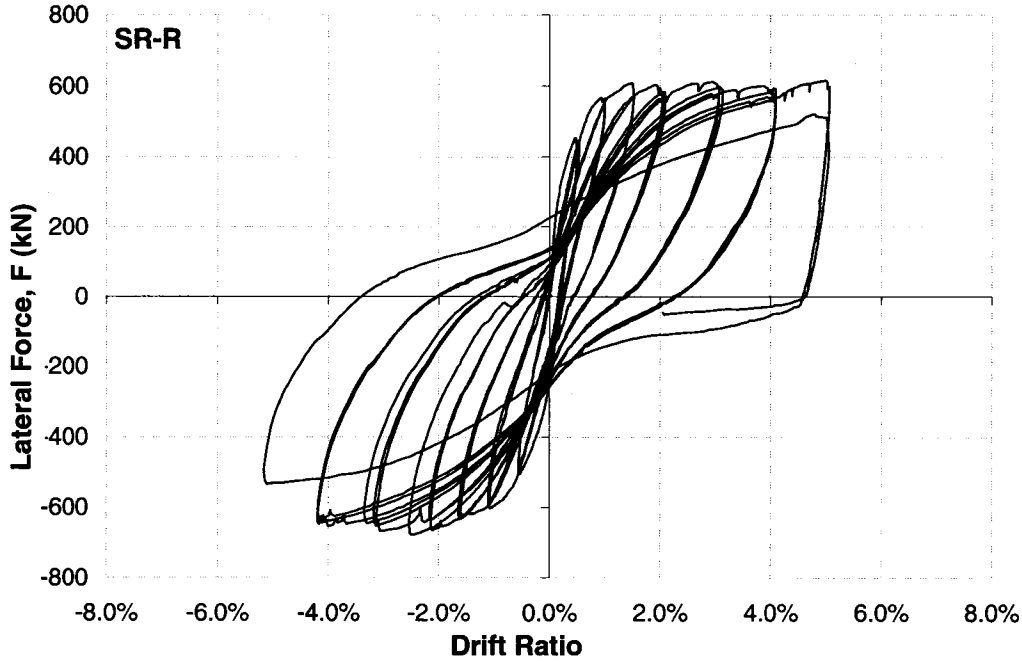

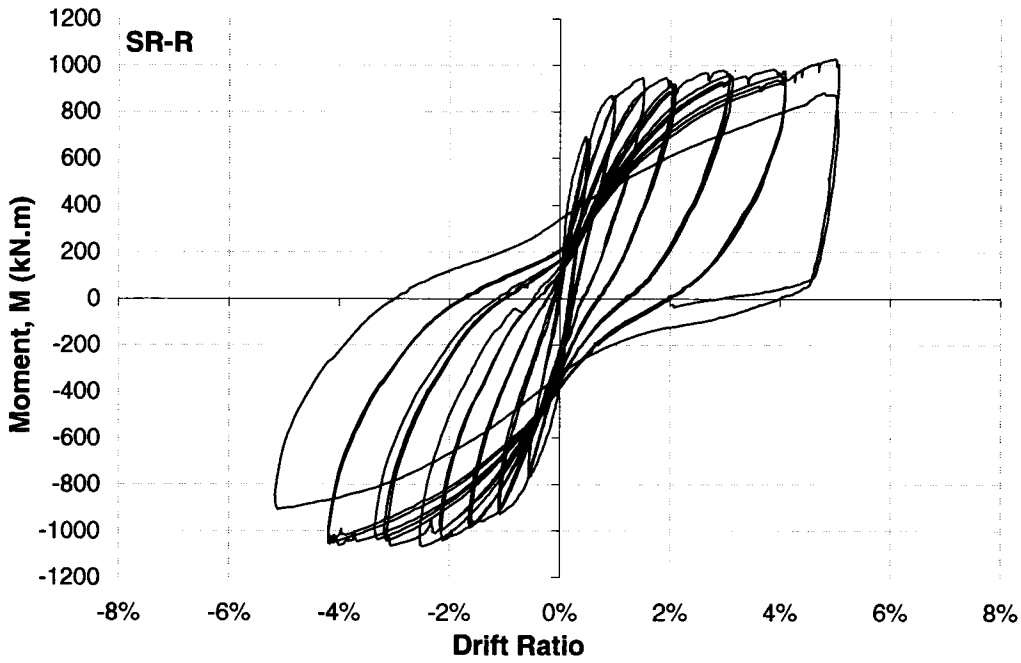

Figure 3.6 Hysteretic relationships for column SR-R (Force-drift &Moment-drift)

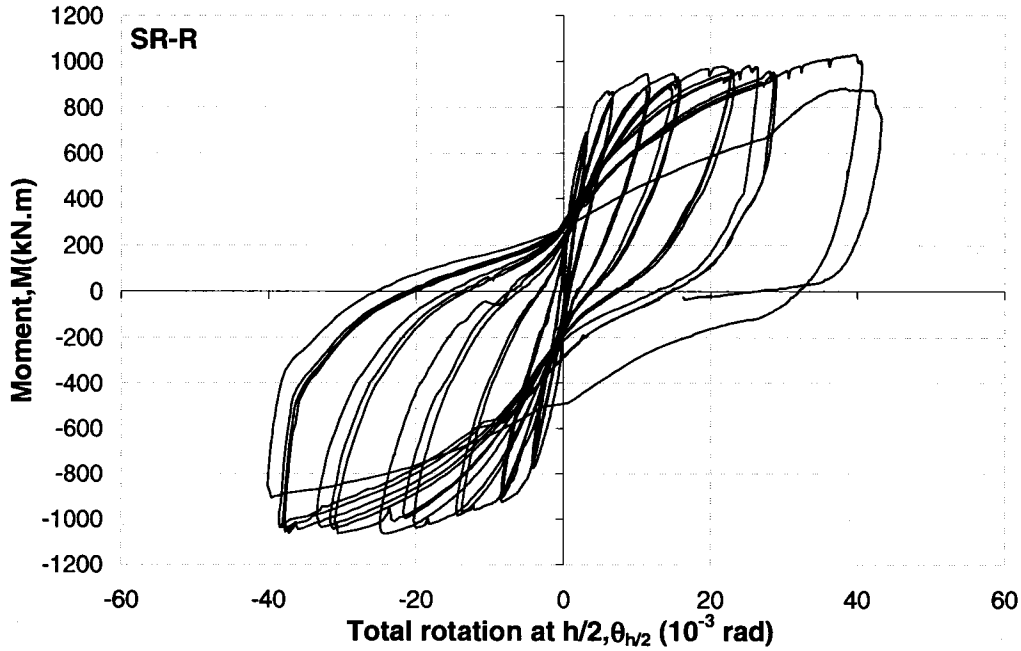

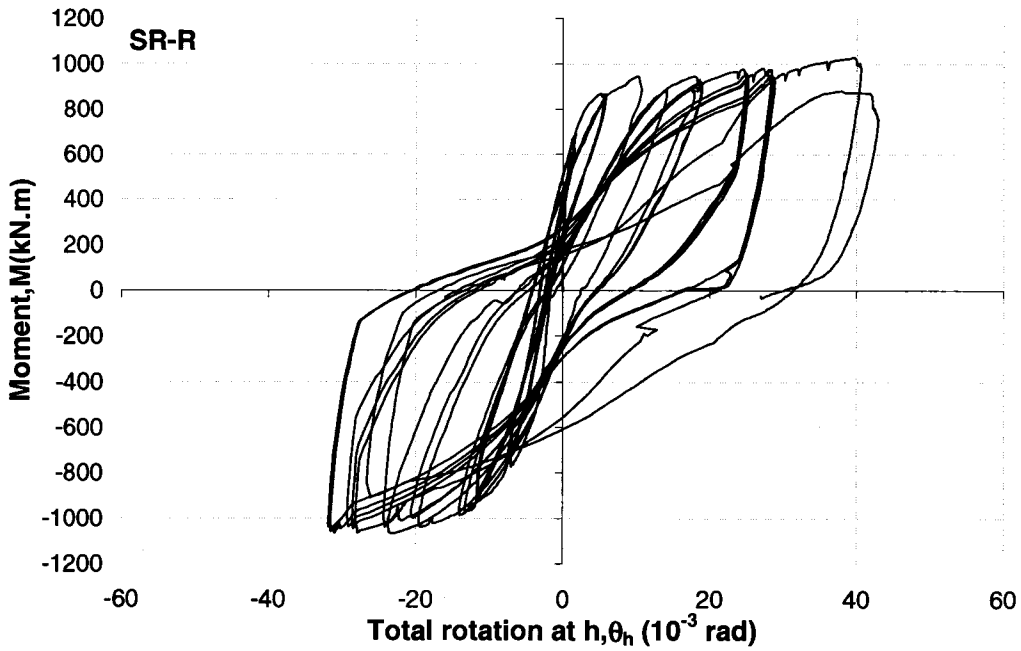

Figure 3.7 Rotation of the hinging region for column SR-R

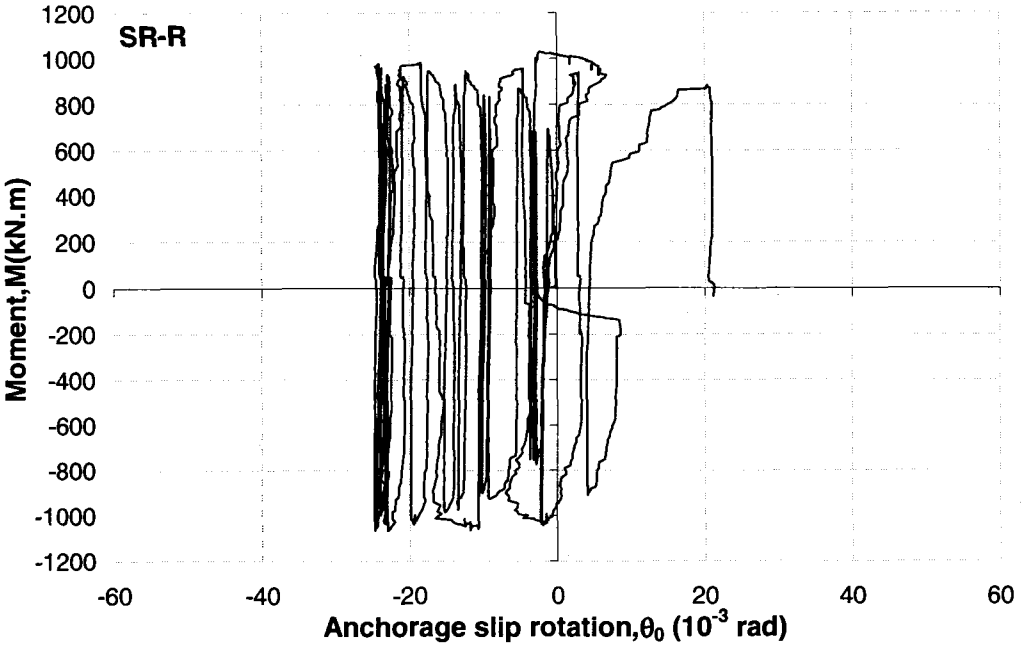

Figure 3.8 Anchorage slip at the column footing interface for column SR-R

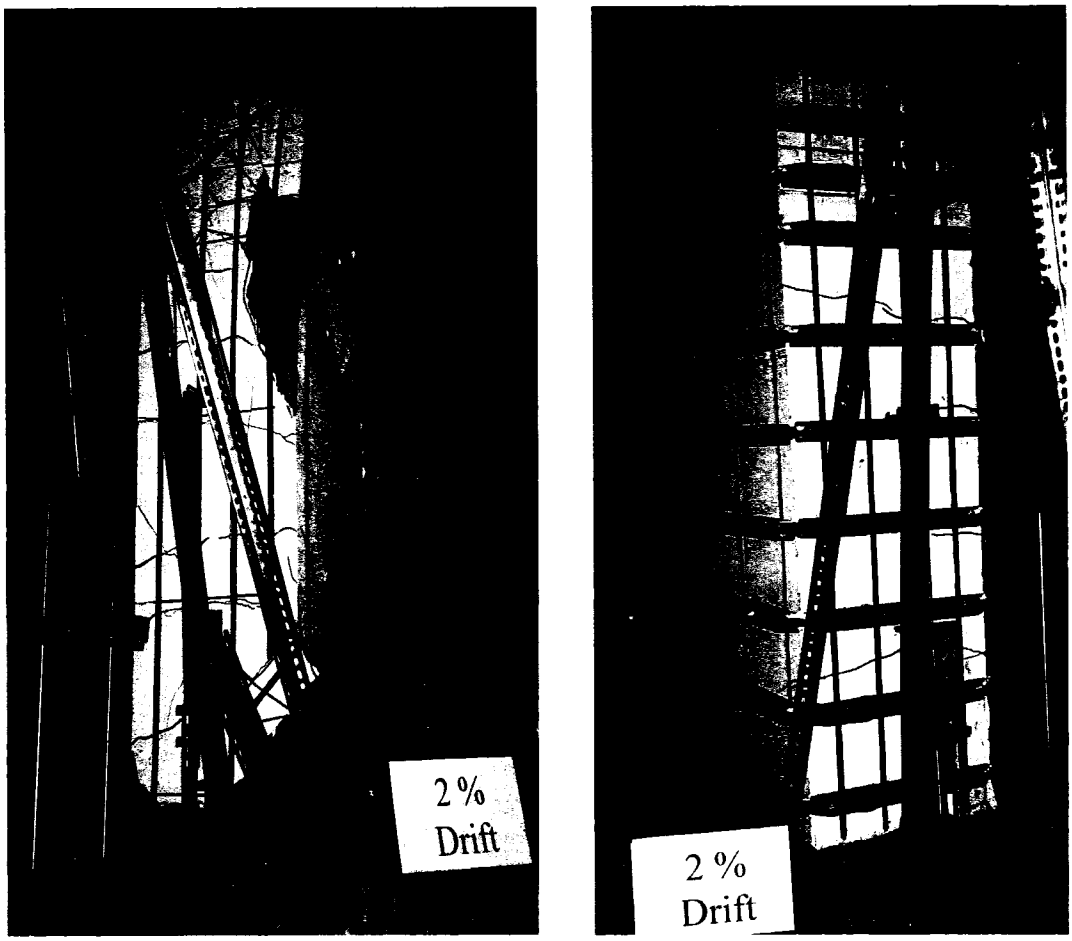

a) SR-C at 2% Drift Level **b) SR-R at 2% Drift Level**

Figure 3.9 Comparison of columns SR-C and SR-R after the test (Pictures)

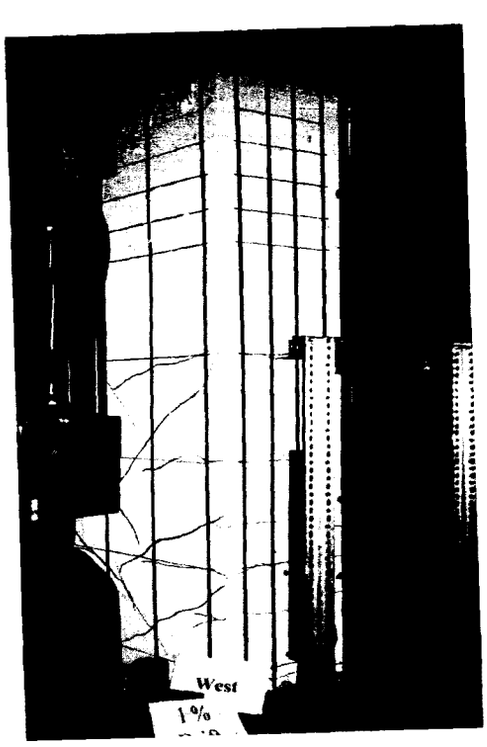

a) 1% drift

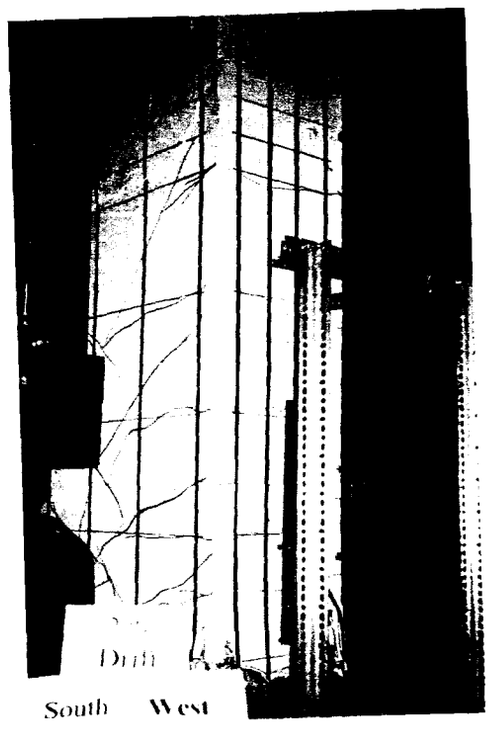

b) 2% drift

c) After the test

Figure 3.10 Behaviour of Column LR-C

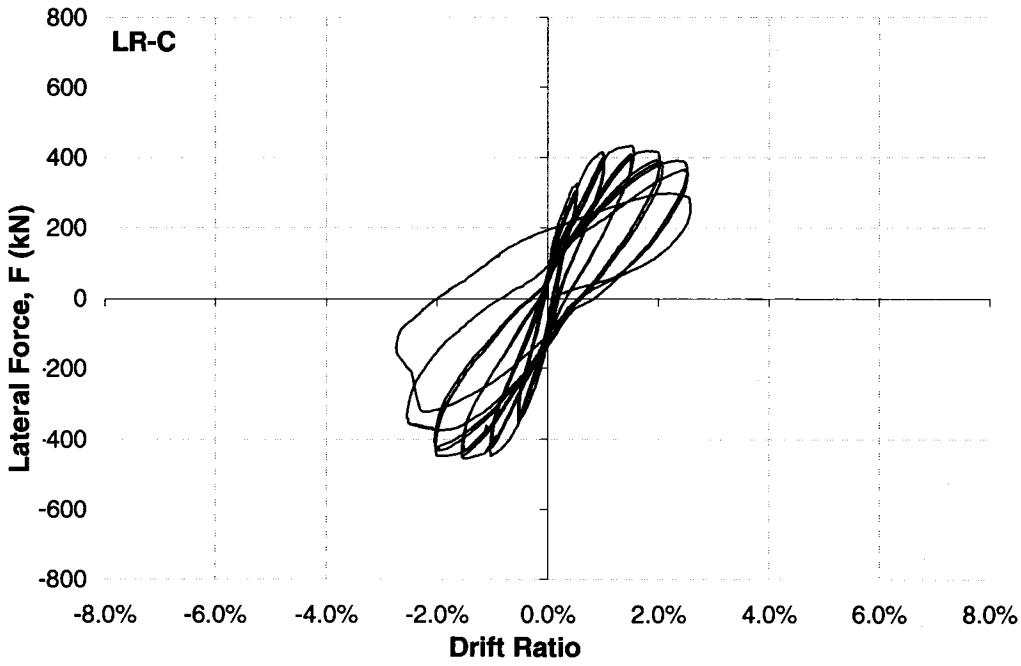

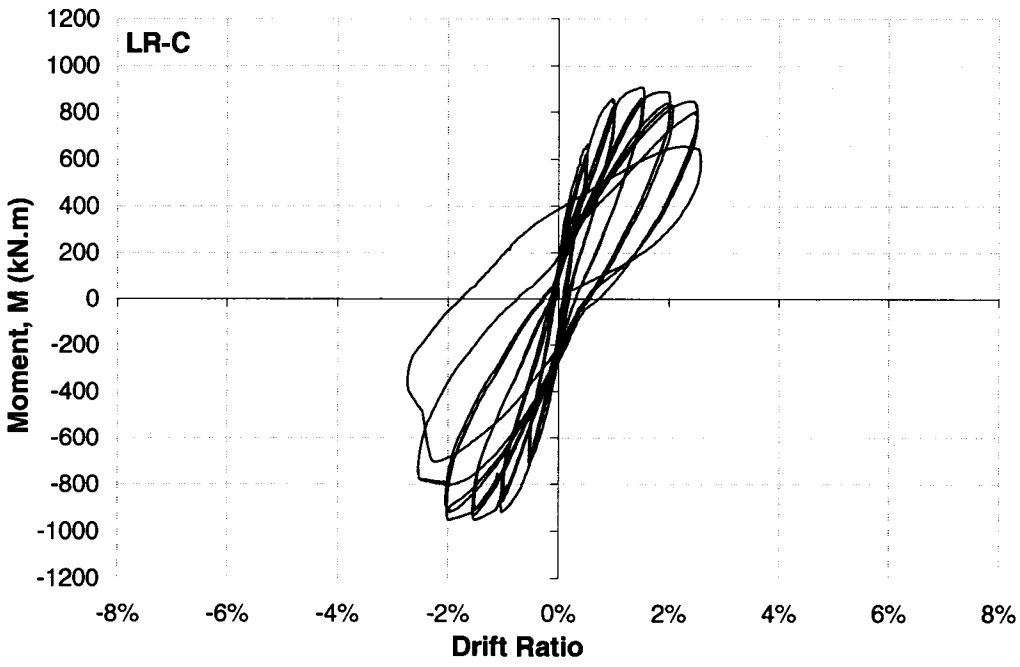

Figure 3.11 Hysteretic relationships for column LR-C (Force-drift &Moment-drift)

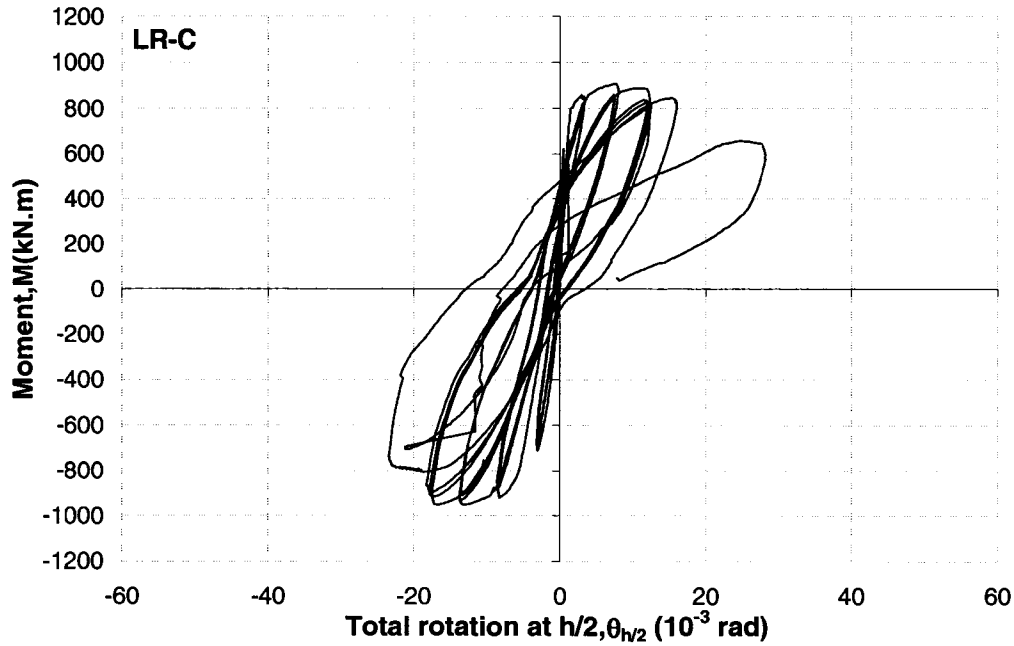

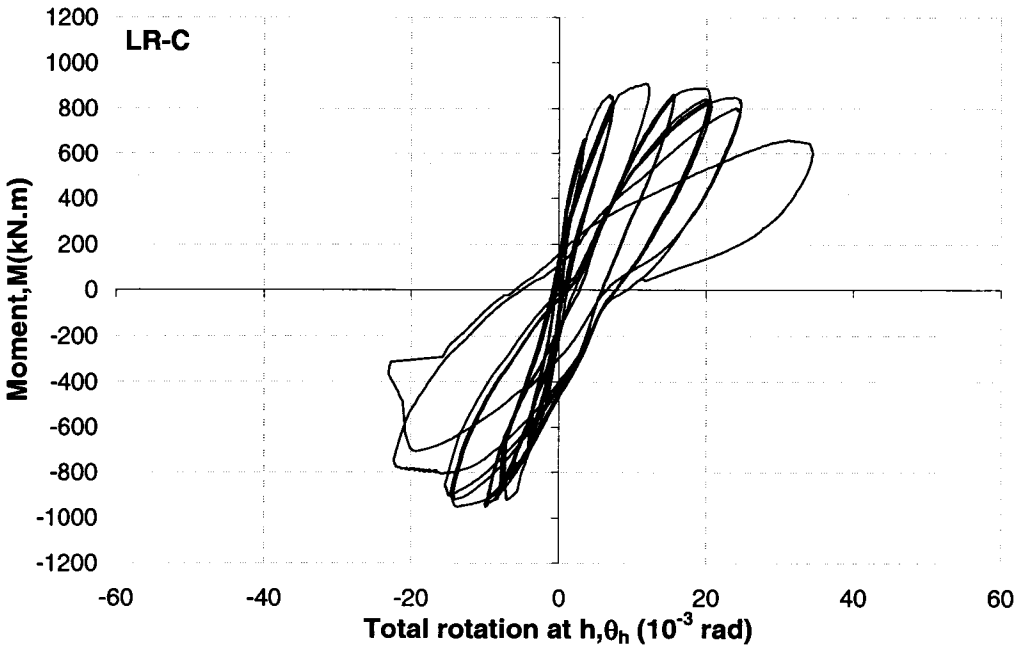

Figure 3.12 Rotation of the hinging region for column LR-C

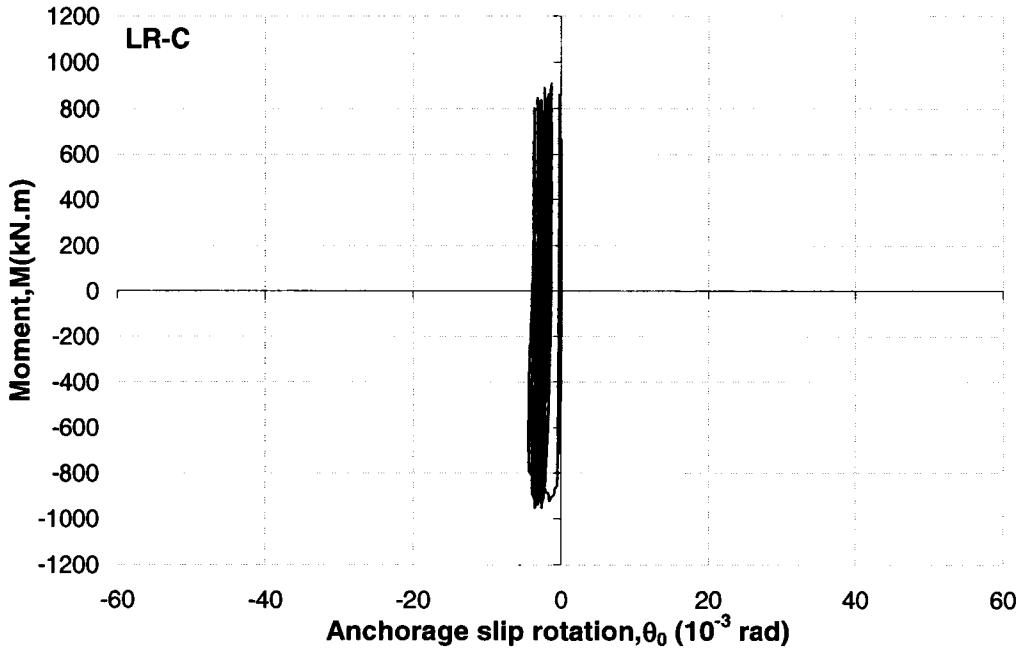

Figure 3.13 Anchorage slip at the column footing interface for column LR-C

a) 1.5% drift

b) 2% drift

c) 3% drift

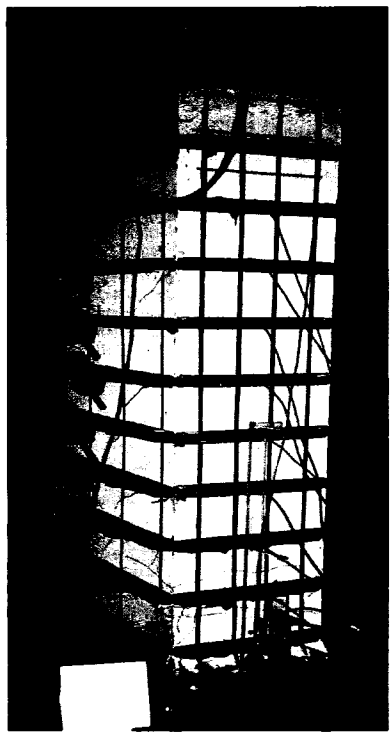

d)4% drift

Figure 3.14 Behaviour of Column LR-R

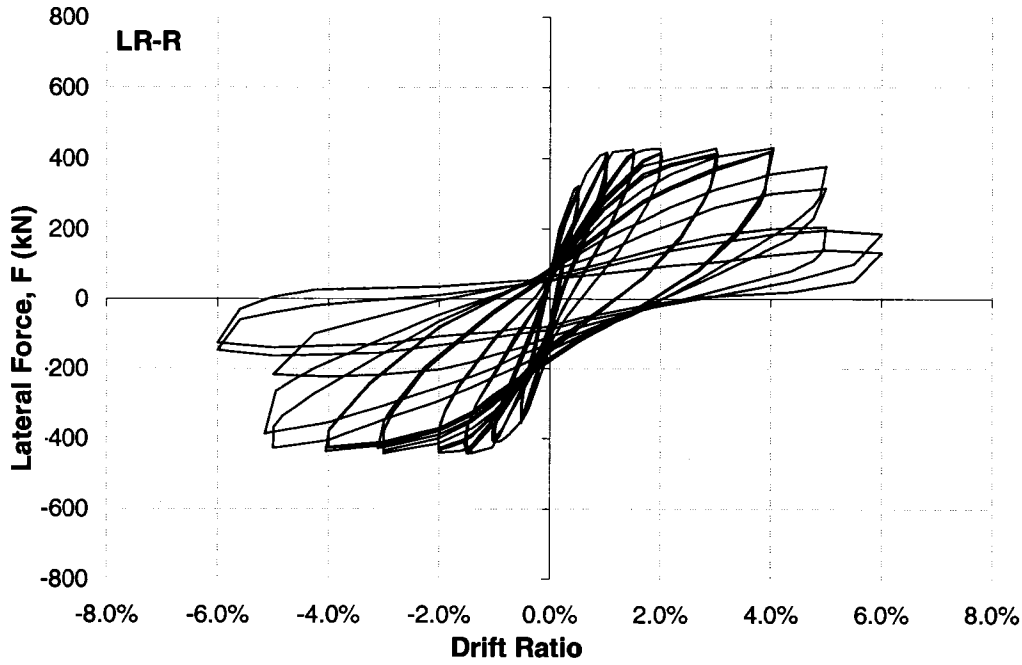

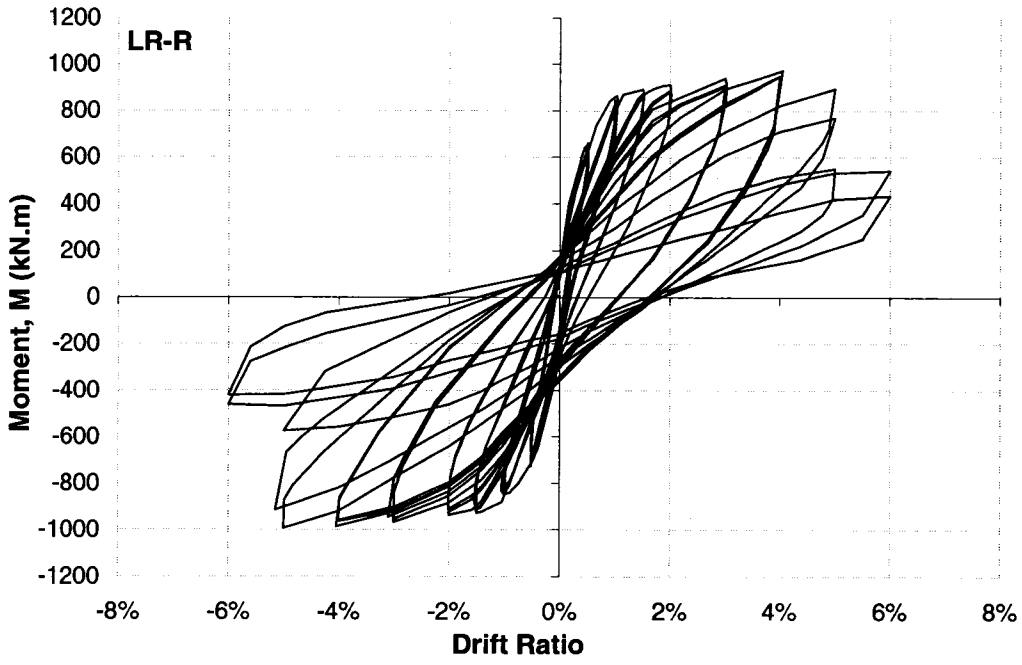

Figure 3.15 Hysteretic relationships for column LR-R (Force-drift &Moment-drift)

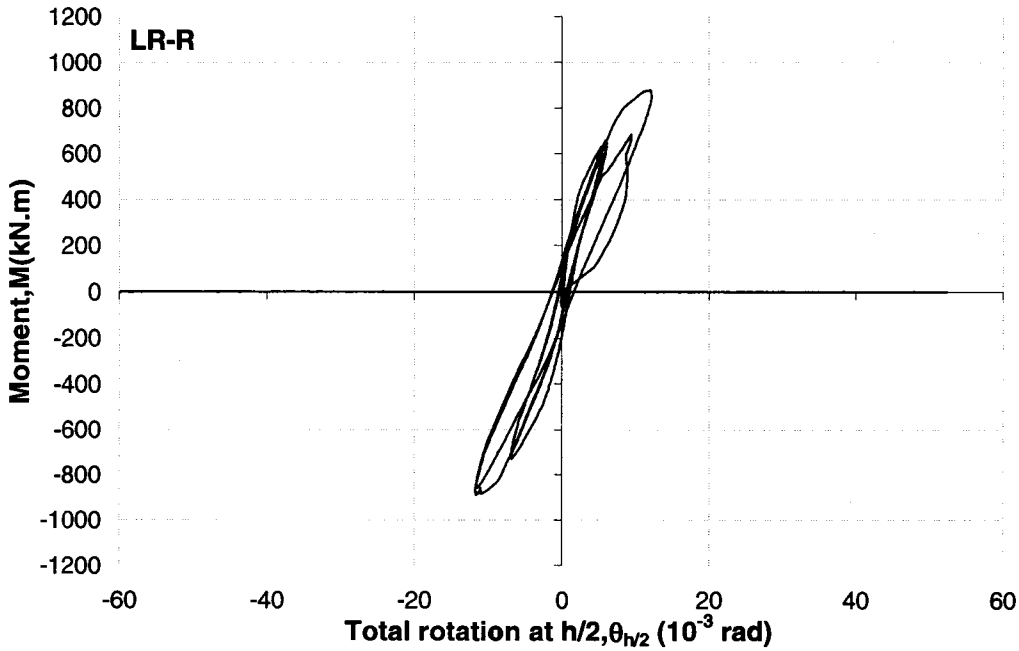

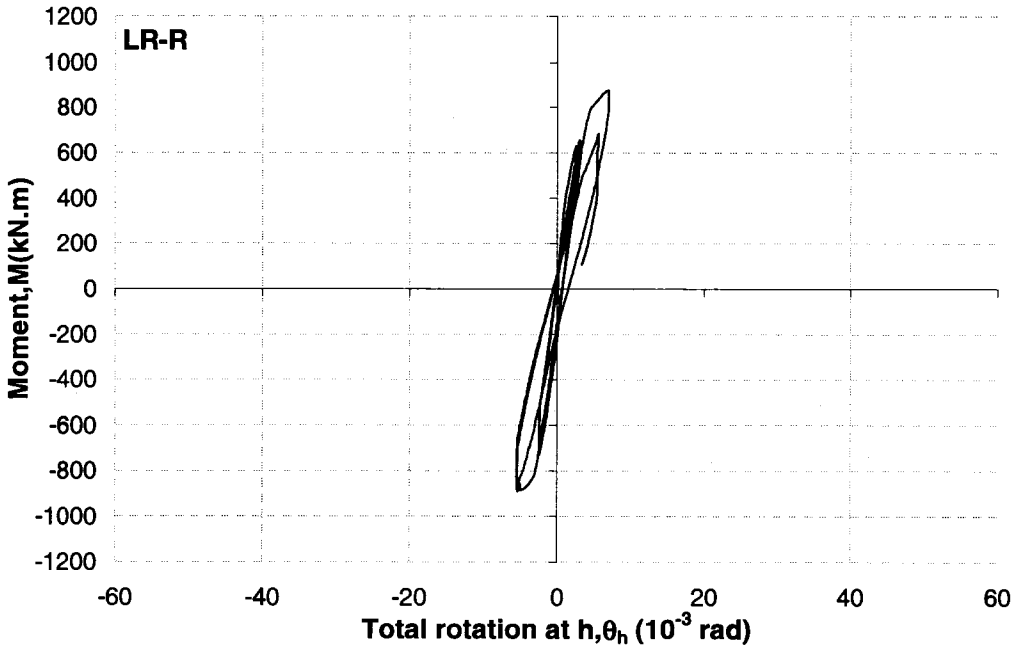

Figure 3.16 Rotation of the hinging region for column LR-R

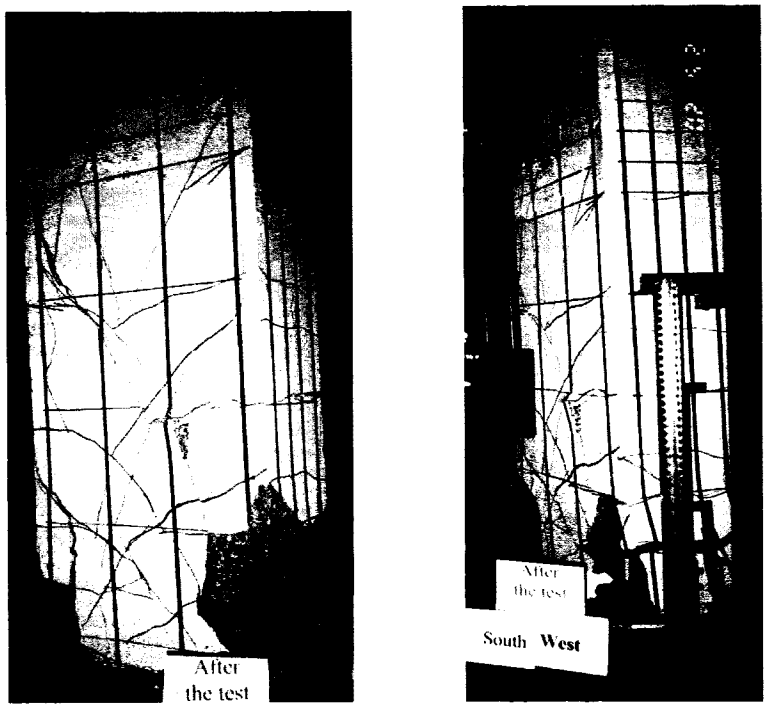

a) Control Column after Test (2% Drift)

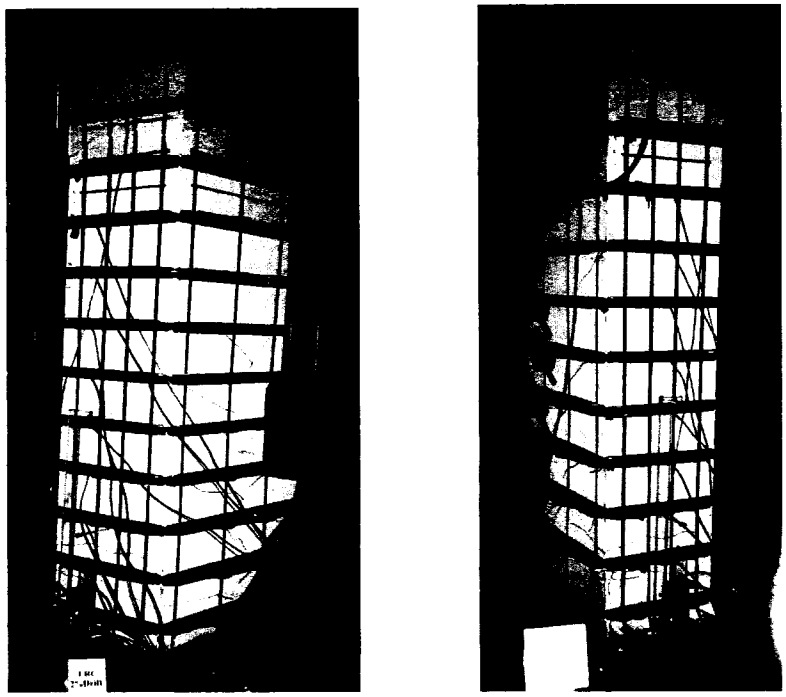

2% drift **4% drift**

b) Retrofitted Column (2%, 4% drift)

Figure 3.17 Comparison of columns after the test

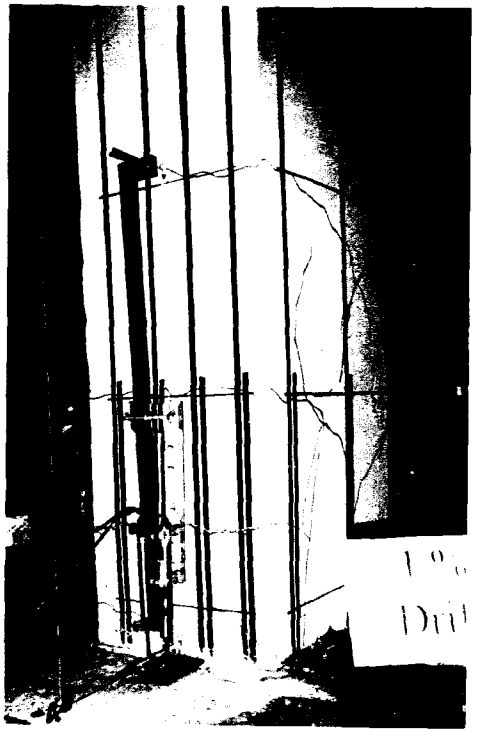

a) 1% drift

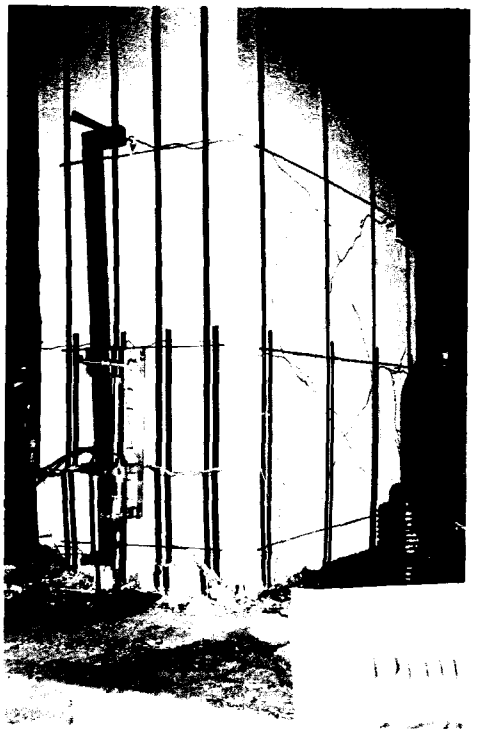

b) 1.5%drift

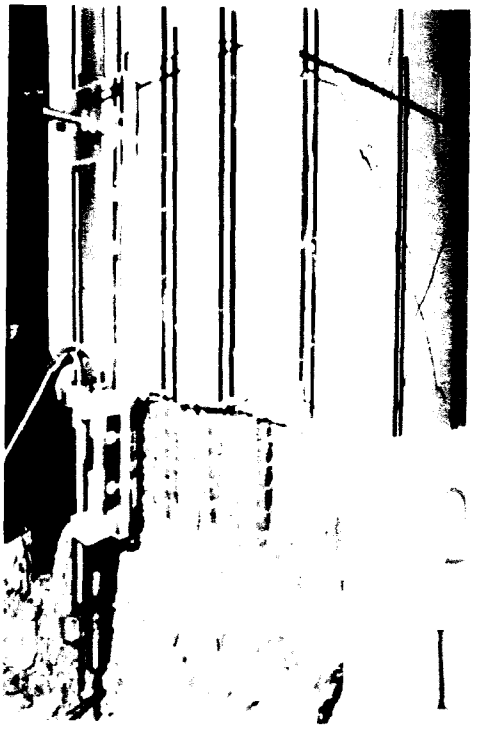

c) 2% drift

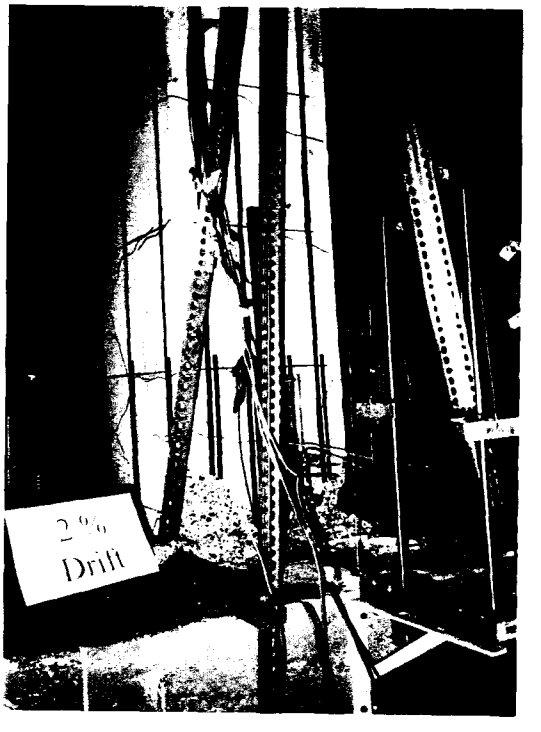

d) 2 % drift

Figure 3.18 Behaviour of Column LS-C

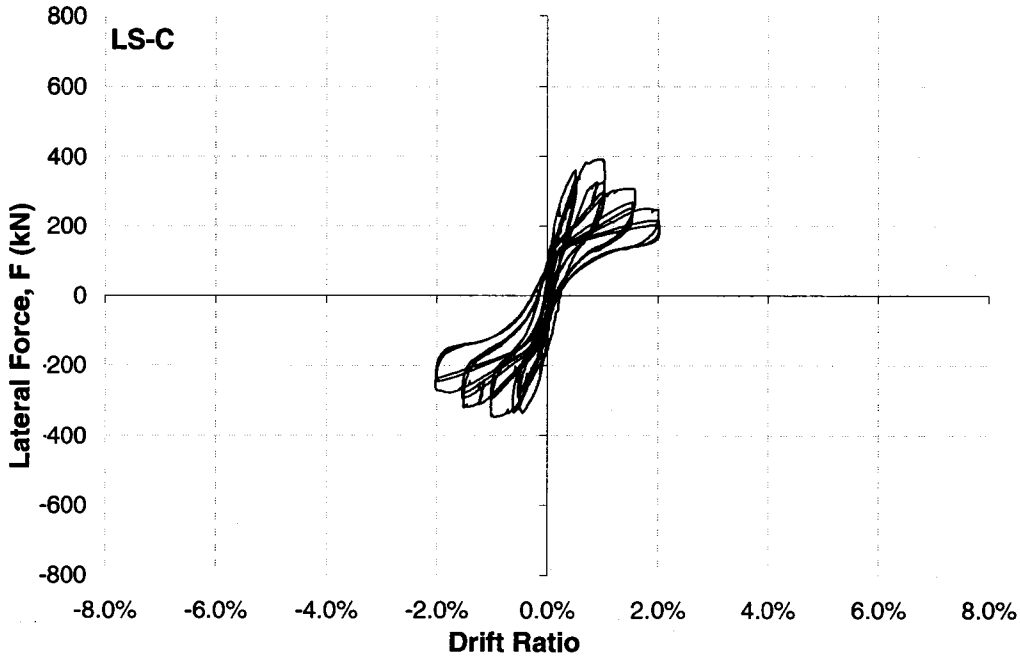

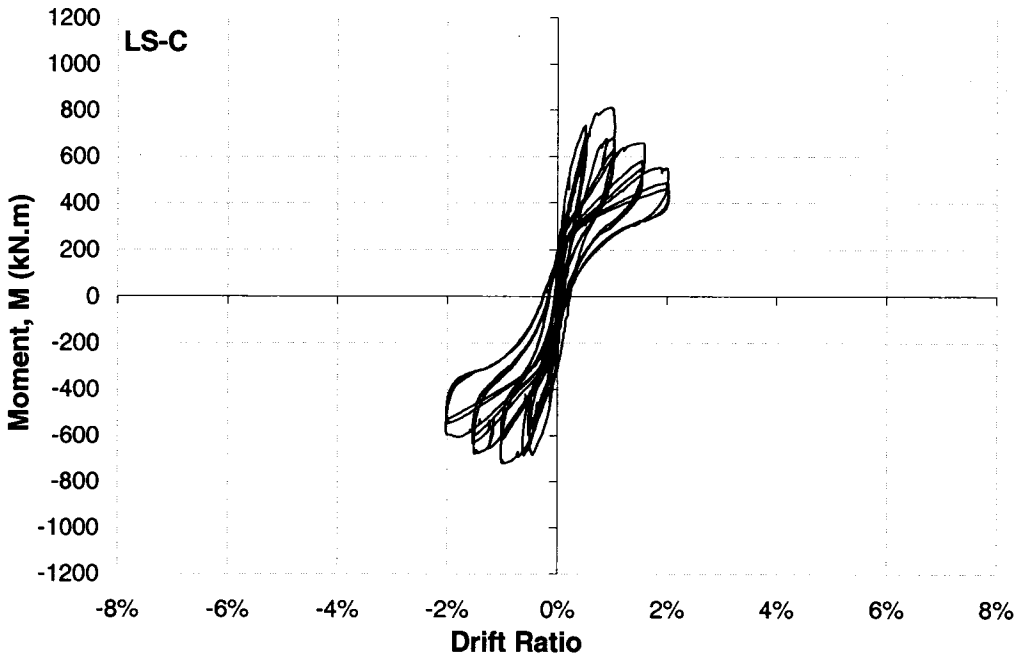

Figure 3.19 Hysteretic relationships for column LS-C (Force-drift &Moment-drift)

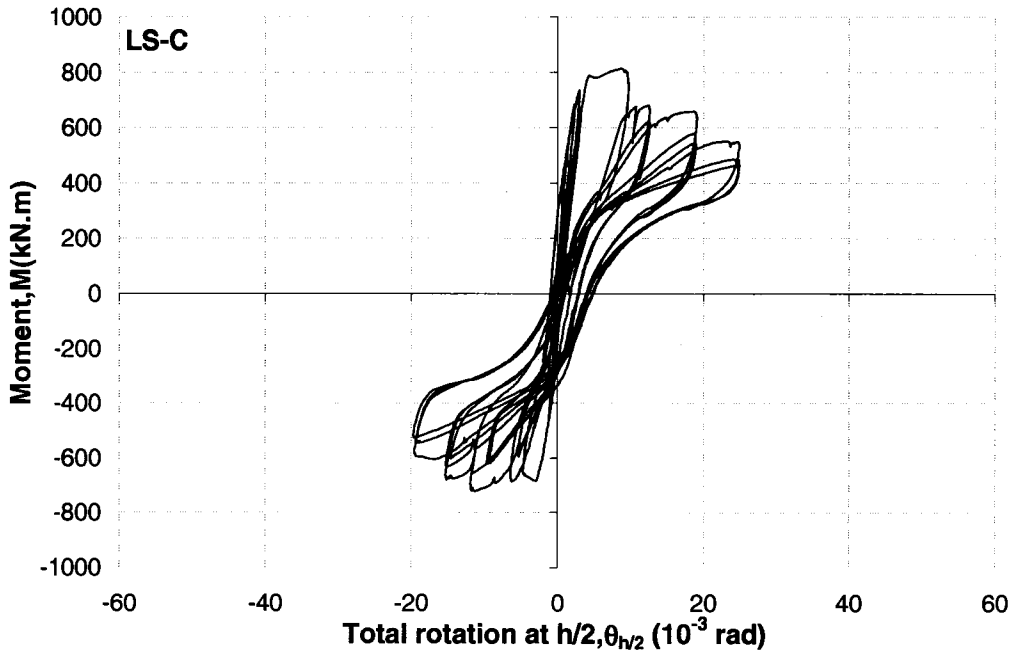

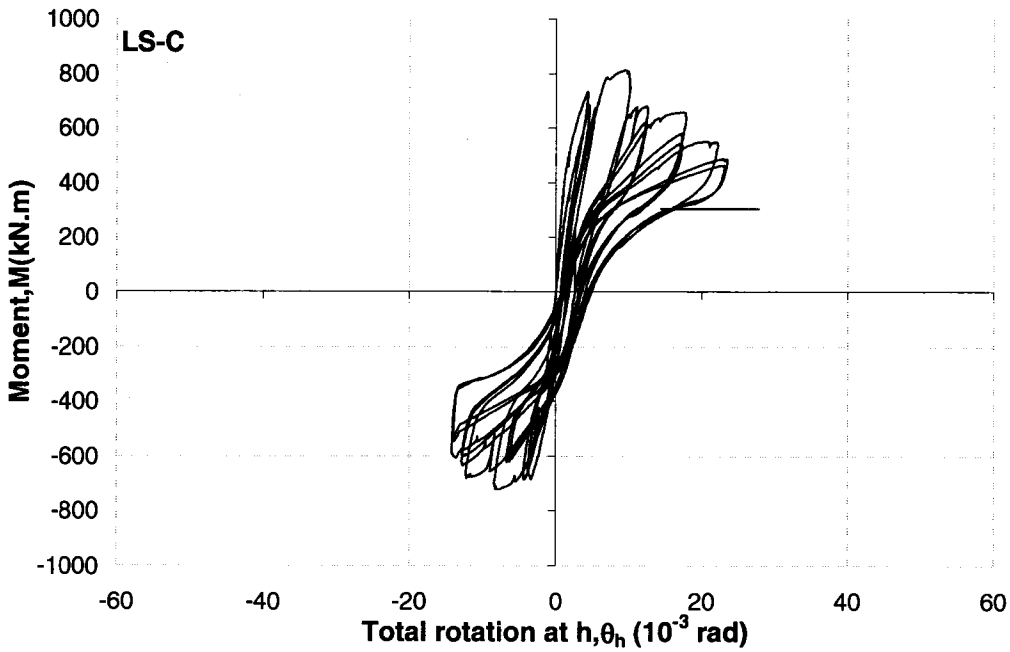

Figure 3.20 Rotation of the hinging region for column LS-C

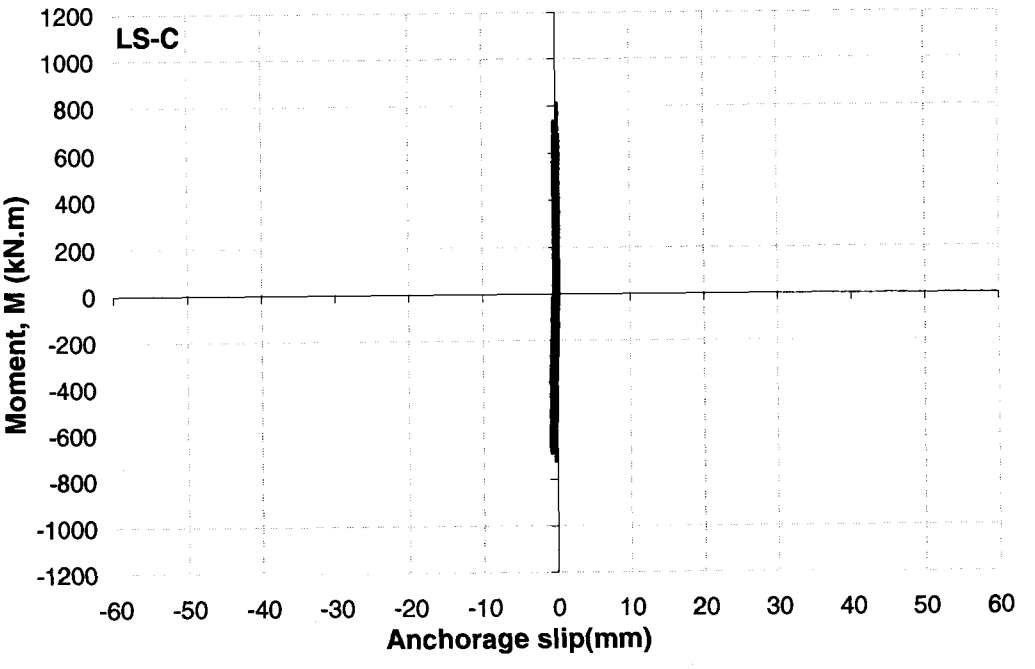

Figure 3.21 Anchorage slip at the column footing interface for column LS-C

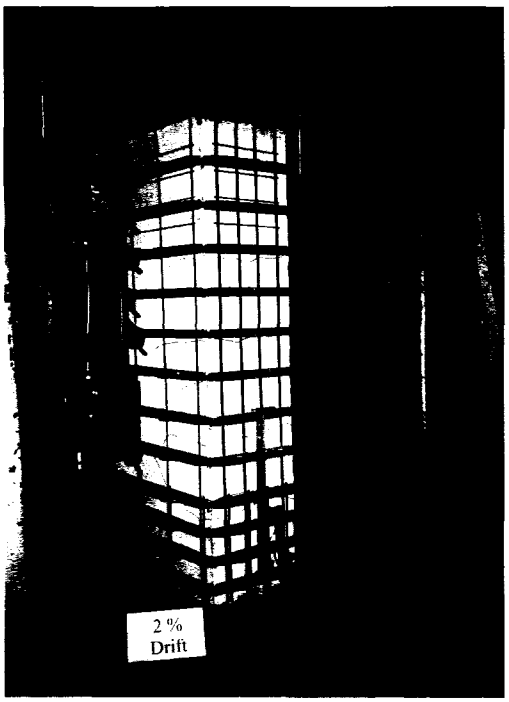

a) 2% drift

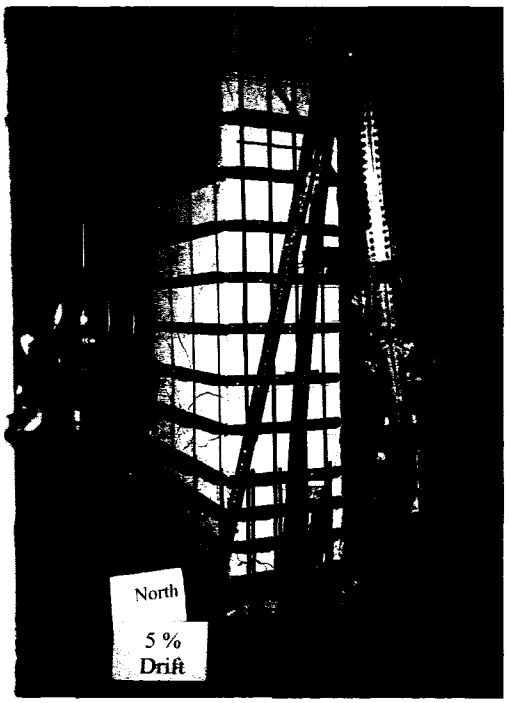

b) 5% drift

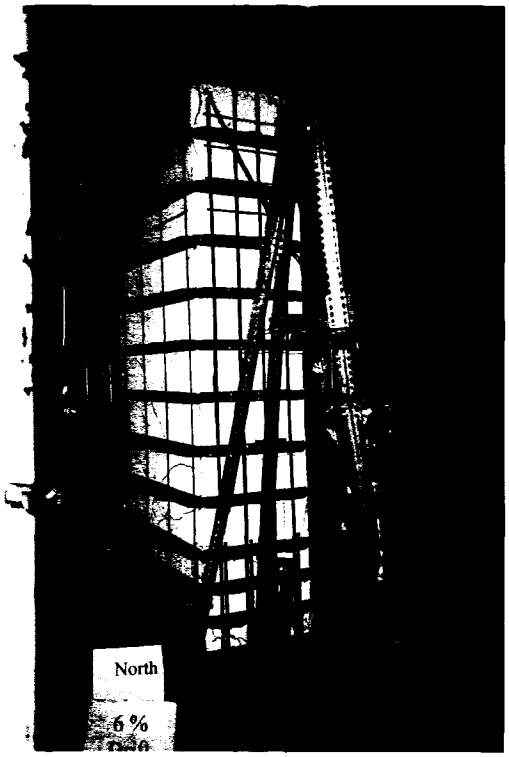

c) 6% drift

d) 6% drift

Figure 3.22 Behaviour of Column LS-R

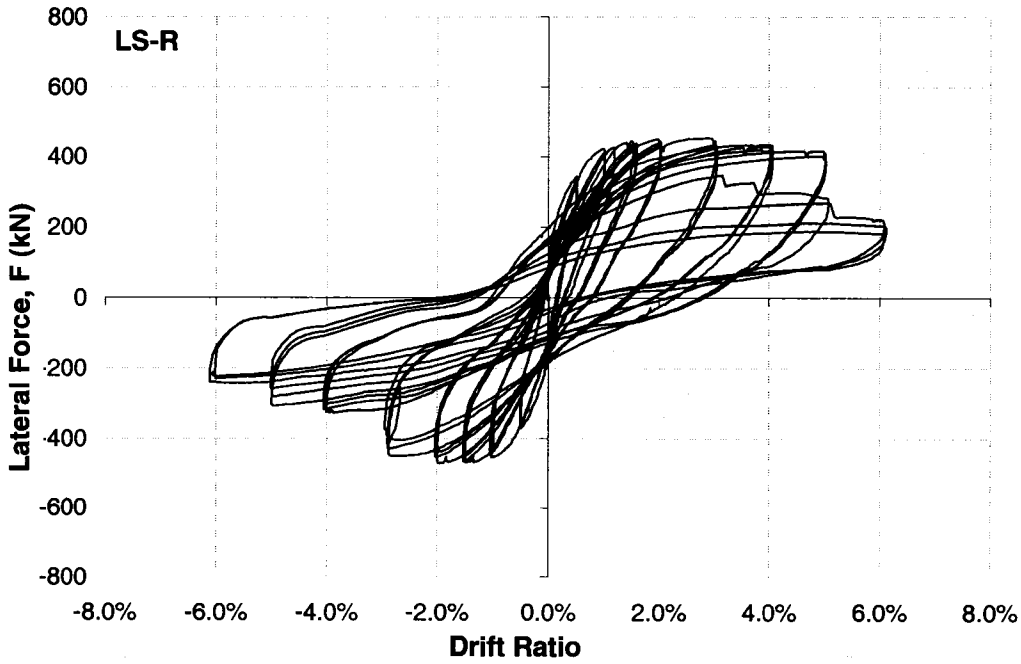

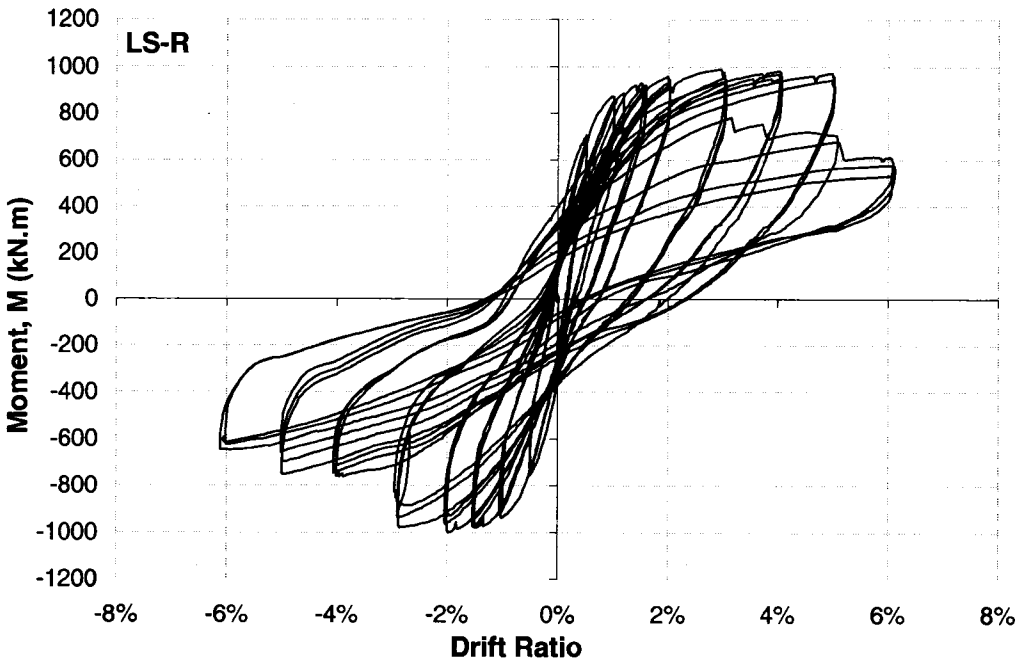

Figure 3.23 Hysteretic relationships for column LS-R (Force-drift &Moment-drift)

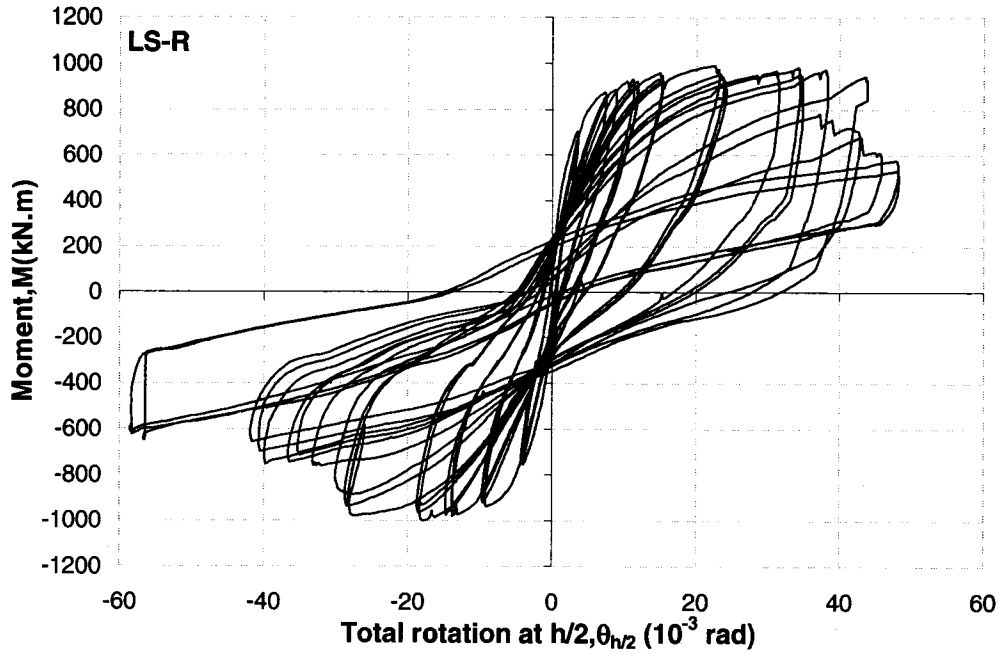

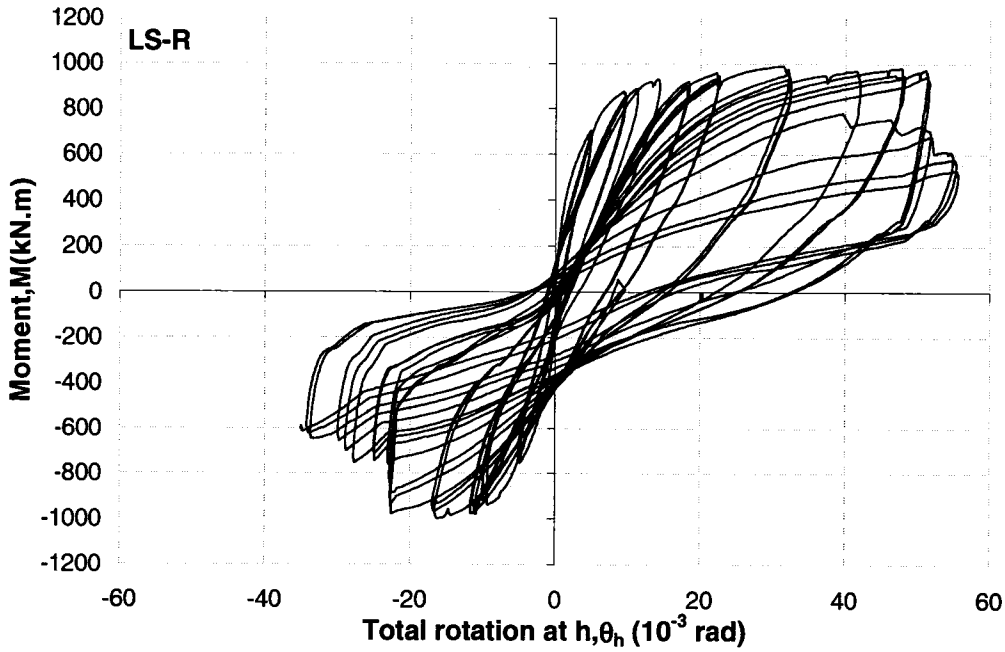

Figure 3.24 Rotation of the hinging region for column LS-R

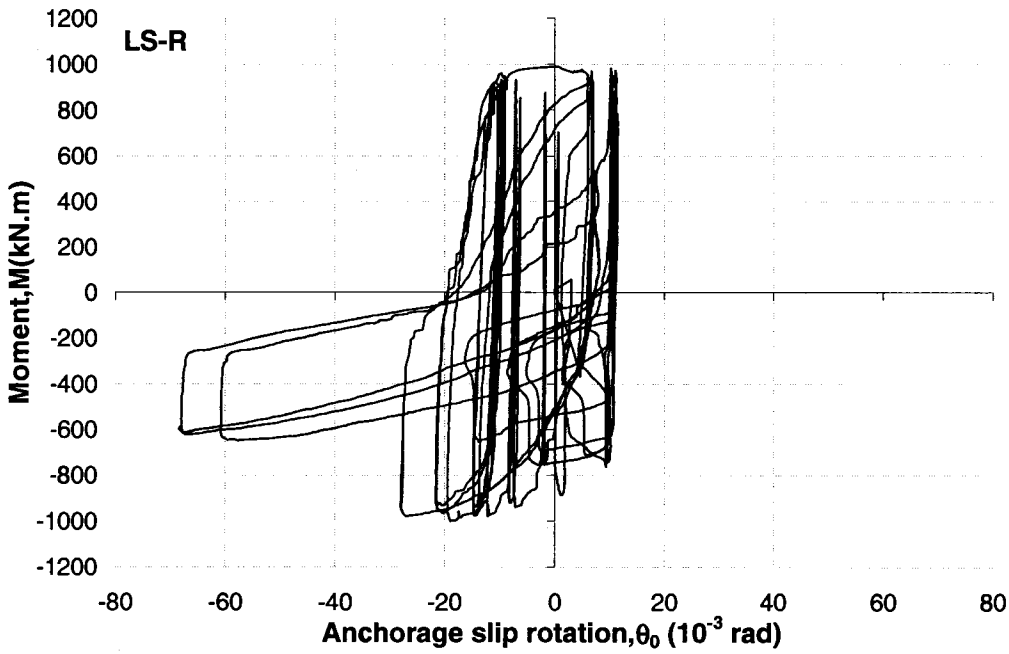

Figure 3.25 Anchorage slip at the column footing interface for column LS-R

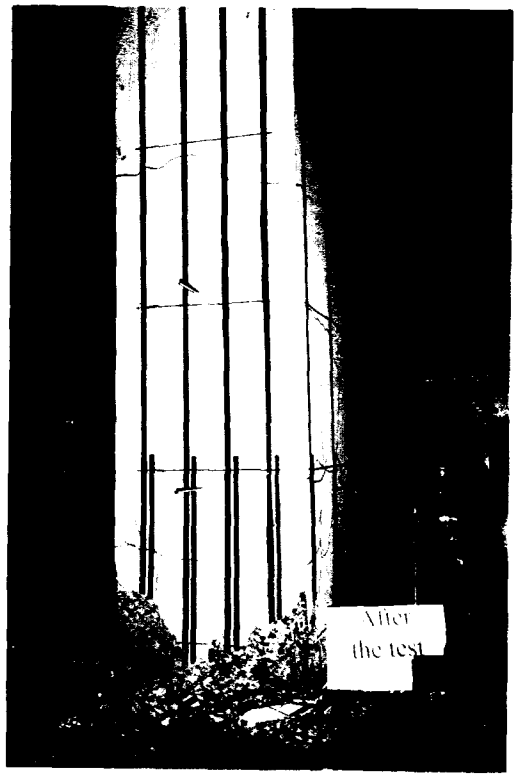

a) Control column after the test (2% drift)

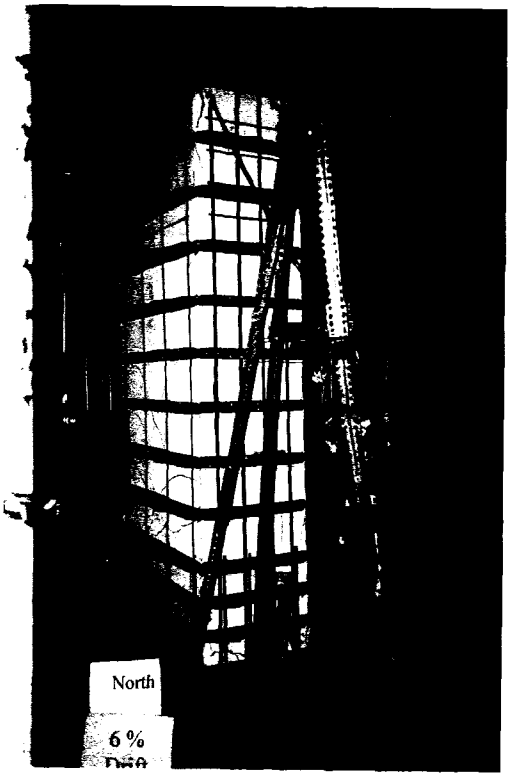

b) Retrofitted column (6% drift)

c) Control column after the test (2% drift)

d) Retrofitted Column (6 % drift)

Figure 3.26 Comparison of columns LS-C and LS-R

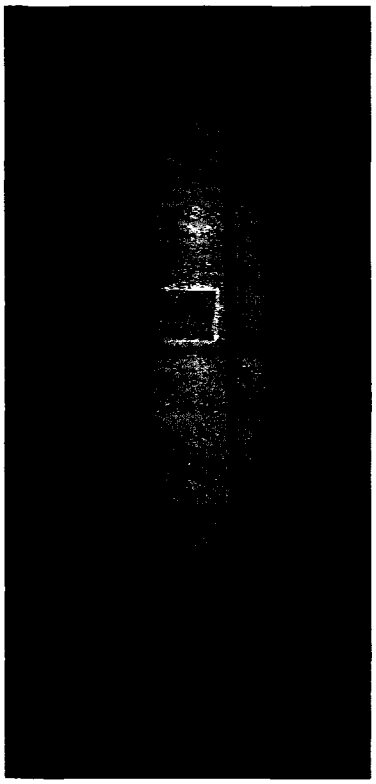

a) 0.5% drift

b) 1% drift

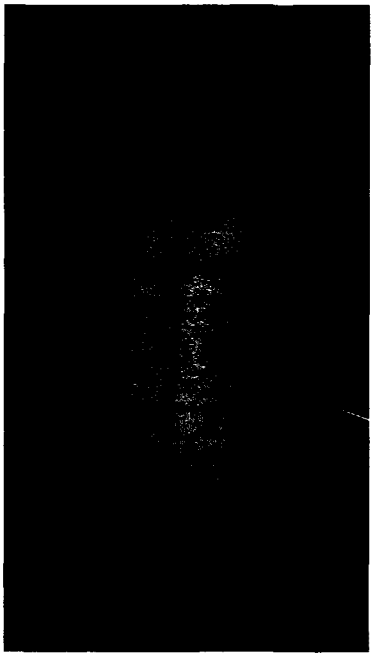

c) 1.5 % drift

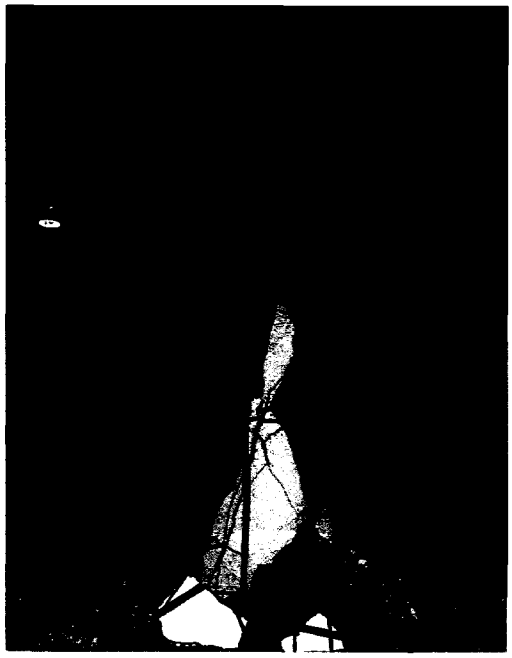

d) After the test

Figure 3.27 Behaviour of Column CR-C

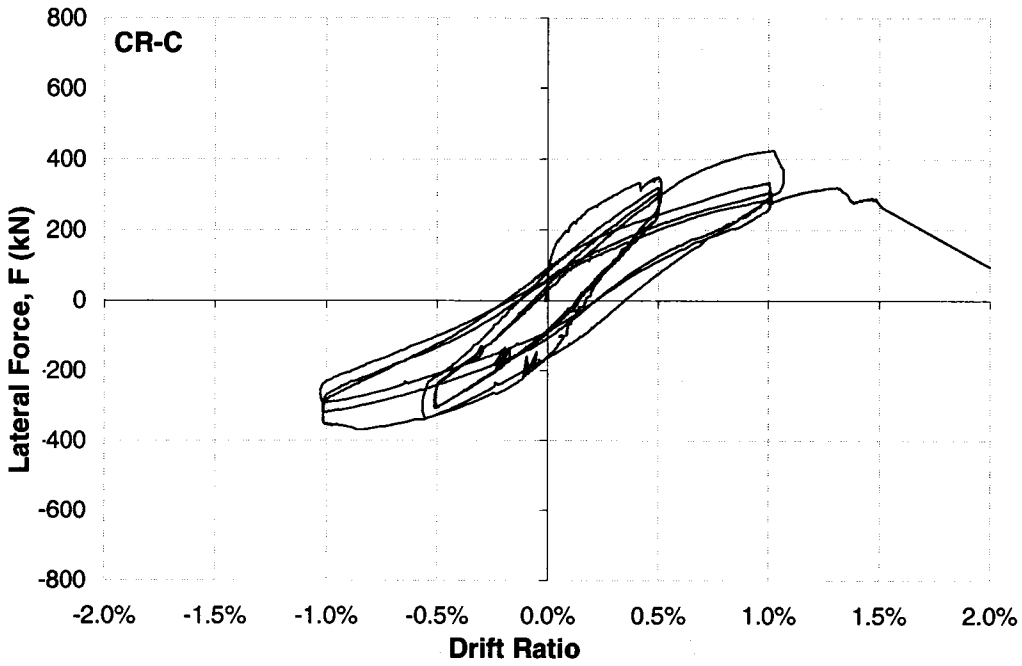

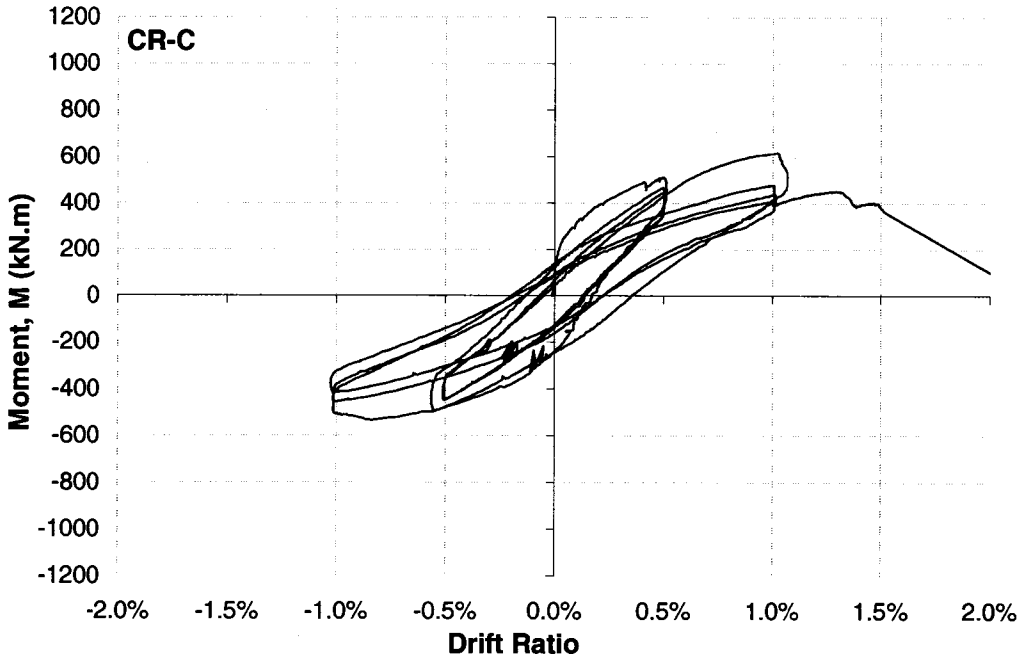

Figure 3.28 Hysteretic relationships for column CR-C (Force-drift &Moment-drift)

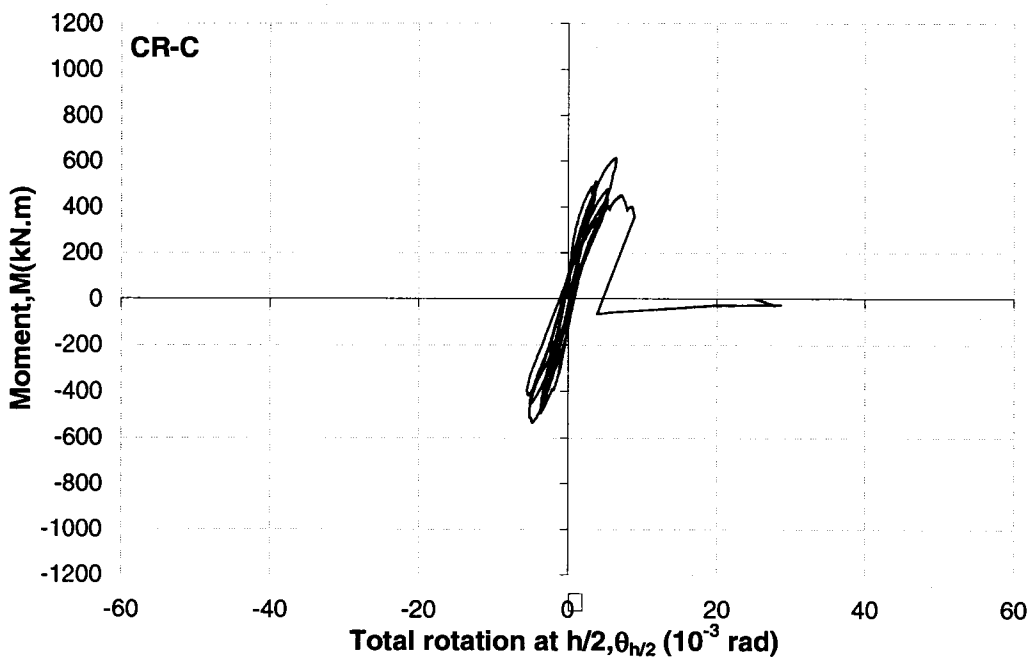

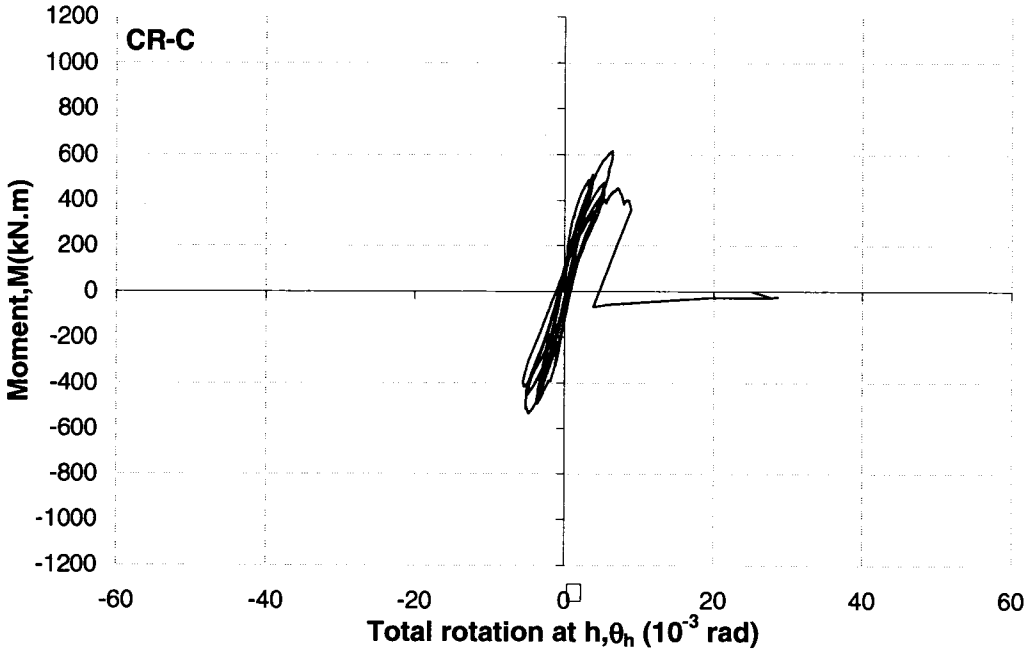

Figure 3.29 Rotation of the hinging region for column CR-C

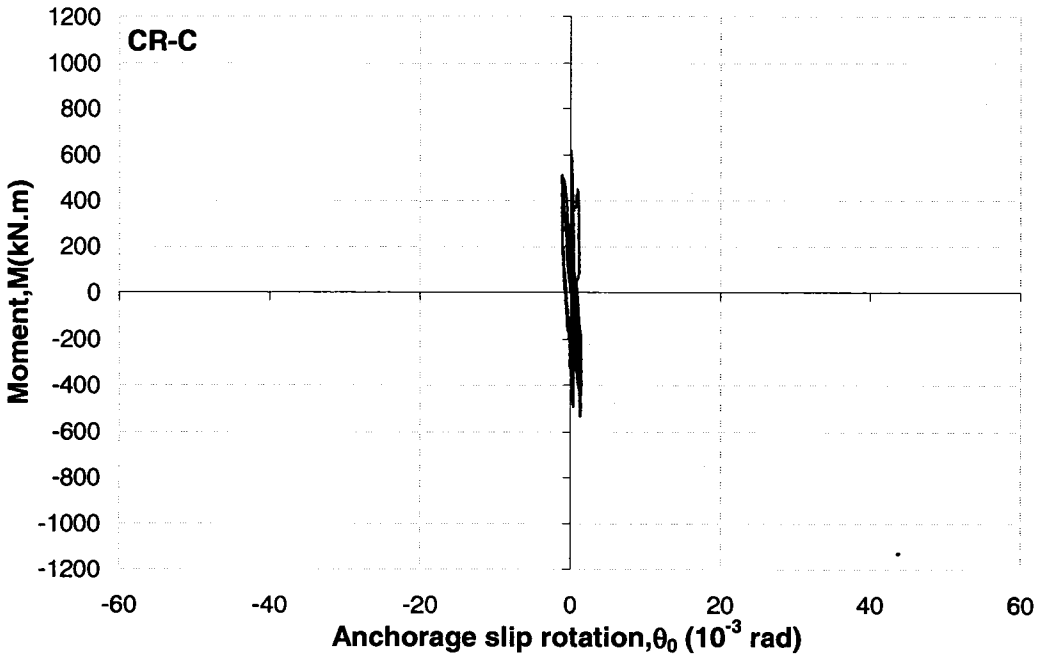

Figure 3.30 Anchorage slip at the column footing interface for column CR-C

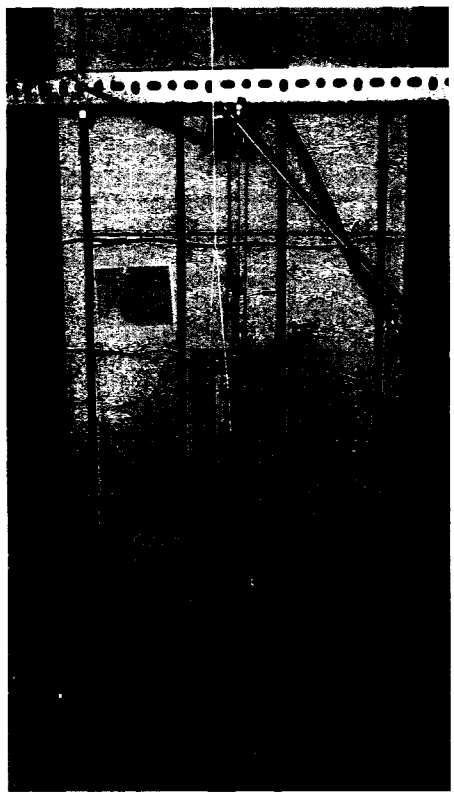

a) 0.5% drift

b) 1% drift

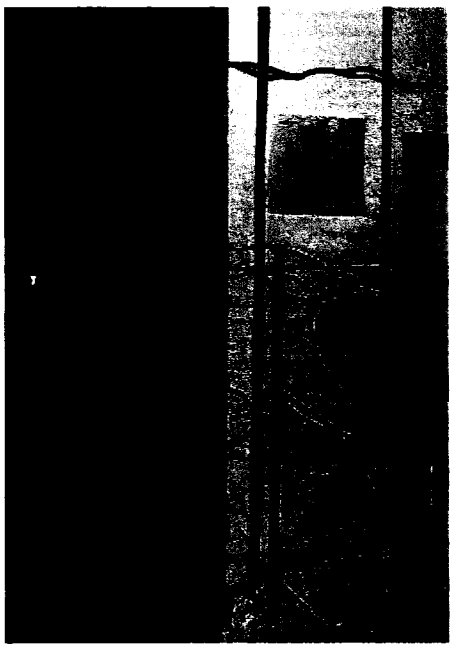

c) 1.5% drift

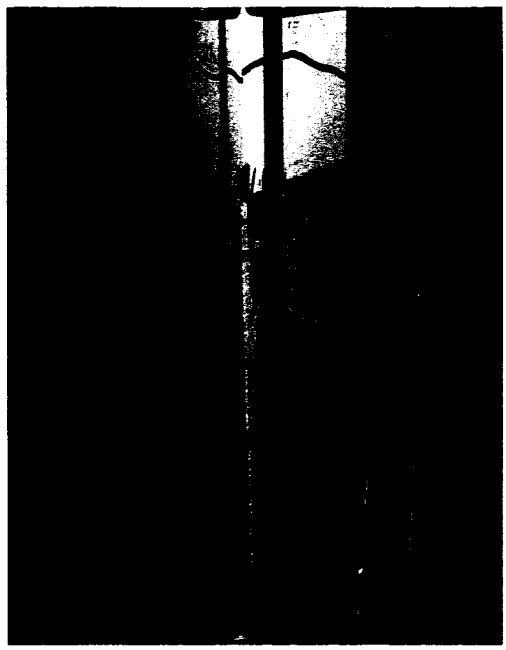

d) 1.5% drift

Figure 3.31 Behaviour of Column SSR-C

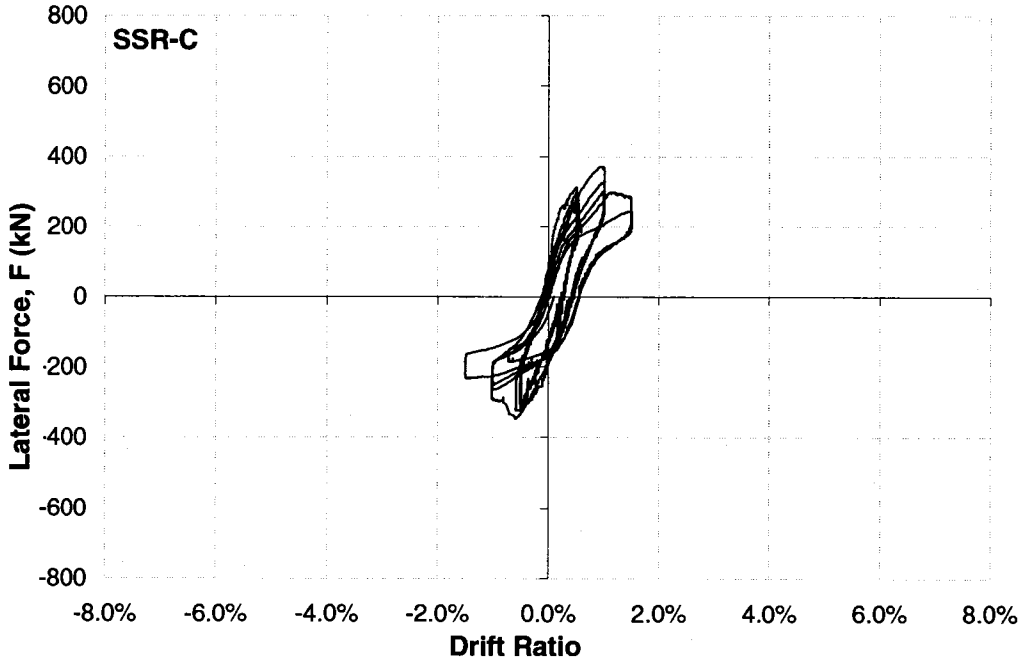

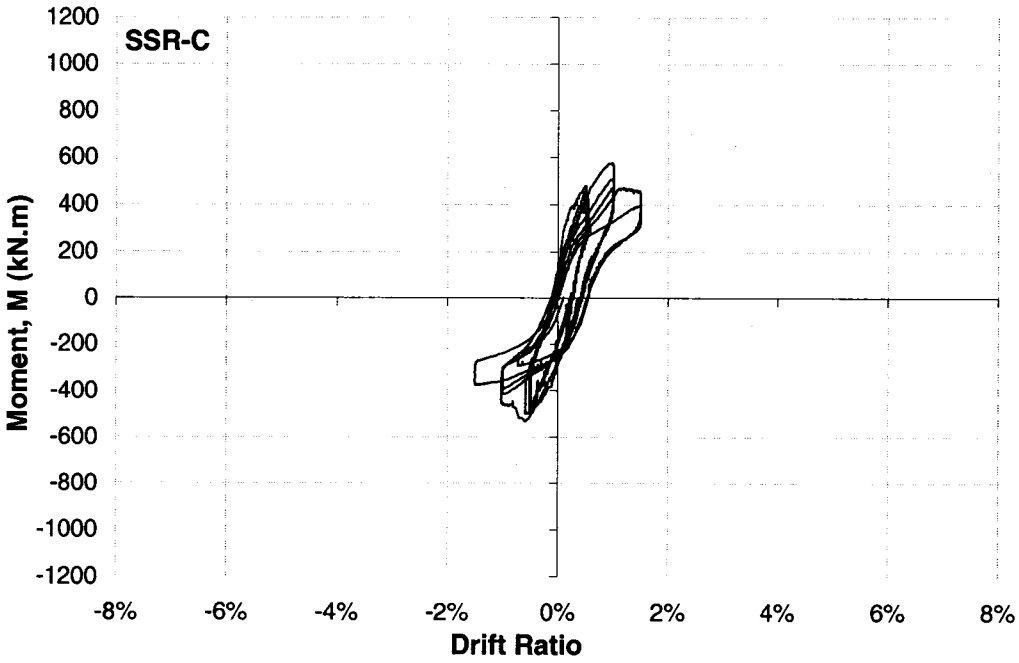

Figure 3.32 Hysteretic relationships for column SSR-C (Force-drift &Moment-drift)

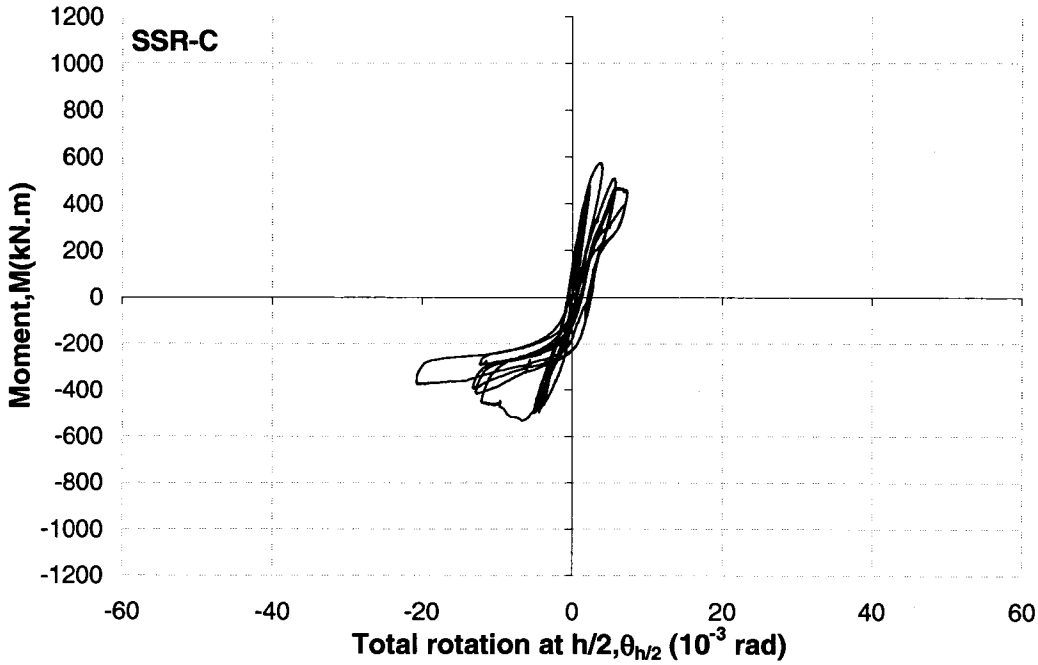

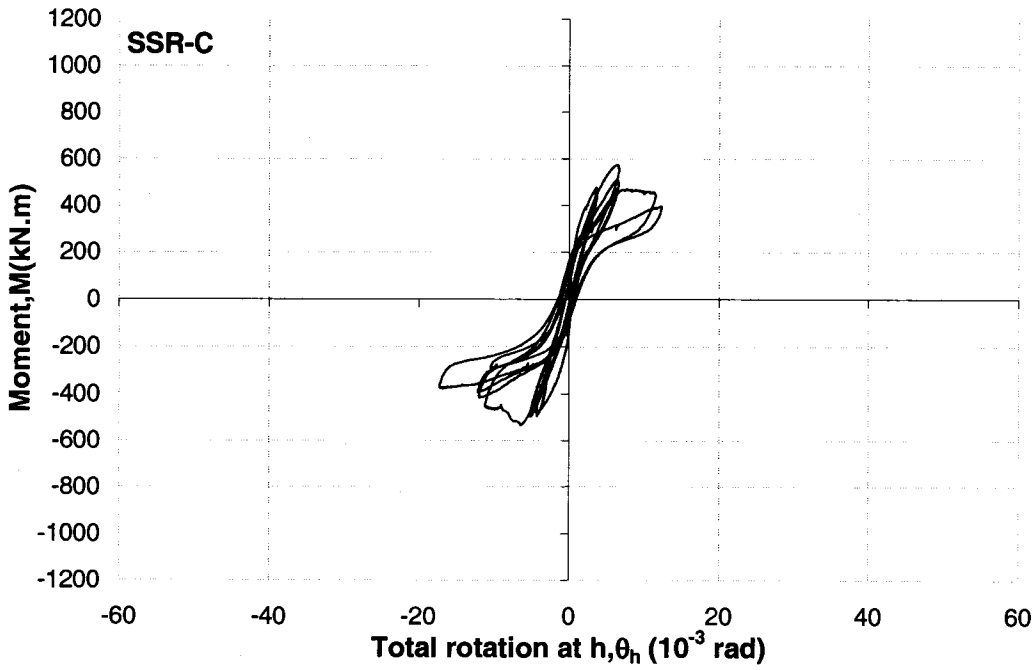

Figure 3.33 Rotation of the hinging region for column SSR-C

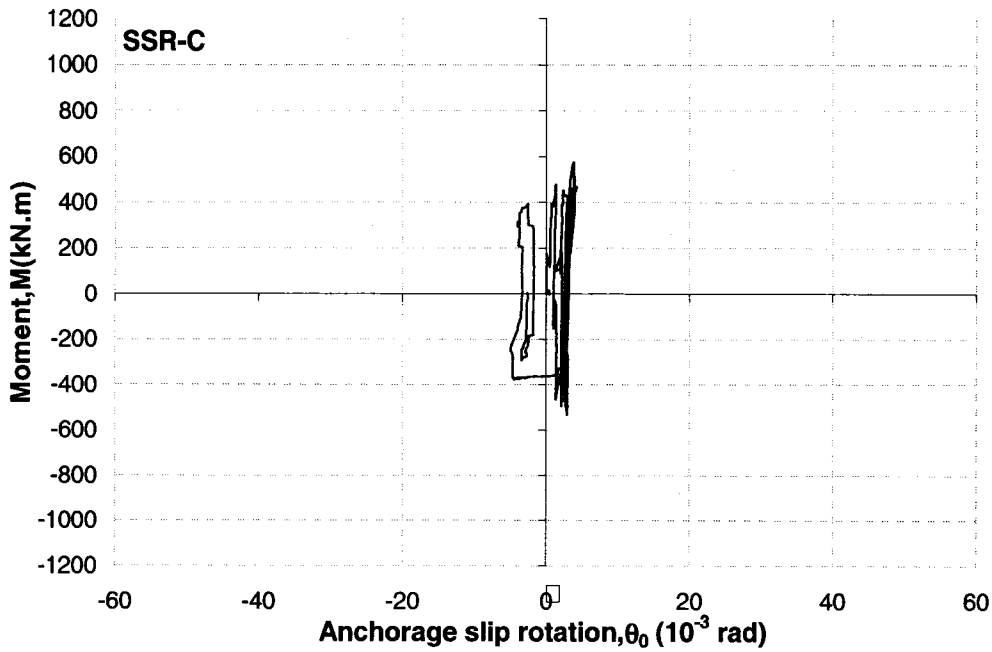

Figure 3.34 Anchorage slip at the column footing interface for column SSR-C

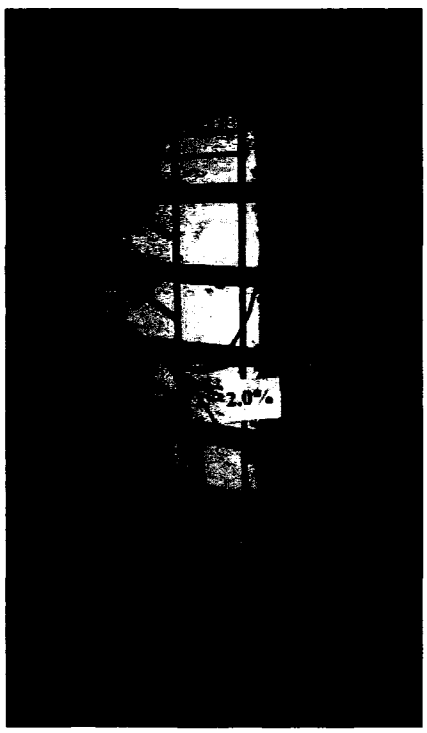

a) 2% drift

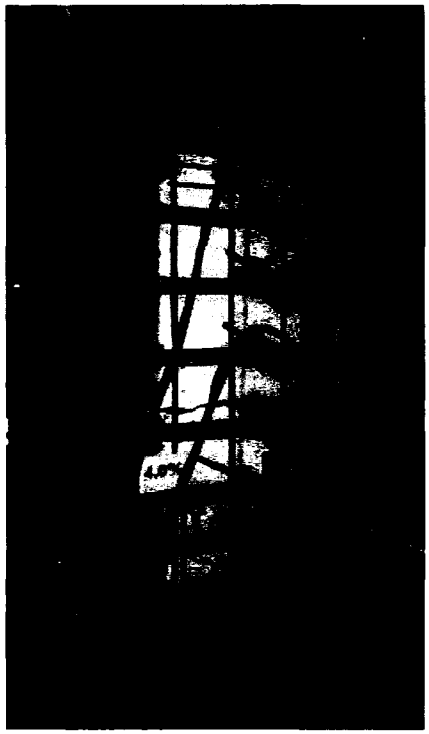

b) 4% drift

a) 9% drift

b) 10% drift

Figure 3.35 Behaviour of Column SSR-R

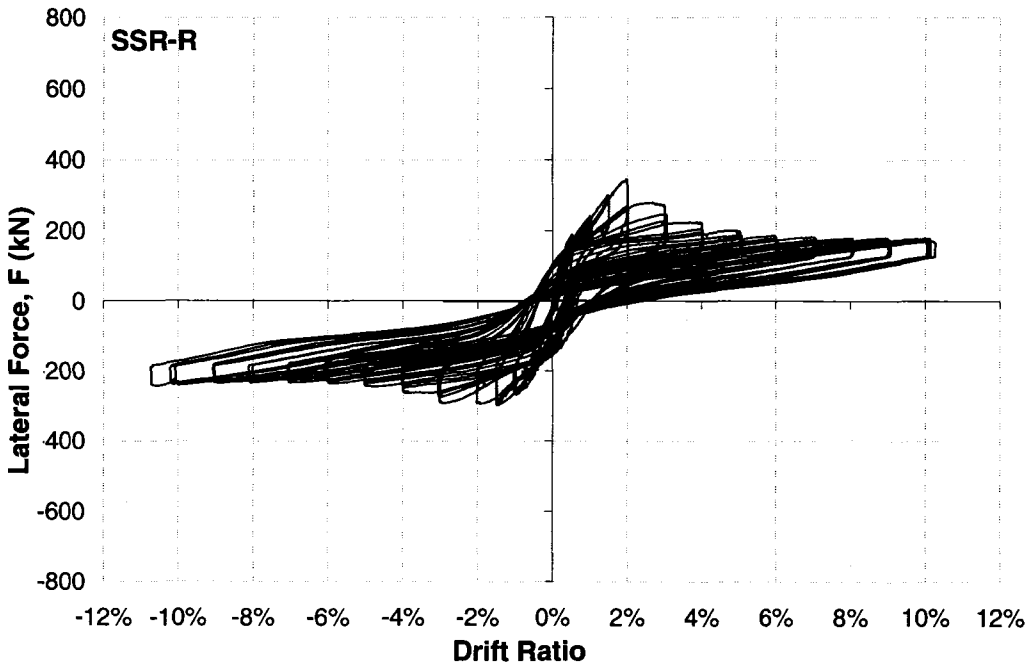

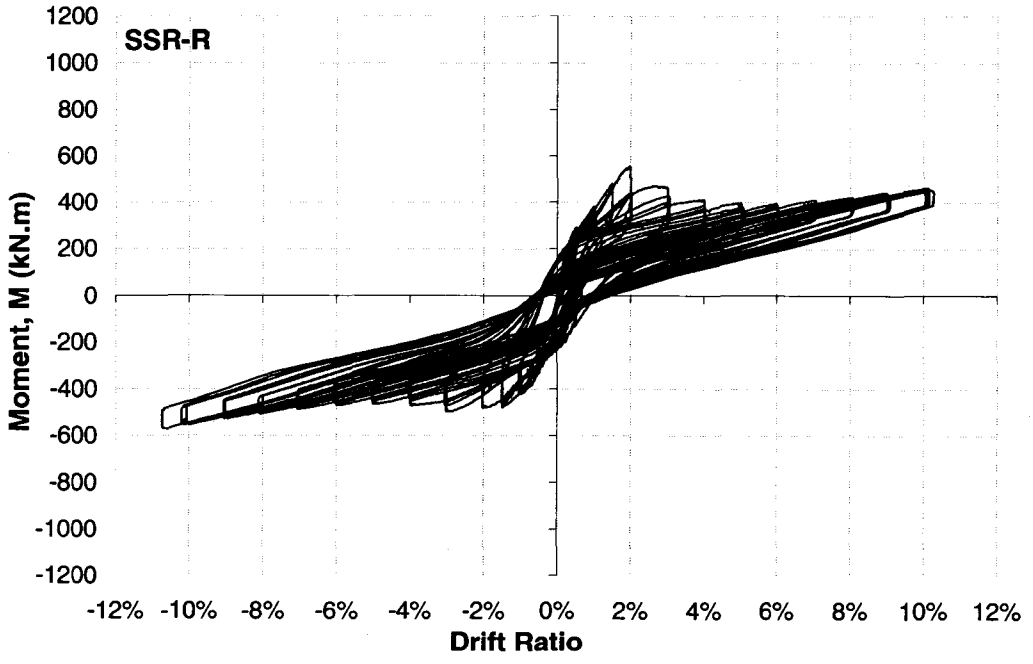

Figure 3.36 Hysteretic relationships for column SSR-R (Force-drift &Moment-drift)

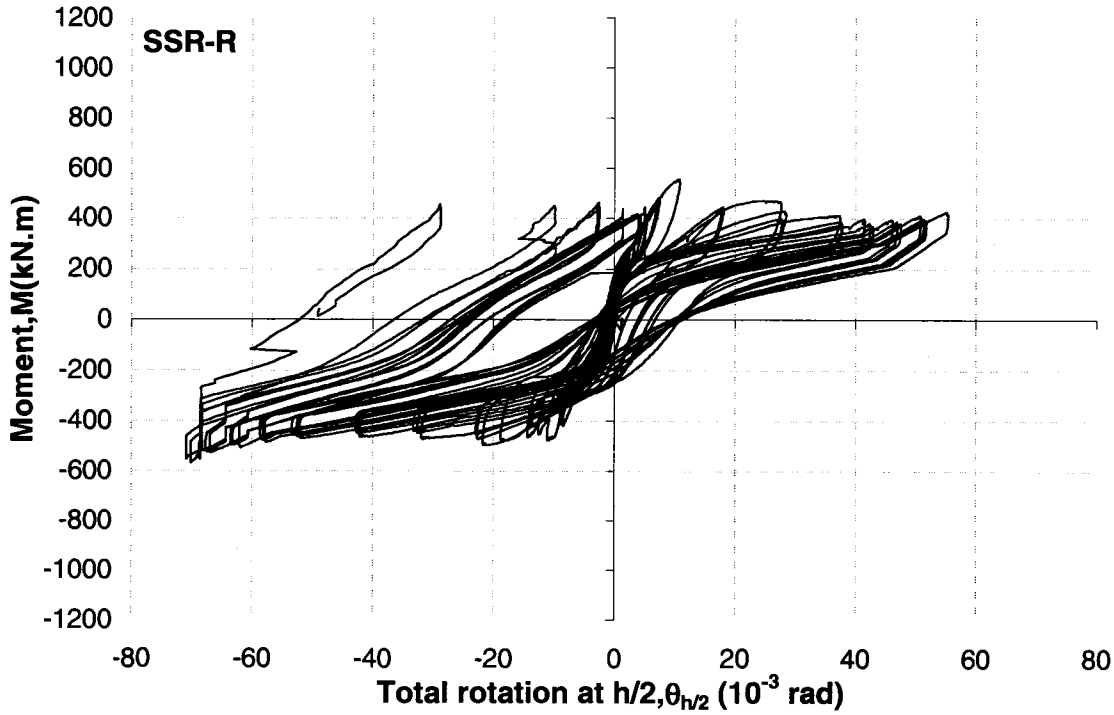

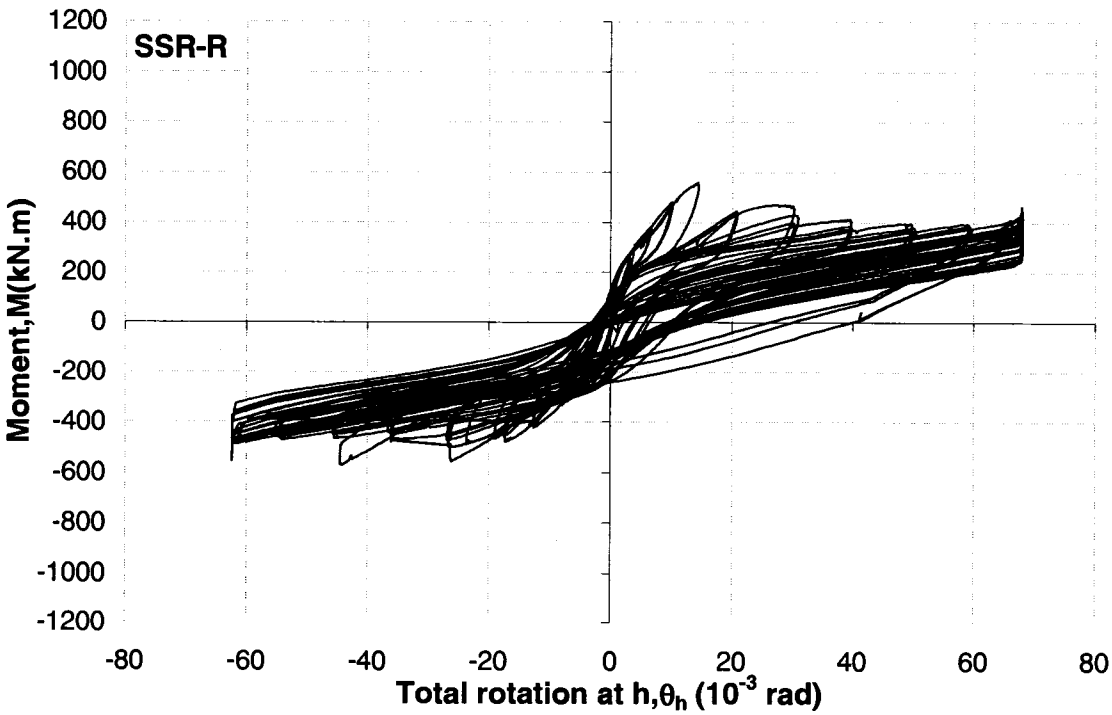

Figure 3.37 Rotation of the hinging region for column SSR-R

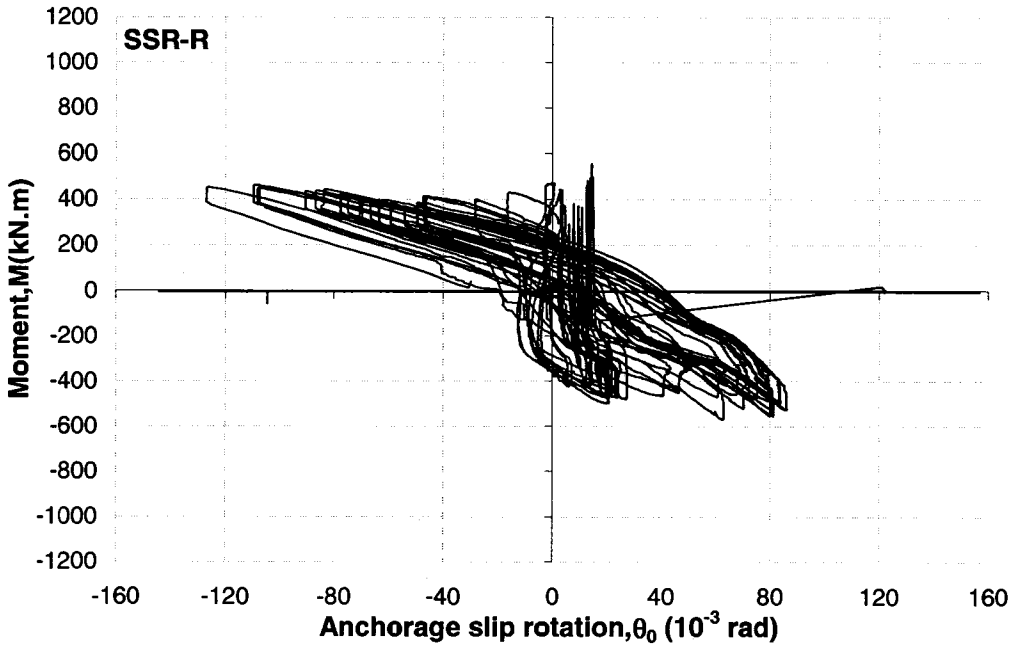

Figure 3.38 Anchorage slip at the column footing interface for column SSR-R

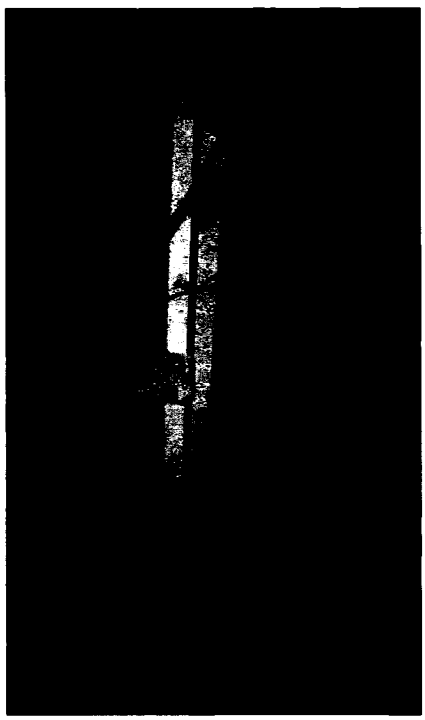

a) 0.5% drift

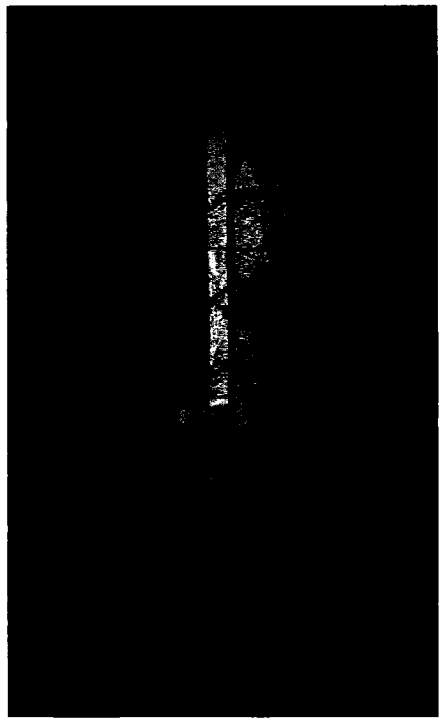

b) 1% drift

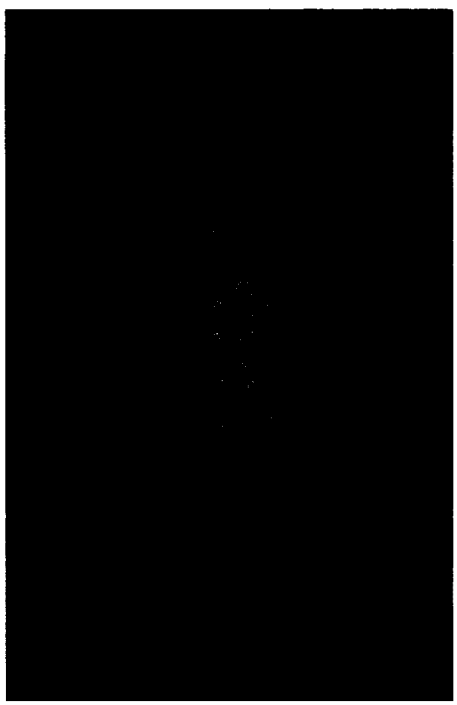

a) 1% drift

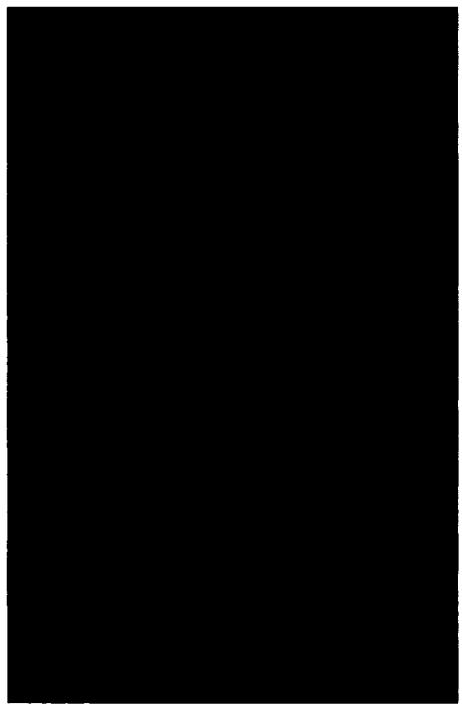

b) 1% drift

Figure 3.39 Behaviour of Column RR-C

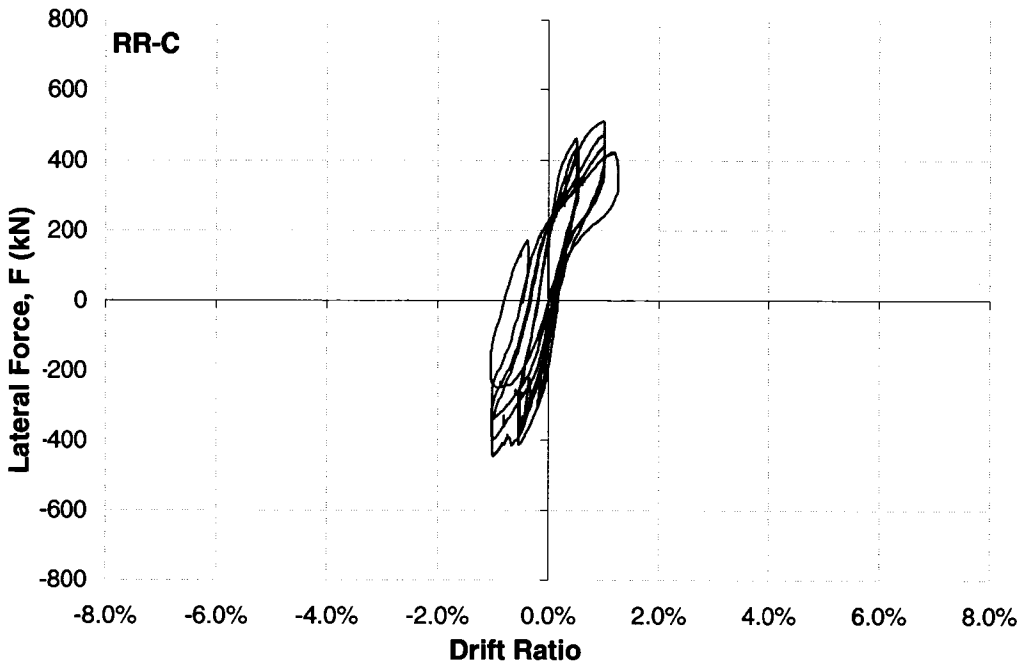

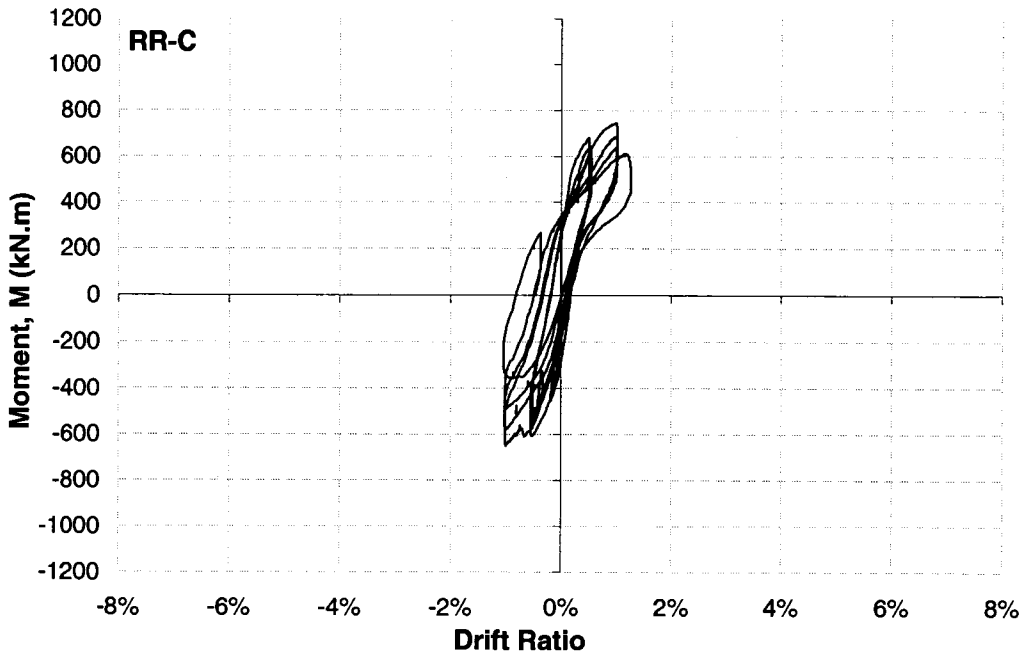

Figure 3.40 Hysteretic relationships for column RR-C (Force-drift &Moment-drift)

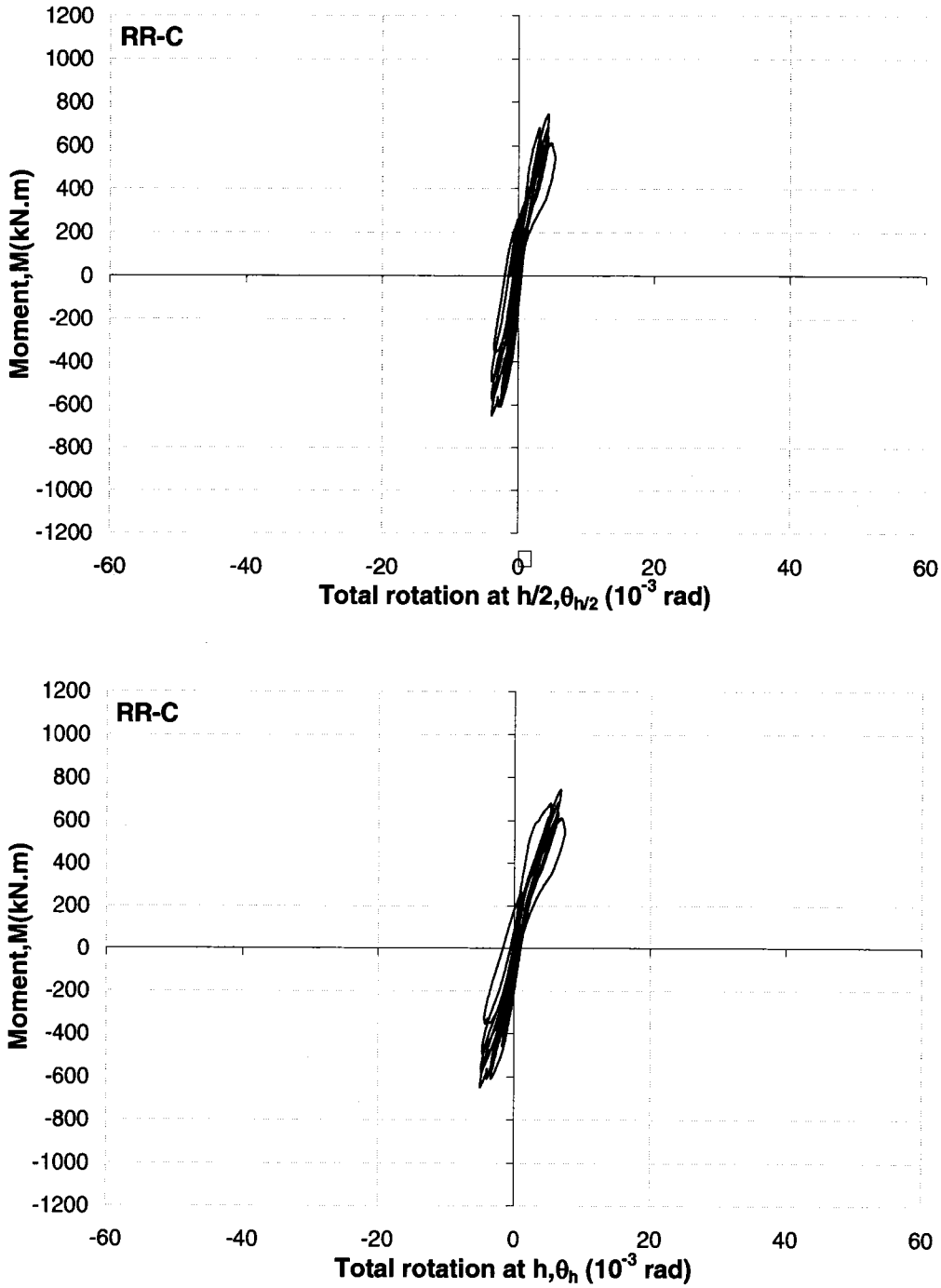

Figure 3.41 Rotation of the hinging region for column RR-C

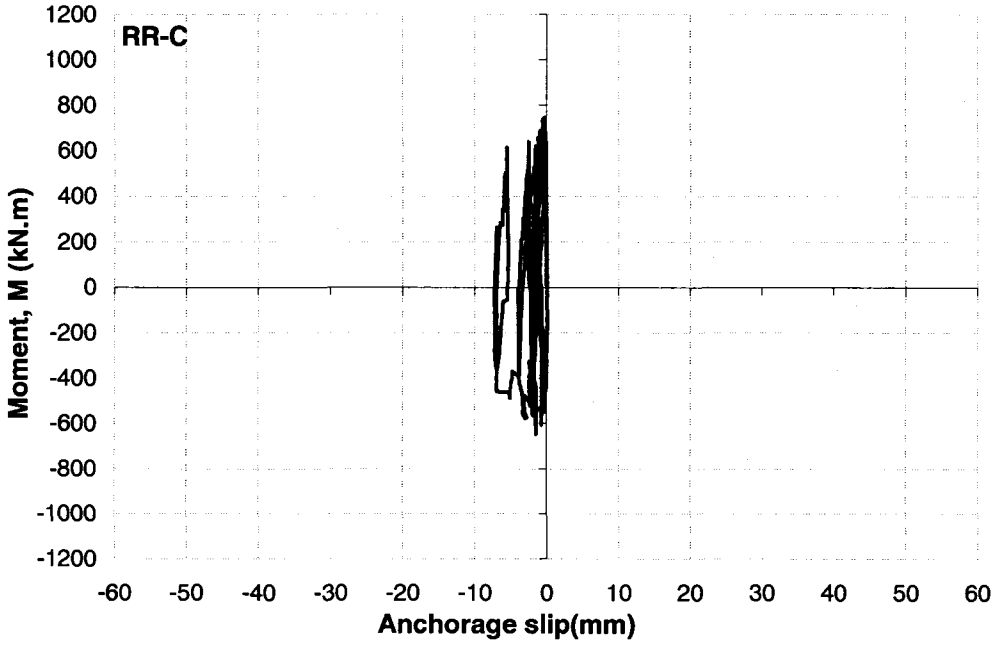

Figure 3.42 Anchorage slip at the column footing interface for column RR-C

a) 3% drift

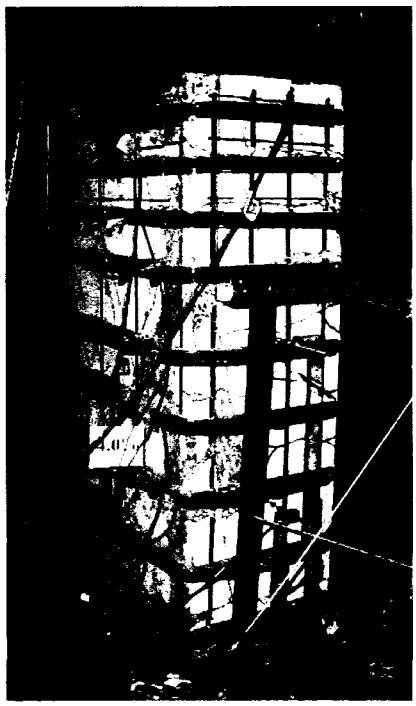

b) 4% drift

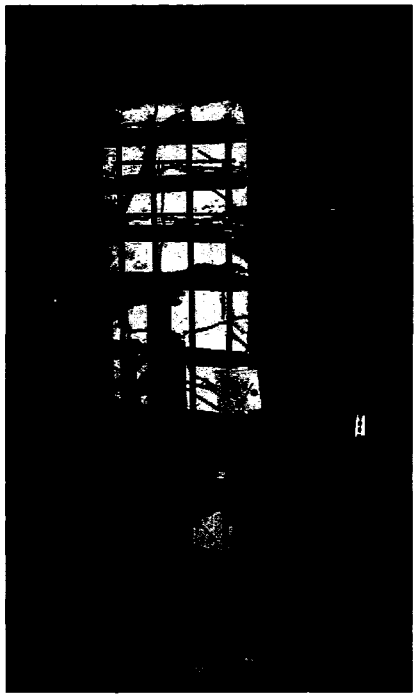

a) 5% drift

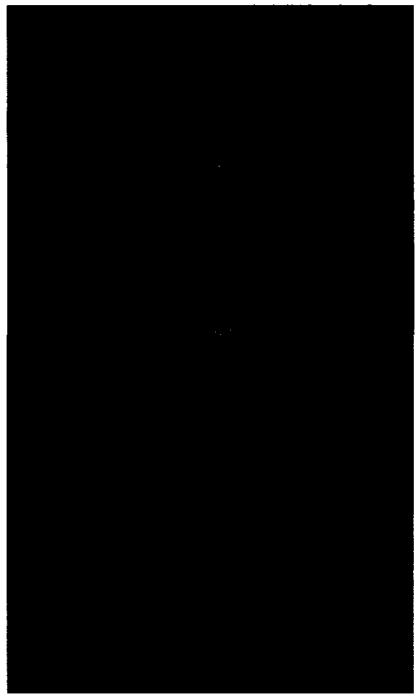

b) 6% drift

Figure 3.43 Behaviour of Column RR-R

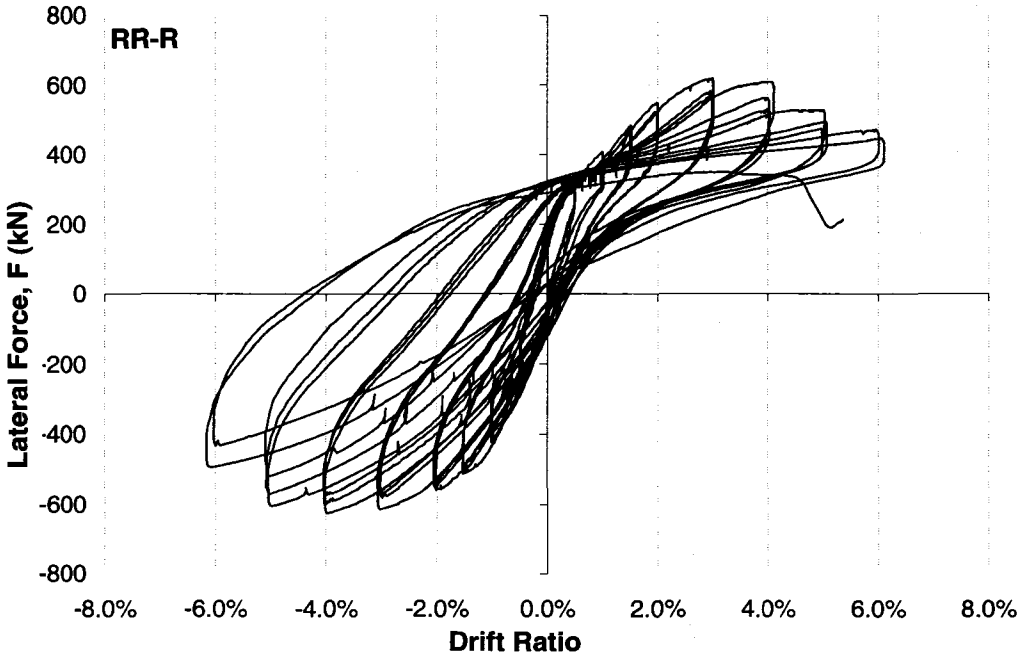

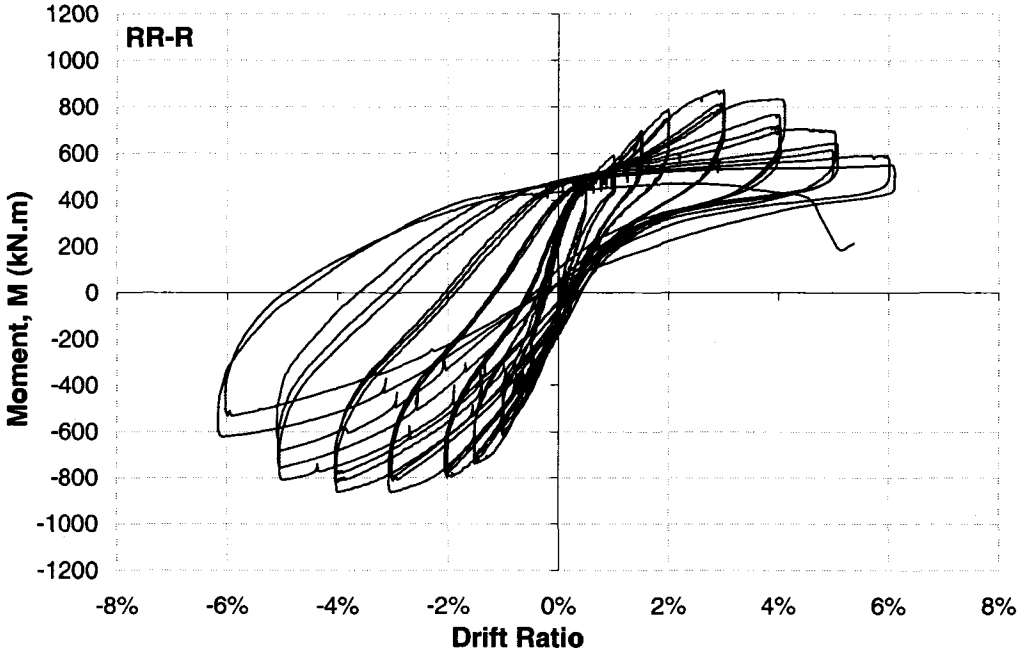

Figure 3.44 Hysteretic relationships for column RR-R (Force-drift &Moment-drift)

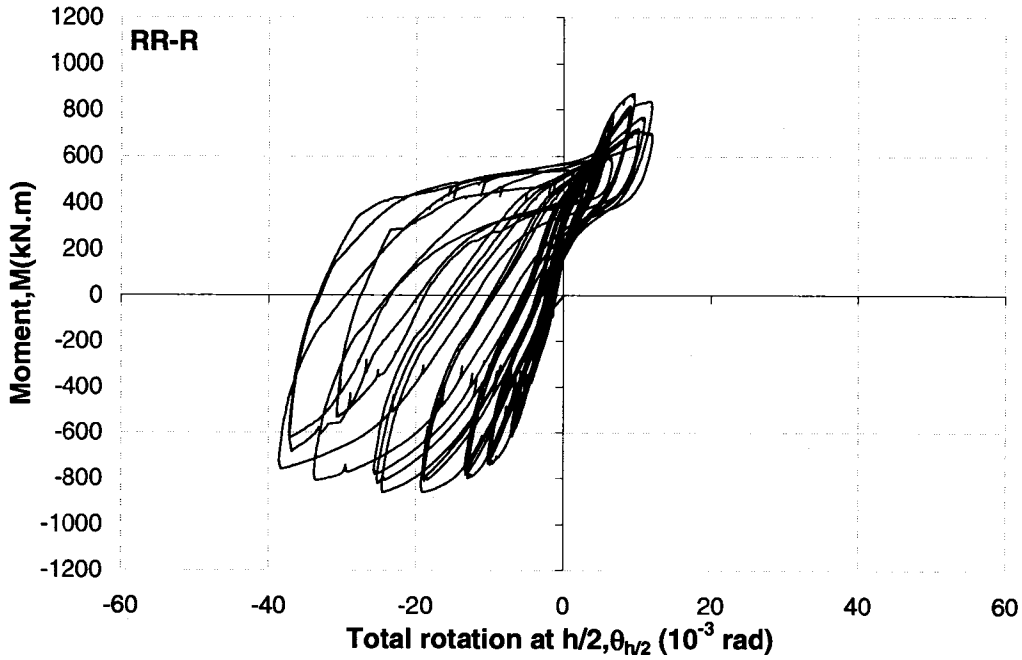

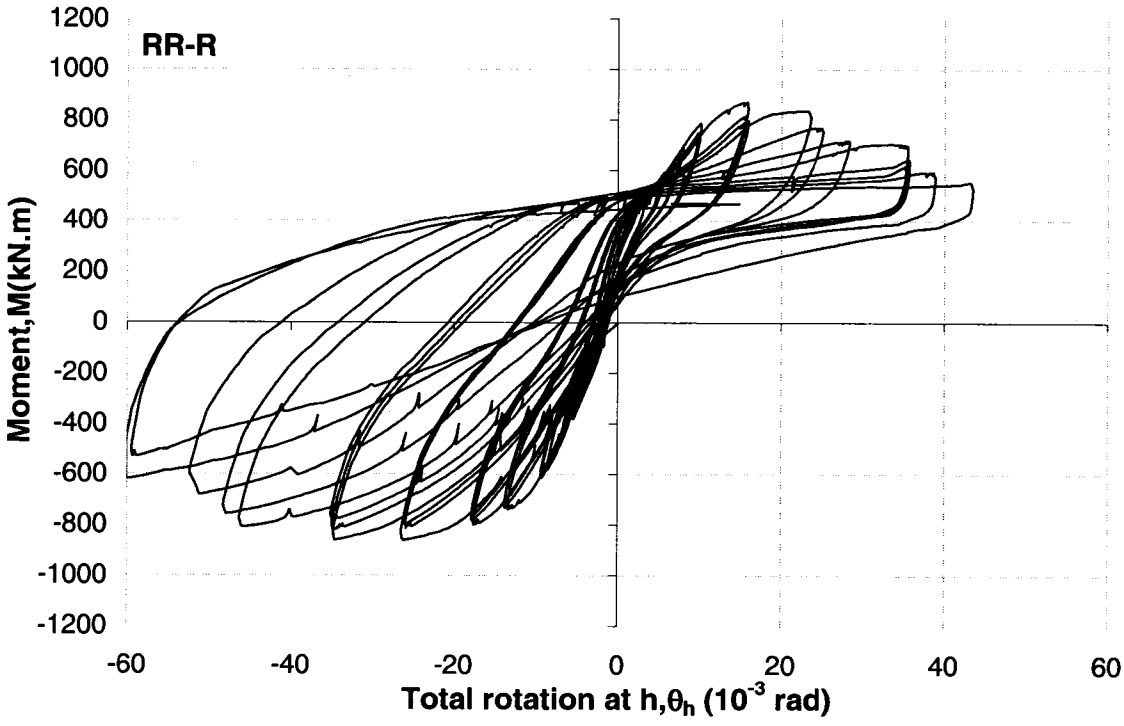

Figure 3.45 Rotation of the hinging region for column RR-R

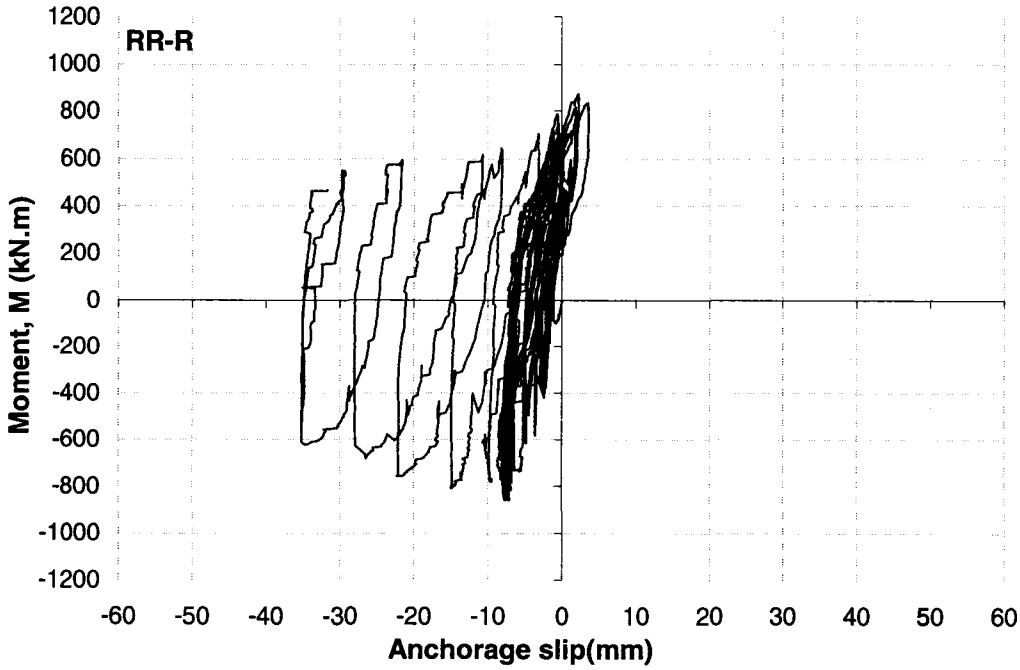

Figure 3.46 Anchorage slip at the column footing interface for column RR-R

a) Installation of raiser frames

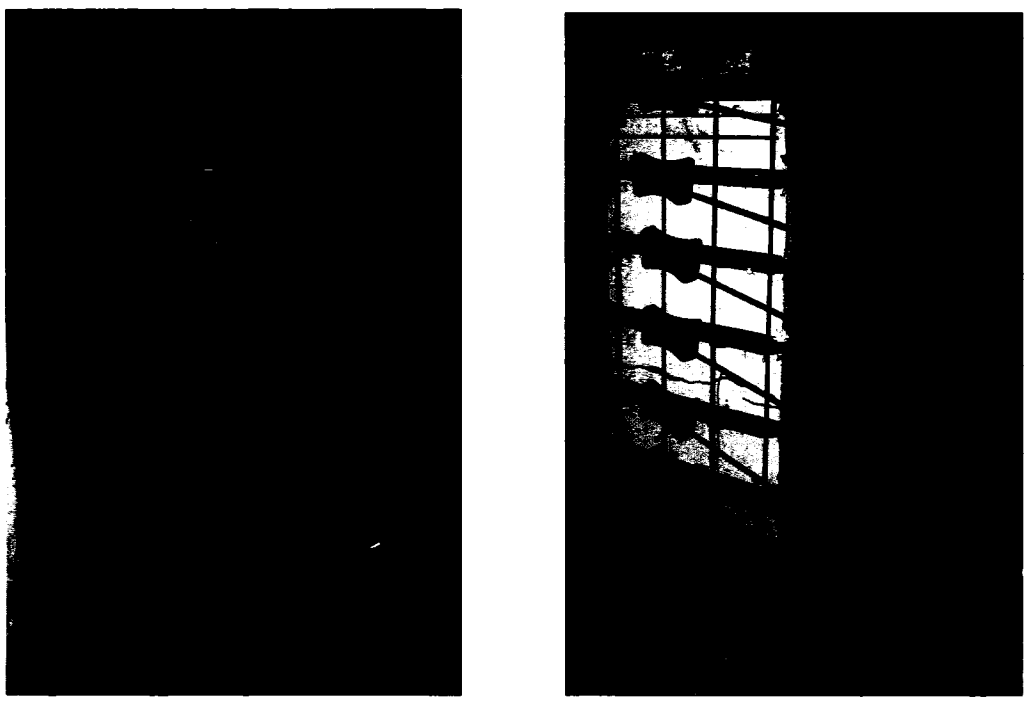

b) Installation of prestressing strands

Figure 3.47 Installation of raiser frames and prestressing strands

Chapter 4

Analysis of Columns and Development of Retrofit and Repair Design Procedures

4.1 General

Analytical research was conducted to verify the applicability of existing analytical techniques to externally prestressed bridge columns for flexure and shear. It also included the development of design procedures for column retrofit and repair using the Retro-belt technology. A computer program was developed to conduct flexural analyses of columns. The program employed the plane-section analysis to generate sectional response within the entire range of inelastic deformations. This necessitated the incorporation of existing material models, including a confined concrete model which was adapted to incorporate the effects of active confinement pressure caused by transverse prestressing. The sectional analysis resulted in the construction of moment-curvature relationships, which were used to conduct member analysis to establish moment-lateral drift relationships. The effects of yield penetration into column footing, which led to anchorage slippage, were also incorporated into the flexural analysis.

The columns tested were further analyzed using the available analytical techniques for shear. North American code approaches were considered for this purpose, including the Modified Compression Field Theory, with appropriate modifications to account for the presence of transverse prestressing. The analysis results provided the verification of analytical techniques for use in practice.

The last task in research involved the extension of the retrofit design procedures developed earlier for concrete confinement, shear resistance and lap splice deficiencies in circular and square columns to columns with rectangular sections. The design methodology was further extended to develop a design procedure for repairing damaged columns. The results of analytical research, including recommended design procedures are presented in this Chapter.

4.2 Flexural Analysis

Flexural analysis of columns was conducted in two stages; i) column sectional analysis and ii) column member analysis.

4.2.1 Sectional Analysis for Flexure

Standard plane-section analysis of reinforced concrete sections was conducted by using the assumption of plane sections before bending remaining plane after bending, enabling a linear relationship between sectional strains across the depth of a section. The contribution of tension concrete to sectional capacity was neglected. Material constitutive models were used to establish the relationships between strains and stresses for concrete and reinforcing steel. A computer program was developed to carry out the iterative process required to compute moment resistance corresponding to different strain profiles, enabling the computation of moment-curvature relationships throughout the entire range of inelastic deformations.

Confined Concrete Model

An important aspect of the retrofit and repair strategy was to improve the confinement of compression concrete to enhance inelastic deformability. Therefore, it was essential to adopt an appropriate constitutive model for confined concrete. The model

proposed by Saatcioglu and Razvi (1992) was incorporated into the computer software for this purpose. This model was developed to construct the stress-strain relationship of confined concrete on the basis of the concept of equivalent uniform confinement pressure. The model is applicable to normal strength concrete, though a modified version (1999) of the same model is also available for high-strength concrete. It incorporates the relevant parameters of confinement, such as the type, volumetric ratio, spacing, yield strength and arrangement of transverse reinforcement, as well as the cross-sectional geometry and strength of concrete. The confined concrete strength and corresponding strain are expressed in terms of equivalent uniform confinement pressure provided by reinforcement cage. This feature is especially attractive for application to current research in which not only the passive confinement pressure had to be computed, but active pressure induced by external prestressing had to be accounted for. Figure 4.1 shows the model, which consists of a parabolic ascending branch, followed by a linear descending segment. The model reduces to that proposed by Hognestad (1951) if the effect of confinement is negligible. The following expressions define the stress-strain relationship for ascending and descending branches, respectively.

$$f_c = f_{cc}' \left[2\left(\frac{\varepsilon_c}{\varepsilon_1}\right) - \left(\frac{\varepsilon_c}{\varepsilon_1}\right)^2 \right]^{\frac{1}{1+2K}} \qquad \varepsilon_c \le \varepsilon_{01} \qquad [4.1]$$

$$f_c = f_{co}' - (\varepsilon_c - \varepsilon_{01}) \left(\frac{0.15 f_{co}'}{\varepsilon_{085} - \varepsilon_{01}} \right) \qquad \varepsilon_{01} < \varepsilon_c \le \varepsilon_{cu} \qquad [4.2]$$

Where, f_c and ε_c are concrete stress and strain. The unconfined concrete strength in member and the corresponding strain are denoted as f_{co}' in MPa and ε_{01}. Strain at 85% of strength is denoted by ε_{085}.

Figure 4.2 illustrates the confinement pressures induced by different arrangements of column reinforcement. The confined concrete strength (f_{cc}') is computed using equivalent uniform confinement pressure in MPa (f_{le}), which is less than the average pressure (f_l) or the actual pressure peaks at corner or nodal points where transverse reinforcement legs are present. The confined concrete strength can be computed as the sum of unconfined strength in column and the incremental effect of equivalent uniform lateral pressure, as shown in Eq.

4.3. It was experimentally observed that the rate of increase in concrete strength due to lateral pressure decreases with the magnitude of pressure (Saatcioglu and Razvi 1982). This is introduced into Eq. 4.3 through coefficient k_1.

$$f_{cc}' = f_{co}' + k_1 f_{le} \quad [4.3]$$

where;

$$k_1 = 6.7(f_{le})^{-0.17} \quad [4.4]$$

$$f_{le} = k_2 f_l \quad [4.5]$$

$$f_l = \frac{\sum_{i=1}^{q}(A_{st} f_{st} \sin\alpha)_i}{sb_c} \quad [4.6]$$

$$K = \frac{k_1 f_{le}}{f_{co}'} \quad [4.7]$$

k_2 is the coefficient that relates the average confinement pressure acting on column face to equivalent uniform pressure, reflecting the efficiency of confinement reinforcement. It assumes a smaller value for widely spaced reinforcement and can reach up to 1.0 when full efficiency of concrete confinement is attained as in the case of circular hoops/spirals and closely spaced and laterally supported longitudinal reinforcement. Eqs. 4.8 and 4.9 define the confinement efficiency coefficient k_2.

$$k_2 = 0.15\sqrt{\left(\frac{b_c}{s}\right)\left(\frac{b_c}{s_l}\right)} \le 1.0 \quad \text{For rectilinear reinforcement} \quad [4.8]$$

$$k_2 = 1 \quad \text{For closely spaced circular spirals} \quad [4.9]$$

For columns with asymmetric reinforcement in two orthogonal directions, the confinement pressure in each direction may be different. For these cases, a weighted average value of equivalent uniform pressure may be used, as shown in Eq. 4.10.

$$f_{le} = \frac{f_{lex} b_{cx} + f_{ley} b_{cy}}{b_{cx} + b_{cy}} \quad [4.10]$$

f_{lex}, f_{ley} are the equivalent lateral pressures perpendicular to core dimensions b_{cx} and b_{cy} measured center to center of perimeter hoop in x and y directions, respectively.

The descending branch of the proposed model for confined concrete consists of a linear segment originating from the peak concrete stress and the corresponding strain (ε_1), sloping down to a strain (ε_{85}) corresponding to 85% of the peak stress. This linear segment continues with a decaying slope down to a strain level corresponding to 20% of the peak stress. The residual strength is then kept constant at 20% of peak strength, simulating an average contribution of damaged concrete to strength (Figure 4.1).

$$\varepsilon_1 = \varepsilon_{01}(1+5k_3k) \quad [4.11]$$

$$\varepsilon_{85} = 260k_3\rho_c\varepsilon_1(1+0.5k_2(k_4-1))+\varepsilon_{085} \quad [4.12]$$

The above model was developed for reinforced concrete elements that develop passive confinement pressures. While it could be used for the control columns tested in the experimental phase of research, it can not be used to incorporate the active pressure imposed on columns by transverse prestressing. Therefore, the method of computation for confinement pressure was modified to adopt a procedure similar to that used for the computation of equivalent pressure on concrete imposed by a prestressing strand with a parabolic tendon profile having a maximum tendon eccentricity of "e" and an effective prestressing force of "F". This is shown in Eq. 4.13. In this equation, "q" is the equivalent uniform force per linear length due to a parabolic tendon profile and "l" is the length of the parabolic segment.

$$F.e = \frac{q.l^2}{8} \quad [4.13]$$

In order to compute the equivalent pressure "q", it is important to estimate the force in prestressing strands when the peak confinement is attained prior to strength decay in column. This was done by using the experimentally recorded strain values. Since most of the strands yielded at the corners, the yield strength of the prestressing strands (f_{ys}) was used to compute the maximum force in strands, as indicated in Eq. 4.14.

$$F = f_{ys}.A_{str} \quad [4.14]$$

Where A_{str} is the area of one leg of strand, f_{ys} is the yield strength of prestressing strands and "e" is the maximum eccentricity of the strand relative to column face due to the presence of raiser disks on steel frames. The product of the applied force and the eccentricity over the length the force was applied (l) resulted in force per unit length, and was denoted by "q."

$$q = \frac{8(F.e)}{l^2} \qquad [4.15]$$

The amount of equivalent uniform lateral pressure (both active and passive) can then be expressed as:

$$f_{le} = \frac{q}{s_{st}} \qquad [4.16]$$

Where s_{st} is the spacing of strands (Retro-belts). The confinement model, with the above modification was used to compute the effect of Retro-belt on confining retrofitted and repaired columns.

Model for Longitudinal Reinforcement

The longitudinal column reinforcement was modeled with a bi-linear stress-strain relationship, followed by a strain hardening region. The strain hardening segment consisted of four linear segments, idealizing the curved portion of stress-strain relationship between the onset of strain hardening and the steel rupturing in tension. This was done by idealizing the experimentally obtained stress-strain relationship between 1.0% strain at the onset of strain hardening and 13% strain at steel rupturing. Figure 4.3 illustrates the analytical model used for longitudinal reinforcement. It should be noted that the stress-strain relationship in compression was assumed to be the same as that in tension.

4.2.2 Member Analysis for Flexure

Once the sectional response was established in the form of moment-curvature relationship, flexural deformations were then computed over the length of columns by constructing the distribution of curvatures over column height. Incrementally increasing and linearly varying moments between the column tip and the critical column section at the footing interface enabled the construction of curvature distributions at selected stages of

loading. Integration of curvatures resulted in column rotations and the moments of the area under the curvature diagrams relative to the tip of columns provided horizontal column displacements due to flexure. The ratio of horizontal column displacement and column height resulted in a drift ratio. Drift ratios at selected stages of loading were computed. These points corresponded to; i) cracking moment, ii) first yielding of extreme tension reinforcement, iii) onset of strain hardening of extreme tension reinforcement, iv) peak moment resistance, v) 80% of peak moment resistance beyond the peak (at 20% strength decay), and vi) a point between the peak and the 80% strength decay corresponding to the average of curvatures at these two moment resistances. For each point, the moment and corresponding curvature was obtained from the analytical moment-curvature relationship, established as described in Sec. 4.2.1.

Beyond the peak moment resistance, as the member starts experiencing plastic deformations and decay under increasing curvatures, a plastic hinge starts forming. The prediction of the length of plastic hinge region and the extent of curvatures along this region is a challenging task. The plastic hinge length is usually idealized by assuming a region of constant curvature. A number of empirical expressions were suggested by previous researchers for this constant curvature segment (plastic hinge length) at ultimate (Corley 1966, Mattock 1964, Sawyer 1964). The expression suggested by Sawyer, given in Eq. 4.17, was used for the computation of ultimate deformation at 20% strength decay beyond peak resistance (point v above). Figure 4.4 illustrates the distribution of curvatures at each of the control points used to compute lateral drift.

$$l_p = 0.25d + 0.075Z \qquad [4.17]$$

l_p is the plastic hinge length , d is the effective depth of section, measured to the centroid of extreme layer of tension reinforcement, and Z is the distance between the critical section and the point of inflection (shear span).

4.3 Rotation and Lateral Drift Due to Anchorage Slip

Reinforced concrete members, subjected to significant flexural inelasticity at member ends experience yield penetration into the adjoining members. Yielding of anchored

longitudinal reinforcement within the adjacent member results in the elongation and possible slippage of reinforcement outside the element (within the adjacent member). This results in significant softening of anchorage, generating additional deformations at member ends which are not accounted for in flexural analysis. This phenomenon, known as "anchorage slip" can be as significant as those caused by flexure, especially if the reinforcement enters into the strain hardening range of deformations. Tests on concrete columns show that anchorage slip plays an important role on total rotation of columns under lateral loading. In the case of bridge columns where the axial compression is low (10% to 20% of the column concentric capacity), anchorage slip has a larger effect than building columns under heavier axial compressive loads. Anchorage slip generates permanent rigid body rotations at member ends, contributing significantly to lateral drift. In this research program, lateral drift caused by anchorage slip was computed based on the procedure suggested by Alsiwat and Saatcioglu (1992). Accordingly, the embedded bar experiences two components of inelastic deformation; i) due to the extension of anchored reinforcement and ii) the slippage of the bar as a whole, prior to anchorage failure. Well anchored bar, with sufficient embedment length do not experience slippage. Often, the slippage is prevented and the anchorage is improved by using hooks.

4.3.1 Extension of Reinforcement

Extension of reinforcement near the end of a member results in an accumulated elongation of reinforcement at the interface of two adjacent members. Therefore, the extension of column reinforcement within its footing results in an elongation of column longitudinal reinforcement which generates a wide crack at the column-footing interface. According to Alsiwat and Saatcioglu (1992), this elongation can be computed by constructing the strain distribution along the embedment length of reinforcement and calculating the area under the strain diagram. This area gives the extension (elongation) of reinforcing bar within the adjoining element. Figure 4.5 illustrates a typical strain distribution of an embedded re-bar with elastic and inelastic segments. The inelastic segment consists of yield plateau and strain hardening regions. If the reinforcement is embedded in an element with unreinforced cover concrete, the end segment pulls-out with a cone of concrete. This region is referred to as the "pull-out cone", with strains in steel remaining

constant. The length of each segment of the embedded re-bar can be computed using bond stress between steel and concrete, and the principles of equilibrium. Once the strain distribution and length of each segment are established, the strain profile can then be integrated to find the extension of reinforcement. The computation of bond stresses and segmental lengths are explained in the following paragraphs.

Elastic Region

Re-bars are strained elastically under increasing tension, until the strained segment approaches their development length. Though the estimation of bond stress is a challenging task, it is generally acceptable to employ an average empirical value for elastic bond, as established by tests. The elastic bond, as recommended by ACI Committee 408, has been adopted in the model used in the current investigation. The expressions for elastic bond (u_e) and the elastic bar length are presented below.

$$u_e = u_{ACI} = \frac{f_y d_b}{4 l_d} \qquad [4.18]$$

Where,

$$l_d = \frac{440 A_b}{K' \sqrt{f_c'}} \frac{f_y}{400} \geq 300mm, \quad K' = 3d_b \qquad [4.19]$$

f_y is the nominal yield strength of steel reinforcement in MPa, d_b is the bar diameter in mm, l_d is the development length in mm, and f_c' is the concrete compression strength in MPa. Once the bond stress is calculated, l_e the elastic length can be derived from;

$$l_e = \frac{f_s d_b}{4 u_e} \qquad [4.20]$$

and f_s is the maximum stress in steel and it reaches f_y when the elastic bar length reaches the development length.

Yield Plateau Region

As the tension force in steel increases, the bar starts yielding. Further straining of the bar results in the penetration of yielding. If the yield plateau has a positive (non-zero) slope, the length of this region also becomes non-zero. Increased post-yield strains result in the

development of frictional bond (u_f) between concrete and steel. The value of average constant frictional bond stress can be determined experimentally. One such expression suggested by Pochanart and Harmon 1989 is shown in Eq. 4.21.

$$u_f = \left(5.5 - 0.07\frac{S_L}{H_L}\right)\sqrt{\frac{f_c'}{27.6}} \qquad [4.21]$$

S_L is the clear spacing between the lugs (deformations) of the bar and H_L is the height of these lugs above the reinforcement surface. By knowing the frictional bond stress (u_f), the yield plateau length can be computed as;

$$L_{yp} = \frac{\Delta f_s d_b}{4u_f} \qquad [4.22]$$

where, Δf_s is the difference in steel stress between the start and end points of yield plateau region.

Strain Hardening Region

Further straining of reinforcement, under increasing inelasticity of the attached member, results in the strain hardening of steel which begins at approximately 1% strain. Strain hardening provides additional reserved capacity, which may be as high as 125% of yield strength. The bond stress in this region can be assumed to be equal to the frictional bond. The concept of force equilibrium and the assumption of constant frictional bond within the segment can be used to establish the length of this region, as illustrated in Eq. 4.23.

$$L_{sh} = \frac{\Delta f_s d_b}{4u_f} \qquad [4.23]$$

Pullout Cone Region

Pullout cone occurs when concrete (usually the cover) breaks loose at the onset of yielding. The length of the cone is usually equal to the cover concrete. The pullout cone does not occur if this region is reinforced. When cover is small, the effect of the pull-out cone may be negligible. In this research project, the effect of the pull-out cone was neglected.

Total Extension of Reinforcement:

Bar extension can be computed through the integration of strains along the embedment length (Figure 4.5) and can be determined from the following equation:

$$\delta_{ext} = \varepsilon_s L_{pc} + 0.5(\varepsilon_s + \varepsilon_{sh})L_{sh} + 0.5(\varepsilon_{sh} + \varepsilon_y)L_{yp} + 0.5\varepsilon_y L_e \qquad [4.24]$$

4.3.2 Hook Deformation

If the elastic segment is not sufficiently long to develop the yield force, then the bar begins to slip. If the bars are hooked, which is the case for the columns tested in the current project, the hook is stressed providing a resisting force of P_h while deforming. The hook force-hook deformation relationship was developed experimentally (Soroushian and Choi 1991) and it was used to calculate the contribution of the hook to reinforcement extension, as illustrated below.

$$P_h = A_s f_s - \pi . d_b . l_e . u_e \qquad [4.25]$$

Where, f_s is the max steel stress in the elastic range of deformations. Ultimate hook force can be derived from;

$$P_{hu} = 271(0.05 d_b - 0.25) \qquad [4.26]$$

By knowing the hook force (P_h) and the ultimate hook force (P_{hu}), the hook deformation can be computed, using Eq. 4.27.

$$\delta_h = 2.54\left(\frac{P_h}{P_{hu}}\right)^5 \qquad [4.27]$$

δ_h is the contribution of hook to the extension of longitudinal reinforcement. Total extension of the embedded hooked bar can be computed using Eq. 4.28.

$$\delta_T = \delta_{ext} + \delta_h \qquad [4.28]$$

The member-end rotation associated with the extension of reinforcement in the adjoining member can be obtained from

$$\theta_e = \frac{\delta_T}{d - c} \qquad [4.29]$$

Where, d and c are the depths of the section measured from the extreme compression fibre to the centroid of the tension steel and the neutral axis, respectively. The effect of the anchorage slip rotation is to induce a linearly increasing displacement profile. The horizontal deflection at the tip of the column can then be computed from the following equation.

$$\Delta_{horz} = L(\theta_e) \qquad [4.30]$$

Where, L is the shear span of column.

4.4 Comparisons of Analytically Generated Moment-Drift Envelopes with Experimentally Recorded Hysteretic Relationships

The analytical procedure explained in the preceding section was used to construct the envelopes of moment-lateral drift relationships for the columns tested. The lateral drifts included inelastic flexural deformations, as well as those caused by anchorage slip. Shear deformations were believed to be small relative to those caused by flexure and negligible in most cases. Hence they were not included in the comparisons.

4.4.1 Columns Tested in the "Retrofit Phase"

Comparisons of analytical and experimental Moment-Drift relationships were made as presented in Figures 4.6 through 4.8 for columns tested in the Retrofit Phase. The first pair of columns compared had a short shear span (SR-C and SR-R) with increased shear stress reversals. The control column (SR-C) showed shear dominant response and failed in shear at about 1.5% lateral drift ratio. However, at about 1% drift the longitudinal reinforcement developed post-yield strains and the column was able to develop its flexural strength, though could not sustain it. Therefore, the strength envelop computed analytically provided excellent agreement with the experimentally recorded hysteretic relationship. However, analytically computed flexural deformations showed higher values than those recorded experimentally because of the degradation of concrete associated with shear in a shear deficient column, which was not considered in the analysis. Analytical and experimental comparisons for the companion retrofitted column (SR-R) showed excellent agreement for both strength and inelastic deformability values until 5% drift ratio. The external prestressing improved the column shear capacity by enhancing the aggregate interlock in concrete and by providing additional transverse reinforcement. The strength

enhancement was about 15% and the ductility improvement was by threefold. The analytical predictions provided excellent strength boundaries throughout the entire range of hysteretic relationship, verifying the applicability of the analysis procedure employed, including the analytical models adopted. However, the monotonic load analysis was continued up to a 20% strength decay point with associated high inelastic deformations, though the test was stopped earlier because of safety concerns as the column was tilting on one side in the orthogonal direction. Therefore, beyond 5% lateral drift, the analysis results show higher deformations than those recorded during the test.

The next comparison was for flexure dominant, long shear-span columns (LR-C and LR-R). The analytically computed envelop curves and experimentally generated hysteretic relationships are shown in Figure 4.7. The comparisons for both confinement- deficient control column (LR-C) and retrofitted column (LR-R) showed excellent agreements up to the onset of strength decay. The columns showed faster decay under reversed cyclic loading at the end of testing, as compared to the analytical envelopes that were intended for monotonic loading. This is to be expected because of the degrading effects of cyclic loading. Furthermore, the analysis method did not consider the buckling of compression reinforcement and associated strength degradation at high levels of inelasticity. The test columns, on the other hand, experienced bar buckling in compression, followed by bar rupturing in tension. This explains the discrepancy observed between the analytical curves and the experimental hysteretic relationships near the end of testing at high levels of deformation. The agreement between computed and recorded force-deformation relationships were excellent for the control and retrofitted columns up to 2.5% and 5% drift ratios, respectively, indicating the applicability of the analysis techniques employed. This was especially true for short and long retrofitted columns (Column SR-R and LR-R), both exhibiting flexure dominant response, validating the type of modification introduced to the confinement model used in incorporating the effects of transverse prestressing with active and passive pressures generated. This observation was used in developing the retrofit design information discussed later in the thesis.

The last pair of columns compared in this phase consisted of splice deficient columns (LS-C and LS-R). An important short coming of the flexural analysis utilized was the lack of a model that could incorporate the mechanism of splice slippage and the resulting strength

decay. Therefore, significant discrepancies were observed for these columns between the analytical and experimental relationships, as depicted in Figure 4.8. The discrepancy was especially pronounced for the control column, though the strength agreement at approximately the yield point of longitudinal reinforcement, just before 1% drift, was reasonably good. The strength was predicted more closely during pushing, which was the first direction of load excursion at each deformation level. Once the reinforcement started slipping within the splice region, the strength during load reversal showed an increased decay. The discrepancy in results became wider as the longitudinal reinforcement continued slipping in the splice region. This slippage was prevented fully in the retrofitted column (LS-R) at least until 3% drift ratio (4% drift in the push direction). This was the beneficial effect of transverse prestressing, which provided clamping force that improved bond within the splice region. The strength decay in the push direction was less severe than that in the pull direction, which was the direction of loading imposed on already damaged column.

4.4.2 Columns Tested in the "Repair Phase"

The "Repair Phase" of experimental research included tests of three shear critical columns with a circular, square and a rectangular cross-section. The columns were first damaged and then repaired and re-tested. The damage induced on the circular column was excessive, leading to sudden failure. Hence this column could not be repaired. All three columns were analyzed using the same procedure and the computer software developed for the comparison of the columns in the "Retrofit Phase".

Figure 4.9 illustrates the comparison of analytically generated envelop curve and the experimentally recorded hysteretic relationship for the shear-critical circular column CR-C. Though the column behaved and failed in shear, the shear-span was such that the column was also subjected to significant flexure, causing the flexural reinforcement to yield as the shear capacity was approached. Therefore, the recorded strength level was close to the computed flexural capacity. As expected, the analytical envelop produced higher deformability in flexure than the actual performance of this shear dominant column exhibited during the test.

The comparisons of force-deformation relationships for the repaired square column are shown in Figure 4.10. Similar to the shear-dominant circular column (CR-C), the

column capacity based on flexural analysis was close to the experimental capacity, especially in the push direction which is the direction of first load excursion. Subsequently the column experienced shear degradation and the test was stopped and the column was repaired using the Retro-belt technology. This column also had spliced longitudinal reinforcement. While the repair technique improved column behavior, by providing sufficiently high shear capacity to change the mode of behaviour from shear to flexure and controlled the slippage of spliced reinforcement to a degree, it was not able to prevent slippage as evidenced by excessive pinching of hysteresis loops. Because of this slippage, the column capacity did not reach the level computed analytically. However, the column did maintain its load resistance after having experienced about 20% to 25% strength decay. It was able to sustain this reduced load resistance up to approximately 10% drift ratio, as also predicted by flexural analysis.

The third column that was repaired and tested had a rectangular cross-section and continuous longitudinal reinforcement (without splicing). The comparisons of analytical envelop curves and the experimental hysteretic relationships after the initial damage and repaired column tests are shown in Figure 4.11. The figure illustrates that the computed flexural capacity was slightly higher than the shear resistance recorded. However, the repair technique did improve the shear capacity significantly, resulting in 30% to 35% increases in column resistance during incrementally increasing deformation cycles. The column shear resistance was fully recovered, and it developed flexural behavior, with strength values reaching to those associated with computed flexural resistance. Figure 4.11 indicates that column strength and deformability could be captured through flexure based analysis, confirming the applicability of the Retro-belt system as a repair technique. The success of the technique was more prevalent in this column than the companion square column since this column did not suffer from splice deficiencies. The examination of the force-deformation relationships further indicate that the stiffness degradation associated with initial flexural cracking could not be recovered by transverse prestressing and the column exhibited somewhat softer response initially. However, as force levels were increased beyond the initial cracking levels, the column stiffness approached to that indicated by flexural analysis, eventually showing an excellent agreement. Another observation that can be made in Figure 4.11 is the asymmetry in hysteresis loops. This was attributed to the

permanent deformation experienced by the column, when it was initially damaged during the push phase of loading prior to repair.

4.5 Flexural Capacities Computed by Building Code Approaches

In addition to the flexural analyses carried out through sectional analysis and using material constitutive models, column moment capacities were also computed by following rectangular stress block simplifications suggested by the American Concrete Institute Building Code (ACI 318-05) and the Canadian Standards Association's CSA A23.3-04 Standard. Table 4.1 lists nominal moment capacities for all columns, computed on the basis of ACI 318-05 and CSA A23.3-04 rectangular stress blocks. The results indicate that the approach followed by the North American design practice provides somewhat conservative, but reasonably accurate results. The flexure dominant control column (LR-C), without the splice deficiency, developed 10% to 15% higher flexural capacity in two directions when compared with the moment capacity computed by rectangular stress blocks. The conservatism of code values increased to approximately 20% when the comparison was made for retrofitted columns, because of the confinement of concrete associated with transverse prestressing, which is neglected by the building code approach. The code approach, however, resulted in slightly higher flexural capacities for the splice-deficient column (LS-C) because of the inadequate splice length provided in the test column. Retrofitting the spliced deficient column (LS-R) resulted in approximately 20% higher moment capacity than that computed by the building code approach, once again illustrating the favorable effect of Retro-belt technique in retrofitting splice-deficient columns. Shear dominant control columns showed slightly lower capacities than those computed by rectangular stress blocks (with the exception of SR-C), mainly because these columns failed in shear, though they did approach their flexural capacities. However, retrofitting as well as repairing these columns shifted the mode of behavior from shear to flexure and exhibited higher moment resistances than those computed. The only exception was the repaired square column, which could not recover its full flexural strength because of the slippage of spliced reinforcement.

The comparisons of flexural capacity computations indicate that the use of rectangular stress block results in conservative results, unless the failure is governed by

shear or splice slippage. The use of Retro-belt system of retrofitting improves moment capacity approximately 20% above those computed by the code approach. One exception is the repair of columns that have already suffered splice slippage, in which case the flexural capacity could be slightly under the code values.

4.6 Shear Strength Analysis

The columns tested were analyzed using selected methods of analysis for shear. The methods considered include; i) ACI 318-2005 Building Code Approach, ii) CSA A23.3 - 2004 Simplified Method and iii) Compression Field Theory (CSA A23.3 General Method and AASHTO LRFD Shear Design Provisions). These analyses were intended to verify the applicability of these existing techniques for the computation of column shear capacity when the columns were externally prestressed in the transverse direction.

4.6.1 ACI 318-2005 Code Approach

ACI 318-2005 Code Approach is based on the computation of concrete and transverse reinforcement contributions to shear. The contribution of concrete was made based on 45-degree truss analogy. Accordingly, the shear failure plane is assumed to occur at a 45-degree inclination relative to the member axis, where diagonal tension reaches the principal tensile stress. The diagonal tension capacity of concrete was established empirically, through a large number of tests. This component of shear resistance, referred to as concrete shear resistance (V_c), in reality reflect the effects of a number of different mechanisms, all lumped in one equation. These include the contribution of uncracked concrete, the aggregate interlock of cracked concrete and the dowel action of the longitudinal reinforcement (Park and Pauly 1975). The effects of shear-flexure interaction and the positive effect of axial compression in terms of delaying the formation of diagonal tension cracks are also introduced empirically. The empirical code expressions for concrete shear resistance are summarized below:

Simplified expression for members subjected to shear and flexure only;

$$V_c = \left(\frac{\sqrt{f_c'}}{6}\right) b_w d \qquad [4.31]$$

Detailed expression for members subjected to shear and flexure;

$$V_c = \left(\sqrt{f_c'} + 120\rho_w \frac{V_u d}{M_u}\right)\frac{b_w d}{7} \qquad [4.32]$$

$$V_c \le 0.3\sqrt{f_c'} b_w d \qquad [4.33]$$

$$\frac{V_u d}{M_u} \le 1.0 \qquad [4.34]$$

For members subjected to axial compression;

$$V_c = \left(1 + \frac{N_u}{14A_g}\right)\left(\frac{\sqrt{f_c'}}{6}\right) b_w d \qquad [4.35]$$

Because the columns tested in the current investigation were subjected to axial compression, Eq. 4.35 was used to determine concrete shear resistance. The results are tabulated in Table 4.2. The contribution of internally placed column tie reinforcement was computed assuming a 45-degree diagonal tension failure plane. Accordingly, the shear force resisted by all legs of transverse reinforcement is specified below:

$$V_s = \frac{A_v f_y d}{s} \qquad [4.36]$$

Where, A_v is the total area, f_y is the yield strength and s is the spacing of non-prestressed transverse reinforcement and d is the effective depth of section. The contribution of transverse steel for each column was computed, as is listed in Table 4.2.

The contribution of transverse prestressing to shear resistance consists of two effects; i) delaying the formation of diagonal tension crack and ii) providing additional shear reinforcement beyond cracking. Both of these effects can be accounted for by using the appropriate strand stress values in Eq. 4.37. The delay of crack formation is associated with initial prestressing that compresses the column concrete in the transverse direction. The transverse compressive strain which has to be offset for concrete cracking can be computed by f_{pi}/E_s where f_{pi} is the initial stress in strands. The additional shear capacity that offsets

this compressive strain is equal and opposite of the initial prestressing force [$V_{pi} = f_{pi}A_{ps}$]. The contribution of strands as additional shear reinforcement depends on the reserve strength of strands, i.e., the difference between the strand capacity and the initial prestressing [$V_{ps} = (f_{pu} - f_{pi})A_{ps}$]. During the column tests, the strands never reached their rupturing strengths at maximum column resistance. Therefore, recorded stresses in strands were used in computing the additional shear resistance provided by prestressing steel [$V_{ps} = (f_{ps} - f_{pi})A_{ps}$]. When the two effects of prestressing are added, i.e., V_{pi} and V_{ps}, then the total resistance provided by external prestressing can be determined as shown in Eq. 4.37.

$$V_p = V_{pi} + V_{ps} = f_{pi}A_{ps} + (f_{ps} - f_{pi})A_{ps} = f_{ps}A_{ps} \quad \textbf{[4.37]}$$

Table 4.2 lists the contribution of transverse prestressing, V_p and associated recorded strand stresses (f_{ps}). The table also includes experimentally recorded maximum applied shear values. For shear-dominant columns, these values correspond to column shear capacities, while for flexure-dominant columns they correspond to maximum shear forces associated with flexural capacities. In the latter case, because the columns failed in flexure, corresponding applied shear forces are expected to be lower than the actual shear capacity.

The computed shear force capacities, based on the ACI 318-2005 Building Code and those recorded experimentally, are compared in Table 4.2. The experimental values correspond to maximum applied shear force (including the horizontal component of vertical actuators) in the push direction, as this is the direction the columns were first subjected to increased drift levels. The results show good agreement in shear capacity calculations based on the above approach and those exhibited experimentally. Column SR-C, is a shear critical short rectangular column with shear deficiency (shear capacity is lower than the shear force associated with flexural capacity). It's capacity was recorded to be only 1% above the ACI 318 expression predicted. Columns LR-C and LS-C are long, flexure-dominant columns with continuous and spliced longitudinal reinforcement, respectively. Their shear capacities were higher than shear forces associated with flexural capacities. Therefore, the ACI approach predicted 28% and 54% higher shear capacities than shear resistances experienced at flexural yielding during testing. The columns tested in the "Repair Phase" were all critical in shear. Column CR-C was a shear critical circular column with less than the minimum

transverse reinforcement required by ACI 318-2005. It developed 15% lower shear capacity than that predicted by the Code expression. Columns SSR-C and RR-C were shear critical square and rectangular columns respectively. These columns also had less than the minimum shear reinforcement specified in ACI 318-2005 to be able to restrain diagonal cracking. The columns developed approximately 4% and 24% higher shear resistances than those predicted by ACI 318 for SSR-C and RR-C, respectively. The comparisons were extended to columns retrofitted by Retro-belt, incorporating the effects of prestressing on shear strength as per Eq. 4.37.

The comparisons show that with the addition of the effects of Retro-belt, the mode of behaviour changed from shear to flexure, and computed ACI shear strength values became higher than maximum shear forces applied during testing, as these shear values corresponded to flexural capacities, i.e., the columns never experienced their shear capacities. Retrofitted short rectangular column (SR-R) developed 70% of the computed capacity, while shear capacities for flexure-dominant columns (LR-R and LS-R) were 112% and 143% higher than shear resistances corresponding to flexural capacities. Similar correlation was obtained for the repaired rectangular column RR-R. The computed shear capacity for this repaired column was 74% higher than the value recorded during testing, which is 47% higher than the computed capacity for the unretrofitted control column (RR-C) indicating a 47% improvement in shear resistance attained by prestressing. However, the computed shear capacity of the repaired square column (SSR-R) could not be sustained during testing, because of the splice failure of longitudinal reinforcement, since this column did contain splice deficiency of longitudinal reinforcement. This observation confirms the earlier experimental observation that repairing a column that has already experienced splice failure was only partially successful and the column could not recover its original strength. Further research is needed in this area, since the experimental program had only one column in this category.

4.6.2 CSA A23.3-2004 Simplified Method

The simplified method presented in CSA A23.3-2004 is permitted for shear design of flexural members not subjected to significant axial tension. The shear resistance is

determined by concrete and steel contributions in a similar manner as the procedure outlined in ACI 318-2005 Building Code.

$$V_r = V_c + V_s \quad \textbf{[4.38]}$$

Where

$$V_c = \varphi_c \lambda \beta \sqrt{f_c'} b_w d_v \quad \textbf{[4.39]}$$

The transverse reinforcement is assumed to be perpendicular to the longitudinal axis of the member and it can be calculated from

$$V_s = \frac{\varphi_s A_v f_y d_v \cot\theta}{s} \quad \textbf{[4.40]}$$

The above expressions provide shear resistance for design purposes, and hence incorporate material resistance factors φ_s and φ_c and the mass density factor λ. For the nominal shear capacities and for normal density concrete, these factors should be taken as 1.0. The values of β and θ used in Eqs. 4.39 and 4.40 are 0.18 and 35, respectively, as per CSA A23.3-2004. Although the columns tested in the current investigation were subjected to axial compression, Eq. 4.38 does not account for the contribution of axial compression to concrete shear resistance. The results obtained from the CSA A23.3 Simplified Method are tabulated in Table 4.3. The two main contributions of transverse prestressing to shear resistance, delaying the formation of diagonal tension cracks and providing additional shear reinforcement beyond cracking, were also evident from the analyses of columns based on the CSA A23.3-2004 simplified method.

Table 4.3 includes experimentally recorded maximum applied shear values and the contributions of transverse prestressing (V_p) and associated recorded strand stresses (f_{ps}). The computed shear force capacities based on the CSA A23.3-2004 Standard and those recorded experimentally are compared in Table 4.3. The shear capacities of shear-dominant columns were listed in the Table, while the shear values presented for the flexure-dominant columns correspond to maximum shear forces associated with flexural capacities. Since these columns failed in flexure, applied shear forces are expected to be lower than the actual shear capacities.

The experimental values correspond to maximum applied shear force (including the horizontal component of vertical actuators) in the push direction, as this is the direction the

columns were first subjected to increased drift levels. The results show good agreement between computed and measured shear capacities. Column SR-C, is a shear dominant short rectangular column with a shear deficiency (shear capacity is lower than the shear force associated with flexural capacity). The experimentally recorded capacity was only 6% above the CSA A23.3 predicted expression. Column LR-C is a long flexure dominant column with continuous reinforcement. The analytically derived shear capacity was 20% higher than the experimentally recorded shear value. Flexure dominant long column LS-C has the same geometric properties as column LR-C except for the spliced longitudinal reinforcement used in the hinging region. The shear capacity for LS-C was 30% higher than the shear forces associated with flexural capacity, as expected.

The columns tested in the "Repair Phase" were all critical in shear. Column CR-C was a shear critical circular column and it developed approximately 12% higher shear resistance that that predicted by CSA A23.3. Columns SSR-C and RR-C were shear critical square and rectangular columns respectively, and they developed approximately 31% and 51% higher shear resistances than those predicted by CSA A23.3.

The comparisons were extended to columns retrofitted and repaired by Retrobelt, incorporating the effects of prestressing on shear strength as per Eq. 4.37. This resulted in the change of mode of behaviour of short columns from shear to flexure. Retrofitted short rectangular column (SR-R) developed 72% of computed capacity. The computed capacities for flexure-dominant columns (LR-R and LS-R) were 205% and 235% higher than experimentally recorded shear resistances corresponding to flexural capacities. The computed shear capacity for the repaired rectangular column RR-R was 191% higher than the computed capacity of control column (RR-C) and 62% more than the experimentally recorded shear resistance of repaired rectangular column RR-C. This indicates more than 80% improvement in shear resistance due to prestressing. However, the computed shear capacity of the repaired square column (SSR-R) could not be sustained during testing, because of the splice failure of longitudinal reinforcement, since this column suffered from splice deficiency of longitudinal reinforcement. This confirms the earlier experimental observation that repairing a column that has already experienced splice failure was only partially successful and the column could not recover its original strength. Further research is needed in this area, since the experimental program had only one column in this category.

4.6.3 Modified Compression Field Theory (CSA A23.3-2004 General Method and AASHTO LRFD Shear Design Provisions)

The Modified Compression Field Theory (MCFT), developed by Vecchio et.al (1986) and Collins et.al (1996) was introduced to CSA Standard A.23.3 and the first edition of AASHTO 1994 Bridge Design Code as generalized shear design methodology. It was subsequently revised in CSA A.23.3-2004 and the annual update for AASHTO that was issued in 2000.

Collins et. al. (1999) showed that the ACI code equations for shear strength of large and lightly reinforced concrete beams, and one way slabs can be unconservative. It was experimentally shown that concrete compressive strength had little effect on observed shear failure loads for such members. It was concluded by Angelakos et.al (2001) that it was necessary to change the current ACI shear provisions for large, lightly reinforced members. The equations presented in the following section have been taken from the paper authored by Angelakos et.al (2001). The shear capacities of columns tested in the experimental program were computed using the Excel spread sheet developed by Bentz (2006). Accordingly, the shear strength of a reinforced concrete section is expressed as;

$$V_n = 0.083\beta\sqrt{f_c'}\,b_v d_v + \frac{A_v f_y}{s} d_v \cot\theta \qquad \textbf{[4.41]}$$

General Method which is a function of concrete strength, with higher strength concretes requiring higher ratios of transverse reinforcement.

$$\frac{A_v f_y}{b_v s} = \sqrt{f_c'}\ (psi\ units) = 0.083\sqrt{f_c'}\ (MPa\ units) \qquad \textbf{[4.42]}$$

The values of β and θ depend on the longitudinal strain which can be calculated for non prestressed members as shown below;

$$\varepsilon_x = \frac{0.5(N_u + V_u \cot\theta) + \frac{M_u}{d_v}}{E_s A_s} \qquad \textbf{[4.43]}$$

where N_u is the axial load normal to the cross section, V_u is the shear force at the section, d_v is the distance measured perpendicular to the neutral axis and can be taken as 0.9d, and A_s is the area of longitudinal reinforcement .

Tensile stresses take place in longitudinal reinforcement on the flexural tension side due to shear forces. If the member has insufficient amount of longitudinal reinforcement, yielding of this reinforcement is the governing shear strength. To avoid such failures, the longitudinal reinforcement is proposed to satisfy the following equation.

$$A_s f_y \geq \frac{M_u}{d_v} + 0.5N_u + (V_u - 0.5V_s)\cot\theta \qquad \textbf{[4.44]}$$

Values of β and θ are derived and presented for members with and without minimum reinforcement in a tabular form in both the CSA Standard A23.3-1994 and AASHTO LRFD Code. However, in the new CSA A.23.3-2004 the tables have been replaced with equations that derive these values. A convenient spreadsheet is provided by Bentz (2006) and is available to generate this data.

The spreadsheet interpolates between the rows of values in the CSA A23.3 Table for given material properties, section geometry and loading to find β and θ for each value of ε_x. For members with at least the minimum amount of transverse reinforcement, the values of β and θ are related to longitudinal strains (ε_x). Concrete shear stress (v) can be derived from;

$$v = \frac{V}{b_v d_v} \qquad \textbf{[4.45]}$$

Table 4.4 includes experimentally recorded maximum applied shear values. It also lists the contributions of transverse prestressing (V_p) and associated strand stresses (f_{ps}). Computed shear force capacities and those recorded experimentally are compared. The Table contains shear capacities of shear-dominant columns while the shear values presented for the flexure-dominant columns correspond to maximum shear forces associated with flexural capacities. Since these columns failed in flexure, the corresponding applied shear forces are expected to be lower than the actual shear capacity.

The experimental values correspond to maximum shear forces applied in the direction of first load excursion. The results show good agreement with those computed based on the Modified Compression Field Theory. The experimentally recorded capacity for short rectangular column (SR-C) with shear deficiency was only 4% above the MCFT predicted expression. The analytically computed shear capacity for the long rectangular

column with continuous reinforcement (LR-C) was 18% higher than the experimentally recorded value. The companion flexure dominant long column with spliced reinforcement (LS-C) developed a shear capacity that was 31% higher than the shear force associated with flexural capacity, as expected.

The columns tested in the "Repair Phase" were all critical in shear. Column CR-C was a shear critical circular column and it developed approximately 17% higher shear resistance than that predicted by MCFT. Column SSR-C was shear critical square column with spliced longitudinal reinforcement within its hinging region. It developed 18% higher shear resistance computed by MCFT. Short shear critical rectangular column RR-C developed approximately 32% higher shear resistance than that predicted by MCFT.

The comparisons were extended to columns retrofitted and repaired by the Retro-belt system, incorporating the effects of prestressing on shear strength as per Eq. 4.37. The comparisons show that with the addition of the effects of Retro-belt, the MCFT approach produced a shear strength value higher than the value observed experimentally. Retrofitted short rectangular column (SR-R) developed 67% of the computed capacity, while shear capacities of flexure-dominant columns (LR-R and LS-R) were 204% and 269% higher than shear resistances corresponding to flexural capacities. Similar correlations were obtained for the repaired rectangular column RR-R. The computed shear capacity for this repaired column is 73% higher than the value recorded during testing. The column repair resulted in a 12% increase in shear resistnace over the unretrofitted control column (RR-C). However, the computed shear capacity of the repaired square column (SSR-R) could not be sustained during testing, because of the splice failure of longitudinal reinforcement. This observation confirms the earlier experimental observation that repairing a column that has already experienced splice failure was only partially successful and the column could not recover its original strength. Further research is needed in this area, since the experimental program had only one column in this category.

4.7 Proposed Design Procedure for Column Retrofitting

Retrofitting seismically deficient bridge columns requires the evaluation of columns to establish the type of deficiency that they suffer from. Three types of seismic deficiencies dominate column performance all of which result from the lack of sufficient transverse

reinforcement. These deficiencies include i) lack of sufficient diagonal tension capacity under seismic shear forces, ii) lack of concrete confinement and resulting brittle behaviour, iii) insufficient splice length in critical column locations. Retro-belt addresses all three deficiencies and provides strength and deformability to the column through transverse reinforcement that induces active and passive lateral pressures. A design procedure for column retrofitting through the use of Retro-belt system was developed by Saatcioglu and Yalcin (2003) and was verified for square and circular columns. The methodology is applied to rectangular columns in the following sections.

4.7.1 Design for Shear

Shear deficiency of columns is caused by wide spacing of column ties of insufficient area that yield prematurely during seismic response. Furthermore, shear force reversals applied on concrete result in diagonal cracks that cross each other leading to the deterioration of concrete if effective crack control is not ensured. This reduces diagonal compression capacity of column under earthquake induced shear. Transverse prestressing through Retro-belt provides enhancements to both diagonal tension and diagonal compression resistance of columns as it improves the integrity of concrete while providing additional shear reinforcement. The required level of enhancement for each component depends on the performance level expected from the structure.

The column may be designed for complete damage control that not only ensures the survival of the column during the design earthquake, but also ensures significant damage control so that it does not require any substantial repair work after the event. This is achieved by providing sufficiently high initial prestressing so that diagonal cracks are controlled and the deterioration of concrete under stress reversals is not permitted. The level of transverse prestressing need not be high enough to eliminate complete diagonal cracking as some tension in concrete can be tolerated for an acceptable level of performance while shear is transferred across the cracks through aggregate interlock. The short columns tests in the current investigation indicated that the damage on concrete could be controlled if the transverse strain is limited to 0.15% to 0.20%, depending on the lateral drift demand. Within this strain level both concrete and internal reinforcement could be relied on for shear resistance. Requirements that satisfy this level of performance are given below.

$$V_e \leq V_c + V_s + V_p \quad \textbf{[4.46]}$$

$$V_c = 0.2\sqrt{f'_c}bd \quad \textbf{[4.47]}$$

$$V_s = A_v f_s \frac{d}{s} \quad \textbf{[4.48]}$$

$$f_s = 0.002E_s \leq f_y \quad \textbf{[4.49]}$$

$$V_p = 2A_{ps}(f_{pi} + 0.002E_p)\frac{h}{s_p} \quad \textbf{[4.50]}$$

$$A_{ps} = \left(\frac{V_e - 0.2\sqrt{f'_c}bd - A_v f_s \frac{d}{s}}{2(f_{pi} + 0.002E_p)} \right) \frac{s_p}{h} \quad \textbf{[4.51]}$$

$$50MPa < f_{pi} \leq 0.5 f_{pu} \quad \textbf{[4.52]}$$

$$s_p \leq \frac{h}{4} \quad \textbf{[4.53]}$$

The above approach is based on the current existing design philosophy in North America, which is based on the computation of concrete and transverse reinforcement to shear resistance. The diagonal tension failure plane is assumed to occur with a 45 degree inclination in deriving the expressions for V_s and V_p. The validity of this approach has been established in Section 4.6, "Shear Strength Analysis".

The level of axial compression on bridge columns often range between 10% to 15% of column concentric capacity, and its effect on improving diagonal tension capacity may be neglected conservatively. Therefore, the concrete shear resistance, V_c in the above procedure

does not incorporate the effect of axial compression. However, if the bridge column is subjected to net tension, V_c term in the above expression may be dropped.

As an alternative to the "damage control" performance level used in deriving the above expressions, "collapse prevention" may be used as a performance criterion. In this case the survival of bridge columns during design earthquake is ensured without collapse. However, the columns may not be protected against relatively wide cracks from occurring, and some repair may be necessary after the earthquake. This performance criterion is ensured by providing the required seismic resistance essentially through transverse reinforcement $(V_s + V_p)$, and allowing the transverse strains to increase beyond a level at which the aggregate interlock mechanism looses its effectiveness. Then, the concrete contribution V_c is conservatively neglected. This implies that the benefits of active lateral pressure are not relied on, and the level of prestressing is kept to a minimum. The following are the design expressions required to implement the collapse prevention performance criterion.

$$V_e \leq V_s + V_p \qquad \textbf{[4.54]}$$

$$V_s = A_v f_y \frac{d}{s} \qquad \textbf{[4.55]}$$

$$V_p = 2A_{ps} f_{py} \frac{h}{s_p} \qquad \textbf{[4.56]}$$

$$A_{ps} = \left(\frac{V_e - A_v f_y \frac{d}{s}}{2 f_{py}} \right) \frac{s_p}{h} \qquad \textbf{[4.57]}$$

$$s_p \leq \frac{h}{4} \qquad \textbf{[4.58]}$$

The prestressing hoops are required to be stressed to a minimum of 50 MPa to remain at least snug-tight around the column. While further stressing does not improve the ultimate shear capacity, it does control damage to concrete, helping the column to approach the damage control performance level.

Shear retrofit does not require the raiser disks used in column tests. These raiser disks are intended to provide near-uniform lateral pressure acting on the surface of column

for concrete confinement. However, it may be argued that shear retrofitting inevitably changes the mode of behaviour from shear to flexure and that the confinement of compression concrete becomes necessary for flexural deformability as well as improving diagonal compression capacity under shear. Figure 4.12 illustrates the shear retrofit scheme for a rectangular column. It is recommended that stress concentration effects in the corners be minimized by using circular disks, as illustrated in the Figure with a minimum diameter of 50 mm.

4.7.2 Design for Concrete Confinement

Compressive stresses in columns often result from a combination of axial force and bending. Sometimes the effects of diagonal compression caused by shear can become significant and may also become a contributing component. Under uniaxial compression, the failure of concrete is attained when it expands laterally due to the Poisson's effect, developing critical transverse tensile strains, resulting in vertical splitting cracks. If the concrete is restrained against lateral expansion, its strength and deformability increases tremendously. The restraining action provided by properly designed transverse ties, together with properly tied longitudinal reinforcement, is referred to as concrete confinement. Concrete confinement has been investigated by numerous researchers in the past, who presented numerous approaches to explain the mechanism of confinement, while also developing analytical models for concrete confinement (Sheikh and Uzumeri 1980 and 1982; Scott et.al 1982; Ozcebe and Saatcioglu 1987; Park et.al 1982; Fafitis and Shah 1985; Sheikh and Yeh 1986 and 1992; Mander 1988). Of the various approached used in the past, that employed by Saatcioglu and Razvi (1992) is of particular significance for the current research program since these researchers used lateral pressure as a basis for explaining the mechanism of confinement, while also quantifying the confinement action as a function of lateral pressure. Though the original concept was intended for passive confinement pressure generated by reinforcement, it can be extended to include the active lateral pressure exerted by lateral prestressing. The application of the model to laterally prestressed concrete exposed to active pressure is demonstrated in Section 4.2.1 "Sectional Analysis for Flexure," and has been verified against test data. The development of confinement design procedure for the

Retro-belt system requires a relationship between lateral confining pressure (active and passive) and column deformability (ductility and/or drift ratio).

A displacement based design procedure was developed for column confinement by Saatcioglu and Razvi (2002), with lateral drift as the performance criterion. It was based on the computed drift capacities of columns under different levels of axial compression, when confined by different levels and efficiency of lateral pressure. An expression was developed for the required transverse reinforcement ratio ρ_c in terms of confinement parameters and design drift ratio δ, as shown below.

$$\rho_c = 14\frac{f'_c}{f_{yh}}\left[\frac{A_g}{A_c}-1\right]\frac{1}{\sqrt{k_c}}\frac{P_f}{\phi P_0}\delta \qquad \textbf{[4.59]}$$

$$\frac{A_g}{A_c}-1 \geq 0.3 \qquad \textbf{[4.60]}$$

$$\frac{P_f}{P_0} \geq 0.2 \qquad \textbf{[4.61]}$$

Where, $(A_g / A_c - 1)$ is cover to core concrete area ratio, P_f/P_o is the ratio of factored axial compression to column concentric capacity, and k_c is the confinement efficiency coefficient reflecting the uniformity of confinement pressure generated by reinforcement with different spacing and arrangement. This coefficient is equal to 1.0 for uniform confinement pressure provided by closely spaced circular reinforcement caused by hoop tension. It approaches 1.0 when closely spaced rectilinear ties, crossties and overlapping hoops are used, producing near uniform pressure. External prestressing applied on rectangular columns becomes near uniform because of the raiser discs placed on spreader frames, generating hoop tension in the strands. Therefore k_c can be taken as 1.00 for the case of external transverse prestressing.

Eq. (4.59) is intended for columns designed with internal confinement reinforcement. However, it can be modified for externally prestressed columns. This can be done by substituting the minimum value specified in Eq. (4.60) for cover-to-core concrete area ratio, since this ratio approaches zero for externally confined columns where the entire column concrete becomes the core concrete. Furthermore, the limiting stress in transverse

reinforcement, f_{yh} should be replaced with the effective prestress f_{pe}. The resulting equation then becomes as follows, when expressed in terms of the strand area, A_{ps}.

$$A_{ps} = 2\frac{f'_c}{f_{pe}}\frac{P}{P_0} h\, s_{ps}\, \delta \qquad \textbf{[4.62]}$$

where, $P/P_0 \geq 0.2$ and "h" is the average of cross-sectional dimensions in two orthogonal directions. The effective stress in prestressing strands consists of two components; i) the initial prestress and ii) stress caused by expanding concrete due to the applied load. The former component results in active confinement pressure on concrete and the latter components results in passive pressure. It was observed in column tests that the internal transverse confinement reinforcement developed a transverse strain of 0.003 to 0.005 in providing passive confinement pressure depending on the level of axial compression and the effectiveness of confinement reinforcement (Saatcioglu and Razvi 2001). In columns retrofitted by externally prestressing, the increase in tensile strains of prestressing strands beyond initial prestressing ranged between 0.002 and 0.003 (Saatcioglu and Yalcin 2001, Mes and Saatcioglu 2006). These values are consistent with the strain values recorded in the current investigation. Therefore, it may be prudent to use 0.002 as a conservative limit for design purposes, especially for bridge columns where the level of axial compression is low and associated lateral expansion is also low. This implies that the effective strand stress can be established conservatively as $f_{pe} = f_{pi} + 0.002\, E_p$, where f_{pi} is the initial prestress in strands, which should not be less than 50 MPa to make sure the strands are tight enough not to become loose during the service life of structure. However, f_{pi} should not be too high to jeopardize the rupturing of strands under heavy compressive loading, especially during a strong earthquake. An upper limit of 50% of the ultimate strength of steel strand may be used as a safe value. Furthermore, the spacing of strands should be limited to h/4 or 150 mm, whichever is smaller, for the mechanism of confinement to be effective (Saatcioglu and Razvi 2001).

The design drift ratio δ depends on the level of performance expected from a column during a seismic activity. Recent codes suggest a design drift level of 2.0% to 2.5% for new construction. For retrofitting, a higher design drift level may be more appropriate and can be achieved without much difficulty or additional cost. A minimum design drift level of 4% is recommended for column retrofit design.

For retrofitting rectangular columns, it is recommended to use raiser discs at a spacing of $h/4$, with a maximum spacing of 150 mm in the vertical direction, with sufficiently high radii to allow for the development of perpendicular force components on column faces. Furthermore, a minimum bend radius of 25 mm is recommended at column corners. The recommended design dimensions for prestressing hardware are specified in Fig. 4.13. Care should be exercised in protecting the retrofitting hardware against corrosion, either by means of shotcreting or other methods of corrosion protection. The prestressing hoops, designed following the above requirements should be provided within the potential plastic hinge region of concrete elements, but should extend at least a distance not less than 1.5 h from the critical section for flexure, where h is the cross sectional dimension in the direction of lateral loading. This segment should not be less than L/4, where L is the shear span (ACI 318-05). The strands may be reduced outside this region by omitting every other strand beyond the plastic hinge region within a distance at least equal to $h/2$, and may be discontinued beyond this section.

4.7.3 Design for Splice Deficiency

Inadequate column splice length, less than 40 times the bar diameter, may result in the slippage of reinforcement, especially in the plastic hinge region. The common practice in the majority of the pre-1970's bridges was to use a splice length of approximately 20 times the longitudinal bar diameter. Therefore, the splice deficient columns tested in the experimental phase of the current research program had 20 times the bar diameter as their longitudinal reinforcement splice length. It was observed during the tests that internal transverse reinforcement was effective in providing clamping force to maintain bond between the spliced reinforcement and concrete until the internal transverse reinforcement strains increased beyond 0.15% to 0.2%. However, the strains measured on external prestressing strands revealed little increase in strains, often limited to 0.05%. Therefore, it may be prudent not to allow any additional straining in strands for design purposes. This implies that the effective strand stress can be taken equal to the initial prestress ($f_{pe} = f_{pi}$). With this level of maximum stress in the strands, the confinement design procedure and Eq. 4.62 may be used to prevent the slippage of spliced reinforcement until the desired level of

lateral drift is attained. The same level of maximum drift recommended for confinement design, i.e., 4%, can be employed for the spliced reinforcement clamping.

4.8 Proposed Design Procedure for Column Repair

A design procedure is recommended for repairing seismically damaged shear-deficient columns, based on the limited tests conducted in the experimental program. The data from two column tests were available for this purpose, i.e., those for columns SSR-R with spliced longitudinal reinforcement and RR-R with continuous longitudinal reinforcement.

The two repaired columns were repaired by applying the Retro-belt technology. The resulting improvement in column shear resistance was found to be approximately equal to the shear resisted by prestressing strands, i.e., V_p. This was especially true for Column RR-R which did not have the additional deficiency in the splice region. The computed retrofit design approach outlined in Sec. 4.7.1 was found to be also applicable as column repair technique, with some judgment required on the part of the structural engineer for the contribution of cracked concrete to shear. Column RR-R did suffer from diagonal cracking which was wide enough to suggest the yielding of internal ties, but did not experience significant strength decay. In this column, transverse prestressing was able to restore concrete contribution to shear, V_c. When in doubt of the extent of concrete damage, it may be prudent to neglect the contribution of cracked concrete to shear in computing the total capacity of repaired column.

Column SSR-R not only experienced diagonal tension cracking, but also experienced the slippage of spliced reinforcement. This column was not able recover its full strength, indicating that external prestressing was not sufficient to restore bond between spliced reinforcement and the surrounding concrete. Further research is needed to develop a repair design methodology for splice deficient columns.

Table 4.1 Nominal moment capacities for columns on the basis of ACI 318-05 and CSA A23.3-04 rectangular stress blocks

Column	f_c' (MPa)	f_y (MPa)	P_n (kN)	$M_n(kN.m)$ CSA	$M_n(kN.m)$ ACI	$M_{exp}(Avg)$ $(kN.m)$	$\frac{M_n(CSA)}{M_{exp}(Avg)}$	$\frac{M_n(ACI)}{M_{exp}(Avg)}$
SR-C	42	458	1386	818	818	870	0.94	0.94
SR-R	38	458	1386	802	808	1047	0.77	0.77
LR-C	42	458	1386	818	818	930	0.88	0.88
LR-R	38	458	1386	802	808	983	0.82	0.82
LS-C	42	458	1386	818	818	766	1.07	1.07
LS-R	38	458	1386	802	808	995	0.81	0.81
CR-C	35	458	1436	592	593	575	1.03	1.03
SSR-C	35	458	1294	545	549	555	0.98	0.99
SSR-R	35	458	1294	545	549	527	1.03	1.04
RR-C	35	458	1294	770	777	698	1.10	1.11
RR-R	35	458	1294	770	777	866	0.89	0.90

Table 4.2 Comparison of the computed shear force capacities, based on the ACI 318-2005 Building Code and experimentally recorded data

Column	f_y (kN)	$V_s(kN)$ ACI	$V_c(kN)$ ACI	f_{pi} (MPa)	V_p (kN)	$V_c+V_s+V_p$ (kN)	$V_{exp}(Avg)$ (kN)	$\frac{Theory}{Exper}$	*Observed Mode of Failure*
SR-C	548	232	337	N/A	N/A	569	563	1.01	**Shear**
SR-R	548	232	321	25%	374	927	646	1.43	**Flexure**
LR-C	548	232	337	N/A	N/A	569	444	1.28	**Flexure**
LR-R	548	232	321	25%	374	927	437	2.12	**Flexure**
LS-C	548	232	337	N/A	N/A	569	370	1.54	**Flexure**
LS-R	548	232	321	50%	572	1125	464	2.43	**Flexure**
CR-C	487	49	385	N/A	N/A	434	370	1.17	**Shear**
SSR-C	487	45	303	N/A	N/A	348	360	0.97	**Shear**
SSR-R	487	45	303	50%	572	920	322	2.86	**Flexure**
RR-C	487	64	302	N/A	N/A	366	452	0.81	**Shear**
RR-R	487	64	302	50%	572	938	539	1.74	**Flexure**

Table 4.3 Comparison of computed shear force capacities based on the CSA A23.3-2004 Building Code and experimentally recorded data

Column	f_{yt} (kN)	$V_s(kN)$ *CSA*	$V_c(kN)$ *CSA*	f_{pi} (MPa)	V_p (kN)	$V_c+V_s+V_p$ (kN)	$V_{exp}(Avg)$ (kN)	$\frac{Theory}{Exper}$	*Observed Mode of Failure*
SR-C	548	298	233	N/A	N/A	531	563	0.94	Shear
SR-R	548	298	222	25%	374	894	646	1.38	Flexure
LR-C	548	298	233	N/A	N/A	531	444	1.20	Flexure
LR-R	548	298	222	25%	374	894	437	2.05	Flexure
LS-C	548	298	233	N/A	N/A	531	370	1.44	Flexure
LS-R	548	298	222	50%	572	1092	464	2.36	Flexure
CR-C	487	63	267	N/A	N/A	330	370	0.89	Shear
SSR-C	487	59	215	N/A	N/A	274	360	0.76	Shear
SSR-R	487	59	215	50%	572	846	322	2.63	Flexure
RR-C	487	84	215	N/A	N/A	299	452	0.66	Shear
RR-R	487	84	215	50%	572	871	539	1.62	Flexure

Table 4.4 Comparison of computed shear force capacities based on the Modified Compression Field Theory (Bentz Spread Sheet) and experimentally recorded data

Column	f_{yt} (kN)	f_{pi} (MPa)	V_p (kN)	V_r (kN)	V_r+V_p (kN)	$V_{exp}(Avg)$ (kN)	$\frac{Theory}{Exper}$	*Observed Mode of Failure*
SR-C	548	N/A	N/A	551	551	572	0.98	Shear
SR-R	548	25%	374	542	916	615	1.42	Flexure
LR-C	548	N/A	N/A	512	512	433	1.15	Flexure
LR-R	548	25%	374	505	879	430	2.01	Flexure
LS-C	548	N/A	N/A	512	512	392	1.39	Flexure
LS-R	548	50%	572	505	1077	454	2.32	Flexure
CR-C	487	N/A	N/A	339	339	396	0.92	Shear
SSR-C	487	N/A	N/A	315	315	371	0.88	Shear
SSR-R	487	50%	572	315	887	345	2.75	Flexure
RR-C	487	N/A	N/A	367	367	484	0.81	Shear
RR-R	487	25%	572	367	939	542	1.74	Flexure

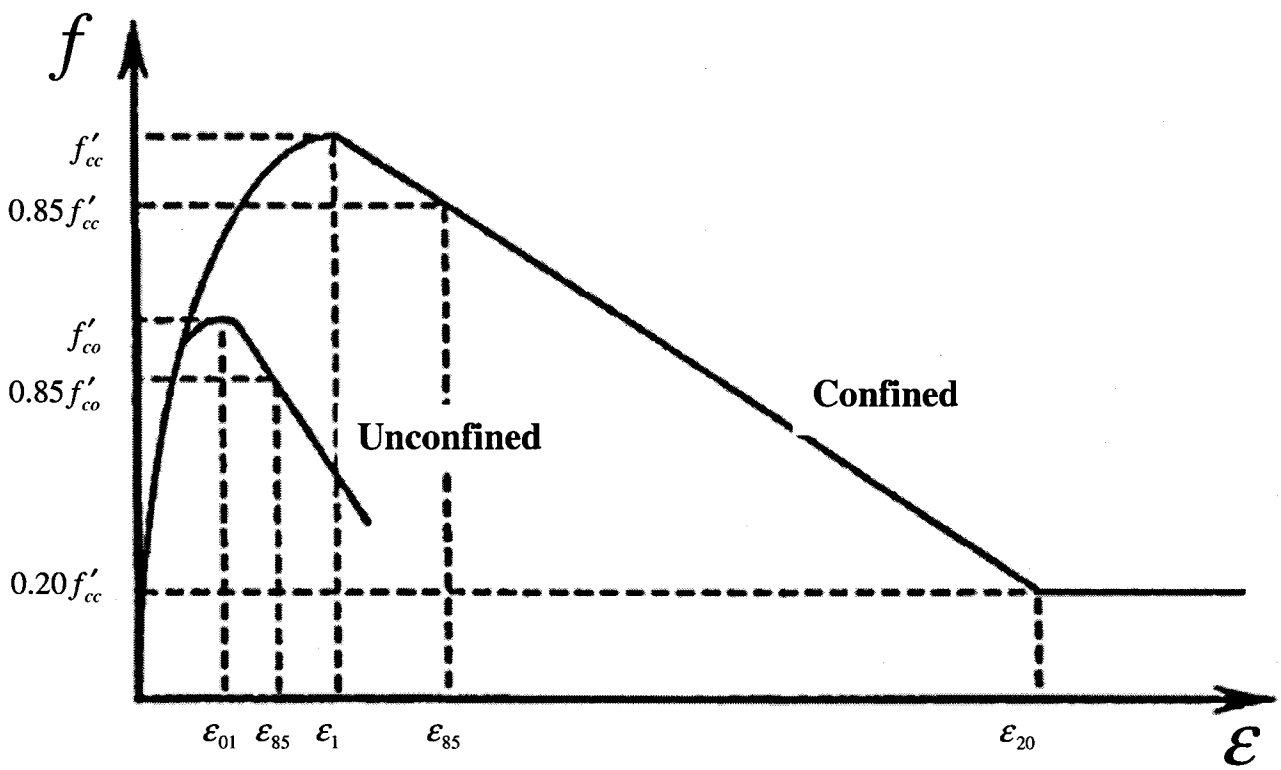

Figure 4.1 Stress-strain relationships for unconfined and confined concrete (Razvi and Saatcioglu, 1999)

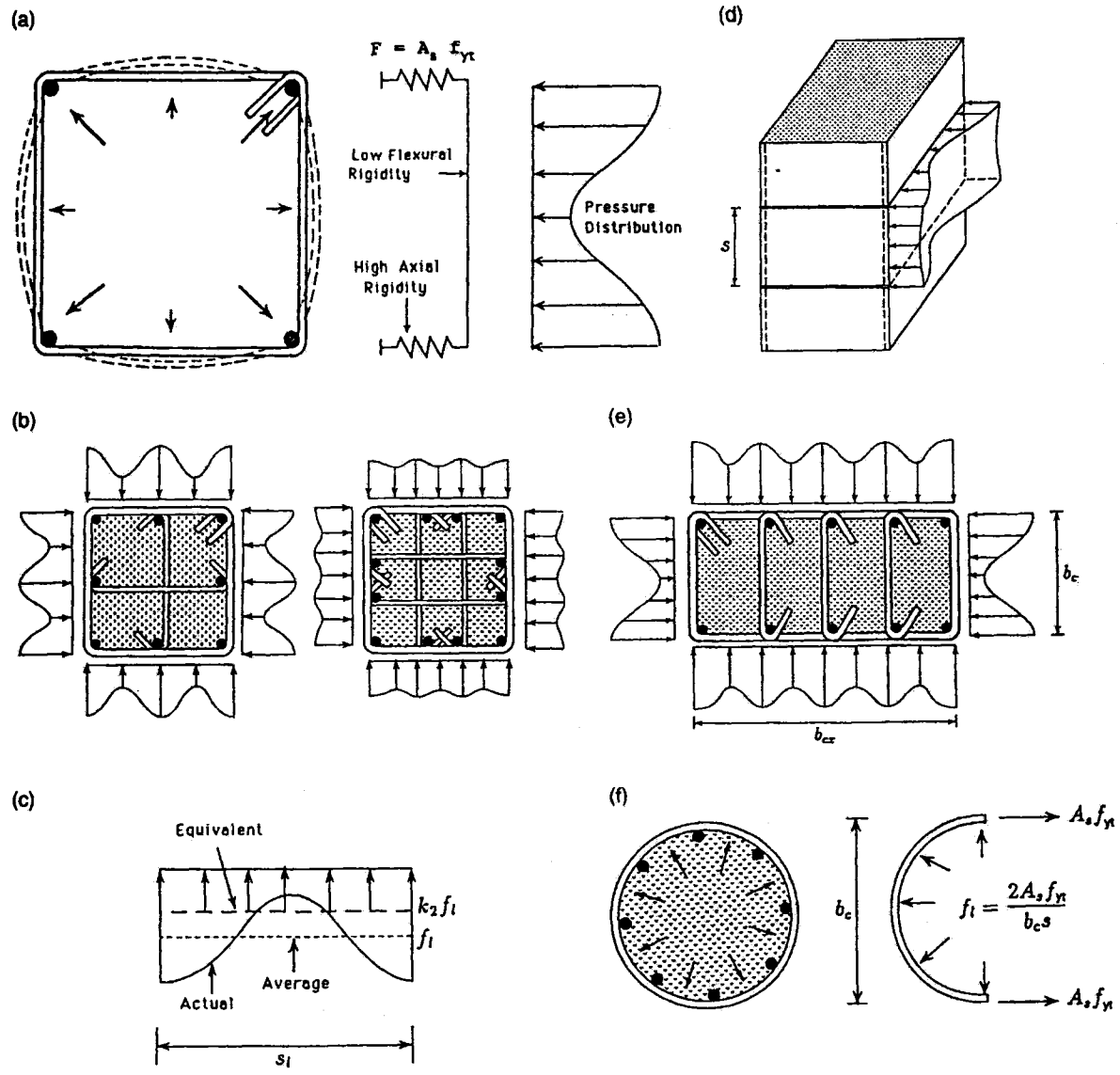

Figure 4.2 Confinement pressures induced by different arrangements of column reinforcement (Razvi and Saatcioglu, 1999)

(a) Development of Passive Confinement Pressure in Square Column; (b) Variation of Confinement Pressure with Reinforcement Arrangement; (c) Uniform Lateral Pressure in Circular Columns; (d) Equivalent Uniform Pressure in Square Column; (e) Confinement Pressure in Rectangular Column

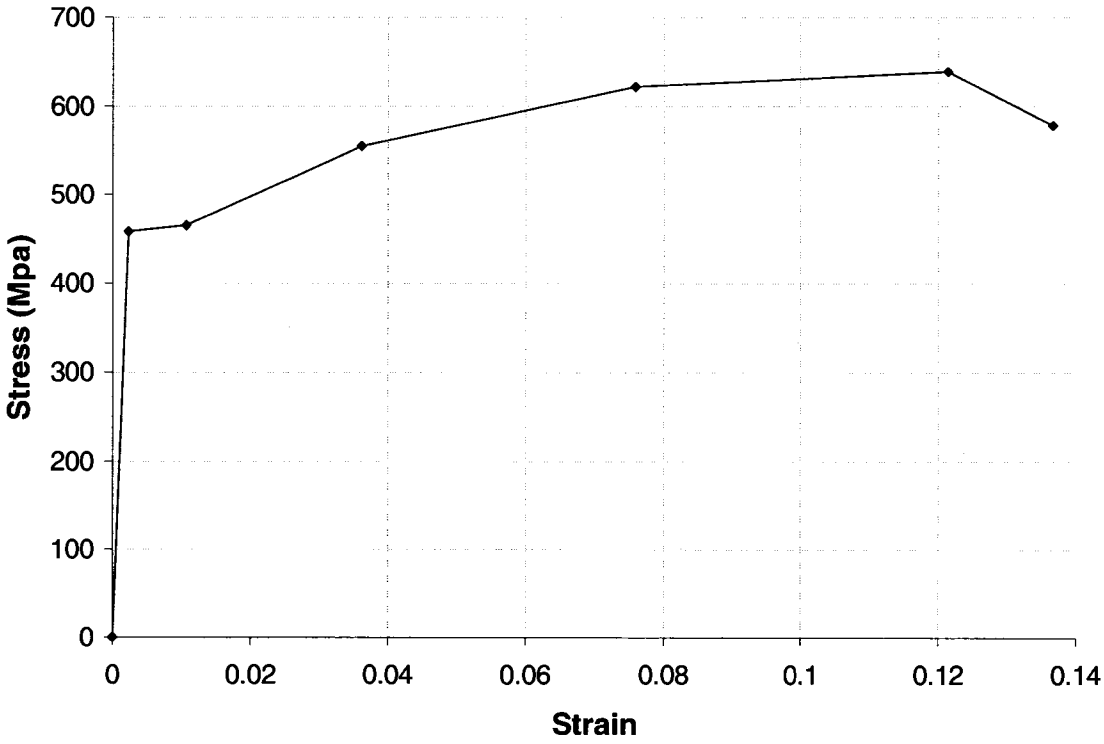

Figure 4.3 Analytical model used for longitudinal reinforcement

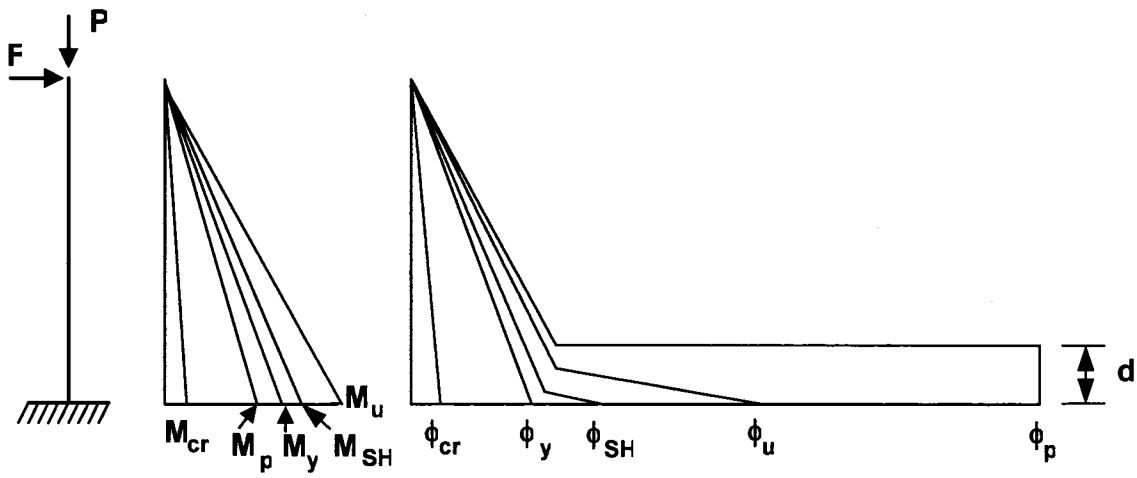

Figure 4.4 Progression of plastic hinging and distributions of curvatures at each of the control points used to compute lateral drift

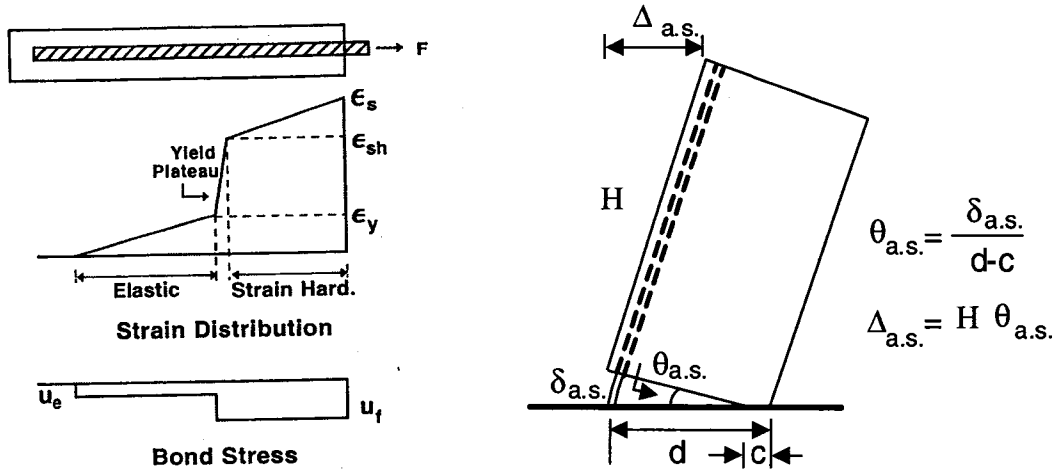

Figure 4.5 Typical strain distribution of an embedded re-bar with elastic and inelastic segments and the extension of anchored reinforcement

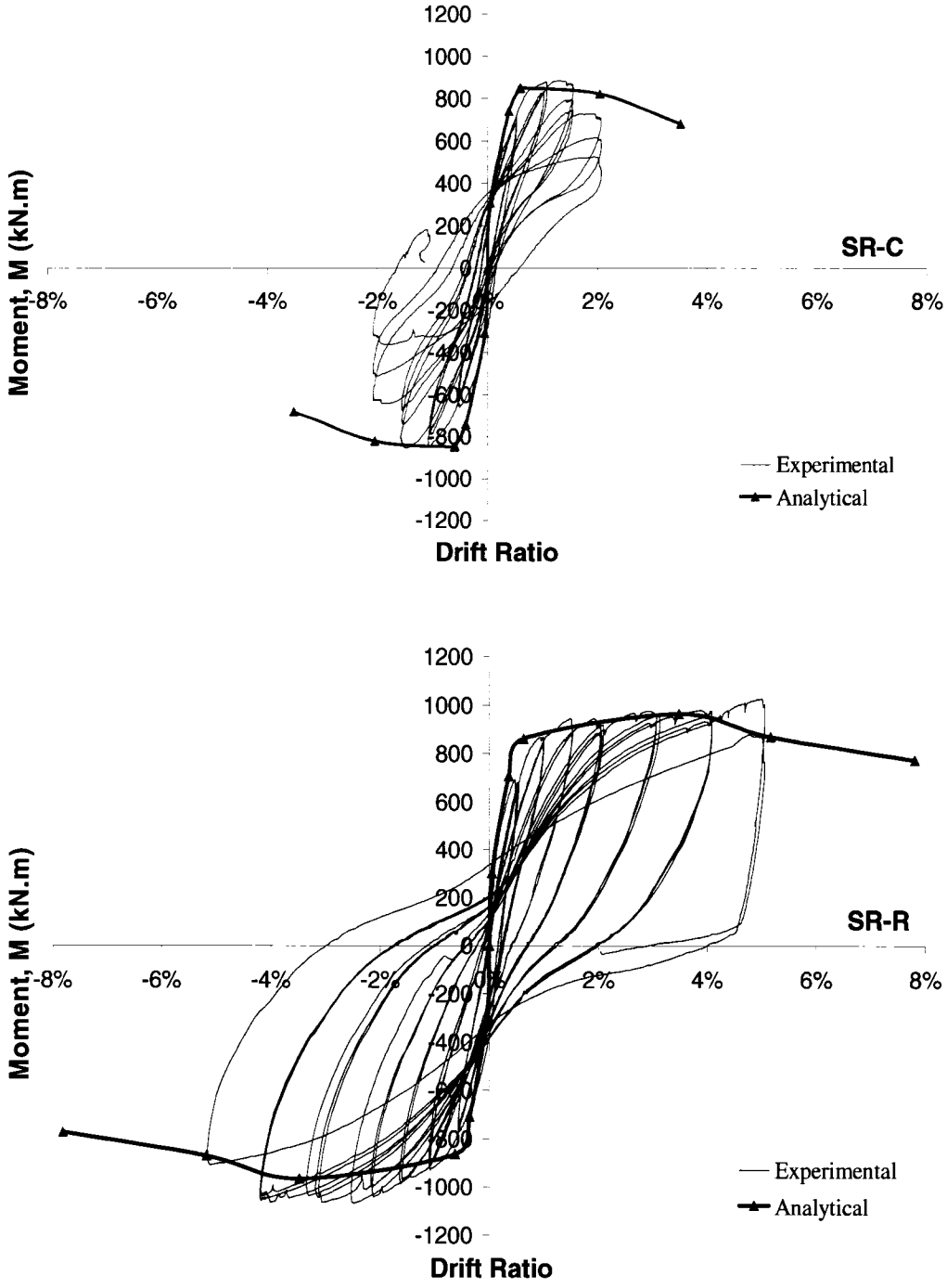

Figure 4.6 Comparison of analytical and experimental Moment-Drift relationships for the columns SR-C and SR-R

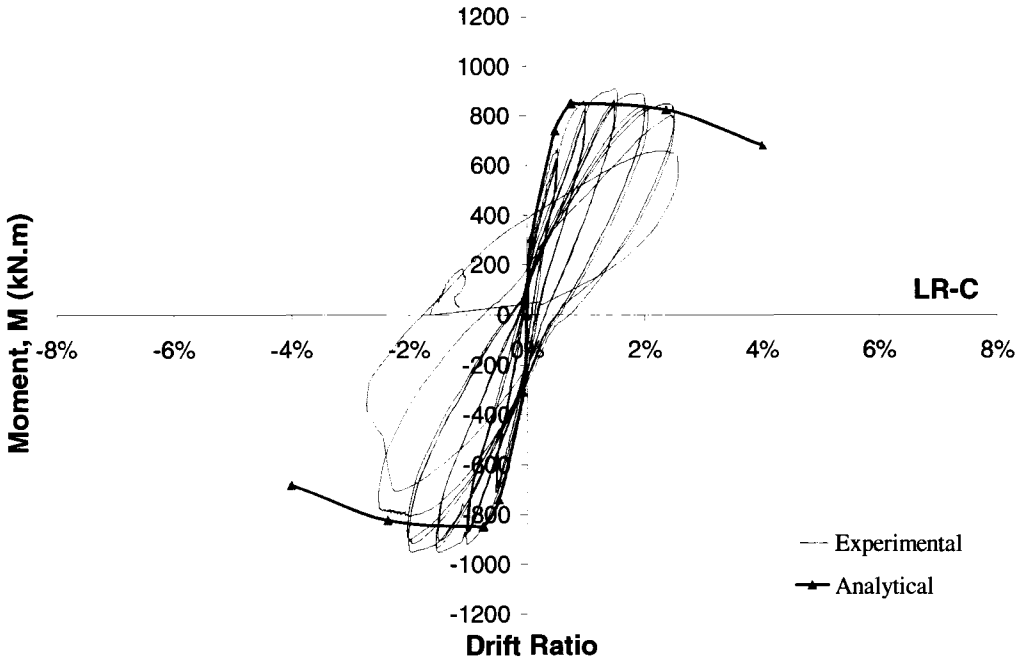

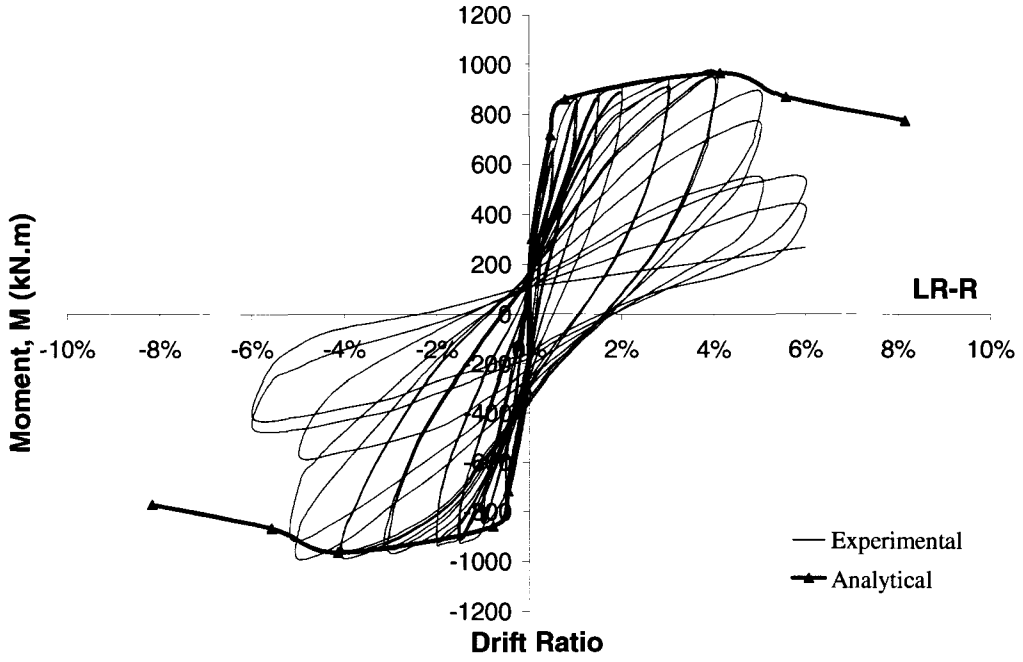

Figure 4.7 Comparison of analytical and experimental Moment-Drift relationships for the columns LR-C and LR-R

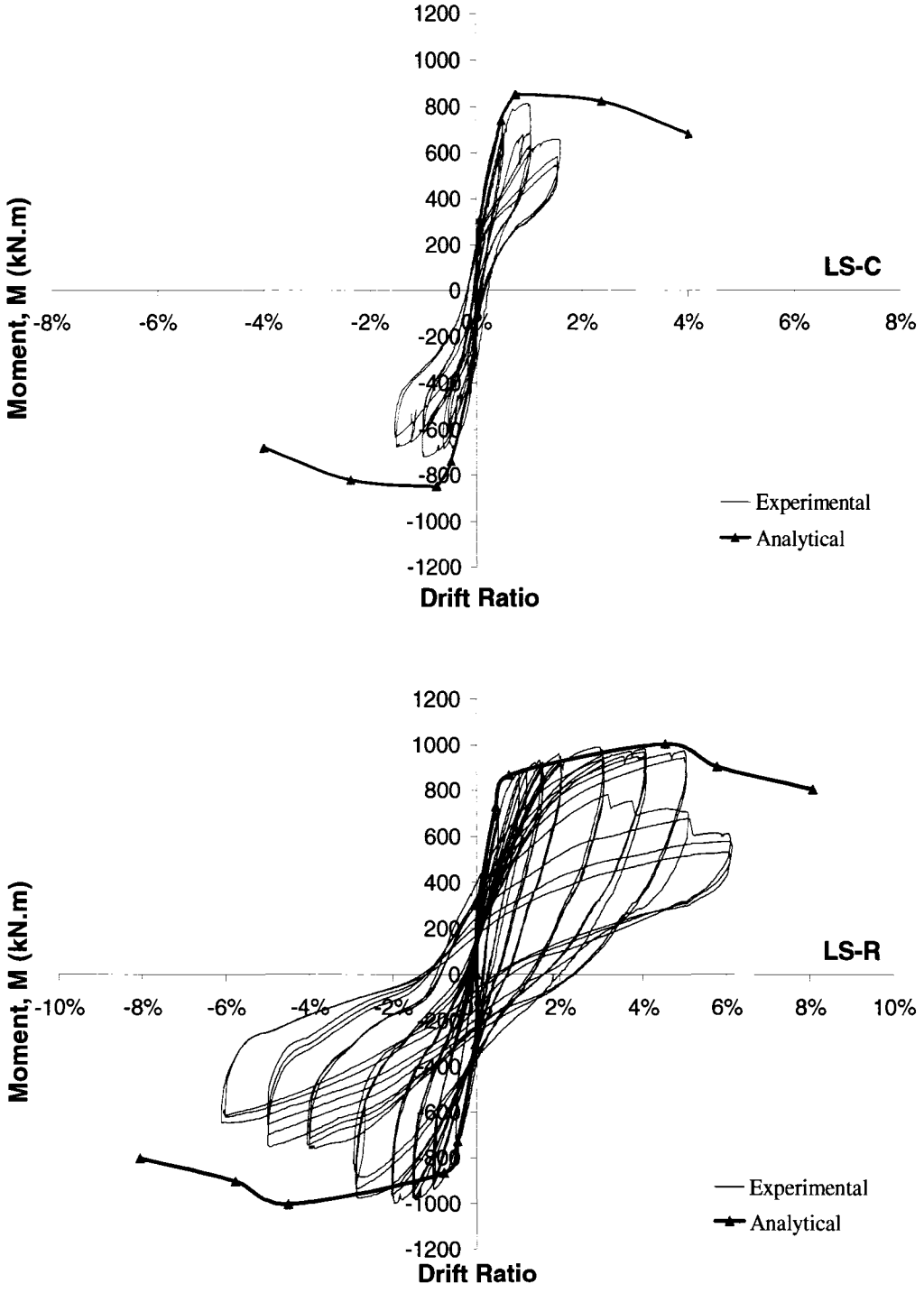

Figure 4.8 Comparison of analytical and experimental Moment-Drift relationships for the columns LS-C and LS-R

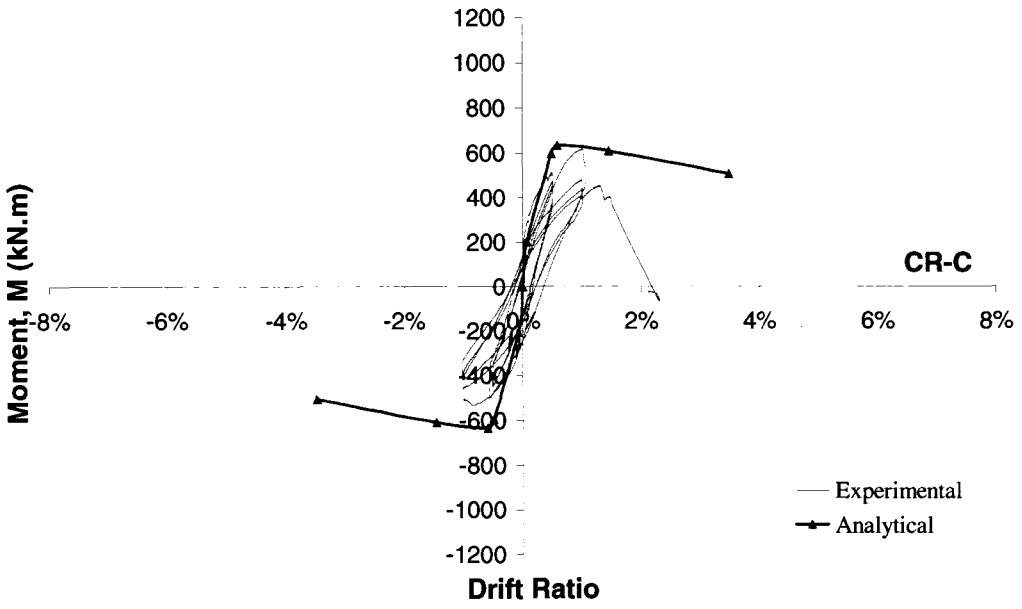

Figure 4.9 Comparison of analytical and experimental Moment-Drift relationships for the column CR-C

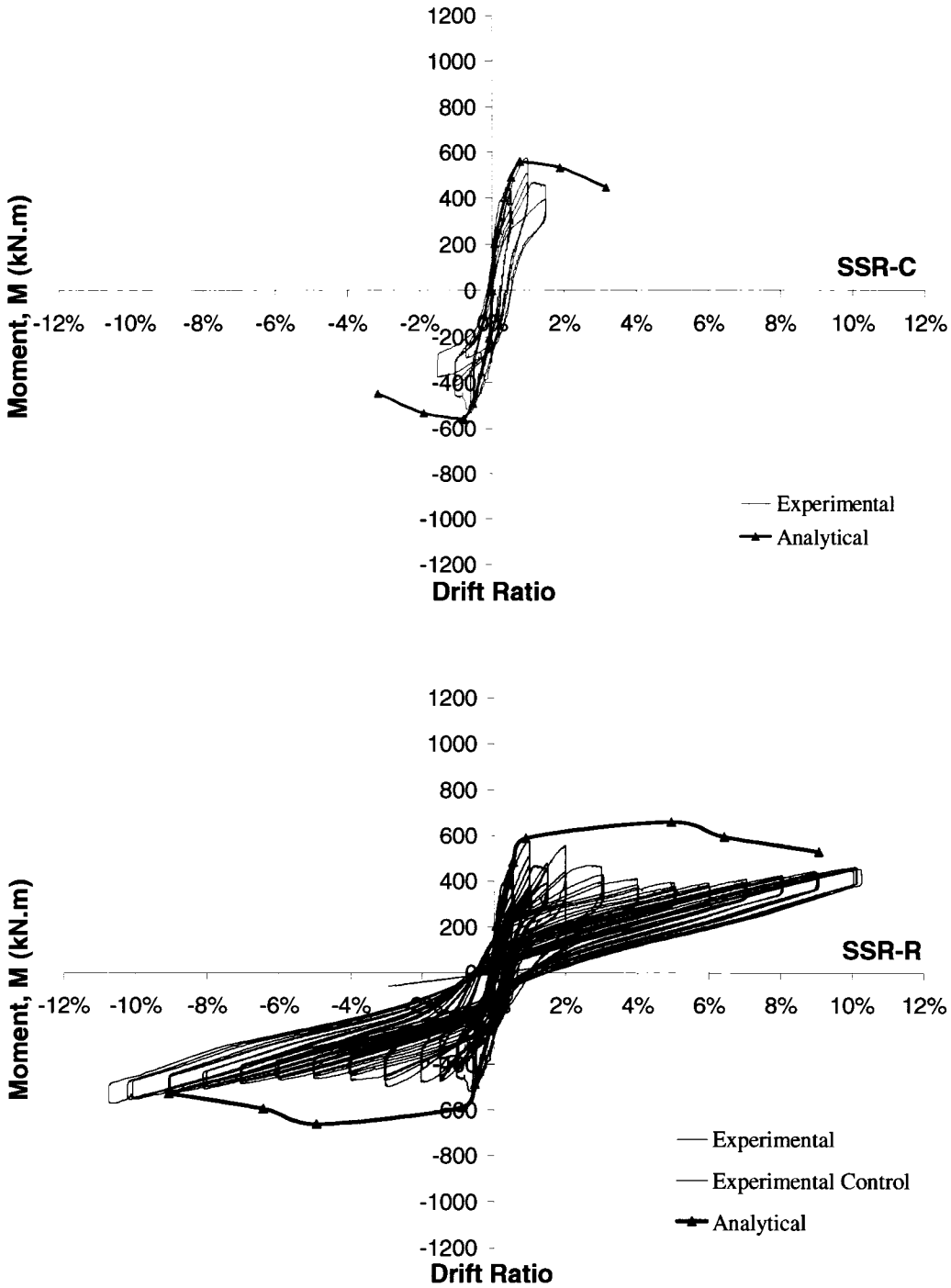

Figure 4.10 Comparison of analytical and experimental Moment-Drift relationships for the columns SSR-C and SSR-R

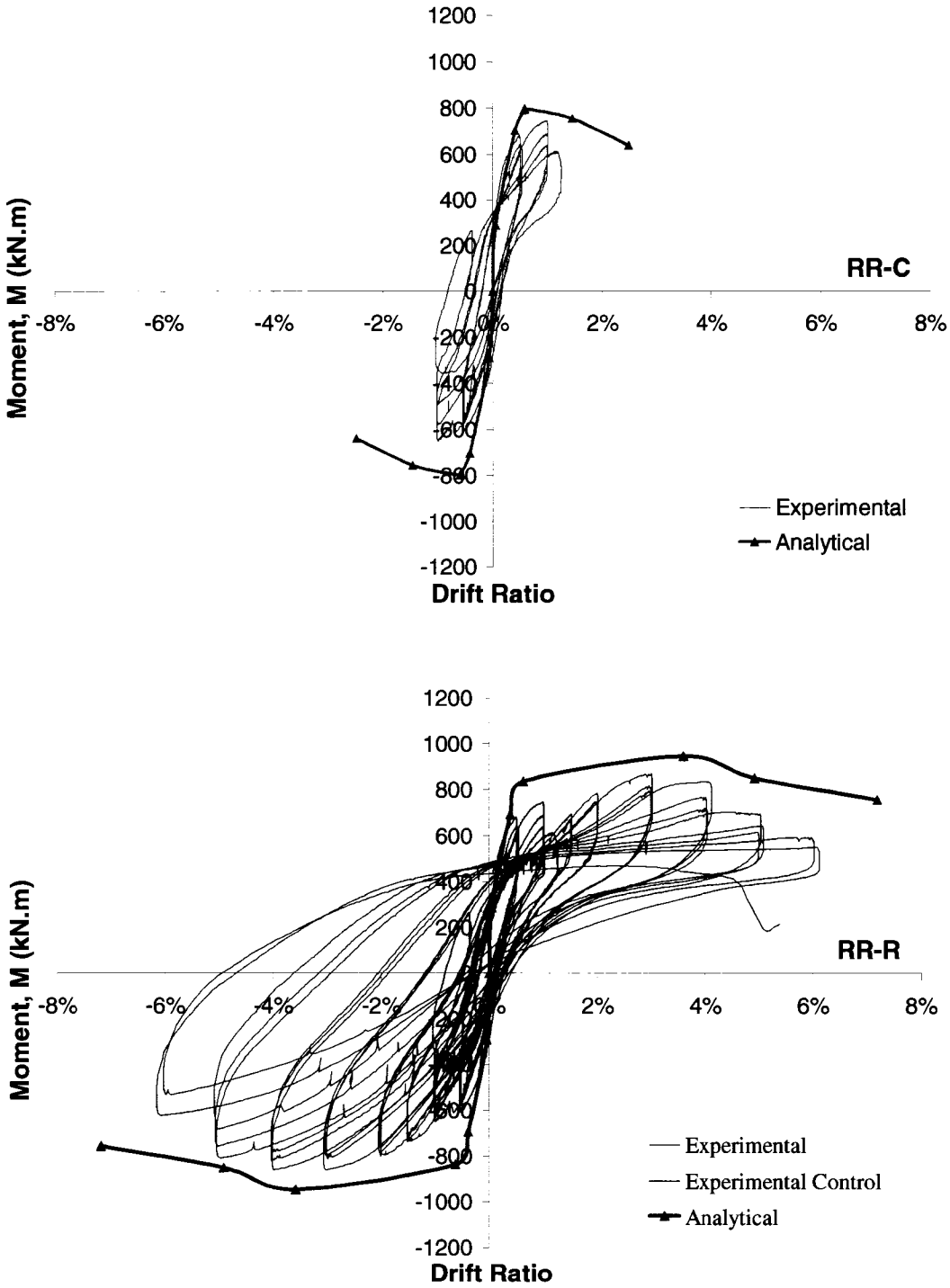

Figure 4.11 Comparison of analytical and experimental Moment-Drift relationships for the columns RR-C and RR-R

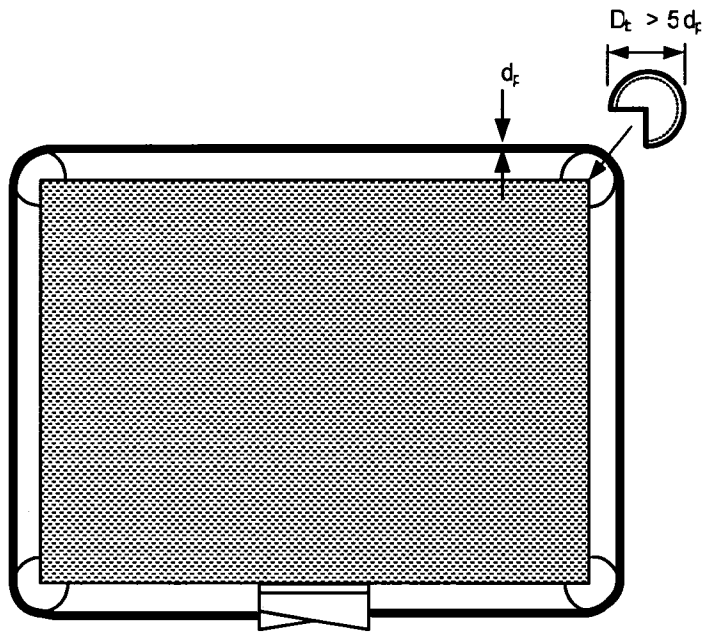

Layout for Shear

Figure 4.12 Shear retrofit scheme for a rectangular column

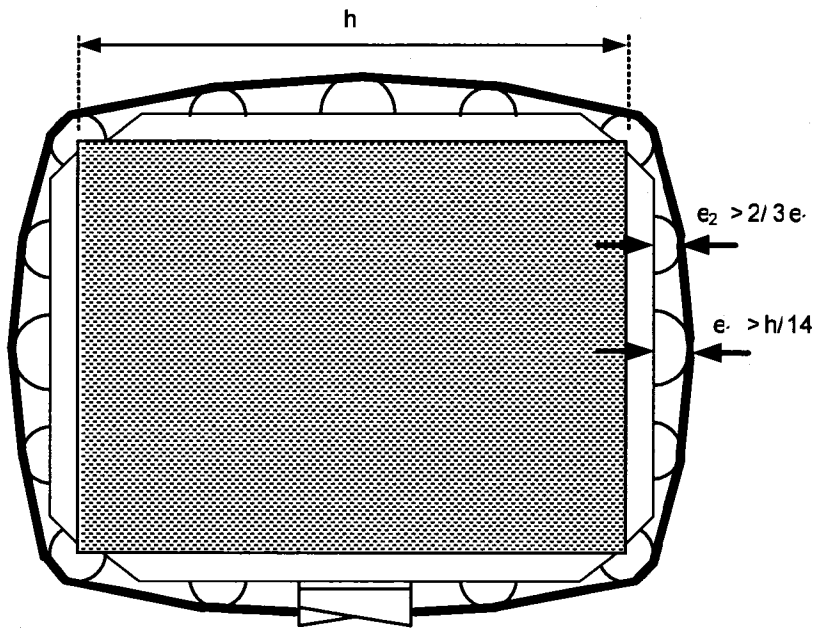

Layout for Shear and Confinement

Figure 4.13 Recommended design dimensions for prestressing hardwaree

Chapter 5

Summary and Conclusions

5.1 General

A comprehensive literature review was conducted on the seismic behavior of concrete columns built prior to the enactment of modern seismic codes. It was found that most columns built before 1970's are seismically deficient and need to be retrofitted. It also indicated the need for a seismic repair technology that could be easily applied in the after math of an earthquake when the need for life line structures is at their peak. Although other retrofit technologies are available, the need for a new technology that is less expensive and time consuming was evident. An extensive experimental and analytical research was conducted to investigate the applicability of the external prestressing technique that was developed at the University of Ottawa, known as "Retro-Belt," to columns with rectangular cross sections. The extension of the technique to repairing damaged columns with different cross-sectional shapes was also undertaken. Columns with shear, confinement and splice deficiencies were investigated. They were built in full scale to obtain the most reliable results for application to real world structures.

The research project was divided in two phases; i) retrofit and ii) repair. The first phase involved three pairs of rectangular columns. Total of six columns with shear, confinement (flexural) and splice deficiencies were designed built and tested. The second phase involved three shear critical short columns with circular, rectangular and square cross sections. The square column also had spliced reinforcement. They were damaged in diagonal tension, repaired using the Retro-belt technique (except for the circular column, which was damaged beyond repair) and re-tested.

The test data obtained from testing of the nine full-size bridge columns were processed. Their characteristics, in terms of strength in flexure and shear, deformability and splice deficiency were assessed by plotting and examining force deformation, moment rotation and reinforcement stress-strain relationships. It was found that shear and splice deficient columns generally had about 1% drift capacity before they developed extensive strength decay. Flexure dominant columns with continuous longitudinal reinforcement had approximately 2% drift capacity. All columns developed their flexural and shear capacities based on current North American design practice. The Retro-belt technology was effective in improving inelastic deformability of columns up to approximately 4% lateral drift ratio. The same technique was shown to be effective in repairing shear damaged columns. Detailed conclusions of the research program are listed in the following section.

5.2 Conclusions

The following conclusions can be drawn from the experimental and analytical investigation reported in this research project:

- Many existing concrete columns, designed and built following the practice of pre-1970's era are seismically deficient. This deficiency is attributed to the large tie spacing of approximately 300 mm, which is not sufficient to control damage caused by reinforcement slippage within spliced regions, concrete crushing due to lack of confinement and shear damage caused by insufficient transverse reinforcement. The control column reflecting as-built conditions had limited drift capacity of 1% in the case of shear and splice deficiencies and 2% when flexural failure of unconfined column occurred. These column need to be seismically retrofitted if they are expected to withstand strong seismic excitations.

- External transverse prestressing technique that was developed earlier at the University of Ottawa and was demonstrated to be effective for circular and square columns is also effective in improving strength and deformability of rectangular bridge columns. Specifically, the transverse reinforcement is effective in controlling diagonal tension cracks, improving shear strength, while confining core concrete and increasing inelastic deformability and bond between spliced reinforcement and the surrounding concrete. The column tests conducted in the current investigation indicated that the resulting improvements produced column deformabilities in access of 3% to 4% drift ratios.
- Transverse prestressing controls/delays the formation of diagonal tension cracks, while also acting as additional shear reinforcement, improving concrete shear resistance. The shear-deficient columns retrofitted with Retro-belt technology resulted in a shift in the mode of behaviour from shear-critical to flexure-critical. The retrofit technique further enhanced column shear capacity by improving diagonal compression resistance through confining the compression struts. The level of initial prestressing plays a role on the level of diagonal cracking permitted after the earthquake. In the columns tested, the prestressing was equal to approximately 25% of the ultimate strand strength of 1800 MPa. This level was sufficient to control cracking such that at about 4% lateral drift, the cracks did not open wide enough to suggest a need for column repair after the event. Seismic retrofitting shear deficient concrete columns by external transverse prestressing prove to be an effective technique that is quick and cost-effective.
- Transverse prestressing applies both active and passive lateral ressure on compression concrete, increasing the effectiveness of confinement mechanism. Flexure dominant columns, retrofitted by Retro-belt technology showed in excess of 4% lateral drift with little damage to concrete. The columns tested indicated that a level of initial prestressing equal to about 25% of the ultimate strand strength of 1800 MPa was sufficient to induce effective confinement, while leaving reserved strength in the strands for further elongation during seismic loading.
- Transverse prestressing longitudinal reinforcement splice regions improve the performance of columns with inadequate splice lengths in potential plastic hinge regions. Based on the earlier test results, the columns tested in the current investigation were pretsressed up to 50% of the strand capacity (i.e., twice the amount of prestressing needed

for shear and confinement deficiency), with the strand spacing reduced from 150 mm to 100 mm. This arrangement was effective in substantially reducing the slippage of spliced reinforcement as evidenced by a marked reduction in the pinching of hysteresis loops, enabling the rupturing of spliced reinforcement at failure.

- The basic concepts used for the design of reinforced concrete columns can be employed in designing column retrofits for flexure and shear. Specifically, the plane section analysis used for flexural strength calculations and the truss analogy adopted by North American Codes (ACI-318 and CSA A23.3) for shear strength calculations can be employed in retrofit designs that involve Retro-belt technology. The effect of transverse prestressing can be incorporated as additional shear and confinement reinforcement. The comparisons of experimental strength values with those generated analytically, following the existing design procedures, as modified to incorporate the effect of transverse prestressing, show good agreement, confirming the aforementioned point.
- The computation of force-deformation envelopes by well accepted analysis procedures for flexure, also incorporating the confining effects of transverse prestressing, can be employed to predict column inelastic deformability.
- The displacement-based design approach adopted for Retro-belt design for confinement-deficient columns in flexure produces good agreement with test results, verifying the applicability of the design procedure.
- The shear design approach adopted for Retro-belt design shows good agreement with test results, verifying its applicability in practice.
- The Retro-belt technique can be employed to repair shear-damaged short concrete columns. Column tests were conducted to verify the parameters involved in the technology. The results indicate improvements in lateral drift capacity from 1% in shear-deficient rectangular column to up to 4% in repaired column. The repair design approach suggested in this thesis can be employed in practice.
- Considerable judgment needs to be exercised to assess whether the level of damage sustained by a column justifies its repair to achieve full reinstatement of its strength. Tests have indicated that spalling of cover concrete and yielding of either longitudinal or transverse reinforcement should not discourage repair. However, if the longitudinal reinforcement has been fractured, buckled, or deformed significantly out of the straight

and/or the diagonal cracks widened significantly to damage the core concrete beyond repair, then column replacement should be considered as a serious option.

- The test results indicated that repairing a column that has experienced significant slippage of longitudinal reinforcement within the splice region may not be possible through Retro-belt. Though some improvement may be attained, restoring the original strength of the column may not be possible. More research is needed in the area before a Retro-belt design strategy can be suggested as a repair technique for splice-deficient columns.

5.3 Recommendations for Future Research

The following are recommended for further research.

- Additional tests on irregular columns with hexagonal and octagonal cross-sections to ensure the applicability of the Retro-belt technique to these columns. The experimental data should be used to devise and/or extend design procedures to cover columns having these geometries, as they are used quite commonly in certain regions of North America, especially along the west coast.
- Further column tests are recommended to investigate the applicability of the new technique to columns with higher axial loads, such as building columns that are critical in shear and flexure. Column deformability decreases with axial compression, and the mode of failure may change with the level of axial compression from longitudinal bar rupturing to concrete crushing. Hence it is important to assess the level of accompanying axial compression on retrofit and repair design.
- Repair technique introduced in this research needs to be further investigated by additional testing. The recommendations outlined in the thesis are based on limited test data and well accepted principles of mechanics. However, the effectiveness of transverse prestressing in restoring damage associated with lateral expansion and/or diagonal cracking need to be assessed.
- Additional analytical and experimental research is needed to address the modeling of spliced regions, with different splice lengths and levels of transverse prestressing for both retrofit and repair applications.

References

Aboutaha, R. S.; Engelhardt M.D.; Jirsa, J.O.; Kreger, M.E. (1999), "Rehabilitation of Shear Critical Columns by Use of Rectangular Steel Jackets", ACI Structural Journal, v 96: 1, pp 68-78.

Aboutaha, R.S.; Engelhardt, M.D.; Jirsa, J.O.; Kreger, M.E. (1999), "Experimental Investigation of Seismic Repair of Lap Splice Failures in Damaged Concrete Columns", ACI Structural Journal, V.96: 2, pp. 297-306.

ACI Committee 318 (1963), "Building Code Requirements for Reinforced Concrete (ACI 318-63)", American Concrete Institute, Farmington Hills, Mich.

ACI Committee 318 (1956), "Building Code Requirements for Reinforced Concrete (ACI 318-56)", American Concrete Institute, Farmington Hills, Mich.

Angelakos, D.; Bentz, E.C..; Collins, M.P. (2001), "Effects of Concrete Strength and Minimum Stirrups on Shear Strength of Large Members", ACI Structural Journal, V.98: 3, pp. 290-300.

Alsiwat, J. (1993), "Effect of Anchorage Slip and Inelastic Shear on Seismic Response of Reinforced Concrete Frames", PhD Thesis, University of Ottawa, Ottawa, Ontario, Canada.

Alsiwat, J.; Saatcioglu, M. (1992), "Reinforcement Anchorage Slip under Monotonic Loading", Journal of Structural Engineering, V.118: 9, pp. 2421-2438.

Beausejour, P. (2000), "Seismic Retrofitting of Concrete Columns with Splice Deficiencies by External Prestressing", M.A.Sc Thesis, University of Ottawa, Ottawa, Ontario, Canada.

Bentz, E.C. (2006), "Calculate Beam and Column Strength" http://www.ecf.utoronto.ca/~bentz/aashto.htm.

Bett, B. J.; Klinger, R.E..; Jirsa, J.O. (1988), "Lateral Load Response of Strengthened and Repaired Reinforced Concrete Columns", ACI Structural Journal, V.85: 5, pp. 4499-508.

Carrasquillo, R.L.; Nilson, A.H.; Slate, F.O.(1981), "Properties of High Strength Concrete Subjected to Short Term Loads", ", ACI Structural Journal, V. 78: 3, pp 171-178.

Chai, Y.H.; Priestly, M. J. N.; Seibel, F. (1991), "Seismic Retrofit of Circular Bridge Columns for Enhanced Flexural Performance", ACI Structural Journal, V. 88: 5, pp 572-584.

Chambers R.E. (1992), "Composite Performance in the Infrastructure", Proceedings of Material Science Conference, ASCE, Atlanta, pp. 532-545.

Chung, H.W. (1981), "Epoxy Repair of Bond in Reinforced Concrete Members", ACI Structural Journal, V.78: 7, pp. 79-82

Ciampi, V.; Eligehausen, R.; Bertero, V.V.; Popov, E. P.(1981), " Analytical model for deformed-bar bond under generalized excitations", Trans. IABSE Colloquium on Advanced Mechanics of Reinforced *Concrete*, Delft, Netherlands.

Ciampi, V.; Eligehausen, R.; Popov E. P.; Bertero, V.V. (1982), "Analytical model for concrete anchorages of reinforcing bars under generalized excitations", Report No. UCB/EERC–82/23. Earthquake Engineering Research Center, University of California, Berkeley.

Collins, M. P.; Mitchell, D.; Adebar, P.E.; Vecchio, F. J. (1996), "A General Shear Design Method", ACI Structural Journal, V.93: 1, pp. 36-45.

Collins, M. P.; Kuchma, D.K. (1999), "How Safe Are Our Large, Lightly Reinforced Beams, Slabs, and Footings?", ACI Structural Journal, V.96: 4, pp. 482-490.

Corley, W.G. (1966), "Rotational Capacity of Reinforced Concrete Beams", Journal of Structural Engineering, ASCE, V.92: 5, pp. 121-147.

Cooper, J. D.; Nimis, R.B.; and Bobb, N.M. (1994), "The Northridge Earthquake: Progress Made, Lessons learned in Seismic Resistant Bridge Design," Public Roads, Summer 1994, V.58, No.1.

Crawford, J.E.; Malvar, L.J.; Wesevich, J.W.; Valancius, J.; Reynolds, A.D. (1997), " Retrofit of Reinforced Concrete Structures to Resist Blast Effects", ACI Structural Journal, V.94: 4, pp. 371-377.

Cusson, D.; Paultre, P. (1994), "High Strength Concrete Columns Confined by Rectangular Ties", Journal of Structural Engineering, ASCE, V.120: 3, pp. 783-804.

Cusson, D.; Paultre, P. (1995), "Stress Strain Model for Confined High Strength Concrete", Journal of Structural Engineering, ASCE, V.121: 3, pp. 468-477.

Ersoy, U.; Tankut, A.T.; Suleiman R. (1993), "Behavior of Jacketed Columns", ACI Structural Journal, V.90: 3, pp. 288-293.

Fafitis, A.; Shah, S.P. (1985a), "Lateral Reinforcement for High Strenght Concrete Columns", SP-87-12, ACI, Detroit, pp. 213-232.

Fafitis, A.; Shah, S.P. (1985b), "Prediction of Ultimate Behavior of Confined Columns Subjected to Large Deformations", ACI Structural Journal, V.82: 4, pp. 423-433.

Filippou, F. C., and Fenves, G. L. (2004), "Methods of analysis for earthquake-resistant structures", Earthquake engineering: From engineering seismology to performance-based engineering, Y. Bozorgnia and V. V. Bertero, eds., Chap. 6, CRC, Boca Raton, Fla.

French, C.W.; Thorp, G.A.; Tsai, W. (1990), "Epoxy Repair Techniques for Moderate Earthquake Damage", ACI Structural Journal, V.87: 4, pp. 416-424.

Haroun, M.A.; Mosallam, A. S.; Feng, M.Q.; Elsanadedy, H.M. (2003), "Experimental Investigation of Seismic Repair and Retrofit of Bridge Columns by Composite Jackets", Journal of Reinforced Plastics and Composites, V. 22: 14, pp.1243-1268.

Jennings, P. C. (1971), Editor, "Engineering Features of the San Fernando Earthquake of Feb. 9, 1971," Report No. EERL 71-02, Earthquake Engineering Research Laboratory, California Institute of Technology, Pasadena, June 1971, pp.512.

Katsumata, H.; Kobatake Y.; Takeda, T. (1988), "A Study on Strengthening with Carbon Fiber for Earthquake-Resistant Capacity of Existing Reinforced Concrete Columns", Proceedings of Ninth World Conference on Earthquake Engineering, Tokyo-Kyoto, Japan, pp.517-522 .

Klaiber, F. W.; Dunker, K. F.; Wipf, T.J.; Sanders, W. W. (1987), "Methods of Strengthening Existing Highway Bridges", NCHRP Rep.293, Transportation Research Board, National Research Council, Washington, D.C.

Lehman, D.E.; Gookin, S.E.; Nacamuli, A.M.; Moehle, J.P. (2001), "Repair of Earthquake-Damaged Bridge Columns", ACI Structural Journal, V.98: 2, pp. 233-242.

Mahin, S.A.; Bertero, V.V.; Chopra, A.K.; Collins, R.G. (1976), "Response of the Olive View Hospital Main Building During the San Fernando Earthquake", Report No. EERC 76-22, Earthquake Engineering Research Center, University of California, Berkeley, Oct.1976.

Mander, J. B.; Priestly, M. J. N.; Park, R. (1988), "Theoretical Stress-Strain Model for Confined Concrete", Journal of Structural Engineering, ASCE, V.114: 8, pp. 1804-1826.

Maruyama, K.; Ramirez, H.; Jirsa, J.O. (1984), "Short RC Columns under Bilateral Load Histories", Journal of Structural Engineering, ASCE, V.110: 1, pp. 120-137.

Mattock, A. H. (1964), "Rotational Capacity of Hinging Regions in Reinforced Concrete Beams", Flexural Mechanics of Reinforced Concrete, Proceedings of the International Symposium, Miami, Florida, Nov.10-12.

Mes, D. (1999), "Seismic Retrofitting of Concrete Bridge Columns by External Prestressing", M.A.Sc Thesis, University of Ottawa, Ottawa, Ontario, Canada.

Nagashima, T.; Sugano, S.; Kimura, H.; Ichikawa, A. (1992), "Monotonic Axial Compression Test on Ultra High Strength Concrete Tied Columns", Proceedings of Tenth World Conference on Earthquake Engineering, Madrid, Spain, pp. 2983-2988.

Ozcebe, G.; Saatcioglu, M. (1987), "Confinement of Conrete Columns for Seismic Loading", ACI Structural Journal, V. 84: 4, pp 308-315.

Park, R.; Priestly, M.J.N.; Gill, W.D. (1982), "Ductility of Square Confined Concrete Columns", Journal of Structural Div., ASCE, V.108: 4, pp. 929-951.

Pochanart, S.; Harmon, T. (1989), "Bond-Slip Model for Generalized Excitations Including Fatigue", ACI Materials Journal, V.86: 5, pp 465-474.

Priestly, M.J.N. (1990), "Flexural Test of High-Strength Fiber Retrofitted Column", SEQAD Consulting Engineers, Report No.90-06, Nov.1990, Solana Beach, California.

Priestly, M. J. N., Seible F., Uang C. M. (1994), The Northridge Earthquake of January 17, 1994:Damage Analysis of Selected Freeway Bridges, Structural System Research Project, Report SSRP-94/06, University of California, San Diego, February 1994, pp.260.

Priestly, M. J. N., Seible F., Calvi G. M. (1996), "Seismic Design and Retrofit of Bridges", John Wiley & Sons, Inc., pp.615.

Priestly, M. J. N.; Seibel, F.; Xiao, Y.; Verma, R. (1994), "Steel Jacket of Reinforced Concrete Bridge Columns for Enhanced Shear Strength-Part 1: Theoretical Consideration and Test design", ACI Structural Journal, V. 91: 4, pp 394-405.

Priestly, M. J. N.; Seibel, F.; Xiao, Y.; Verma, R. (1994), "Steel Jacket of Reinforced Concrete Bridge Columns for Enhanced Shear Strength-Part 2: Test Results and Comparison with Theory", ACI Structural Journal, V. 91: 5, pp 537-551.

Popovics, S (1973), "Analytical Approach to Complete Stress-Strain Curves", Cement and Concreter Res., V.3: 5, pp 583-599.

Razvi, S.R. ; Saatcioglu, M. (1989), "Confinement of Reinforced Concrete Columns with Welded Wire Fabric." ACI Structural Journal, American Concrete Institute, V.86 : 5, , pp.615-623.

Razvi, S. ; Saatcioglu, M. (1991), "Discussion of Deformation Properties and Ductility of High-Strength Concrete." ACI Materials Journal, V.88 : 6, pp 674-675.

Razvi, S.R. ; Saatcioglu, M. (1994), "Strength and Deformability of Confined High-Strength Concrete Columns." American Concrete Institute, Structural Journal, V. 91 : 6, pp. 678-687.

Razvi, S. R. ; Saatcioglu, M. (1998), "Discussion of Stress-Strain Model for Confined Reinforced Concrete in Bridge Piers," ASCE Journal of Structural Engineering, V. 124 : 10, pp. 1227-1228.

Razvi, S. R. ; Saatcioglu, M. (1998) "Discussion of Strain Localization in Confined High-Strength Concrete Columns," ASCE Journal of Structural Engineering, V. 124 : 9 , pp. 1090-1092.

Razvi, S.; Saatcioglu, M. (1999), "Confinement Model for High-Strength Concrete ", Journal of Structural Engineering, ASCE, V.125: 3, pp.281-289.

Razvi, S. R. ; Saatcioglu, M. (1999), "Analysis and Design of Concrete Columns for Confinement." Earthquake Spectra, the Journal of Earthquake Engineering Research Institute, Berkley, California, V. 15: 4, pp. 791-811,.

Razvi, S. R. ; Saatcioglu, M. (1999), "Stress-Strain Relationship for Confined High-Strength Concrete." ASCE Journal of Structural Engineering, V. 125 : 3 , pp. 281-289.

Razvi, S.R.; Saatcioglu, M. (1999), "Circular High-Strength Concrete Columns under Concentric Compression." ACI Structural Journal, V. 96 : 5, , pp. 817-825.

Roberts, J. E. (1991), "Recent Advances in Seismic Design and Retrofit of Bridges", Transportation Research Record, No. 1290, National Research Council, Washington, D.C., 1991, pp.75-79.

Rodriguez, M.; Park, R. (1994), "Seismic Load Tests On Reinforced Concrete Columns Strengthened By Jacketing", ACI Structural Journal, V.91: 2, pp. 150-159.

Saadatmanesh, H.; Ehsani, M.R.; Jin, L. (1996), "Seismic Strengthening of Circular Bridge Pier Models with Fiber Composites", ACI Structural Journal, V.93: 6, pp. 639-647.

Saadatmanesh, H.; Ehsani, M.R.; Jin, L. (1997), "Seismic Retrofitting of Rectangular Bridge Columns with Composite Straps", Earthquake Spectra, V.13: 2, pp. 281-304.

Saadatmanesh, H.; Ehsani, M.R.; Jin, L. (1997), "Repair of Earthquake-Damaged RC Columns with FRP Wraps", ACI Structural Journal, V.94: 2, pp. 206-215

Saatcioglu, M.; Alsiwat, J.; Ozcebe, G. (1992), "Hysteretic Behavior of Anchorage Slip in Reinforced Concrete Members", Journal of Structural Engineering, ASCE, V.118: 9, pp.2439-2458.

Saatcioglu, M.; Elnabelsy, G. (2001), "Seismic Retrofit of Bridge Columns with CFRP Jackets", Proceedings of the International Conference on FRP Composites in Civil Engineering, 12-15 December 2001, Hong Kong, China, pp. 833-838.

Saatcioglu, M.; Razvi, S. (1992), "Strength and Ductility of Confined Concrete", Journal of Structural Engineering, ASCE, V.118: 6, pp.1590-1607.

Saatcioglu, M. ; Razvi, S. R. (2002), "Displacement Based Design of Reinforced Concrete Columns for Confinement." The ACI Structural Journal, American Concrete Inst., V. 90: 1, pp. 3-11.

Saatcioglu, M.; Yalcin, C. (2003), "External Prestressing Concrete Columns for Improved Seismic Resistance", Journal of Structural Engineering, ASCE, V.129: 8, pp.1057-1070.

Saiidi, M.S.; Wehbe, N.I.; Sanders, D.H.; Caywood, C.J. (2001), "Shear Retrofit of Flared RC Bridge Columns Subjected to Earthquakes", Journal of Bridge Engineering, May/June, pp. 189-197.

Satoh, H.; Yamakawa, T.; Nasrollahzadeh Neshli, K.; Inaba, H. (2001), "Seismic and/or Emergency Retrofit of Extremely Short RC Columns Utilizing Prestressed Aramid Fiber Belts and Steel Angles", Proceedings of the International Conference on FRP Composites in Civil Engineering, 12-15 December 2001, Hong Kong, China, pp. 909-916.

Sawyer, H. A. (1964), ''Design of concrete frames for two failure states'', Proceedings of ASCE-ACI Int. Symp. On the Flexural Mech. of Reinforced Concrete, 405–431.

Scott, B.D.; Park, R.; Priestly, M.J.N. (1982), "Stress-strain Behavior of Concrete Confined by Overlapping Hoops at High and Low Strain Rates", ACI Structural Journal, V.79: 1, pp. 13-27.

Selna, L.G; Morrill, K.B.; Ersoy, O.K. (1973), "Shear Colapse, Elastic and Inelastic Biaxial Studies of the Olive View Hospital Psychiatric Day Clinic", Proceedings, U.S-Japan Seminar on Earthquake Engineering, Berkeley.

Sheikh, S. A. (1982), "A Competetive Study of Confinemen Models", ACI Structural Journal, V.79: 4, pp. 296-305.

Sheikh, S. A.; Uzumeri, S. M. (1980), "Strength ad Ductility of Tied Concrete columns", Journal of Structural Engineering, ASCE, V.106:5, pp. 1079-1102.

Sheikh, S. A.; Uzumeri, S. M. (1982), "Analytical Model for Concrete Confinement in Tied Columns", Journal of Structural Engineering, ASCE, and V.108:5, pp. 2703-2723.

Sheikh, S. A.; Yeh, C. C. (1986), "Flexural Behavior of Confined Concrete Columns", ACI Structural Journal, V.86: 2, pp. 389-404.

Sheikh, S. A.; Yeh, C. C. (1992), "Analytical Moment-Curvature Relations for Tied Concrete Columns", Journal of Structural Engineering, ASCE, and V.118:2, pp. 529-544.

Soroushian, P.; Choi, K.B. (1989), "Local Bond of Deformed Bars with Different Diameters in Confined Concrete", ACI Structural Journal, V.86: 2, pp. 217-222.

Soroushian, P.; Choi, K.B. (1991), "Analytical Evaluation of Straight Bar Anchorage Design in Exterior Joints", ACI Structural Journal, V.88: 2, pp. 161-168.

Stallings, J.M.; Tedesco J.W.; El-Mihilmy, M.; McCauly, M. (2000), "Field Performance of FRP Bridge Repairs", Journal of Bridge Engineering, ASCE, V.5:2, pp. 107-113.

Sugano, S. (1981), "Seismic Strengthening of Existing Reinforced Concrete Buildings in Japan", Bulletin of the New Zealand National Society for Earthquake Engineering, V.14, pp.209-222.

Umehara, H.; Jirsa, J.O. (1984), "Short Rectangular RC Columns under Bidirectional Loading", Journal of Structural Engineering, ASCE, V.110: 3, pp. 605-618.

Unjoh, S.; Kawashima, K. (1992), "Seismic Inspection and Seismic Strengthening of Reinforced Concrete Bridge Piers", National Institute of Standards & Technology, C/O US Department of Commerce, Gaithersburg, MD (USA), no. 840, pp. 91-124.

Vecchio, F.J.; Collins, M.P. (1986), "The modified Compression Field Theory for Reinforced Concrete Elements Subjected to Shear ", ACI Journal, Proceedings V.83: 2, pp. 219-231.

Whirley, R.G.; Engelmann, B.E. (1993), "DYNA3D: A Nonlinear Explicit Three Dimensional Finite Element Code for Solid and Structural Mechanics", User Manual, Report UCRL-MA-107254 Rev.1, Lawrence Livermore National Laboratory, Livermore, CA.

Woodward, K.A.; Jirsa, J.O. (1984), "Influence of Reinforcement on RC Short Columns Lateral Resistance", Journal of Structural Engineering, ASCE, V.110: 1, pp. 90-104.

Xiao, Y.; Martin, G. R.; Yin Z.; Ma R.(1995), "Experimental Validation of A Prefabricated Jacketing System for Bridge Column Retrofit", USC Structural Engineering Research Report, No. USC-SERR95/02, Department of Civil Engineering, University of Southern California, 150p.

Yalcin, C. (1998), "Seismic Evaluation and Retrofitting of Existing Reinforced Concrete Bridge Columns", PhD Thesis, University of Ottawa, Ottawa, Ontario, Canada.

Yalcin, C. and Saatcioglu, M. (2000), "Inelastic Analysis of Reinforced Concrete Columns," Computers and Structures, Pergamon Press, V. 77: 5, pp. 539-555.

Yamakawa, T.; Nasrollahzadeh Nesheli, K.; Satoh, H. (2003), "Seismic Retrofitting of RC Columns Using Prestressed Aramid Fiber Belts", Fourth International Conference of Earthquake Engineering and Seismology, 12-14 May 2003 Tehran, Islamic Republic of Iran.

Yoshimura, K.; Kikuchi, K.; Kuroki, M. (1991), "Seismic Shear Strengthening Method for Existing Reinforced Concrete Short Columns", Proceedings of ACI Conference on Evaluation and Rehabilitation of Concrete Structures and Innovations in Design, SP-128, American Concrete Institute, Farmington Hills, Mich., pp. 1065-1079.

Appendix A

Experimentally Recorded Strain Values

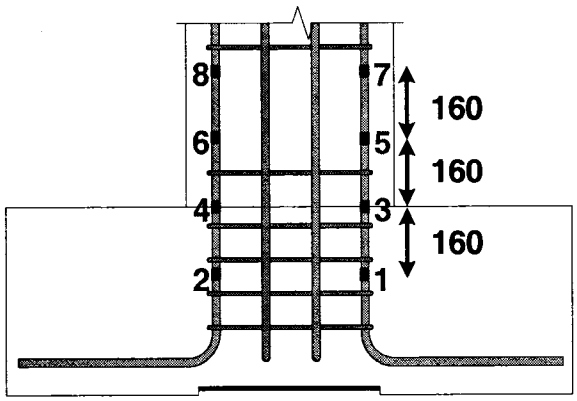

a) Strain gauge location on longitudinal bars

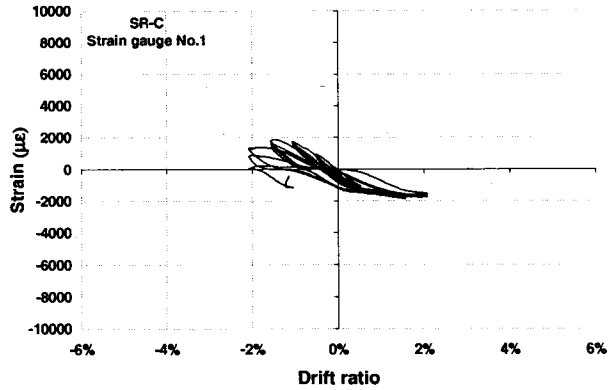

b) Strain gauge No.1

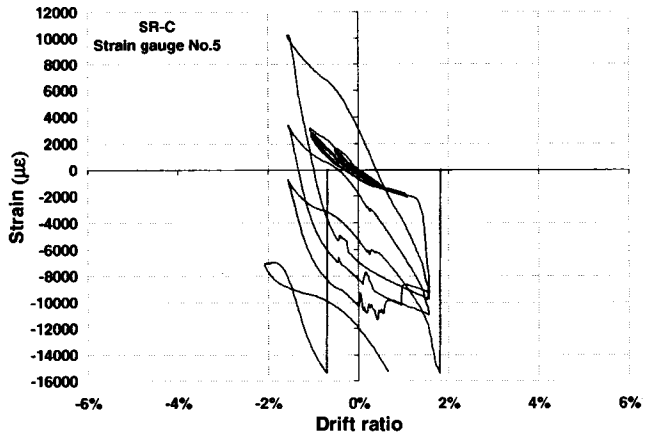

c) Strain gauge No.5

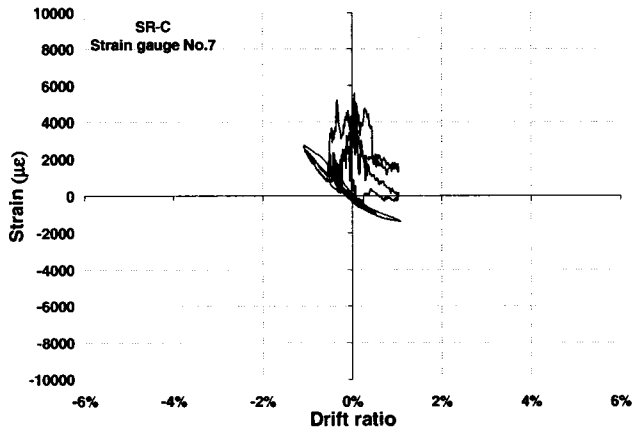

d) Strain gauge No.7

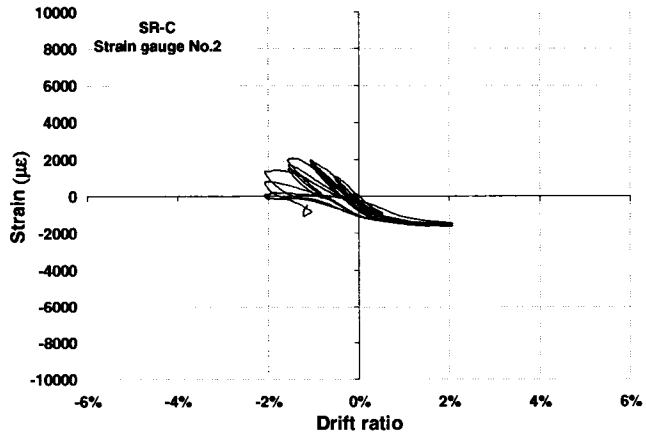

e) Strain gauge No.2

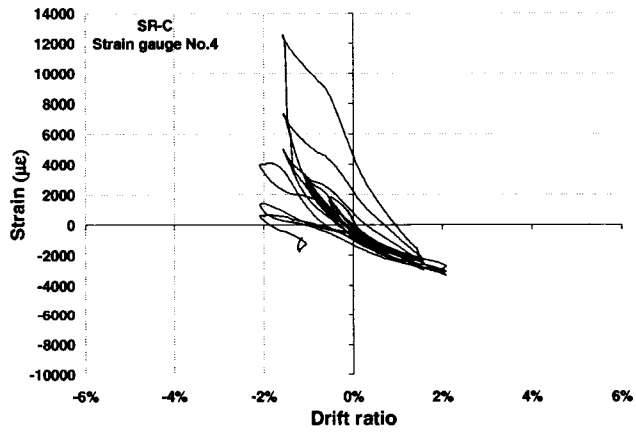

f) Strain gauge No.4

Figure A.1 Longitudinal reinforcement steel strains for column SR-C

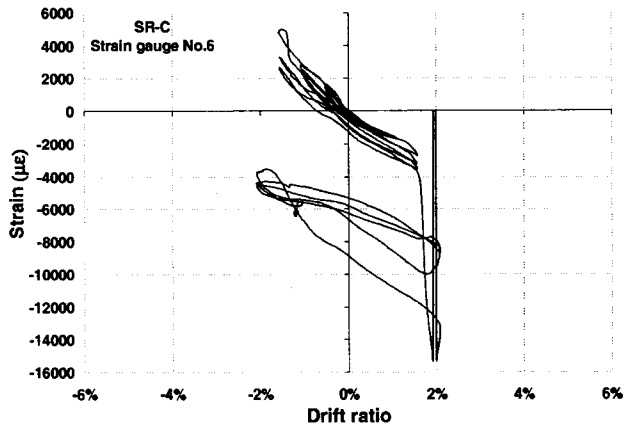

g) Strain gauge No.6

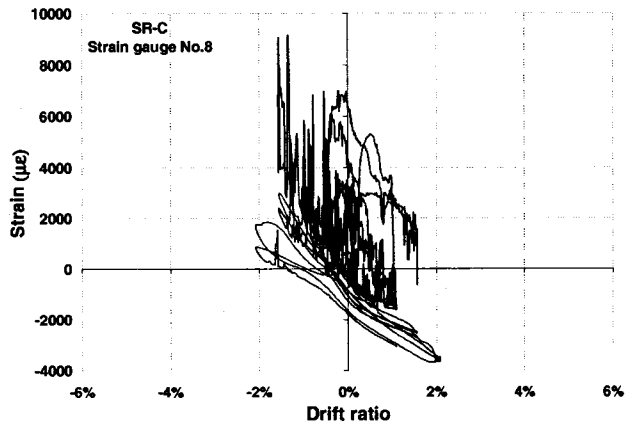

h) Strain gauge No.8

Figure A.1 Longitudinal reinforcement steel strains for column SR-C (Continued)

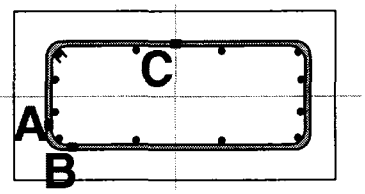

a) Strain gauge location on the 2nd hoop

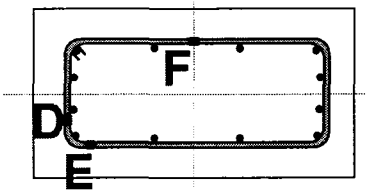

b) Strain gauge location on the 3rd hoop

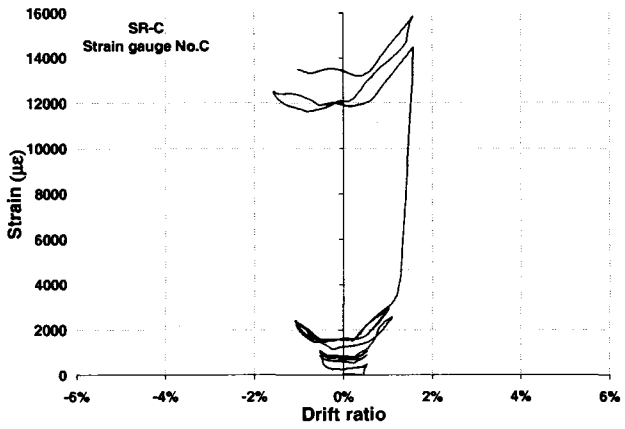

c) Strain gauge No.C

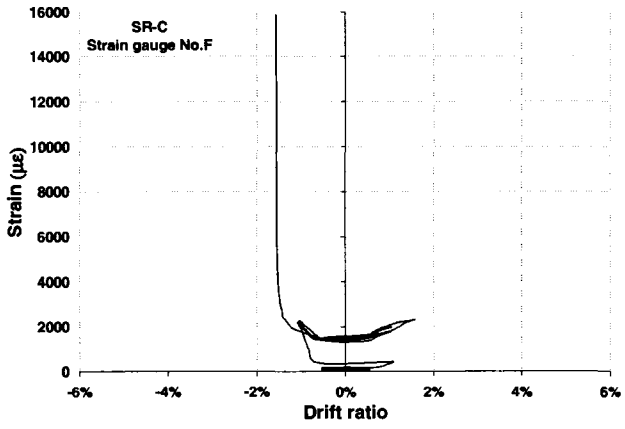

d) Strain gauge No.F

Figure A.2 Transverse reinforcement steel strains for column SR-C

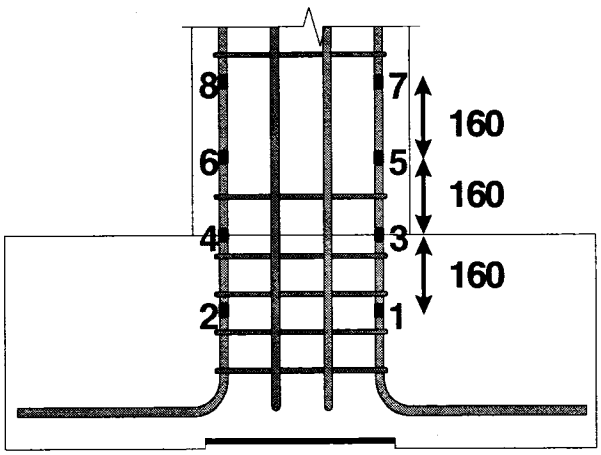

a) Strain gauge location on longitudinal bars

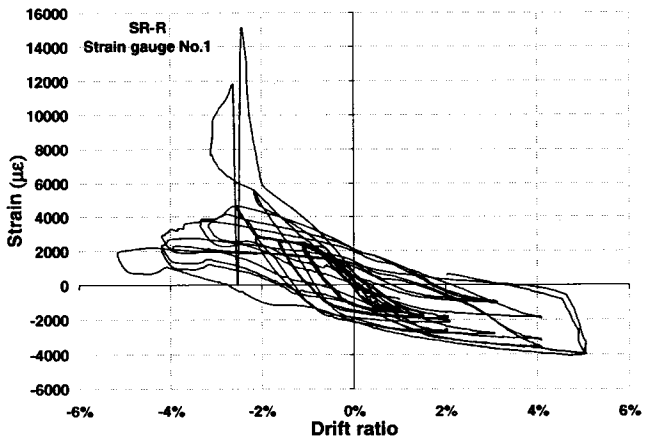

b) Strain gauge No.1

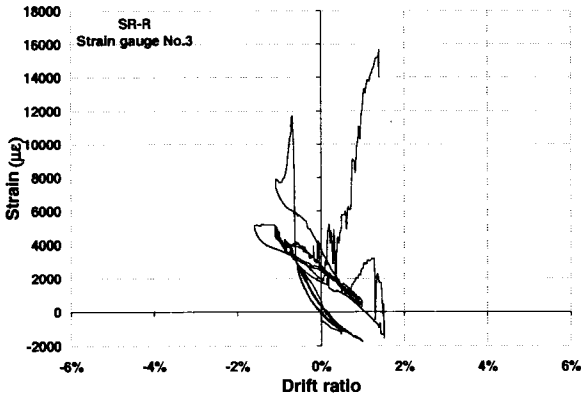

c) Strain gauge No.3

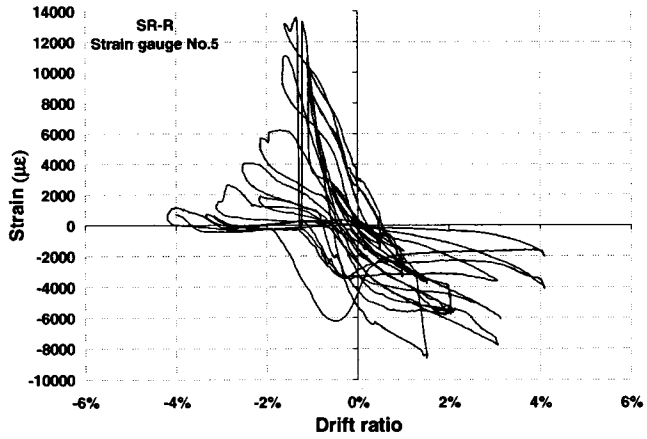

d) Strain gauge No.5

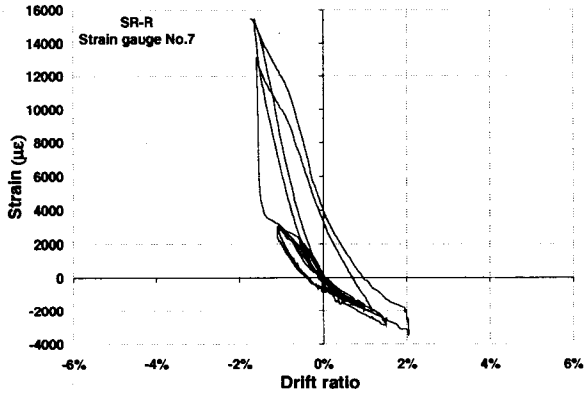

e) Strain gauge No.7

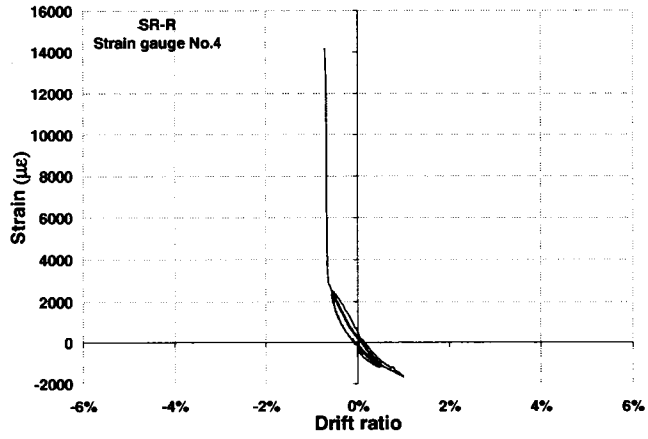

f) Strain gauge No.4

Figure A.3 Longitudinal reinforcement steel strains for column SR-R

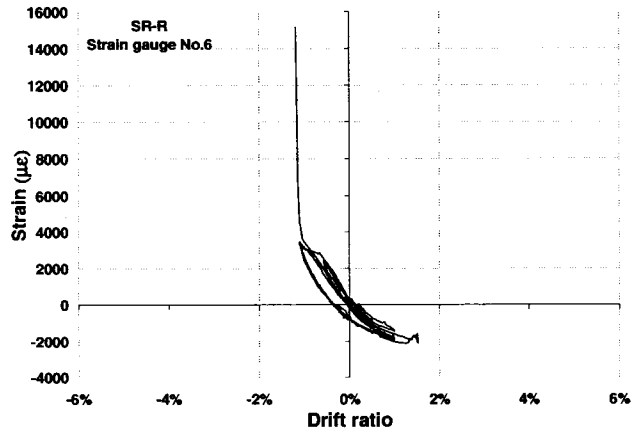

g) Strain gauge No.6

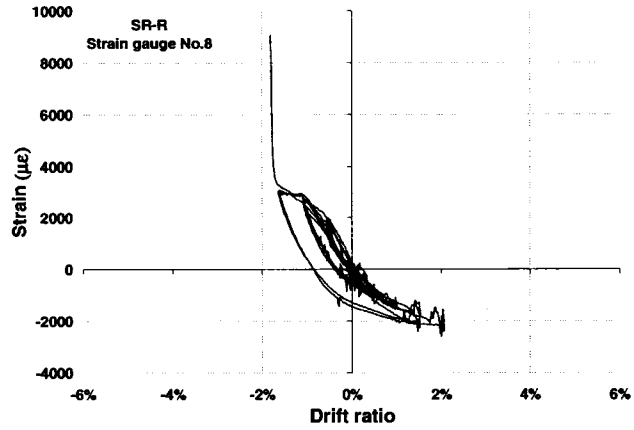

h) Strain gauge No.8

Figure A.3 Longitudinal reinforcement steel strains for column SR-R (Continued)

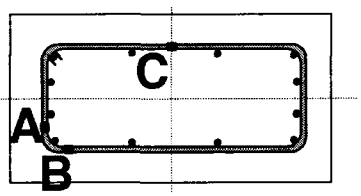

a) Strain gauge location on the 2nd hoop

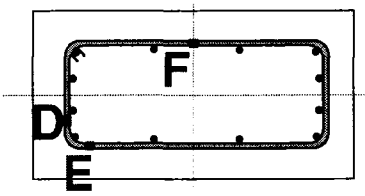

b) Strain gauge location on the 3rd hoop

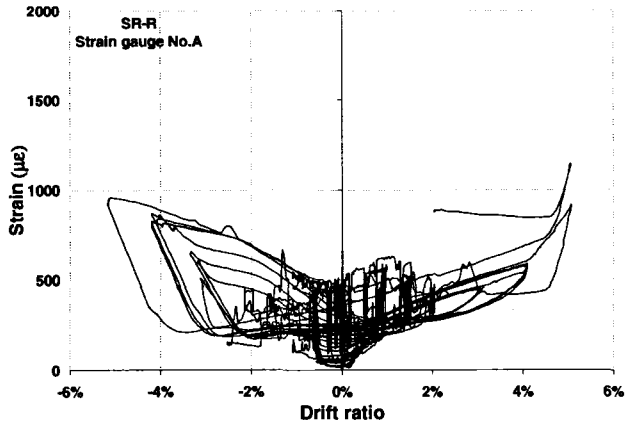

c) Strain gauge No.A

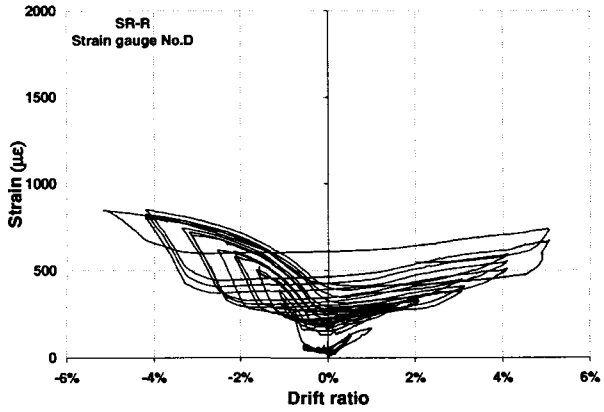

d) Strain gauge No.D

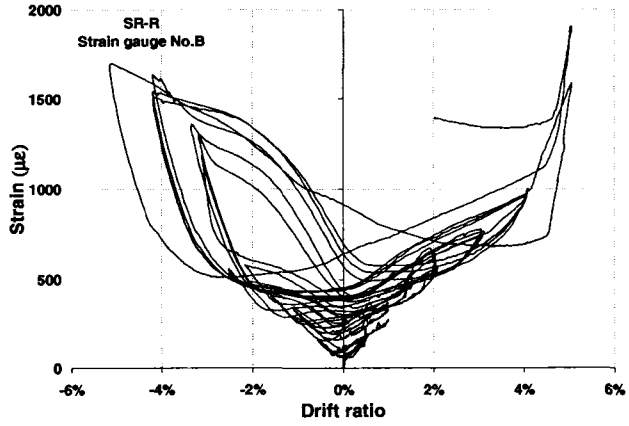

e) Strain gauge No.B

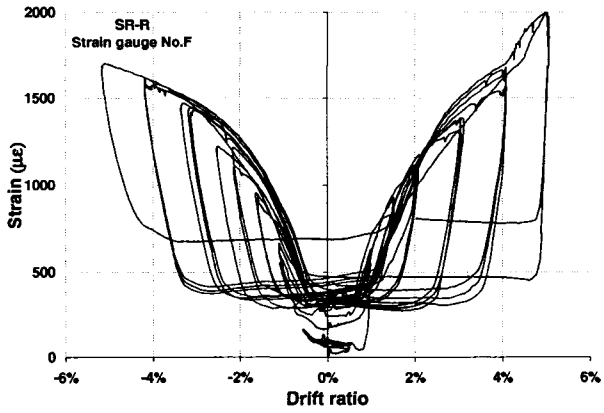

f) Strain gauge No.F

Figure A.4 Transverse reinforcement steel strains for column SR-R

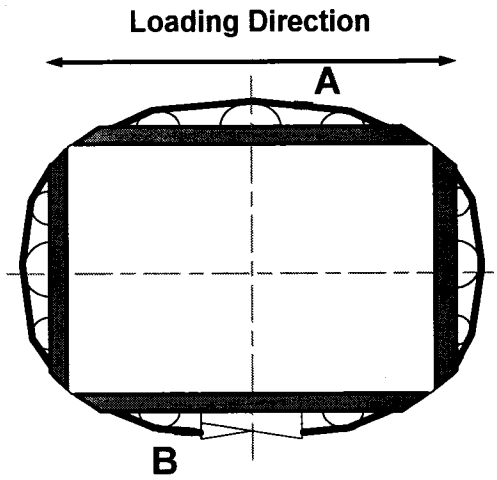

a) Strain gauge location on prestressing strands

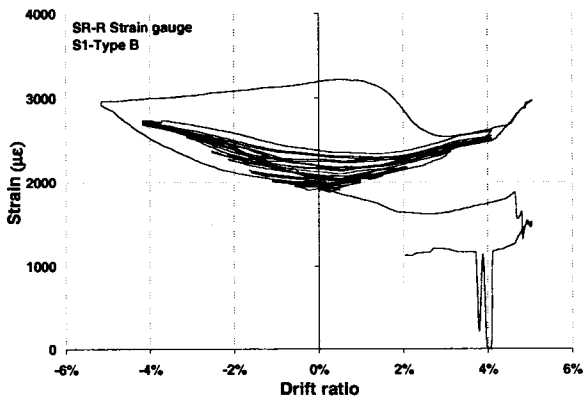

b) 1st Strand(Gauge Type B)

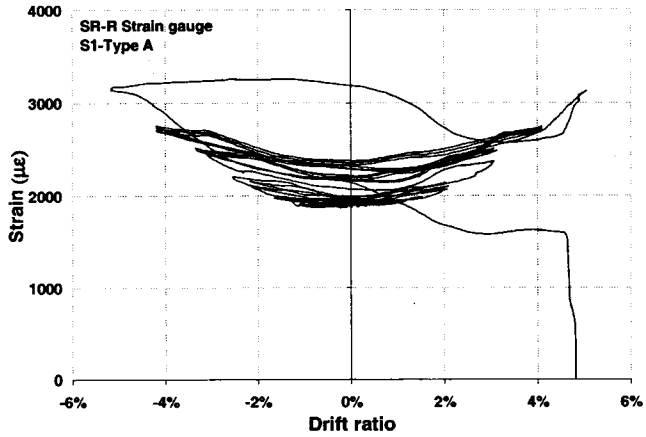

c) 1st Strand(Gauge Type A)

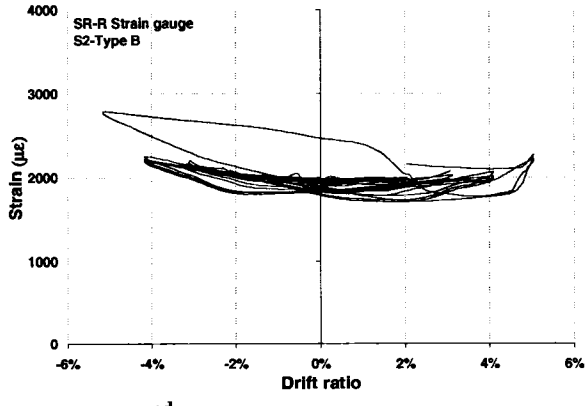

d) 2nd Strand(Gauge Type B)

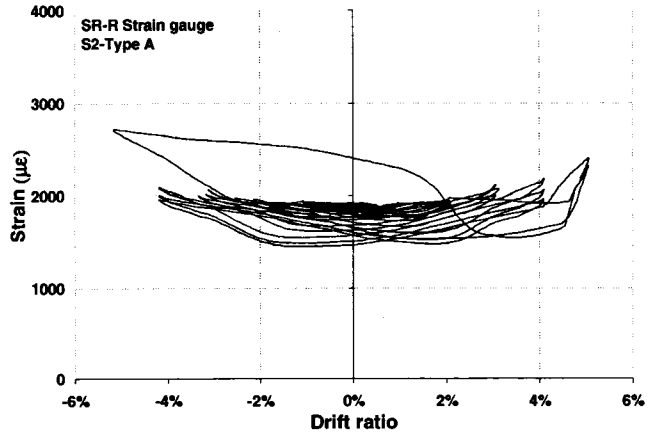

e) 2nd Strand(Gauge Type A)

Figure A.5 Prestressing strand strains for column SR-R

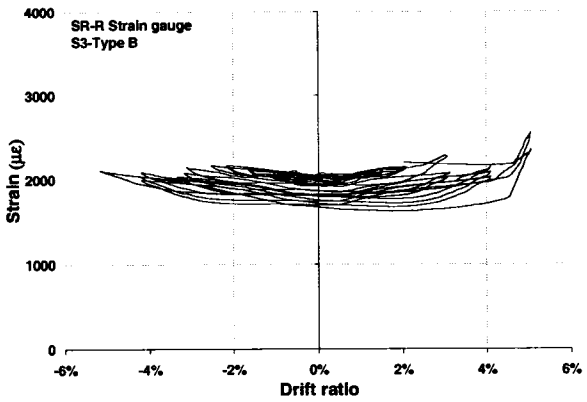

f) 3rd Strand(Gauge Type B)

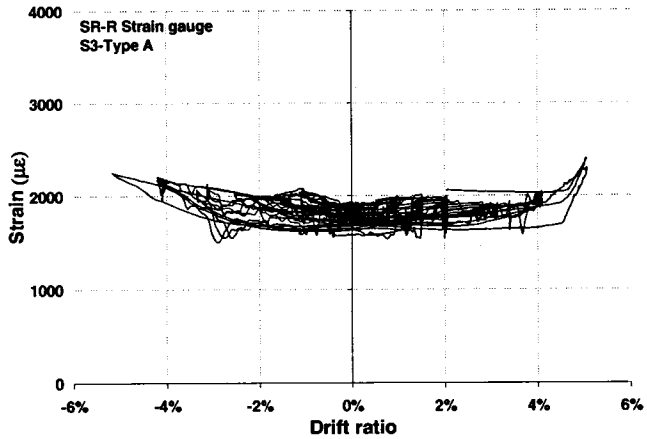

g) 3rd Strand(Gauge Type A)

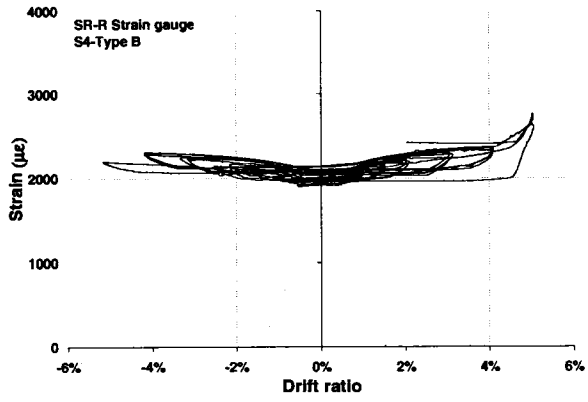

h) 4th Strand(Gauge Type B)

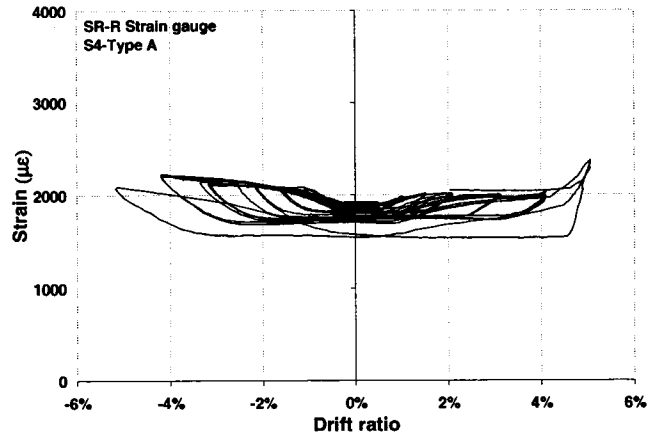

i) 4th Strand(Gauge Type A)

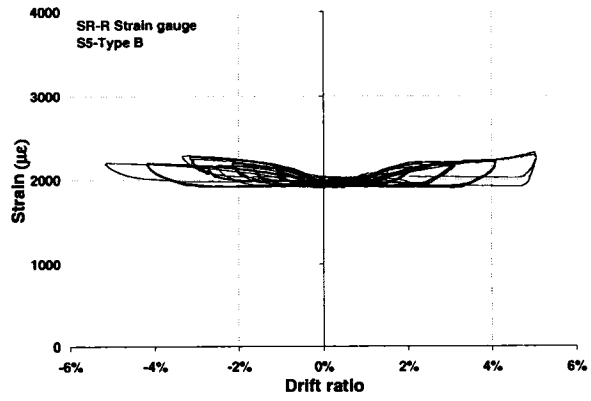

j) 5th Strand(Gauge Type B)

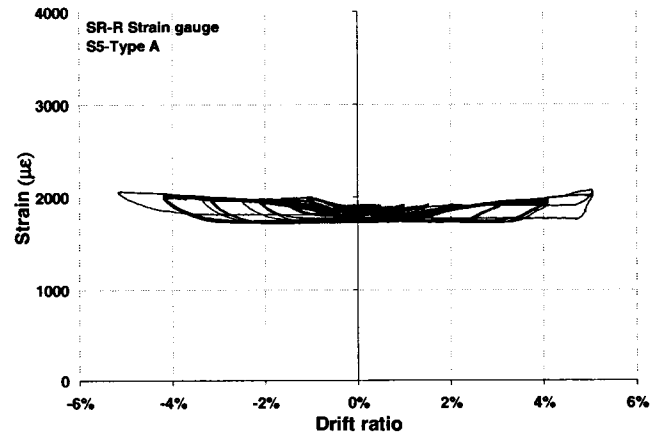

k) 5th Strand(Gauge Type A)

Figure A.5 Prestressing strand strains for column SR-R (Continued)

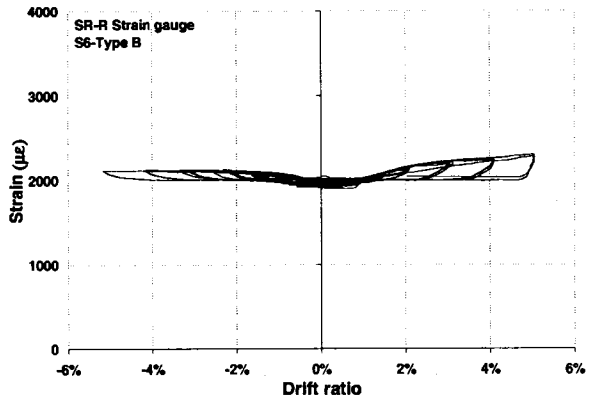

l) 6th Strand(Gauge Type B)

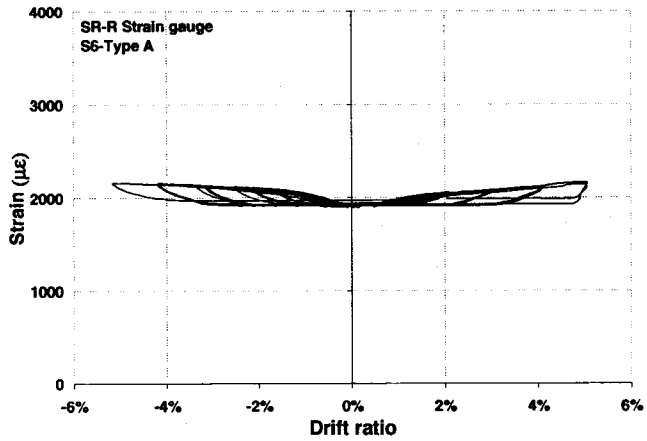

m) 6th Strand(Gauge Type A)

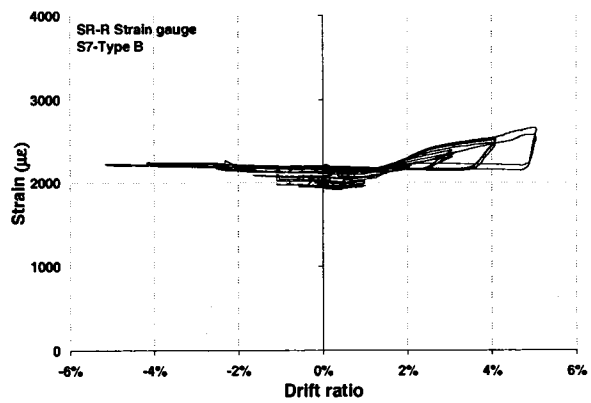

n) 7th Strand(Gauge Type B)

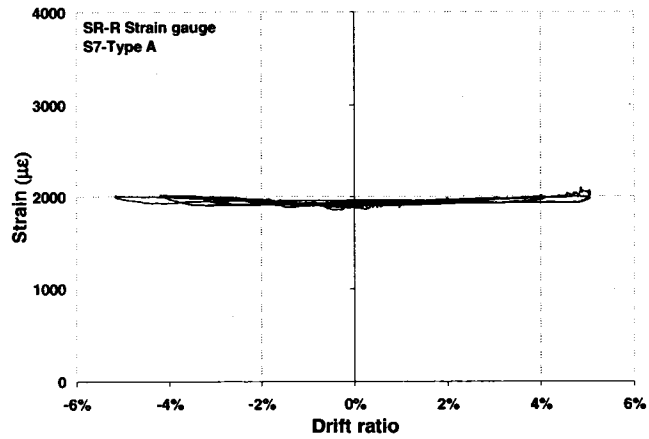

o) 7th Strand(Gauge Type A)

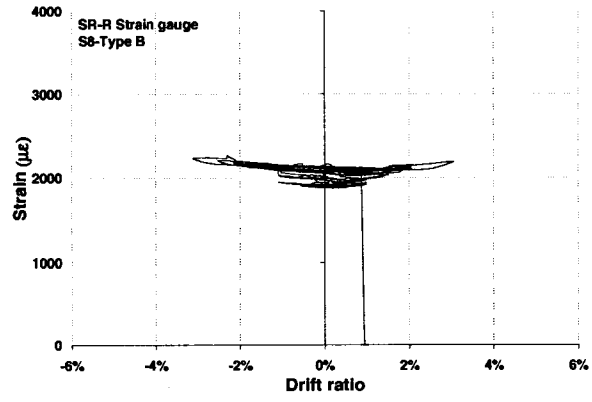

p) 8th Strand(Gauge Type B)

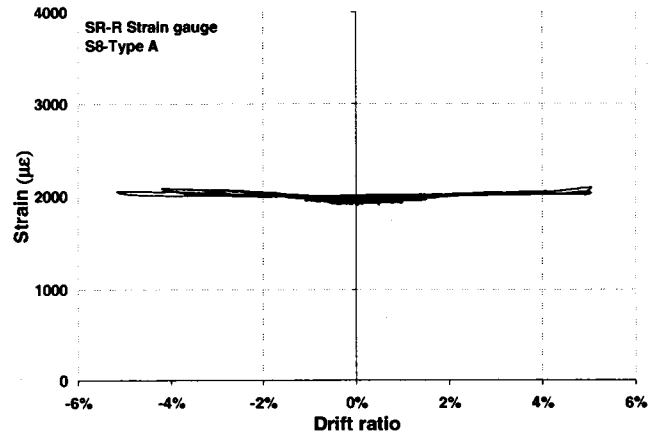

q) 8th Strand(Gauge Type A)

Figure A.5 Prestressing strand strains for column SR-R (Continued)

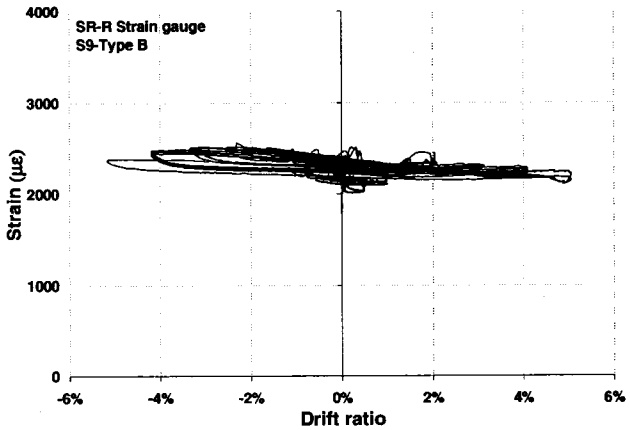

r) 9th Strand(Gauge Type B)

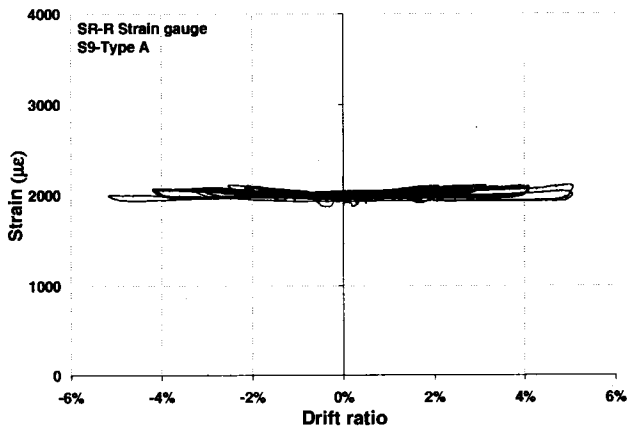

s) 9th Strand(Gauge Type A)

Figure A.5 Prestressing strand strains for column SR-R (Continued)

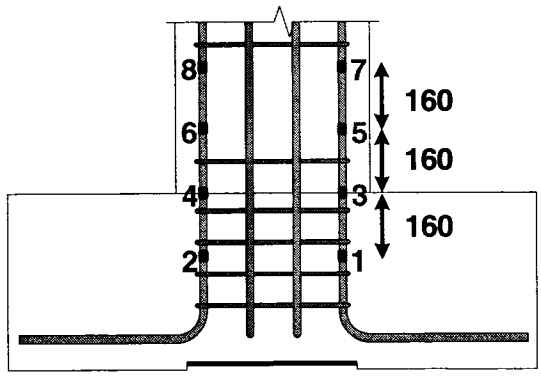

a) Strain gauge location on longitudinal bars

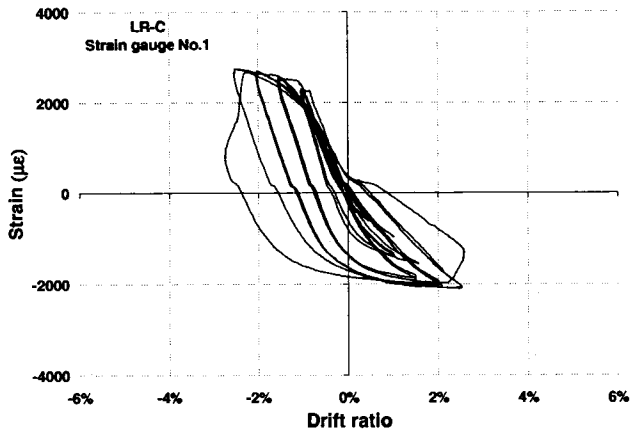

b) Strain gauge No.1

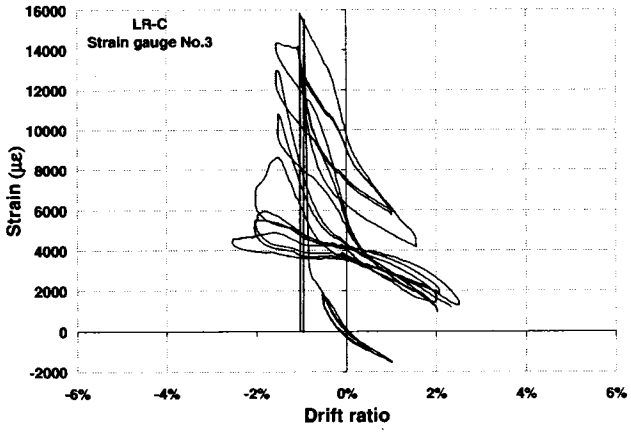

c) Strain gauge No.3

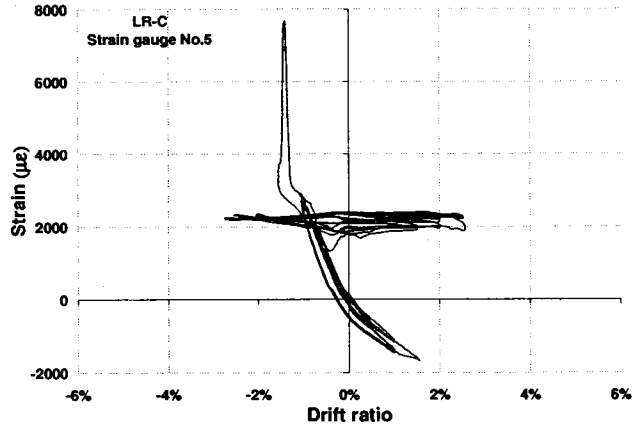

d) Strain gauge No.5

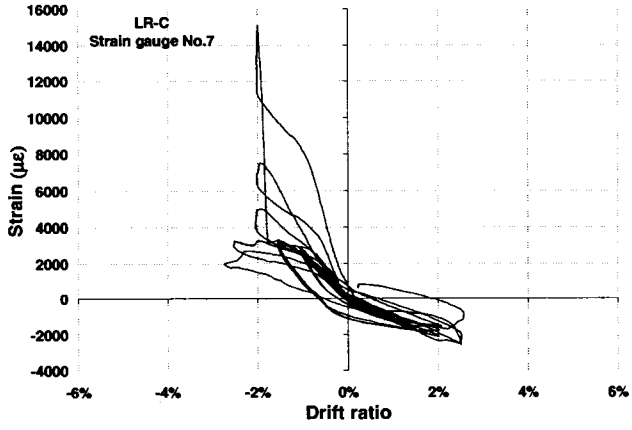

e) Strain gauge No.7

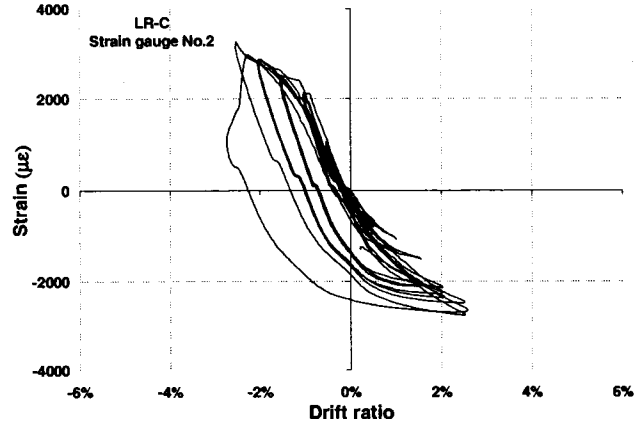

f) Strain gauge No.2

Figure A.6 Longitudinal reinforcement steel strains for column LR-C

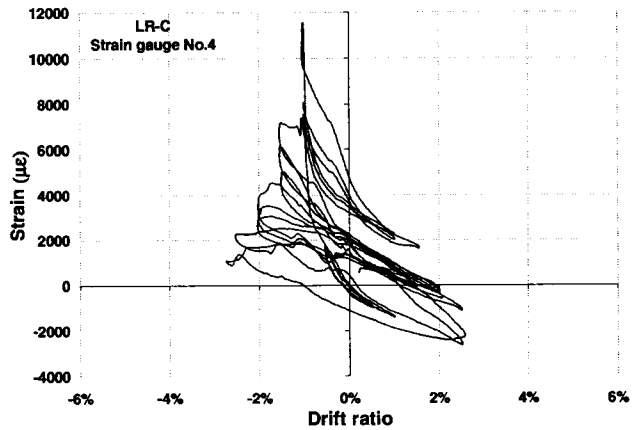

g) Strain gauge No.4

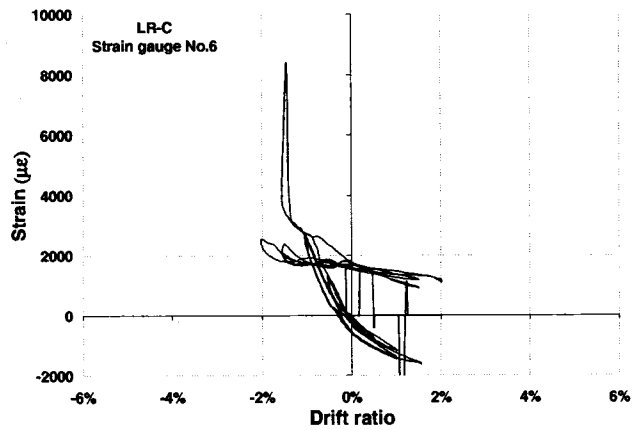

h) Strain gauge No.6

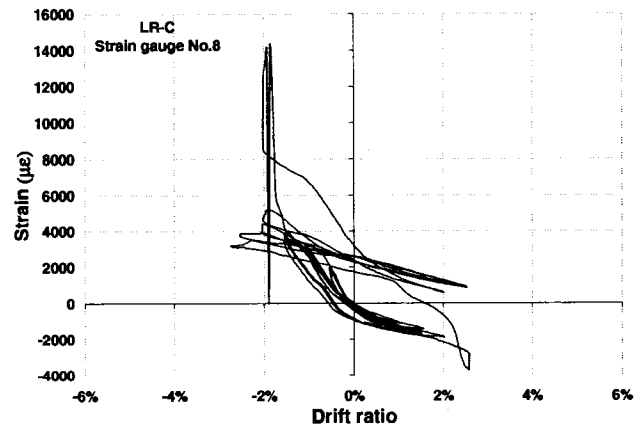

i) Strain gauge No.8

Figure A.6 Longitudinal reinforcement steel strains for column LR-C (Continued)

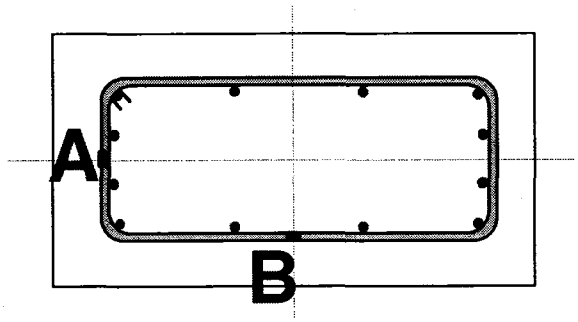

a) Strain gauge location on the 2nd hoop

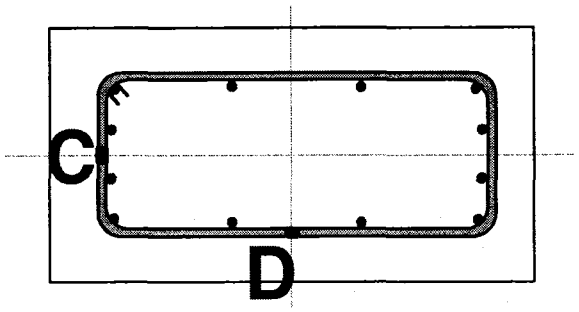

b) Strain gauge location on the 3rd hoop

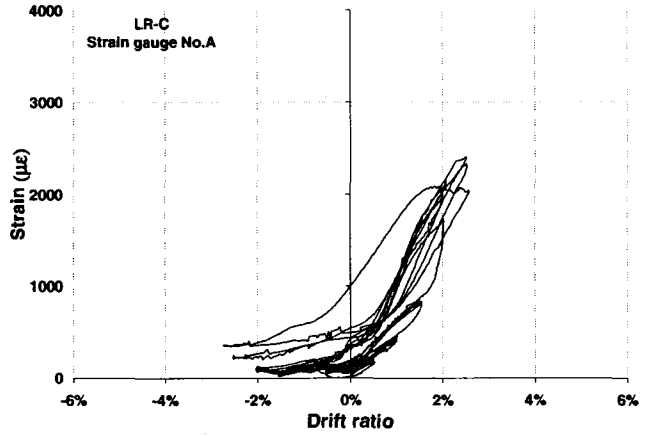

c) Strain gauge No.A

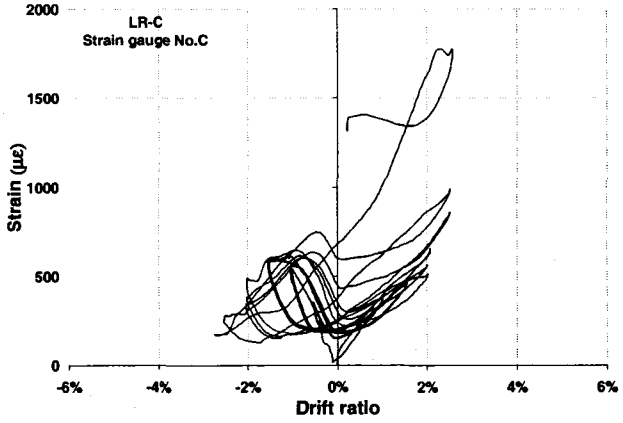

d) Strain gauge No.C

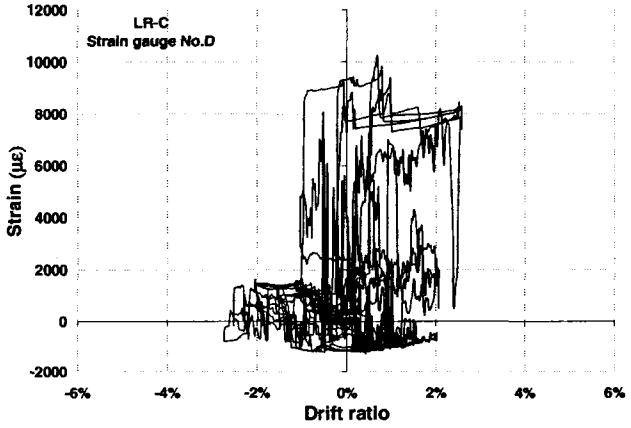

e) Strain gauge No.D

Figure A.7 Transverse reinforcement steel strains for column LR-C

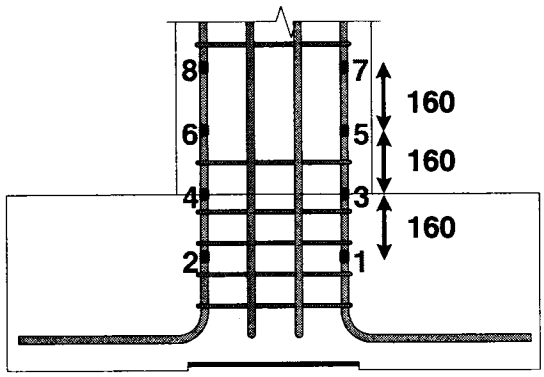

a) Strain gauge location on longitudinal bars

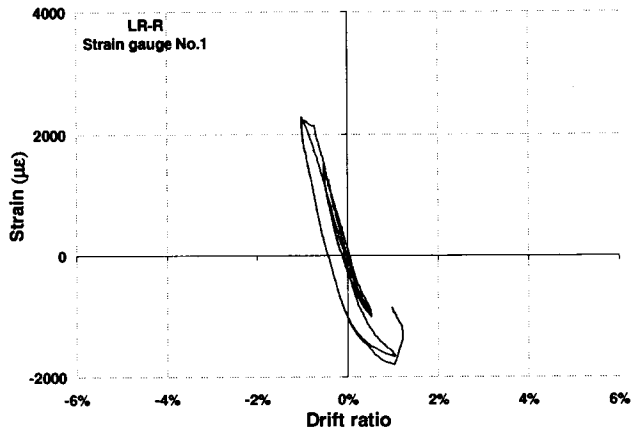

b) Strain gauge No.1

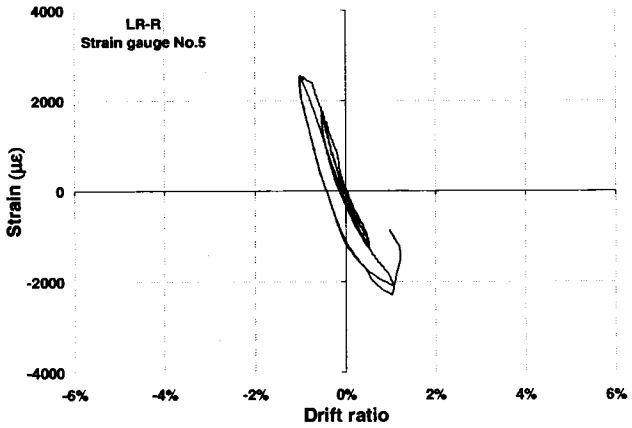

c) Strain gauge No.5

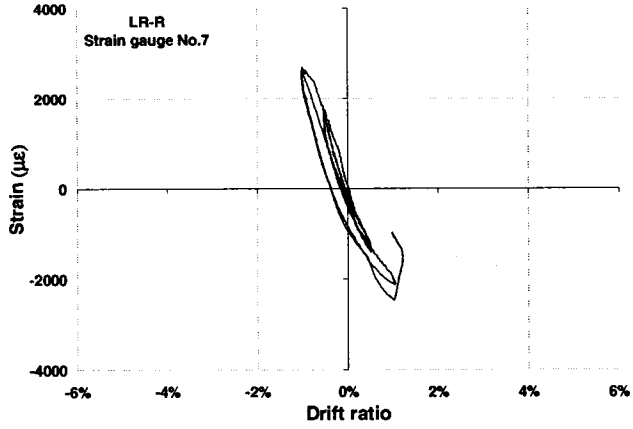

d) Strain gauge No.7

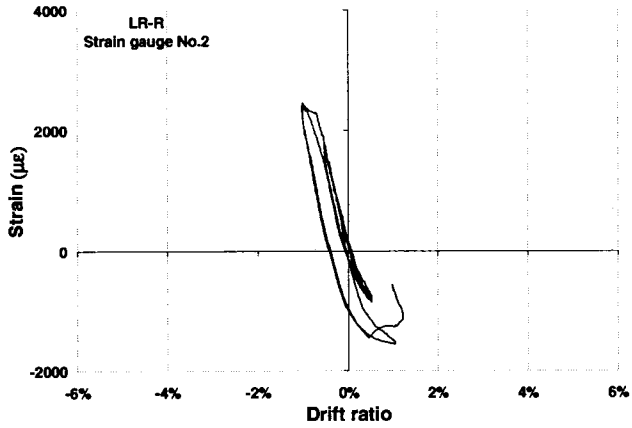

e) Strain gauge No.2

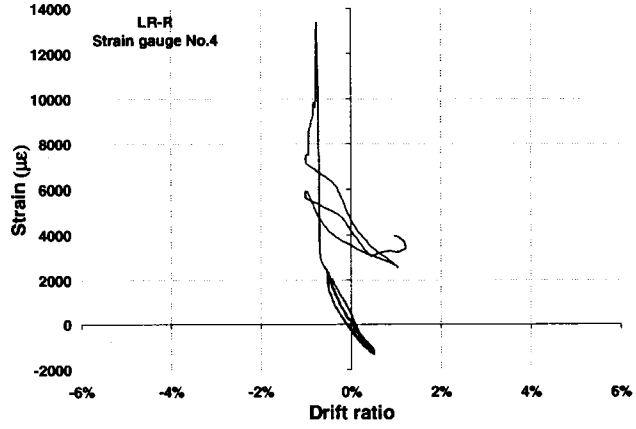

f) Strain gauge No.4

Figure A.8 Longitudinal reinforcement steel strains for column LR-R

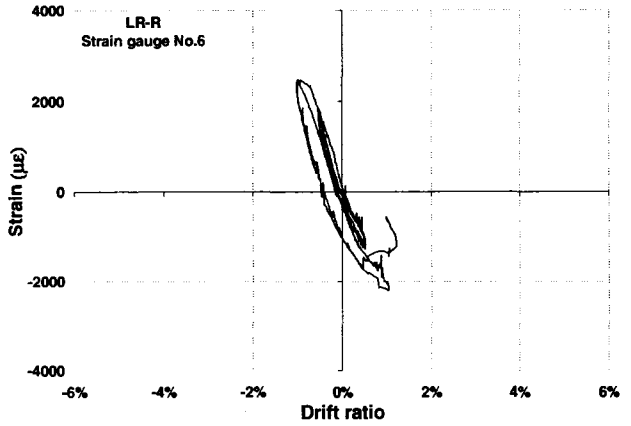

g) Strain gauge No.6

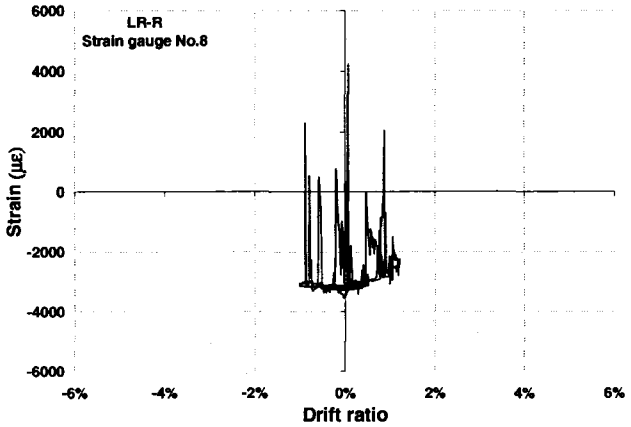

h) Strain gauge No.8

Figure A.8 Longitudinal reinforcement steel strains for column LR-R (Continued)

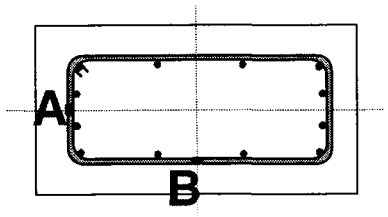

a) Strain gauge location on the 2nd hoop

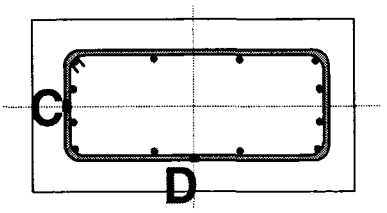

b) Strain gauge location on the 3rd hoop

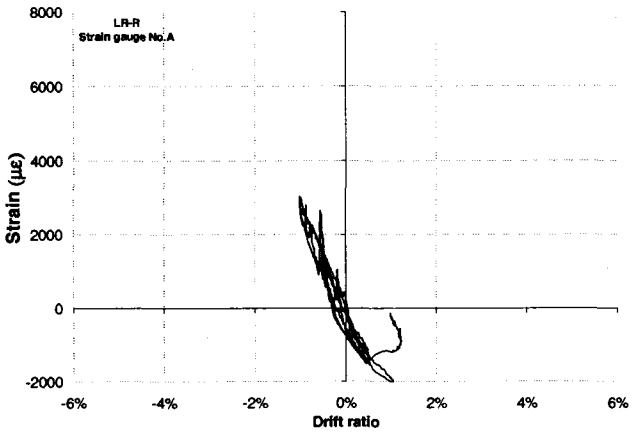

c) Strain gauge No.A

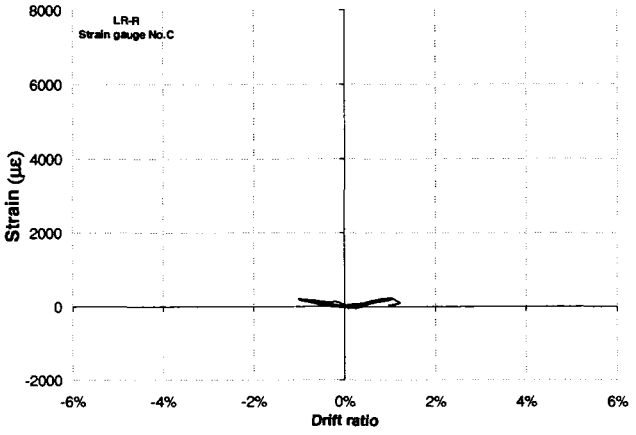

d) Strain gauge No.C

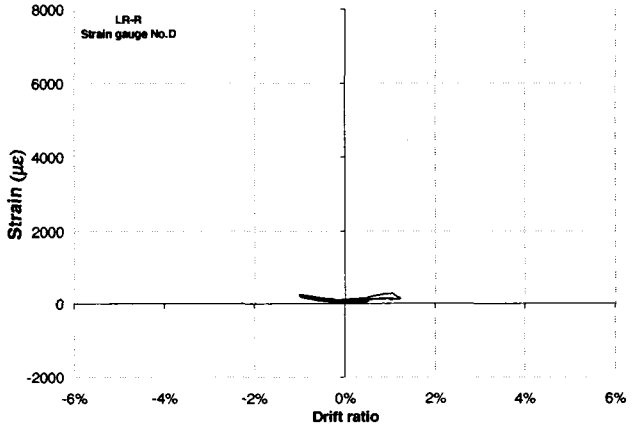

e) Strain gauge No.D

Figure A.9 Transverse reinforcement steel strains for column LR-R

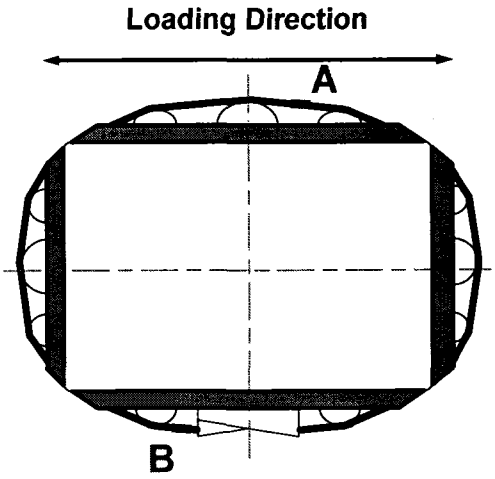

a) Strain gauge location on prestressing strands

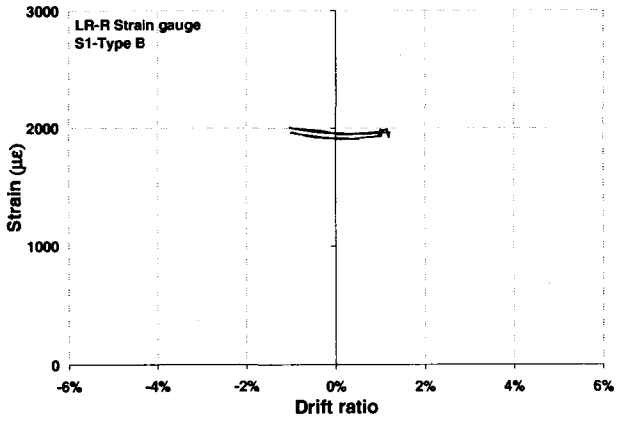

b) 1st Strand(Gauge Type B)

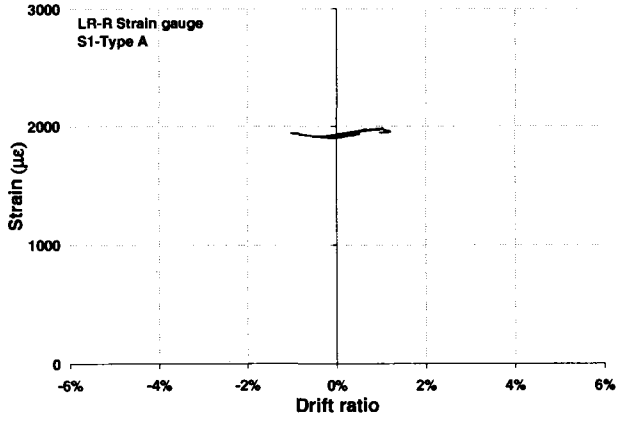

c) 1st Strand(Gauge Type A)

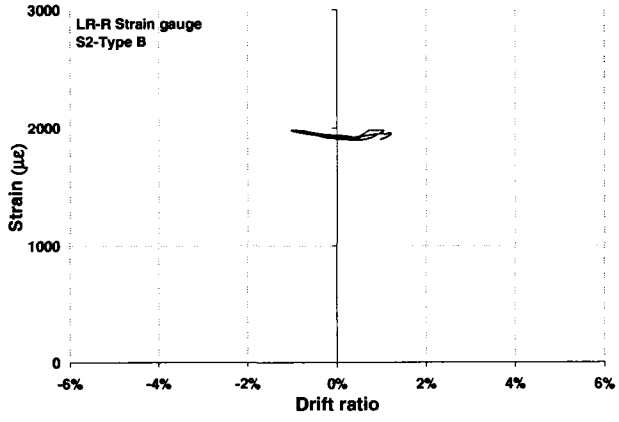

d) 2nd Strand(Gauge Type B)

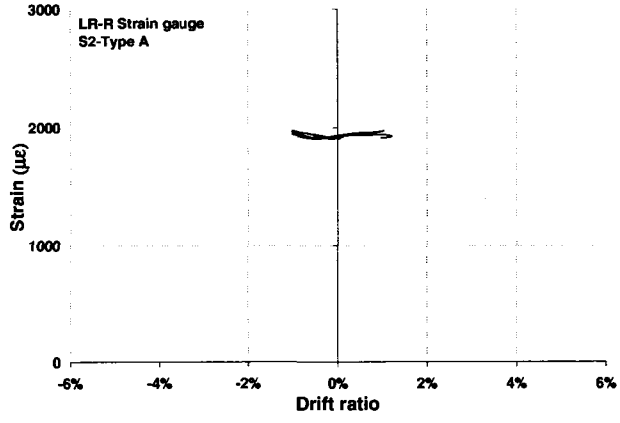

e) 2nd Strand(Gauge Type A)

Figure A.10 Prestressing strand strains for column LR-R

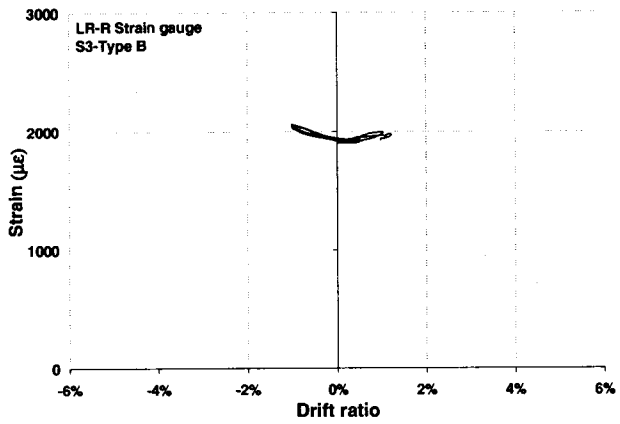

f) 3rd Strand(Gauge Type B)

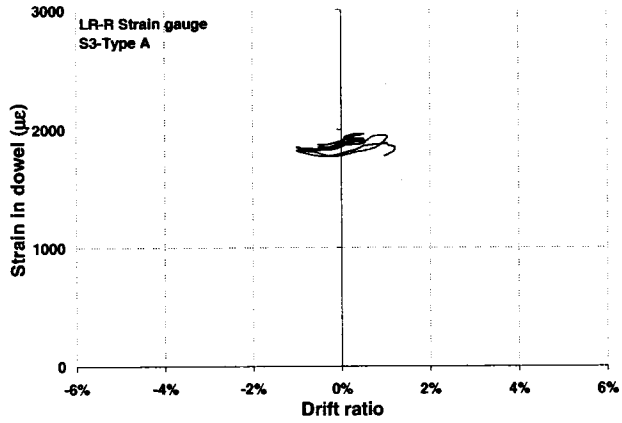

g) 3rd Strand(Gauge Type A)

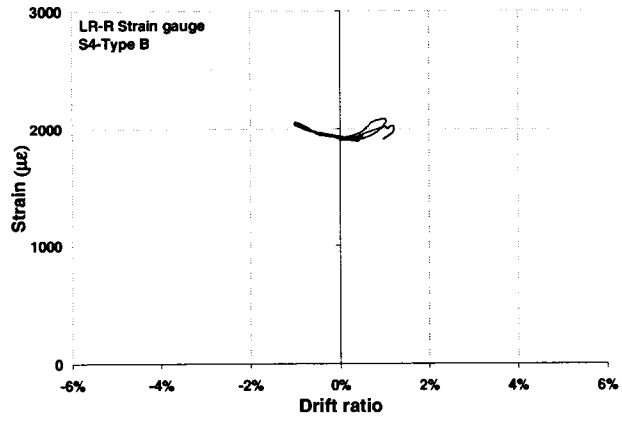

h) 4th Strand(Gauge Type B)

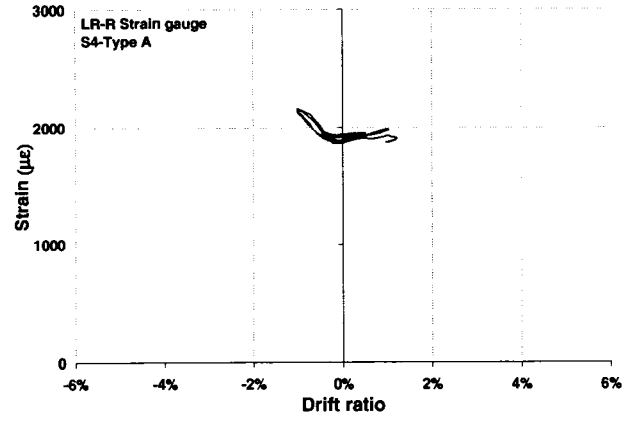

i) 4th Strand(Gauge Type A)

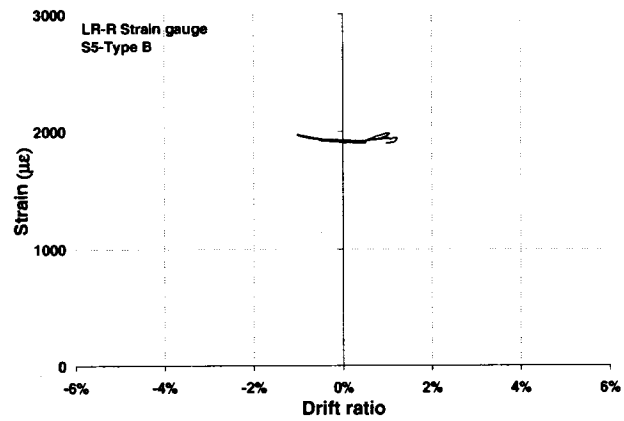

j) 5th Strand(Gauge Type B)

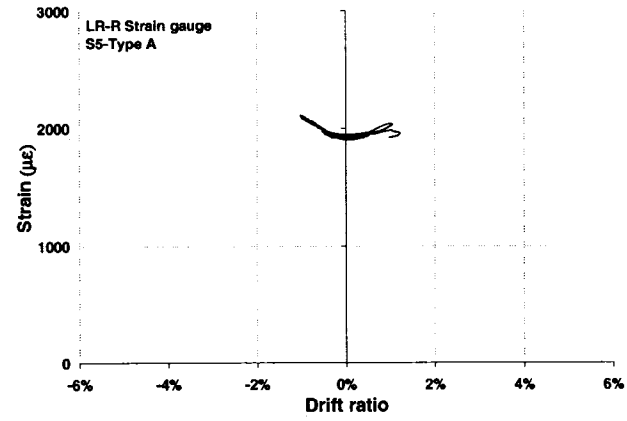

k) 5th Strand(Gauge Type A)

Figure A.10 Prestressing strand strains for column LR-R (Continued)

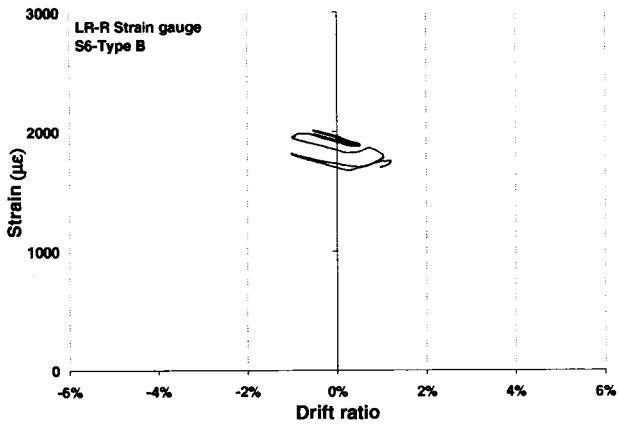

l) 6th Strand(Gauge Type B)

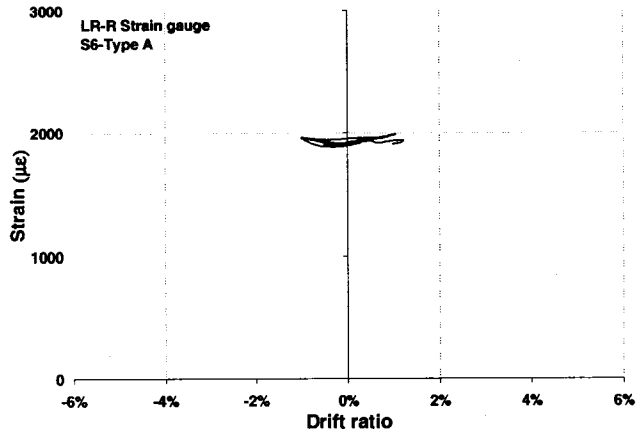

m) 6th Strand(Gauge Type A)

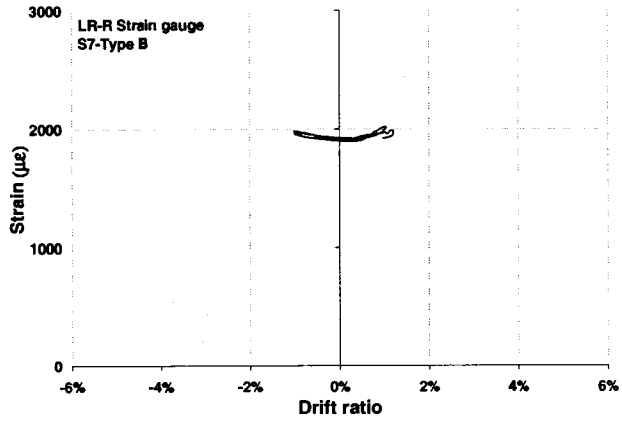

n) 7th Strand(Gauge Type B)

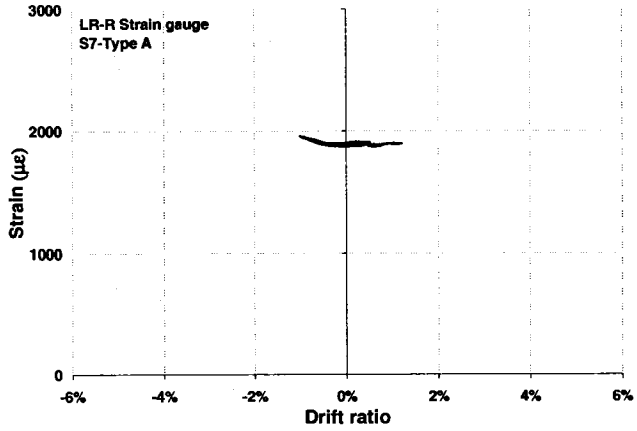

o) 7th Strand(Gauge Type A)

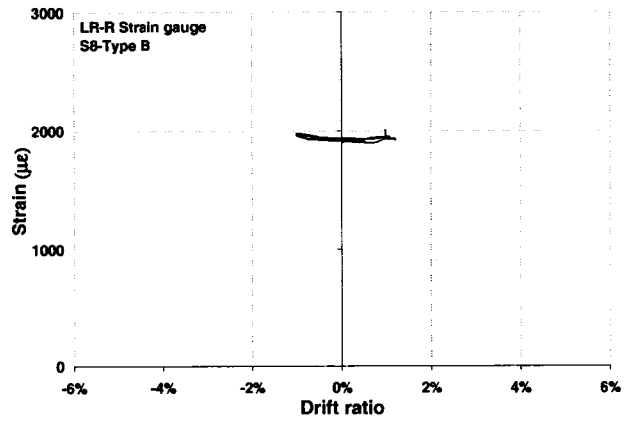

p) 8th Strand(Gauge Type B)

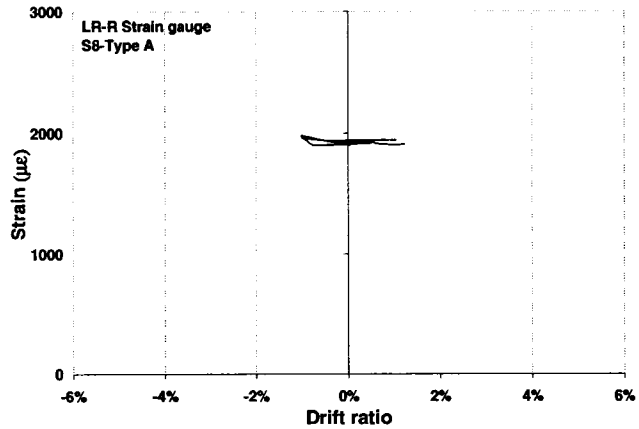

q) 8th Strand(Gauge Type A)

Figure A.10 Prestressing strand strains for column LR-R (Continued)

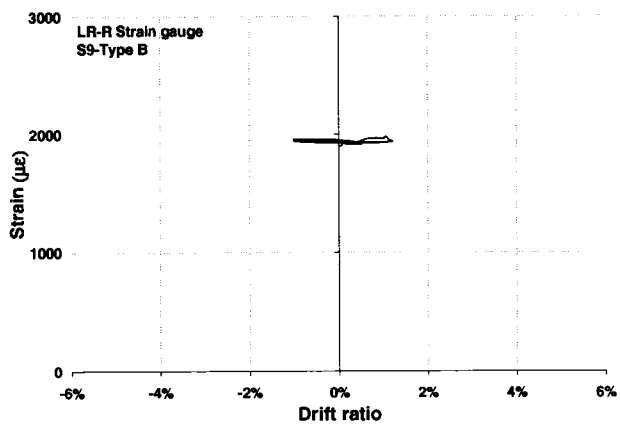

r) 9th Strand(Gauge Type B)

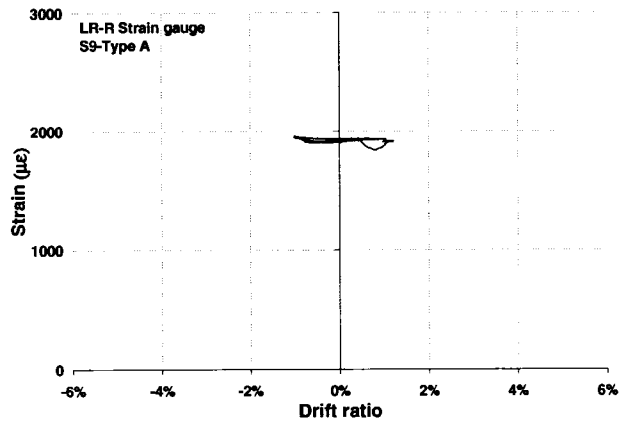

s) 9th Strand(Gauge Type A)

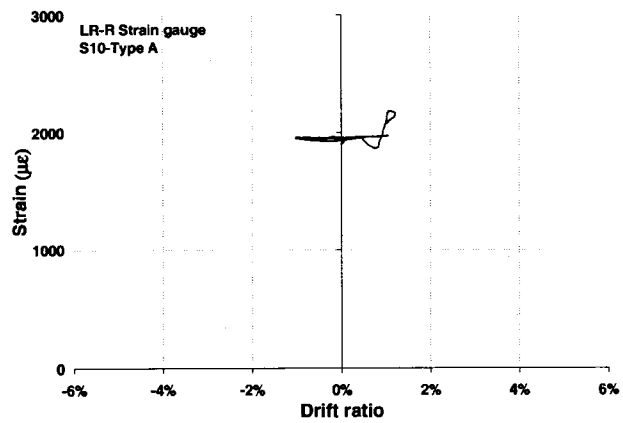

t) 10th Strand(Gauge Type A)

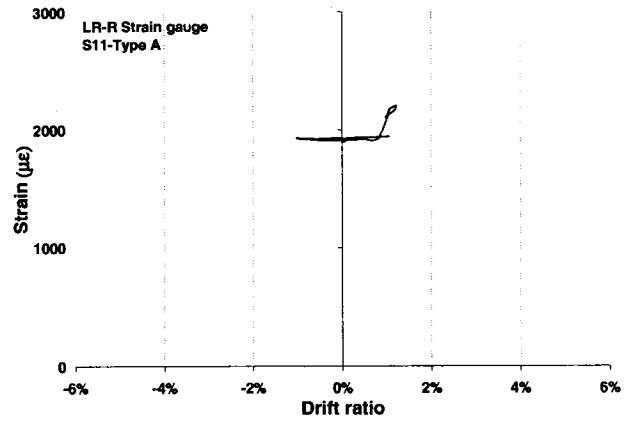

u) 11th Strand(Gauge Type A)

Figure A.10 Prestressing strand strains for column LR-R (Continued)

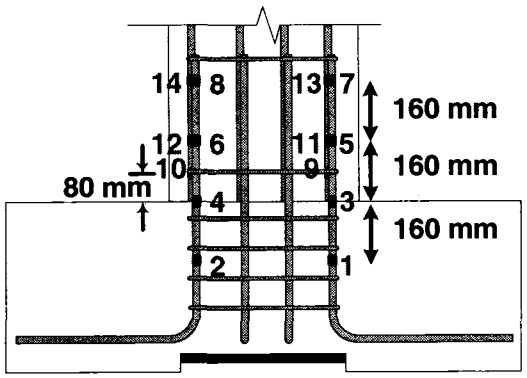

a) Strain gauge location on longitudinal bars

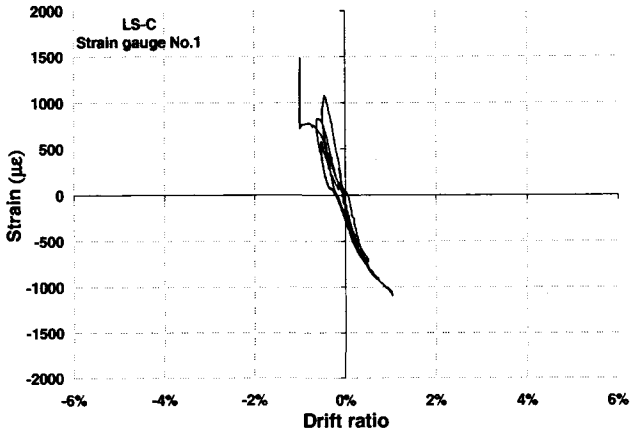

b) Strain gauge No.1

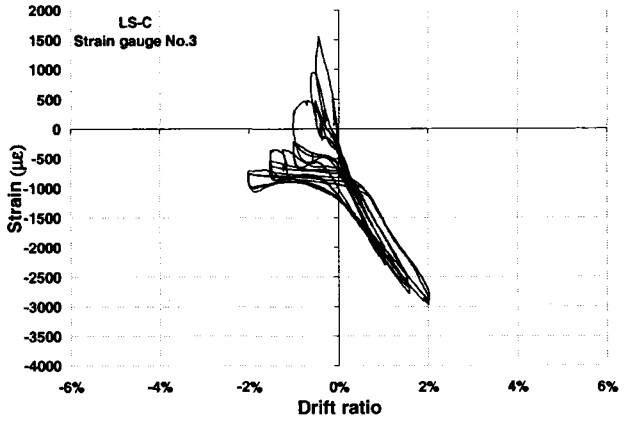

c) Strain gauge No.3

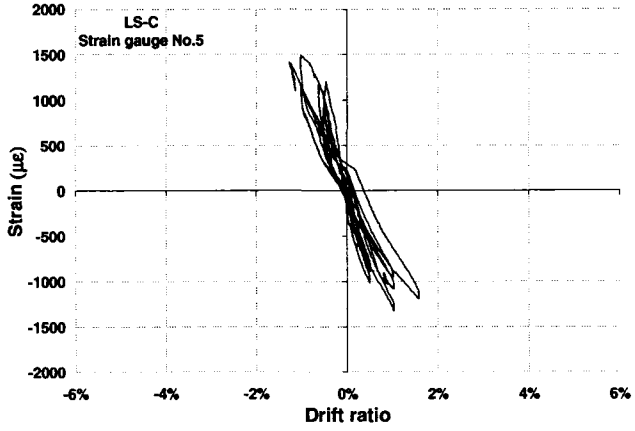

d) Strain gauge No.5

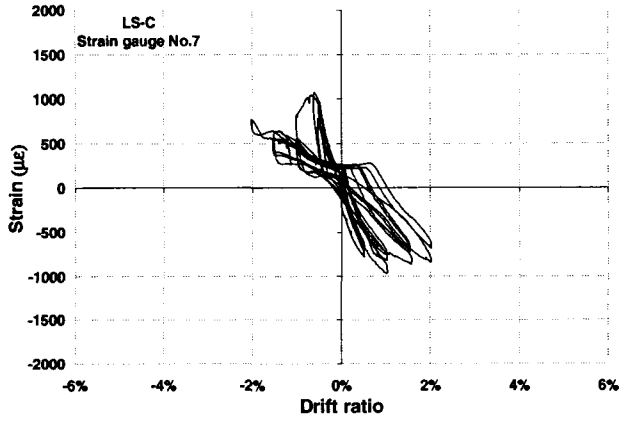

e) Strain gauge No.7

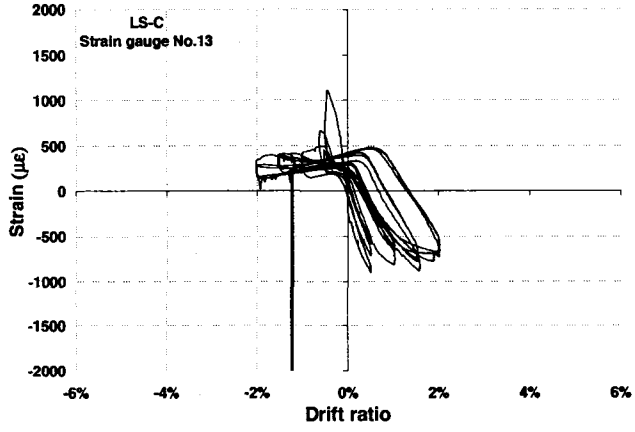

f) Strain gauge No.13

Figure A.11 Longitudinal reinforcement steel strains for column LS-C

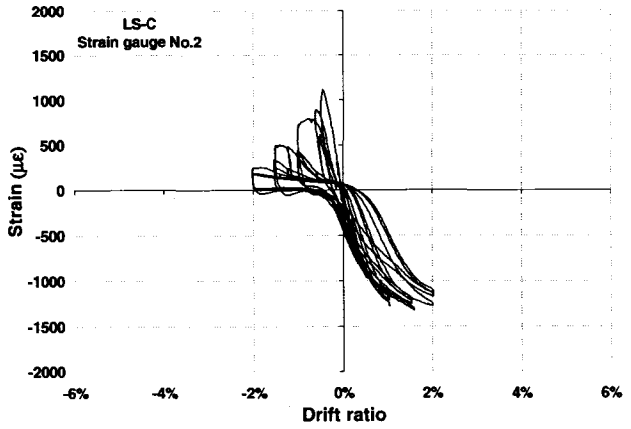

g) Strain gauge No.2

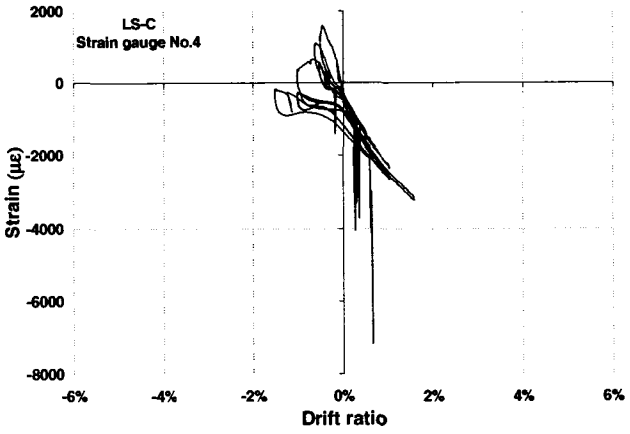

h) Strain gauge No.4

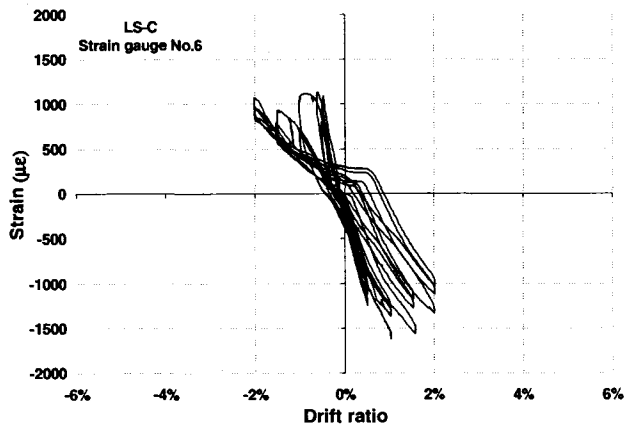

i) Strain gauge No.6

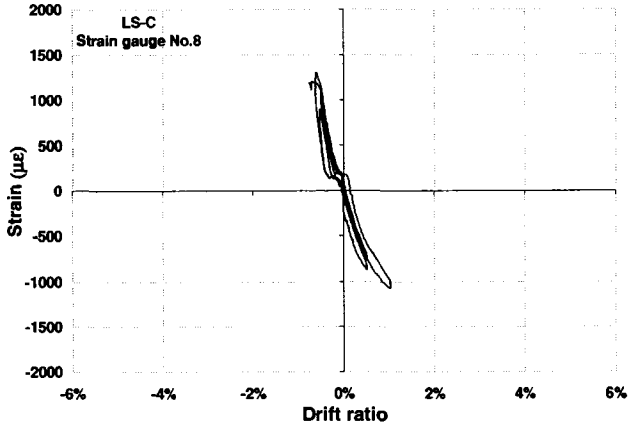

j) Strain gauge No.8

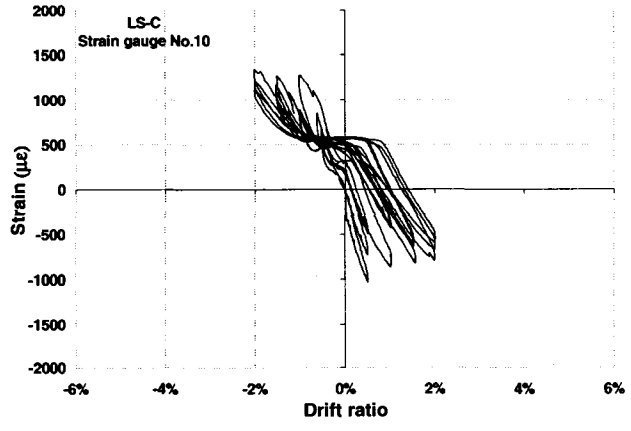

k) Strain gauge No.10

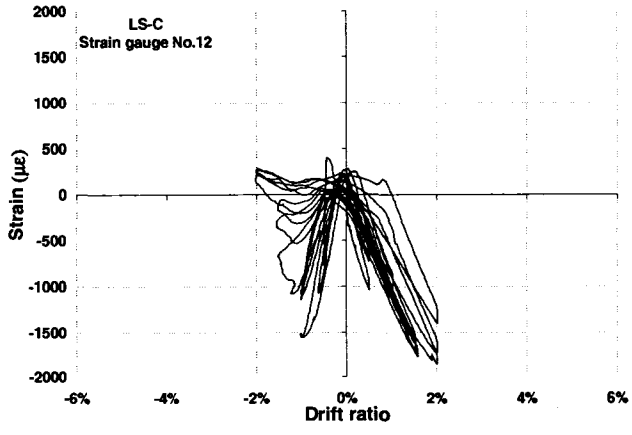

l) Strain gauge No.12

Figure A.11 Longitudinal reinforcement steel strains for column LS-C (Continued)

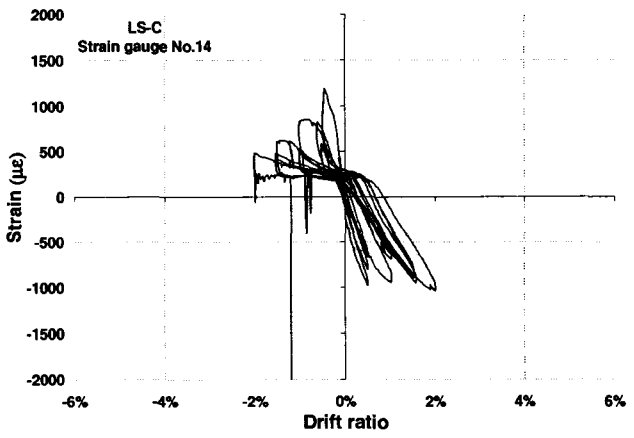

m) Strain gauge No.14

Figure A.11 Longitudinal reinforcement steel strains for column LS-C (Continued)

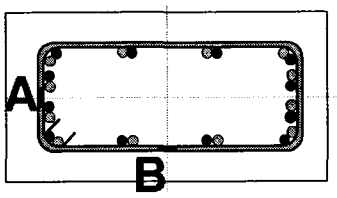

a) Strain gauge location on the 2nd hoop

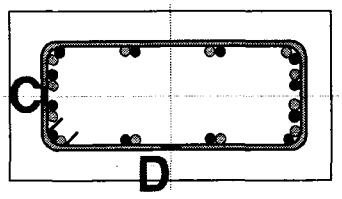

b) Strain gauge location on the 3rd hoop

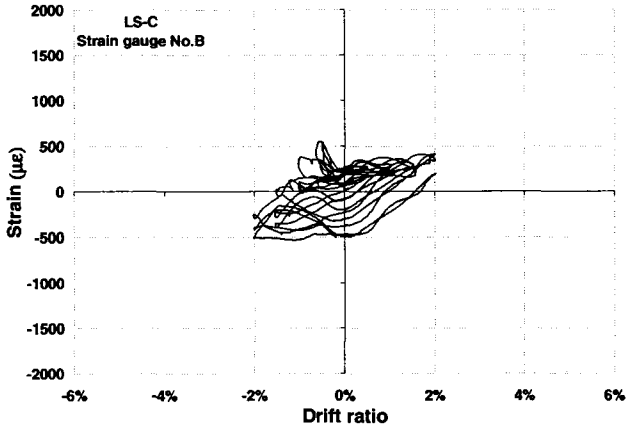

c) Strain gauge No.B

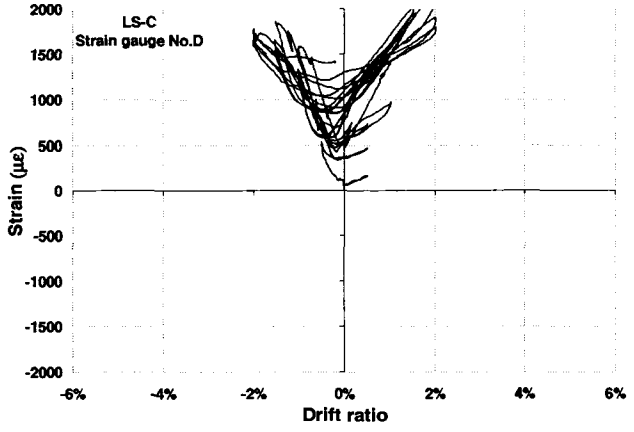

d) Strain gauge No.D

Figure A.12 Transverse reinforcement steel strains for column LS-C

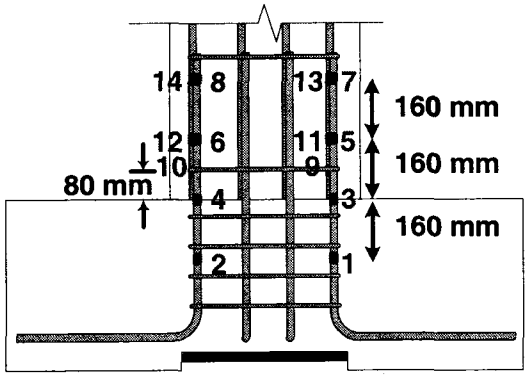

a) Strain gauge location on longitudinal bars

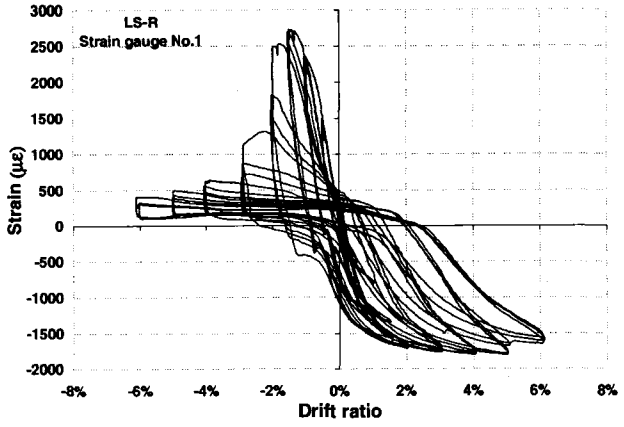

b) Strain gauge No.1

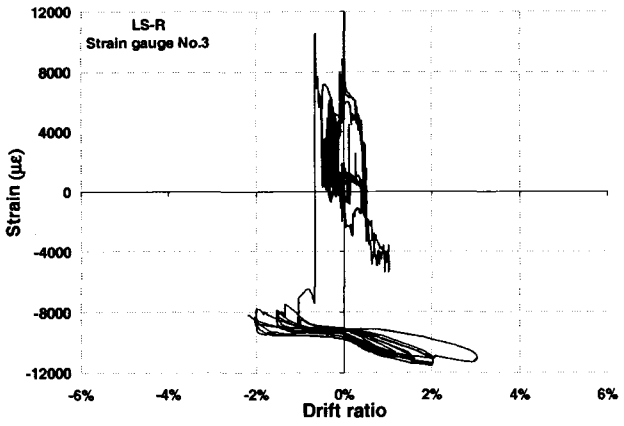

c) Strain gauge No.3

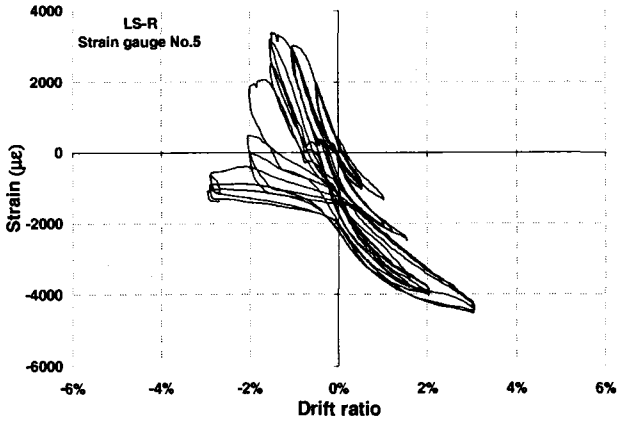

d) Strain gauge No.5

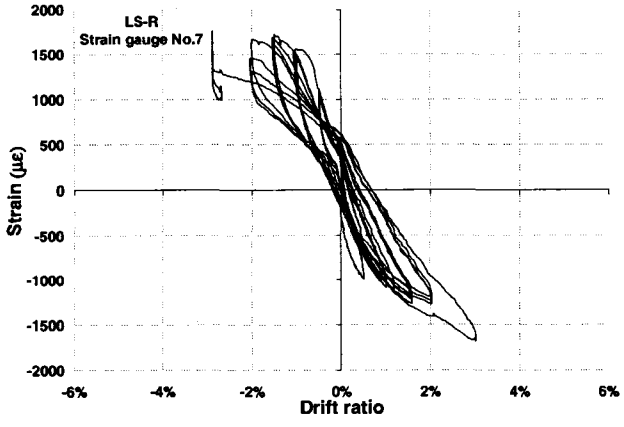

e) Strain gauge No.7

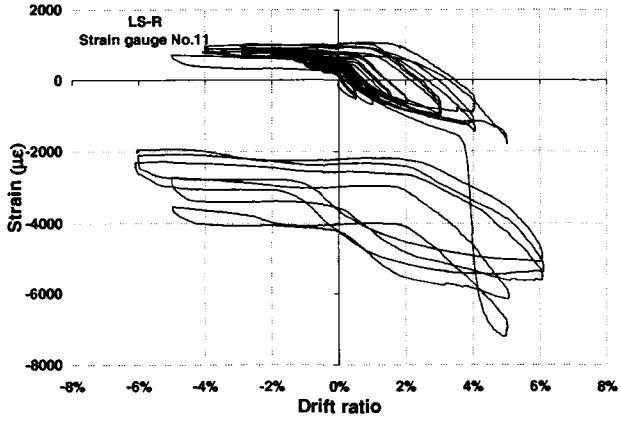

f) Strain gauge No.11

Figure A.13 Longitudinal reinforcement steel strains for column LS-R

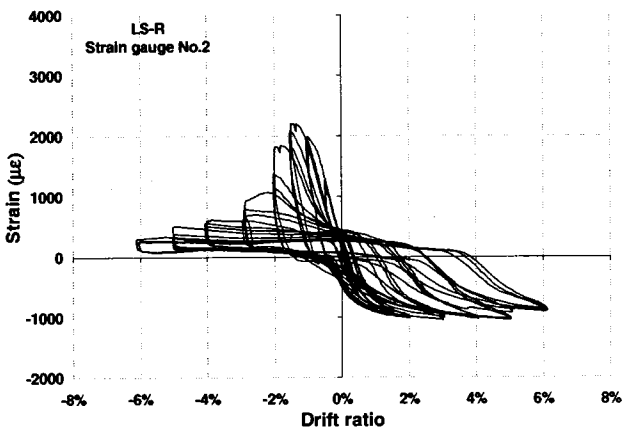

g) Strain gauge No.2

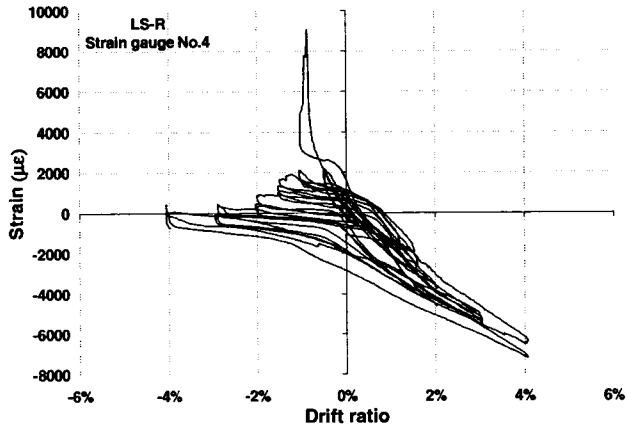

h) Strain gauge No.4

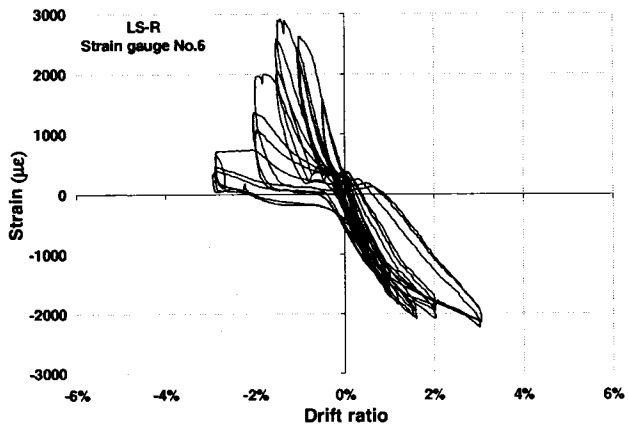

i) Strain gauge No.6

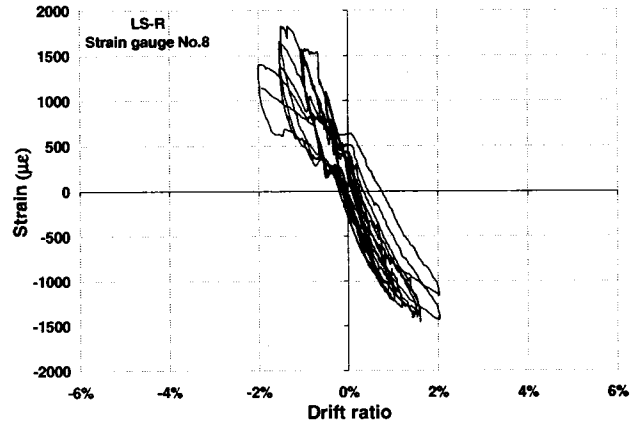

j) Strain gauge No.8

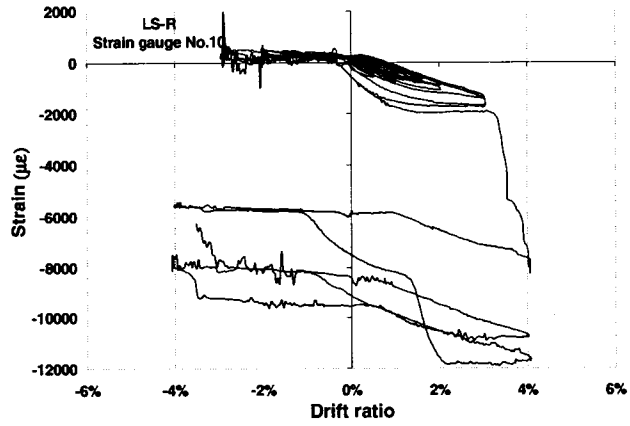

k) Strain gauge No.10

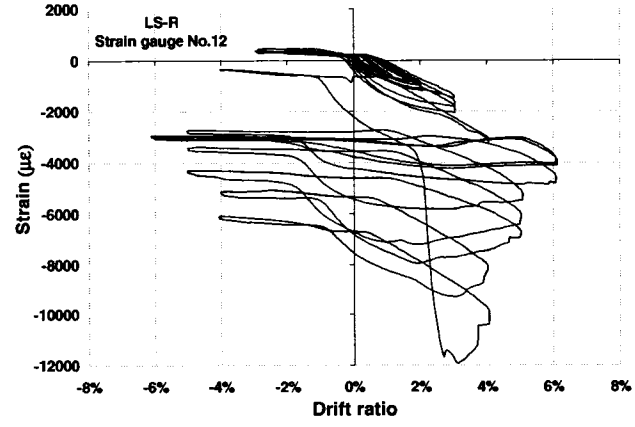

l) Strain gauge No.12

Figure A.13 Longitudinal reinforcement steel strains for column LS-R (Continued)

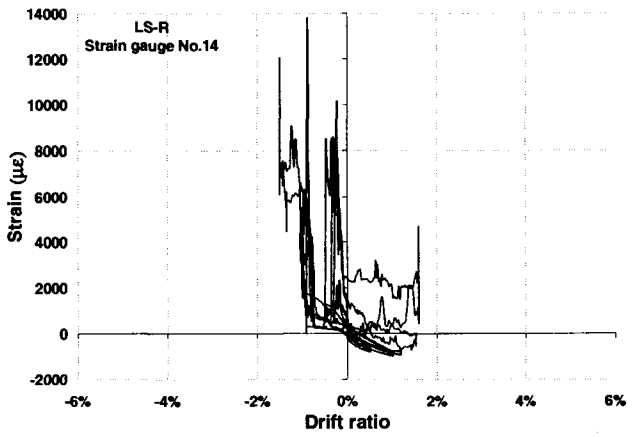

m) Strain gauge No.14

Figure A.13 Longitudinal reinforcement steel strains for column LS-R (Continued)

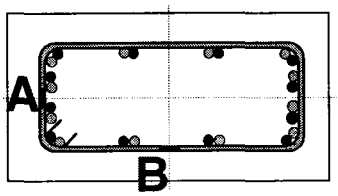

a) Strain gauge location on the 2nd hoop

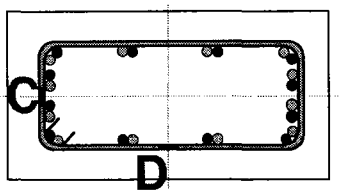

b) Strain gauge location on the 3rd hoop

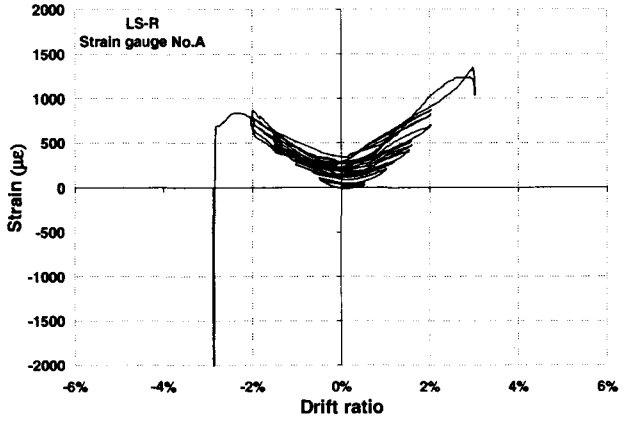

c) Strain gauge No.A

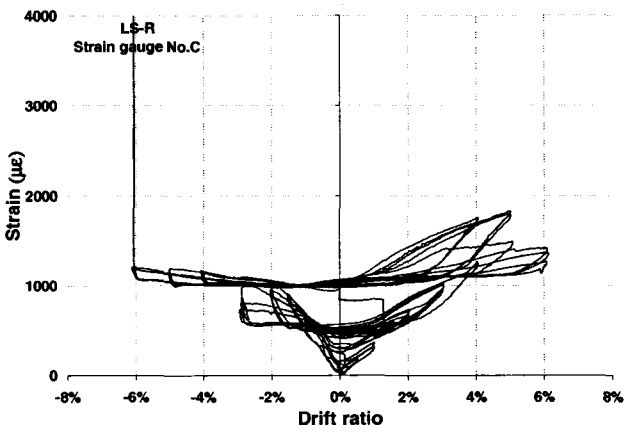

d) Strain gauge No.C

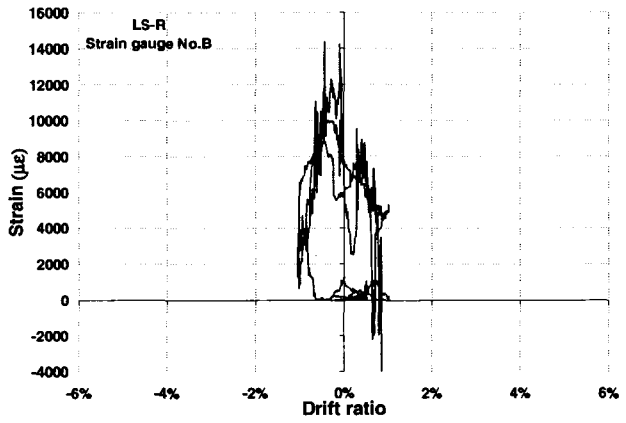

e) Strain gauge No.B

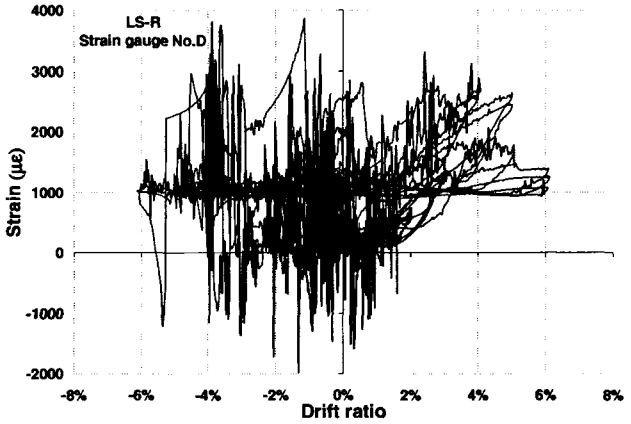

f) Strain gauge No.D

Figure A.14 Transverse reinforcement steel strains for column LS-R

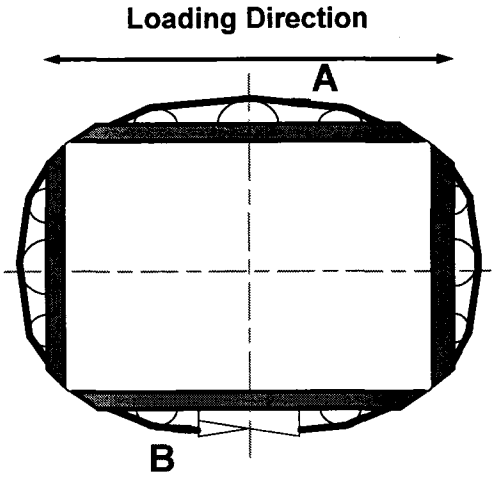

a) Strain gauge location on prestressing strands

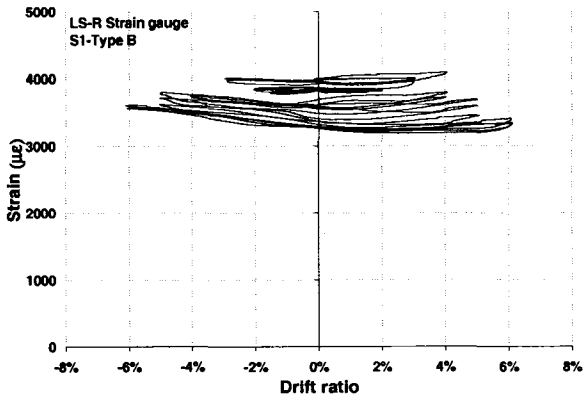

b) 1st Strand(Gauge Type B)

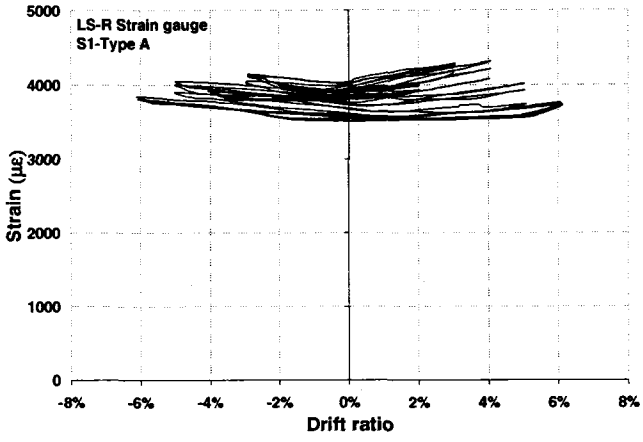

c) 1st Strand(Gauge Type A)

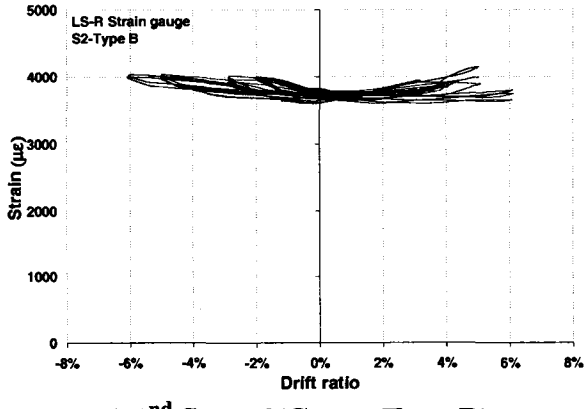

d) 2nd Strand(Gauge Type B)

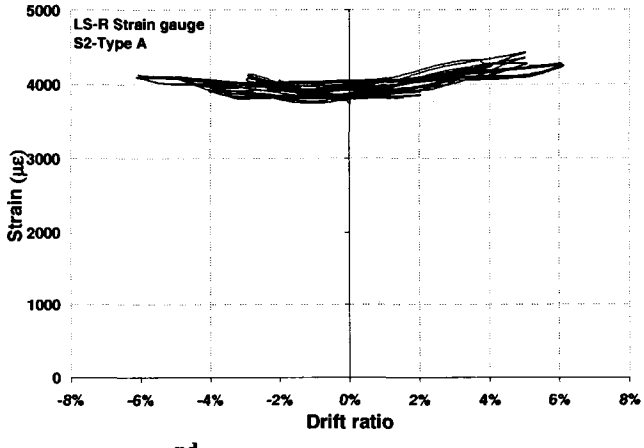

e) 2nd Strand(Gauge Type A)

Figure A.15 Prestressing strand strains for column LS-R

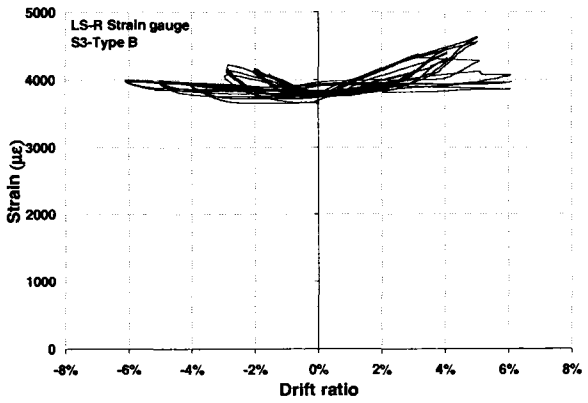

f) 3rd Strand(Gauge Type B)

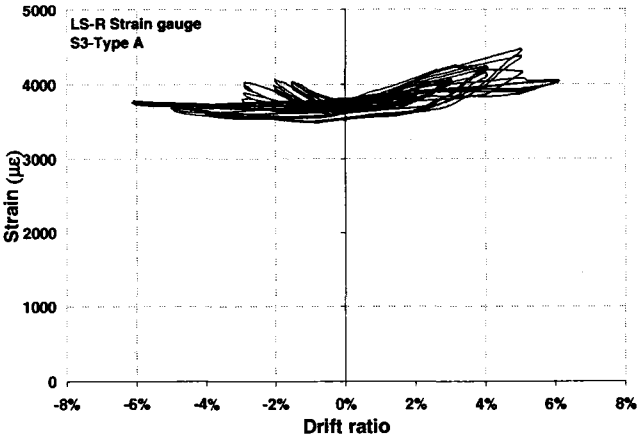

g) 3rd Strand(Gauge Type A)

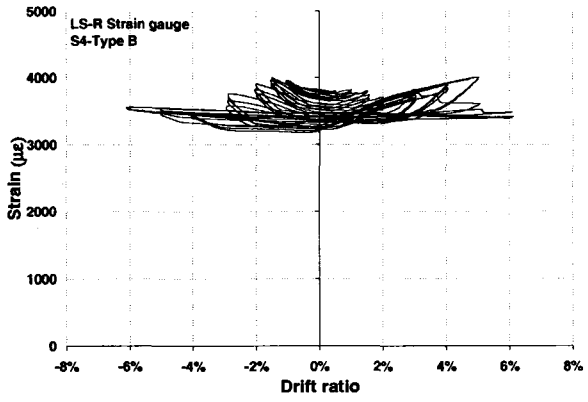

h) 4th Strand(Gauge Type B)

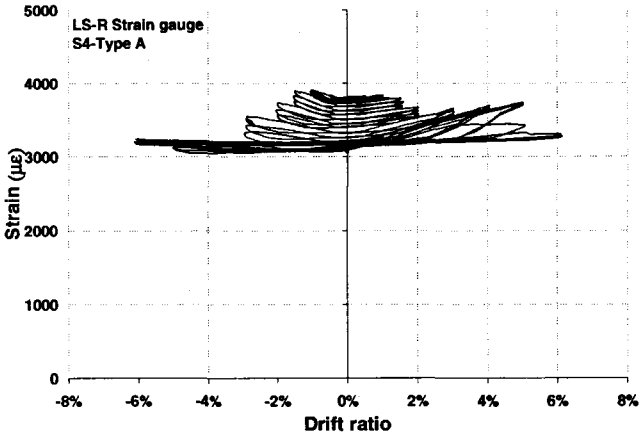

i) 4th Strand(Gauge Type A)

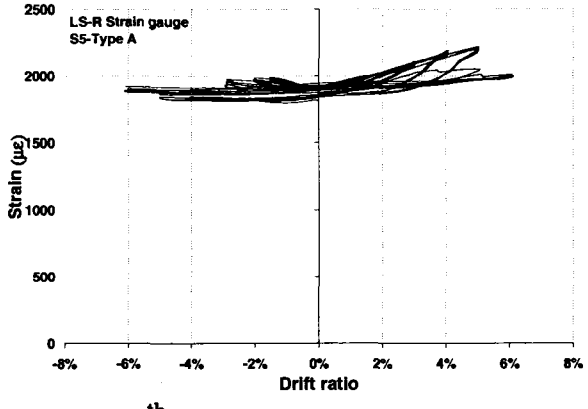

j) 5th Strand(Gauge Type A)

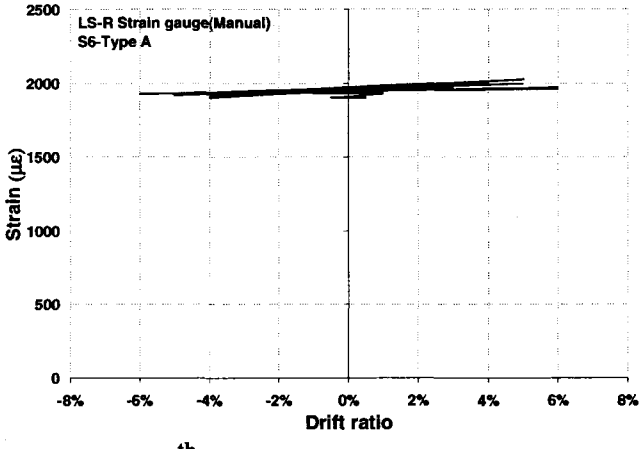

k) 6th Strand(Gauge Type A)

Figure A.15 Prestressing strand strains for column LS-R (Continued)

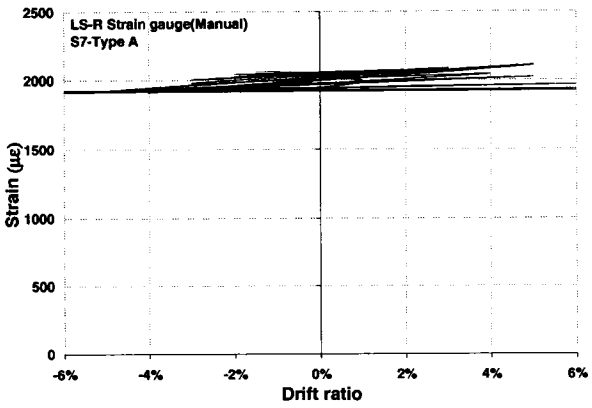

l) 7th Strand(Gauge Type A)

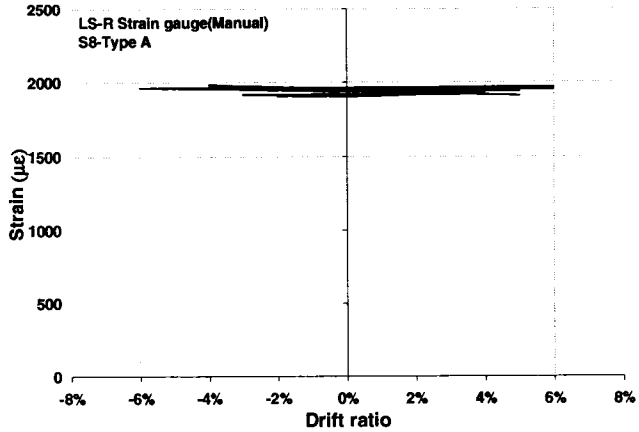

m) 8th Strand(Gauge Type A)

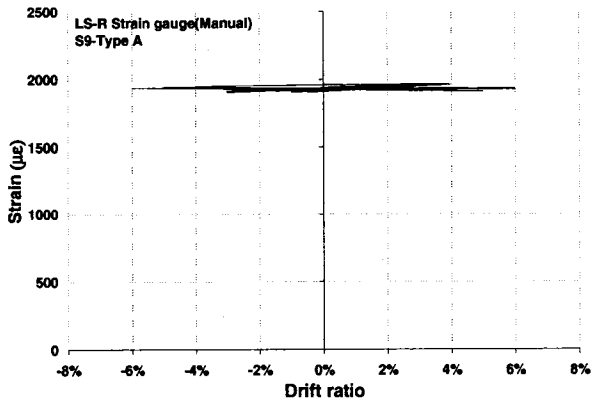

n) 9th Strand(Gauge Type A)

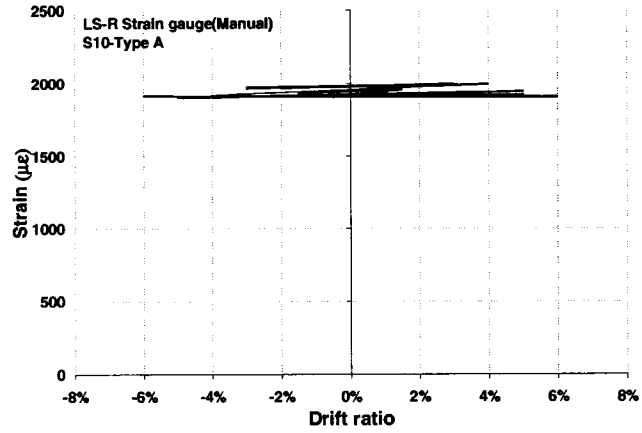

o) 10th Strand(Gauge Type A)

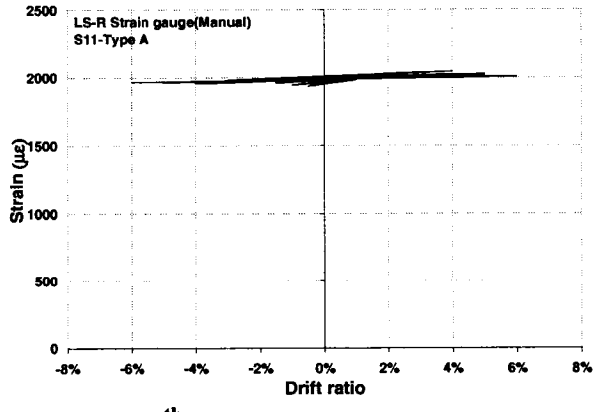

p) 11th Strand(Gauge Type A)

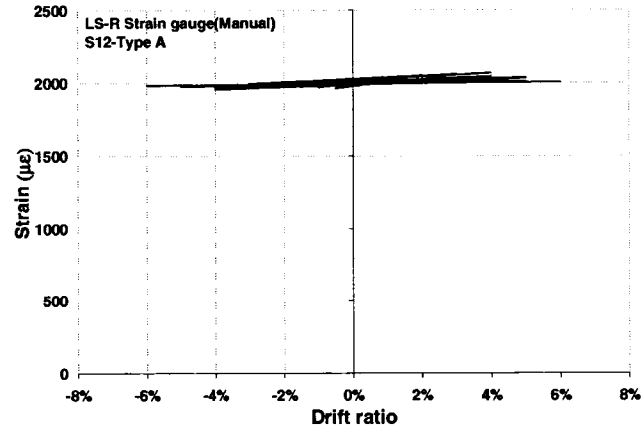

q) 12th Strand(Gauge Type A)

Figure A.15 Prestressing strand strains for column LS-R (Continued)

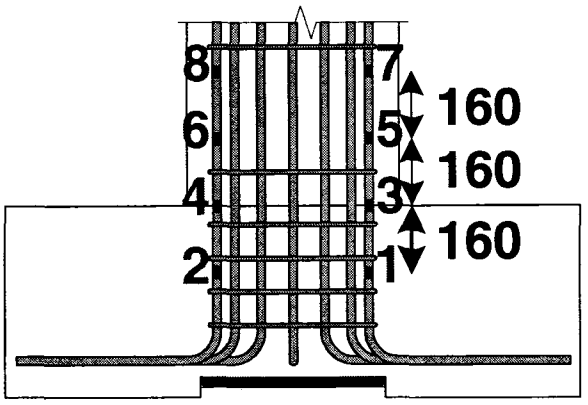

a) Strain gauge location on longitudinal bars

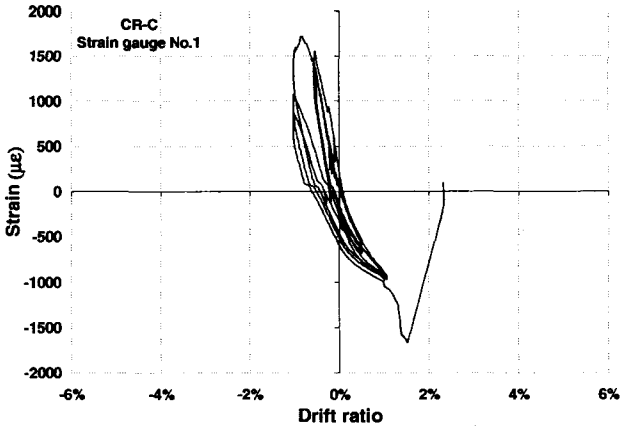

b) Strain gauge No.1

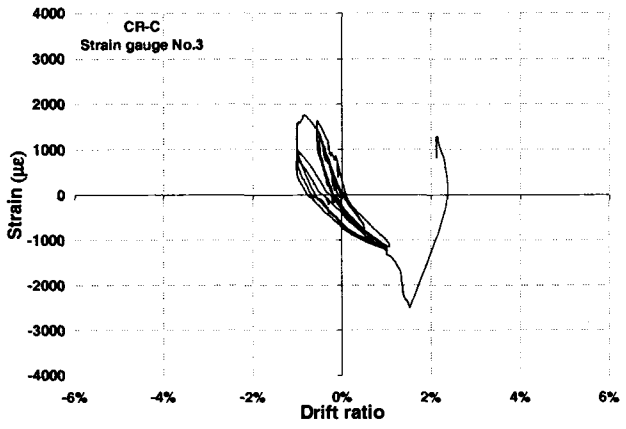

c) Strain gauge No.3

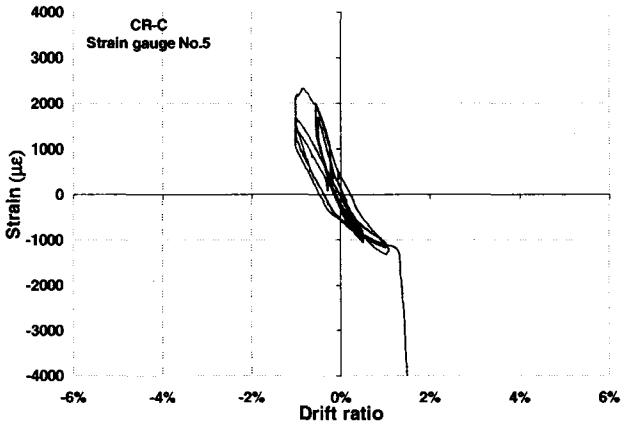

d) Strain gauge No.5

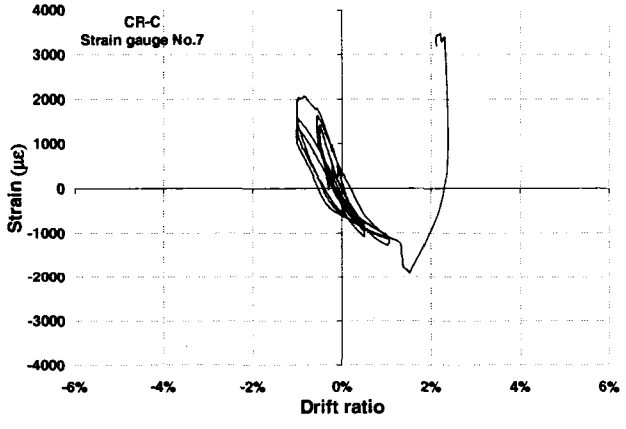

e) Strain gauge No.7

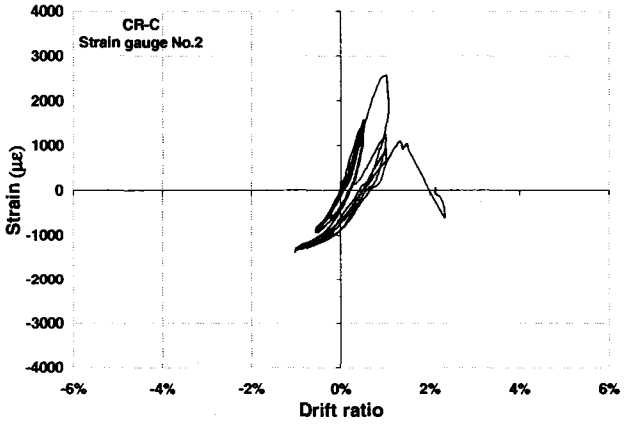

f) Strain gauge No.2

Figure A.16 Longitudinal reinforcement steel strains for column CR-C

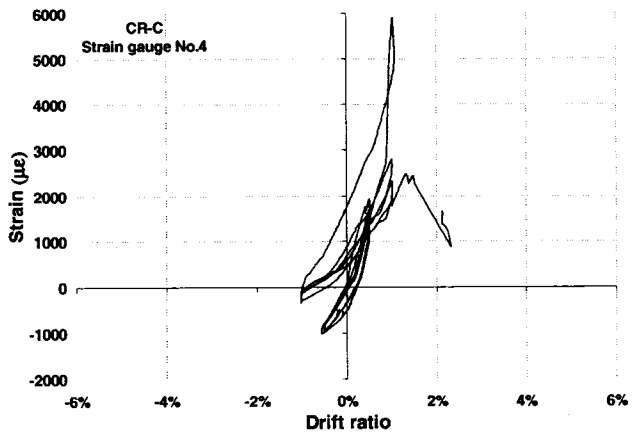

g) Strain gauge No.4

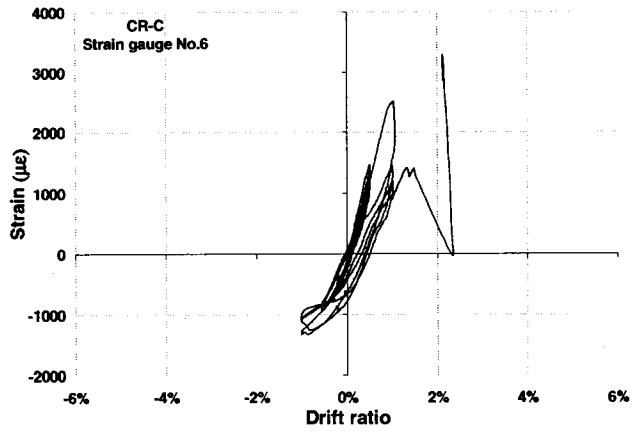

h) Strain gauge No.6

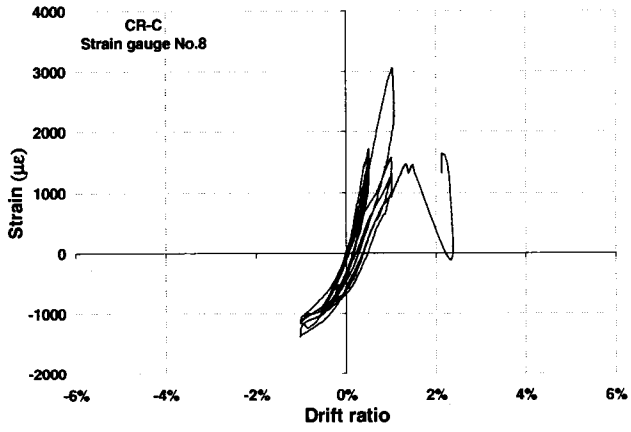

i) Strain gauge No.8

Figure A.16 Longitudinal reinforcement steel strains for column CR-C (Continued)

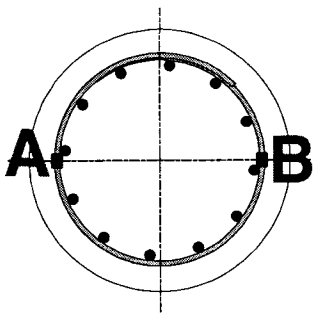

a) Strain gauge location on the 2nd hoop

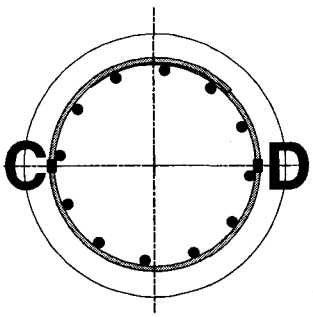

b) Strain gauge location on the 3rd hoop

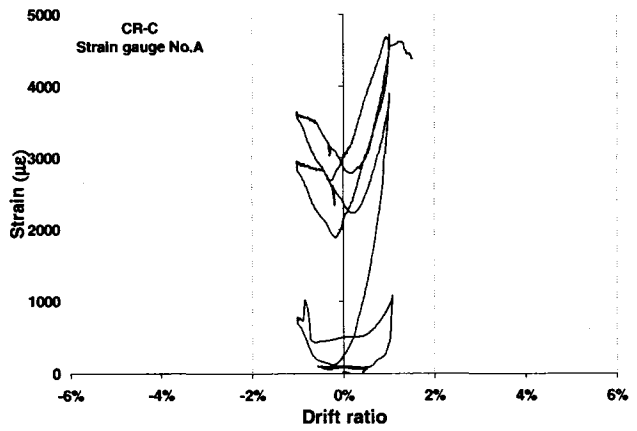

c) Strain gauge No.A

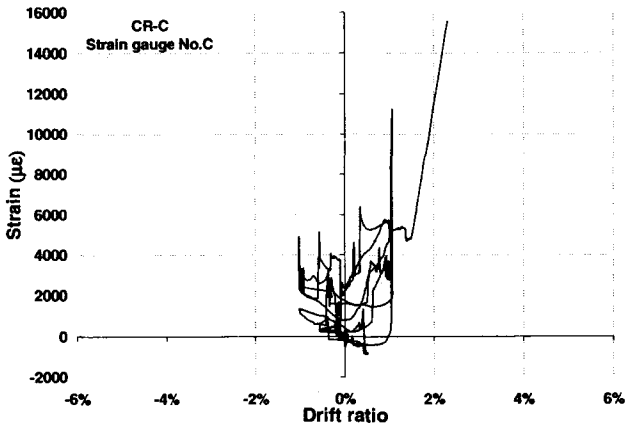

d) Strain gauge No.C

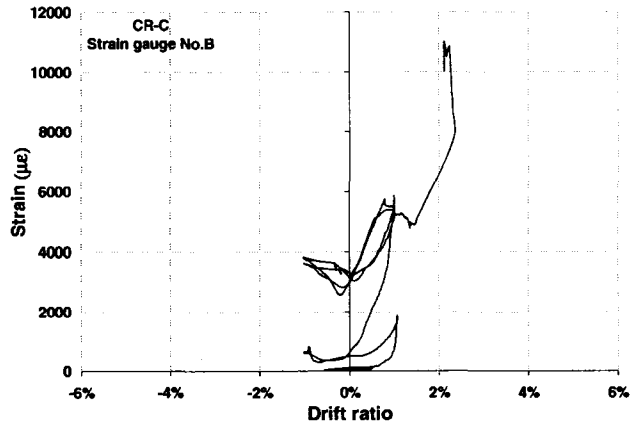

e) Strain gauge No.B

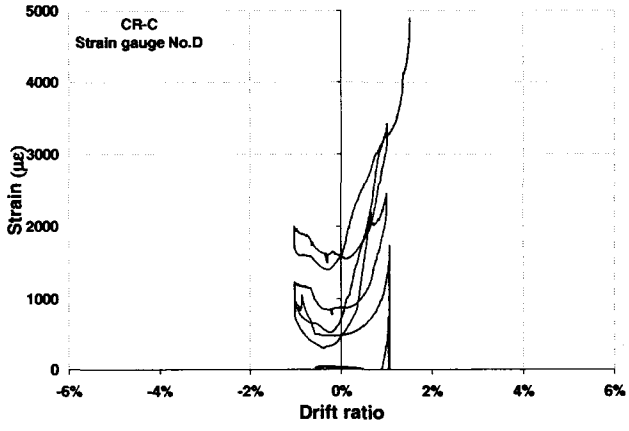

f) Strain gauge No.D

Figure A.17 Transverse reinforcement steel strains for column CR-C

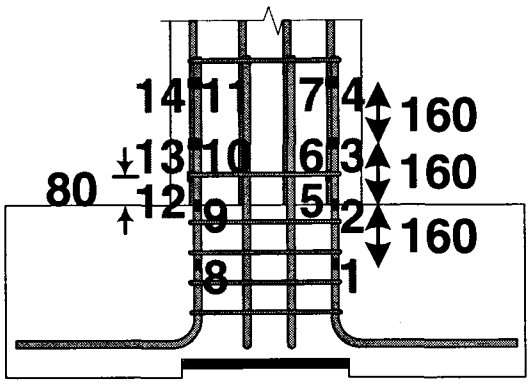

a) Strain gauge location on longitudinal bars

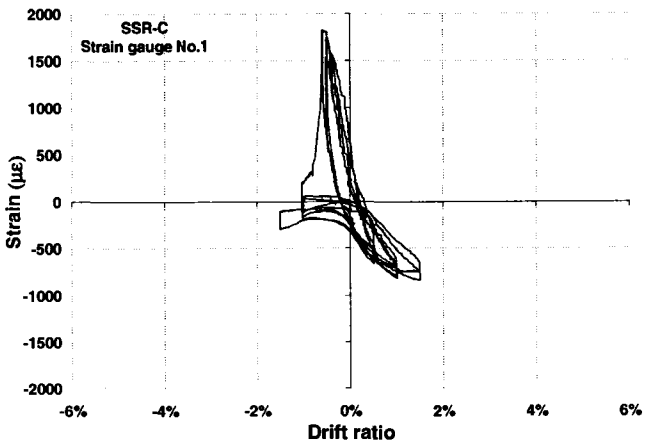

b) Strain gauge No.1

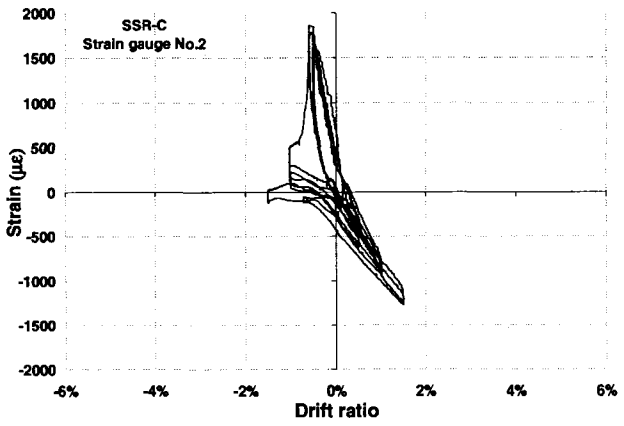

c) Strain gauge No.2

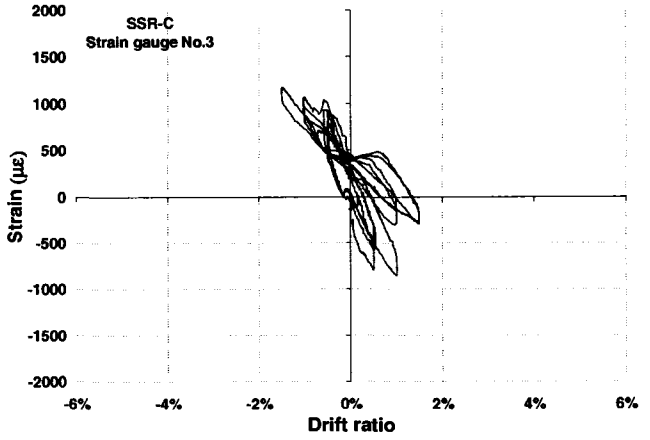

d) Strain gauge No.3

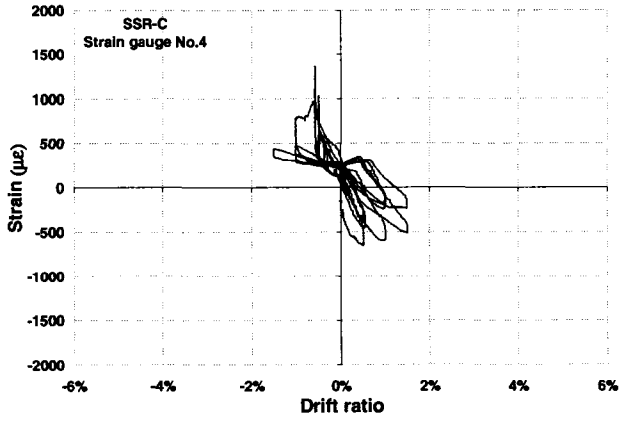

e) Strain gauge No.4

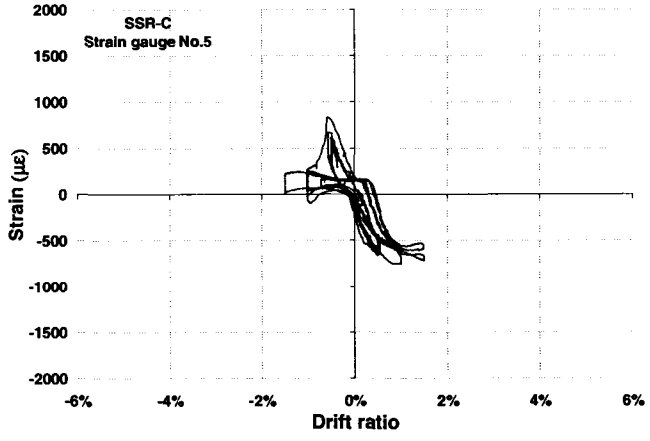

f) Strain gauge No.5

Figure A.18 Longitudinal reinforcement steel strains for column SSR-C

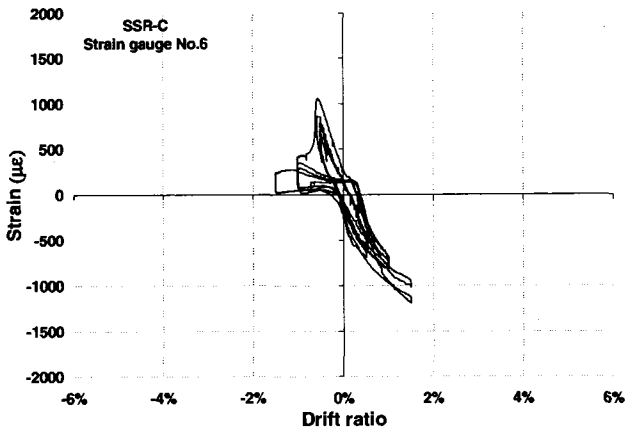

g) Strain gauge No.6

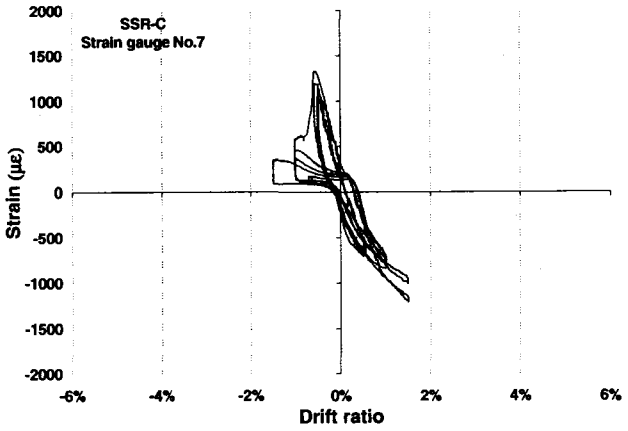

h) Strain gauge No.7

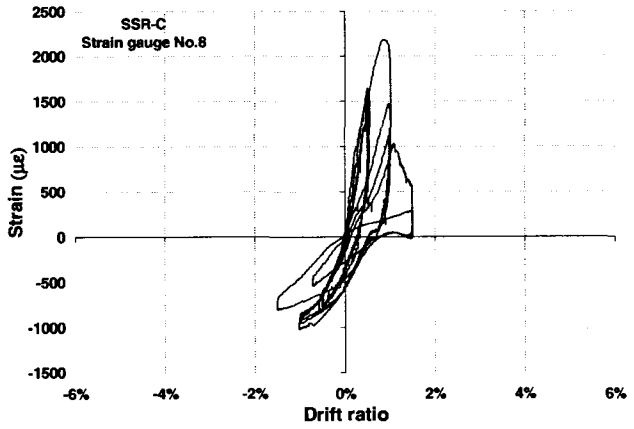

i) Strain gauge No.8

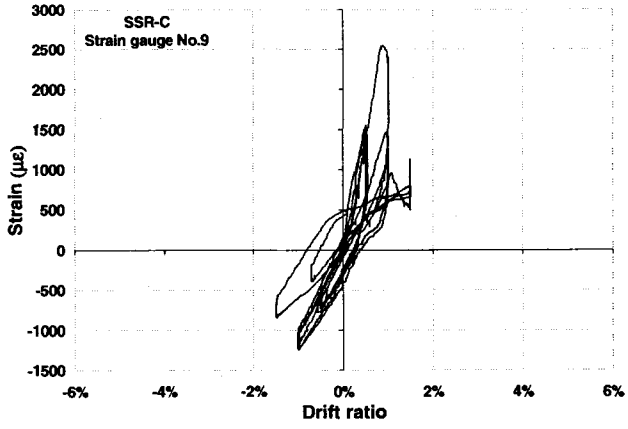

j) Strain gauge No.9

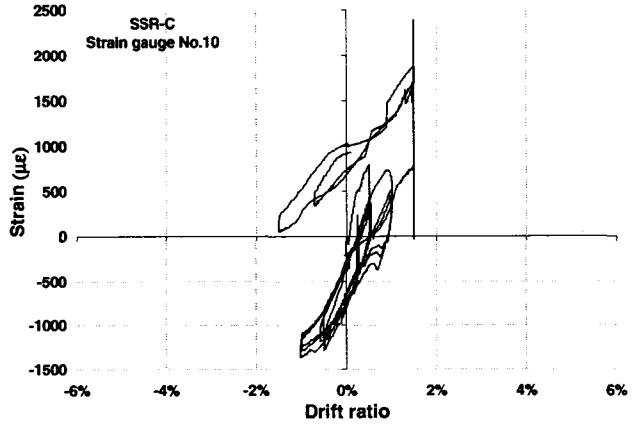

k) Strain gauge No.10

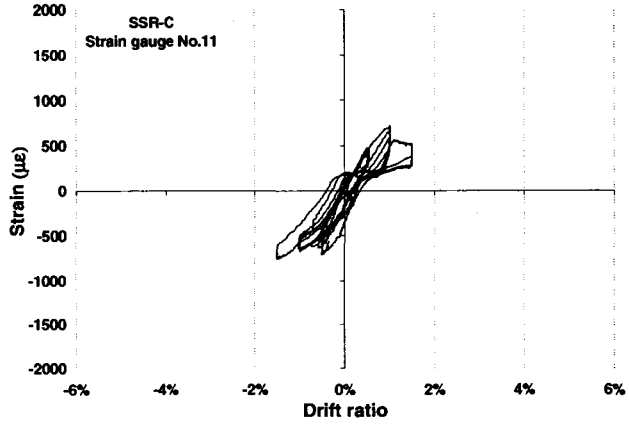

l) Strain gauge No.11

Figure A.18 Longitudinal reinforcement steel strains for column SSR-C (Continued)

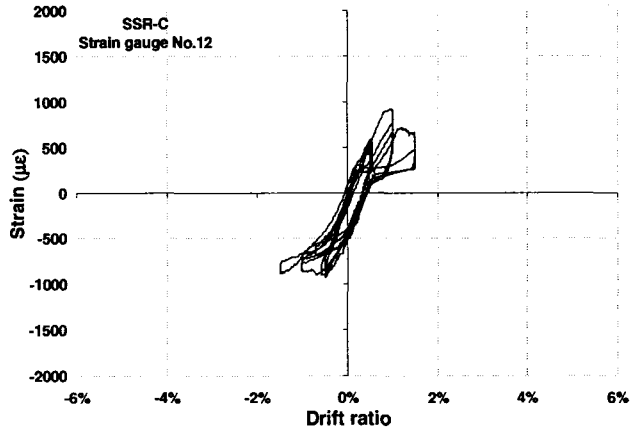

m) Strain gauge No.12

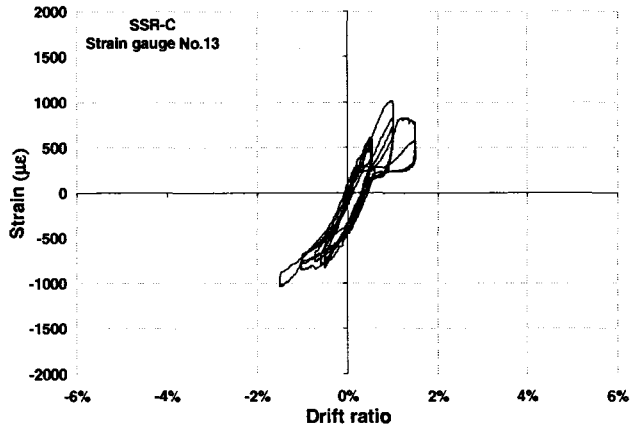

n) Strain gauge No.13

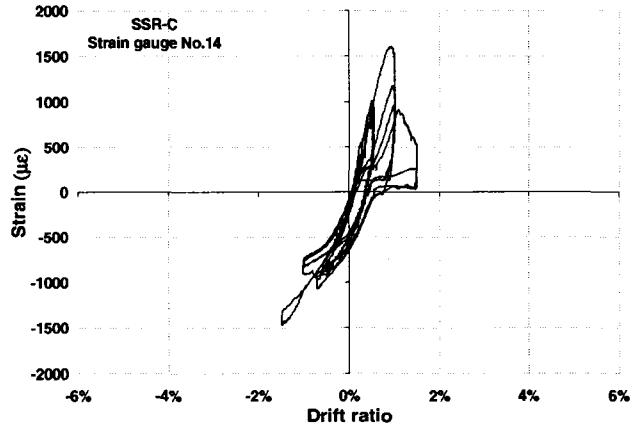

o) Strain gauge No.14

Figure A.18 Longitudinal reinforcement steel strains for column SSR-C

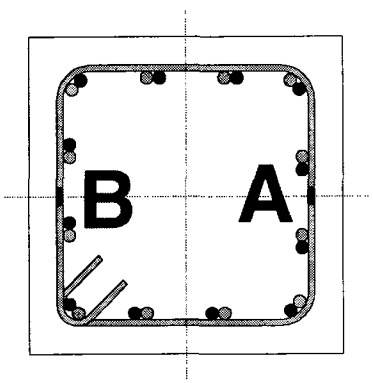

a) Strain gauge location on the 2nd hoop

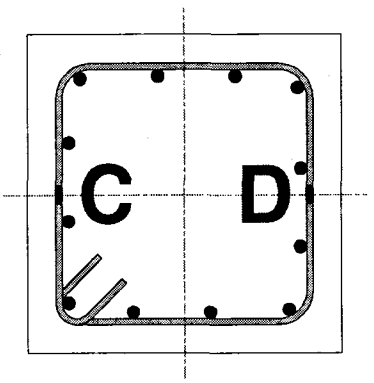

b) Strain gauge location on the 3rd hoop

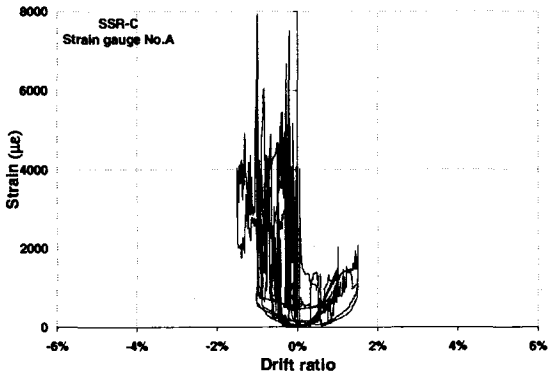

c) Strain gauge No. A

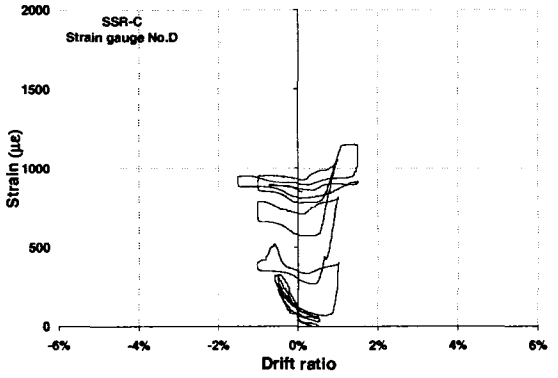

d) Strain gauge No. D

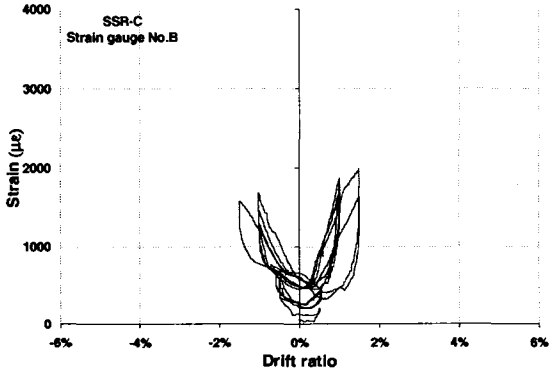

e) Strain gauge No. B

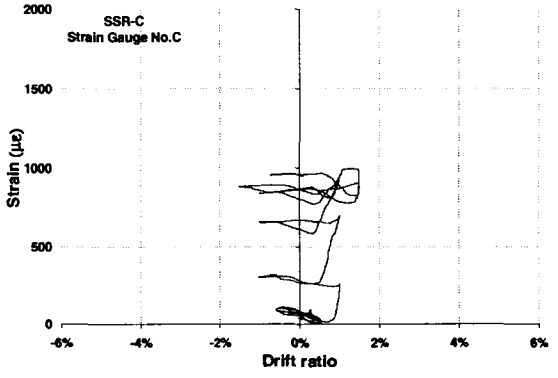

f) Strain gauge No. C

Figure A.19 Transverse reinforcement steel strains for column SSR-C

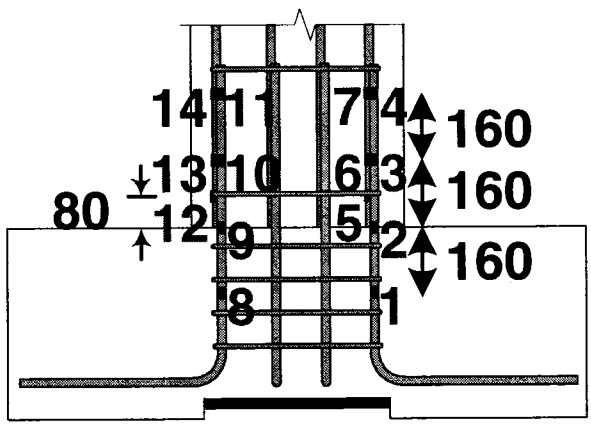

a) Strain gauge location on longitudinal bars

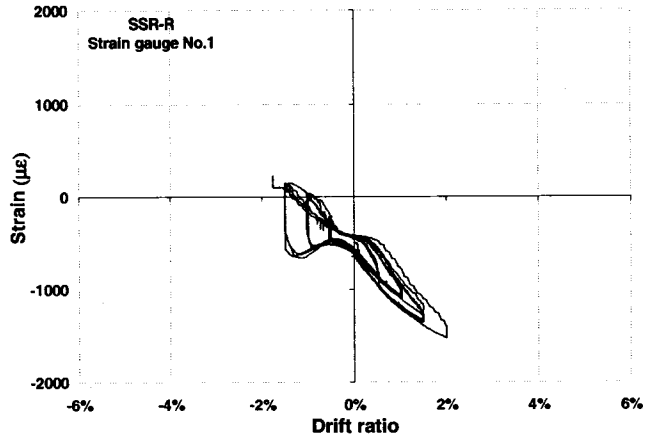

b) Strain gauge No.1

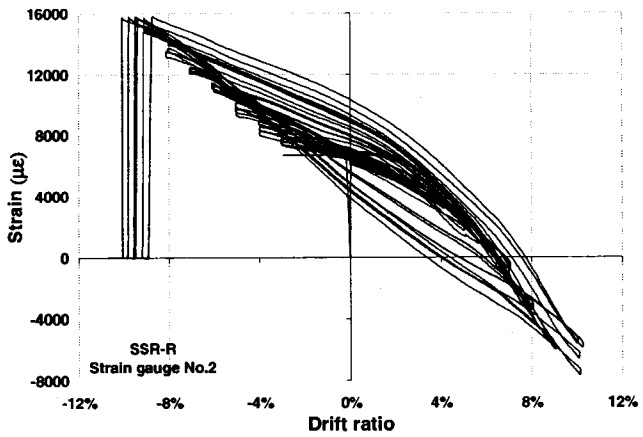

c) Strain gauge No.2

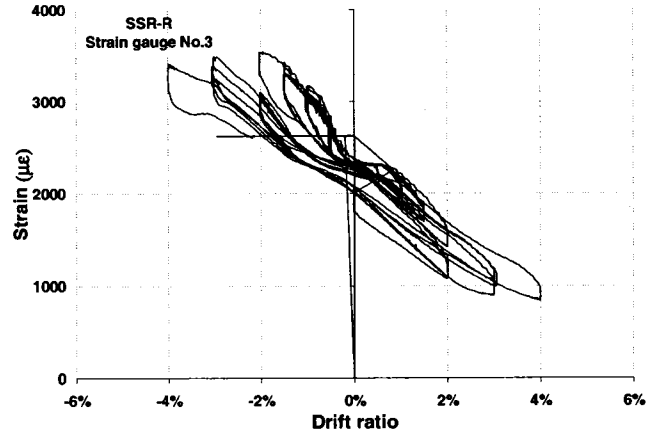

d) Strain gauge No.3

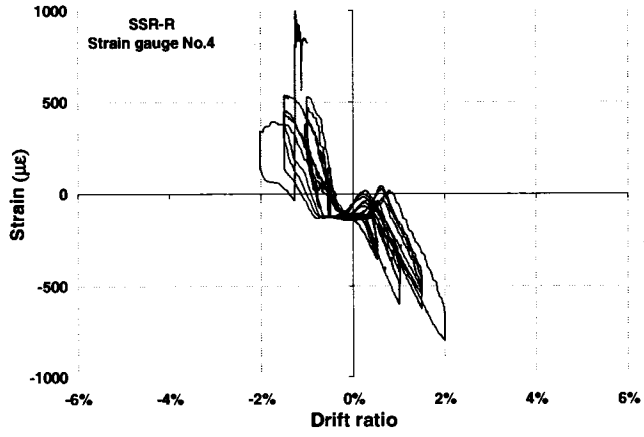

e) Strain gauge No.4

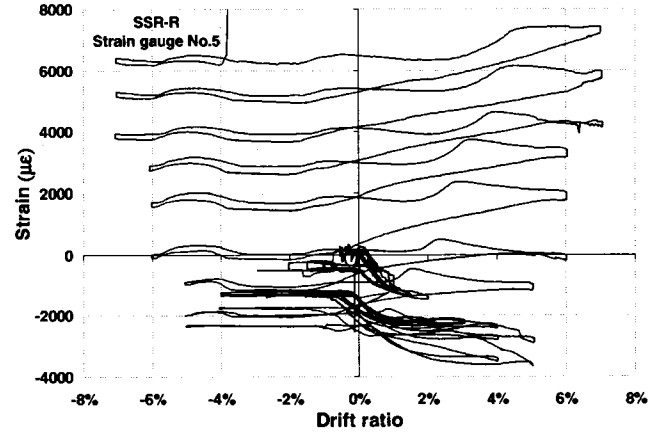

f) Strain gauge No.5

Figure A.20 Longitudinal reinforcement steel strains for column SSR-R

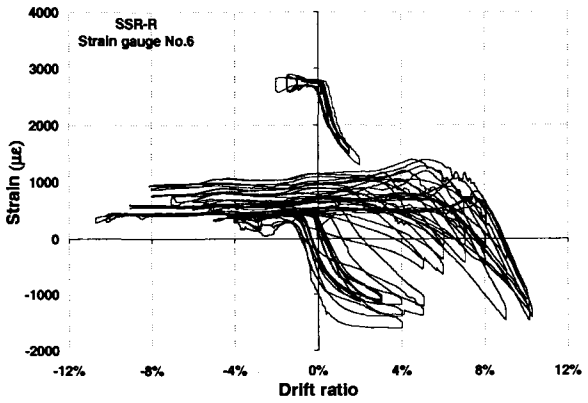

g) Strain gauge No.6

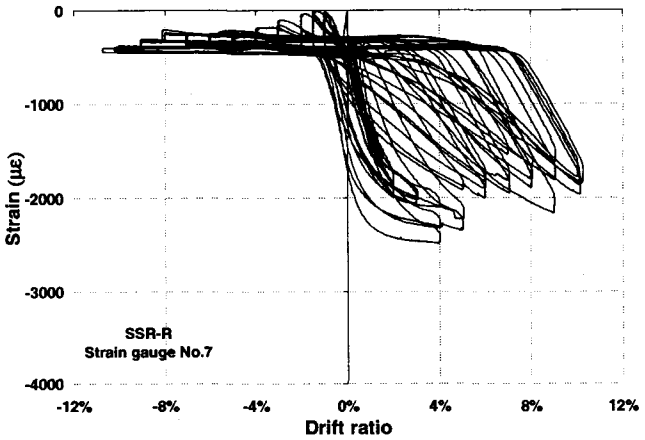

h) Strain gauge No.7

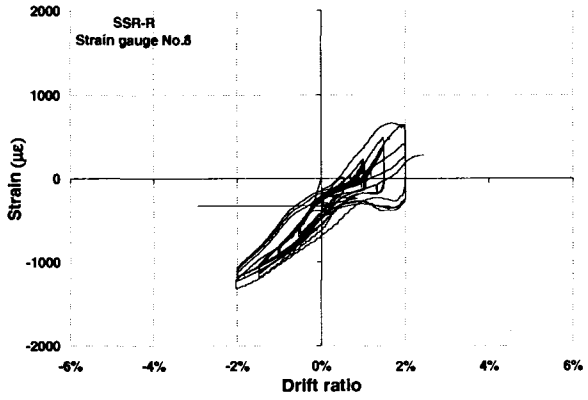

i) Strain gauge No.8

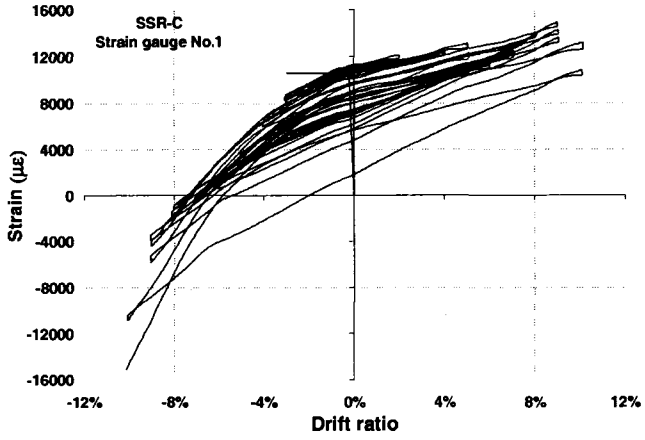

j) Strain gauge No.9

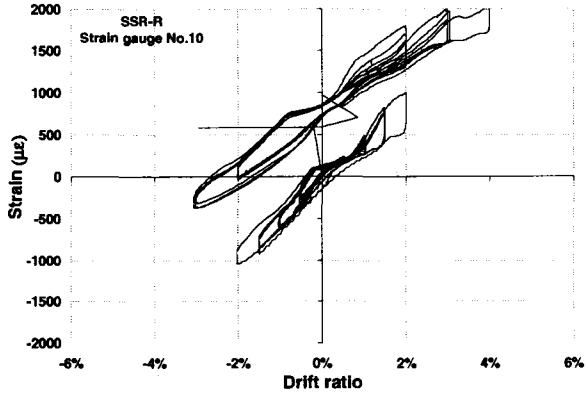

k) Strain gauge No.10

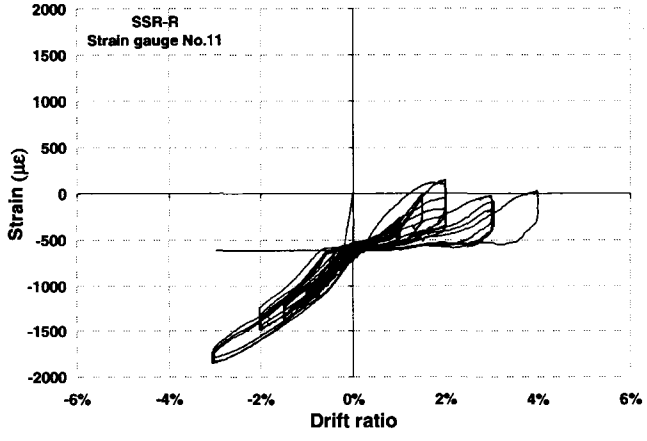

l) Strain gauge No.11

Figure A.20 Longitudinal reinforcement steel strains for column SSR-R (Continued)

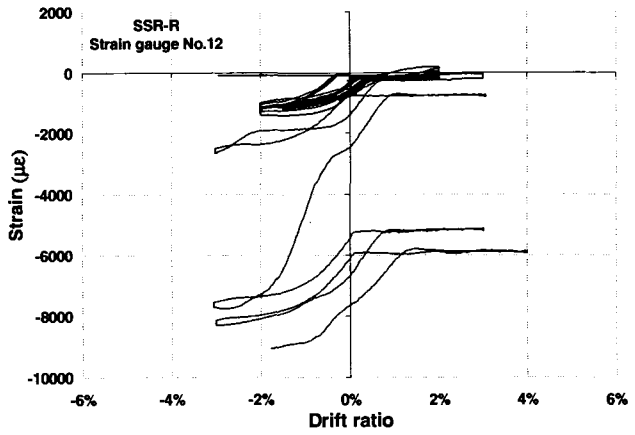

m) Strain gauge No.12

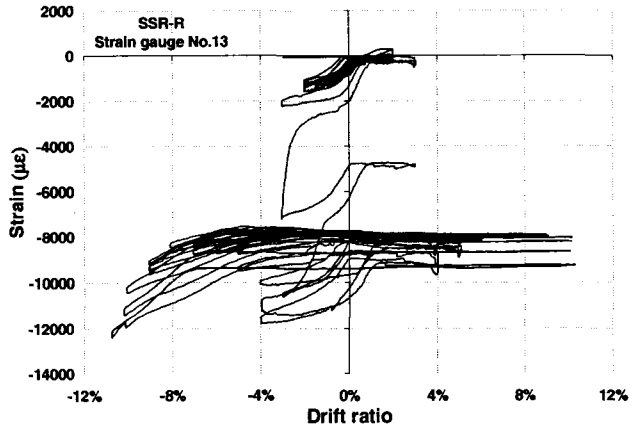

n) Strain gauge No.13

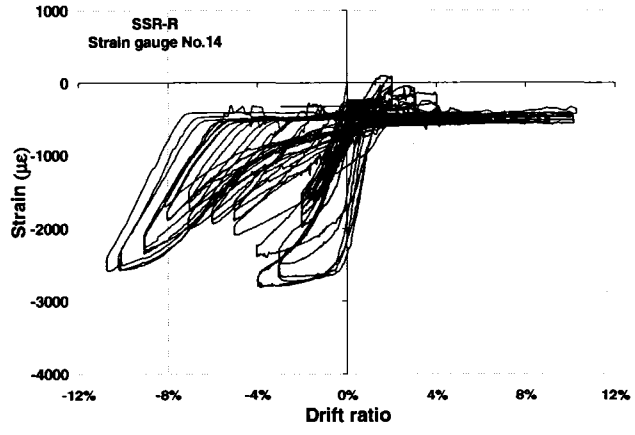

o) Strain gauge No.14

Figure A.20 Longitudinal reinforcement steel strains for column SSR-R (Continued)

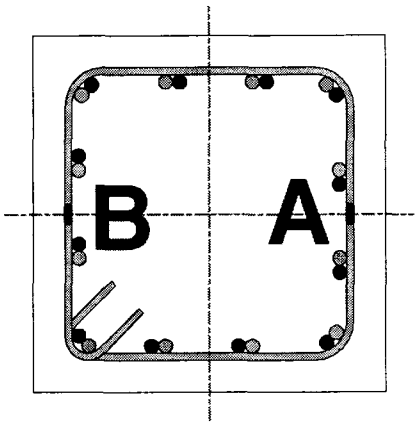

a) Strain gauge location on the 2nd hoop

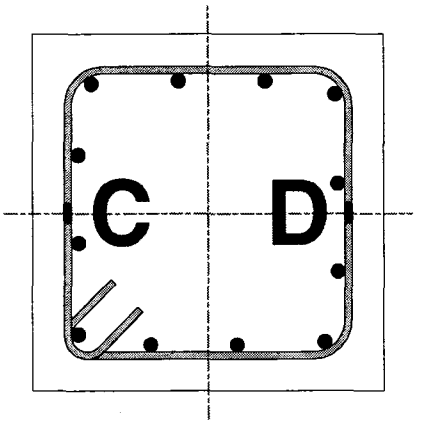

b) Strain gauge location on the 3rd hoop

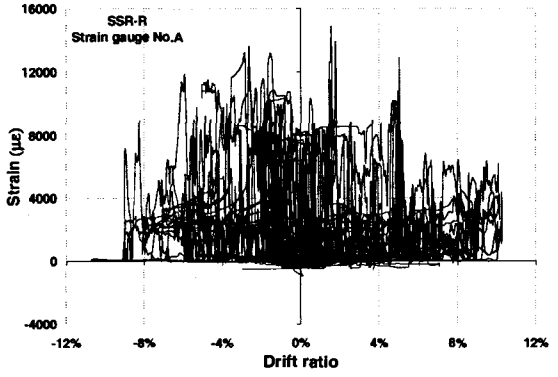

c) Strain gauge No. A

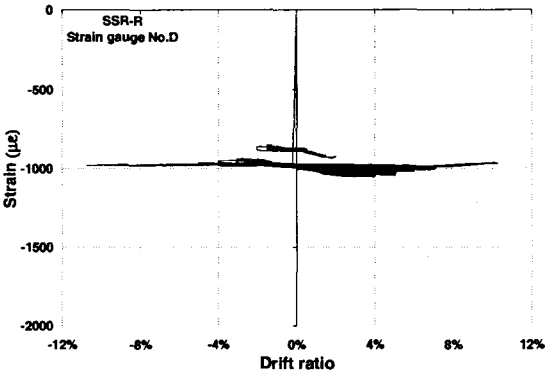

d) Strain gauge No. D

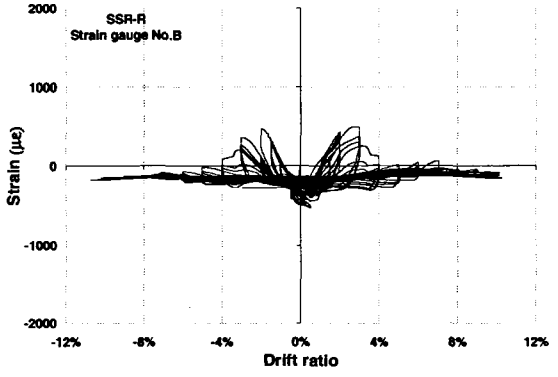

e) Strain gauge No. B

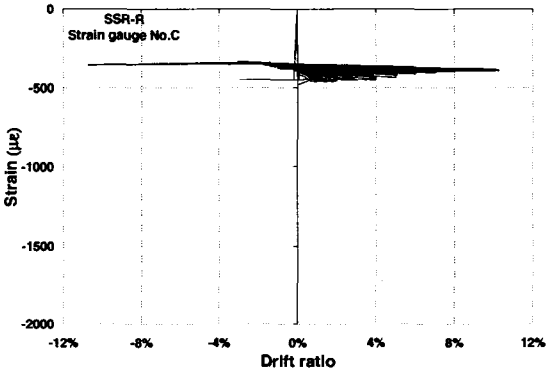

f) Strain gauge No. C

Figure A.21 Transverse reinforcement steel strains for column SSR-R

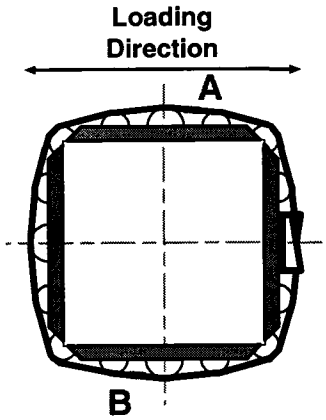

a) Strain gauge location on prestressing strands

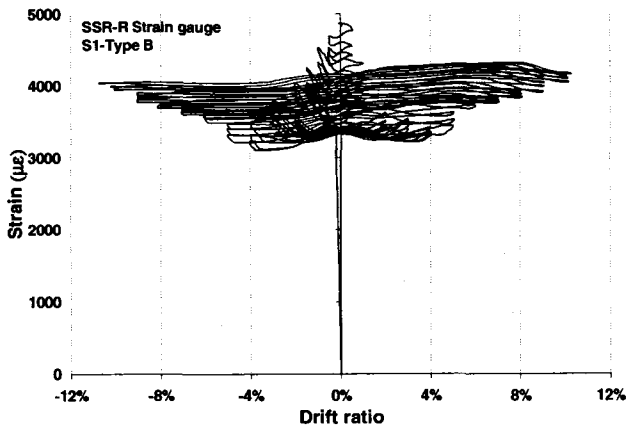

b) 1st Strand(Gauge Type B)

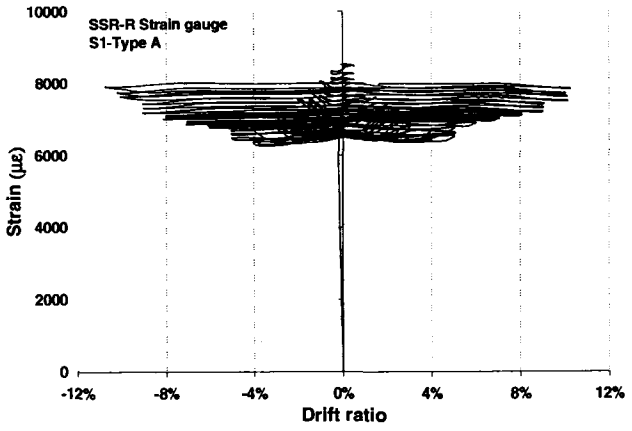

c) 1st Strand(Gauge Type A)

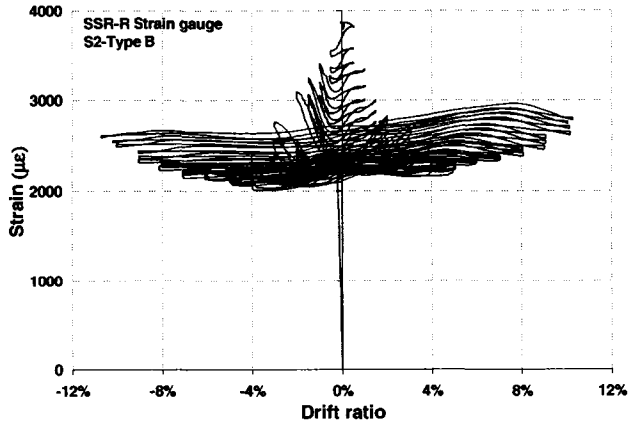

d) 2nd Strand(Gauge Type B)

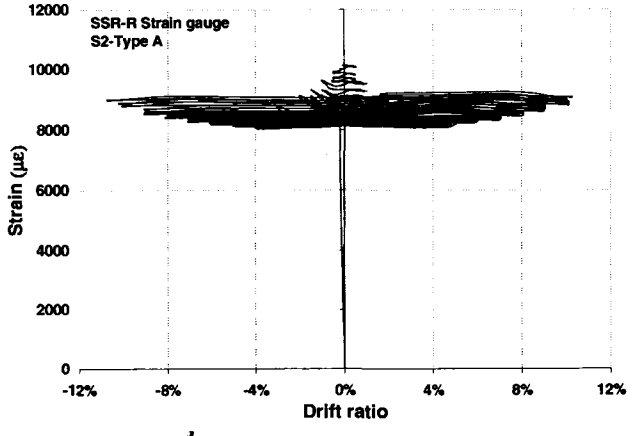

e) 2nd Strand(Gauge Type A)

Figure A.22 Prestressing strand strains for column SSR-R

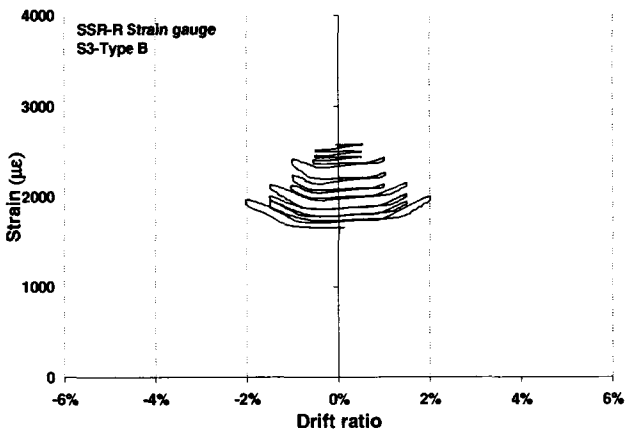

f) 3rd Strand(Gauge Type B)

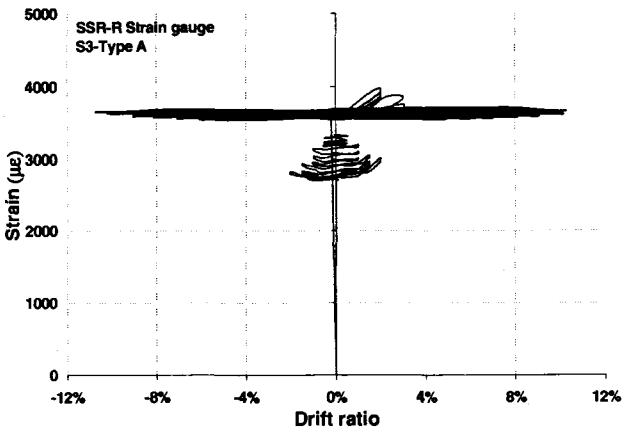

g) 3rd Strand(Gauge Type A)

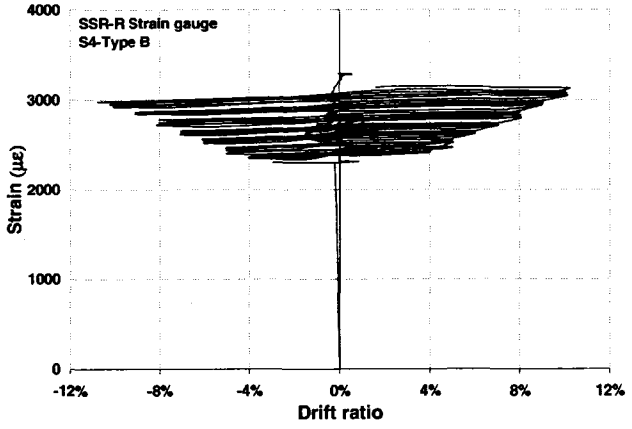

h) 4th Strand(Gauge Type B)

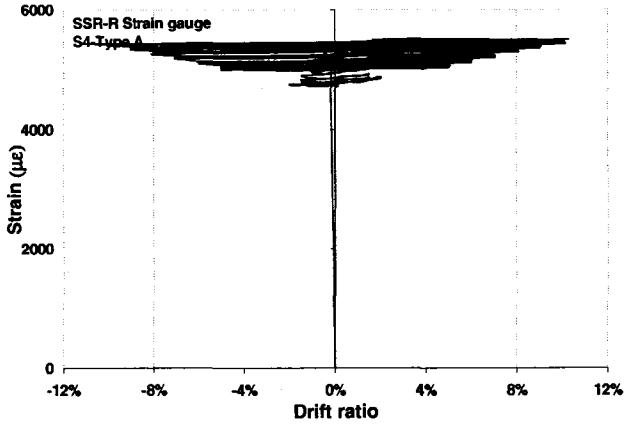

i) 4th Strand(Gauge Type A)

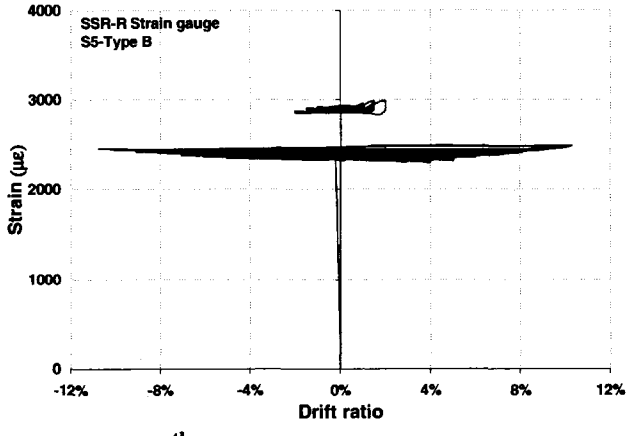

j) 5th Strand(Gauge Type B)

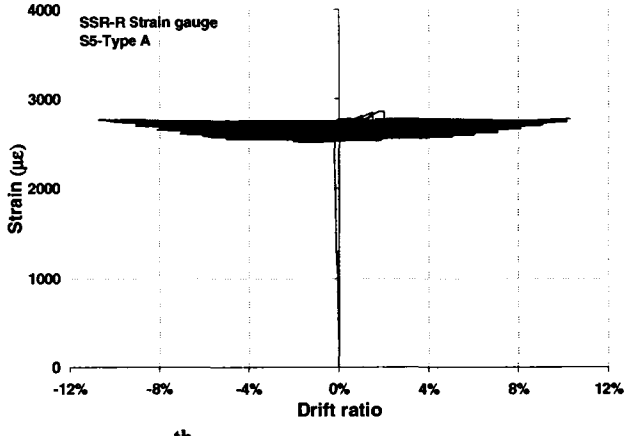

k) 5th Strand(Gauge Type A)

Figure A.22 Prestressing strand strains for column SSR-R (Continued)

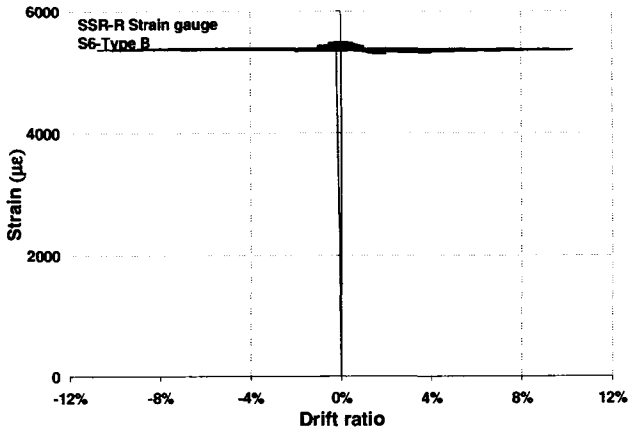

l) 6th Strand(Gauge Type B)

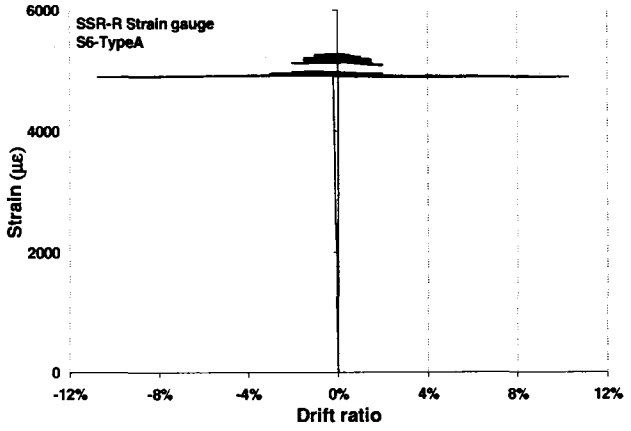

m) 6th Strand(Gauge Type A)

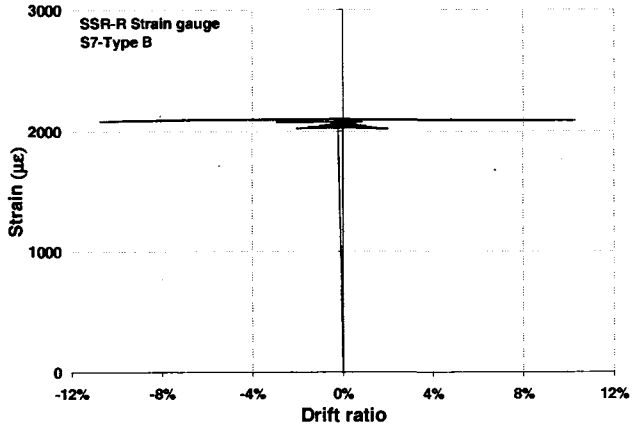

d) 7th Strand(Gauge Type B)

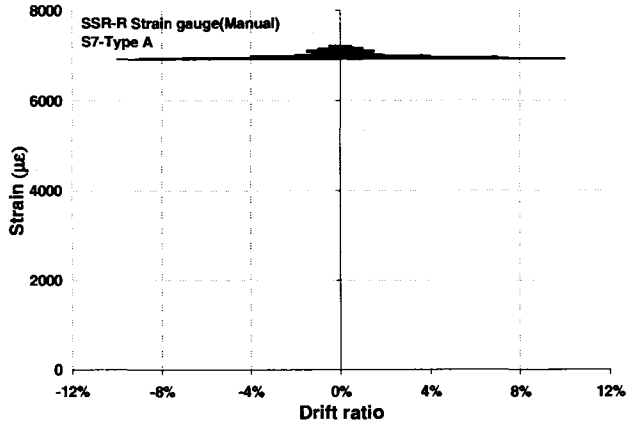

c) 7th Strand(Gauge Type A)

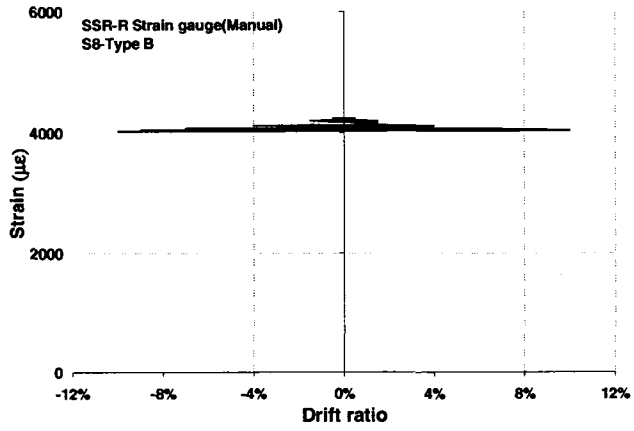

d) 8th Strand(Gauge Type B)

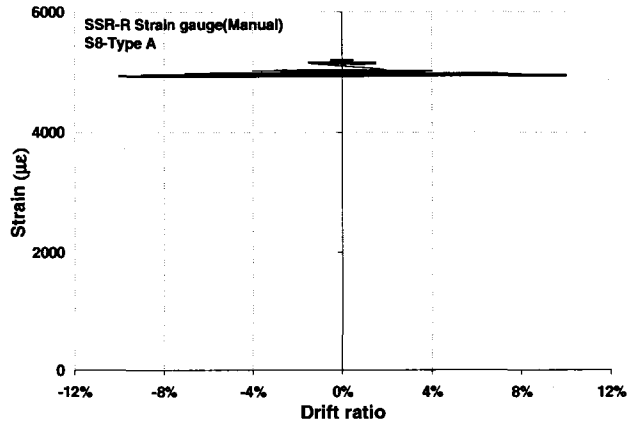

c) 8th Strand(Gauge Type A)

Figure A.22 Prestressing strand strains for column SSR-R (Continued)

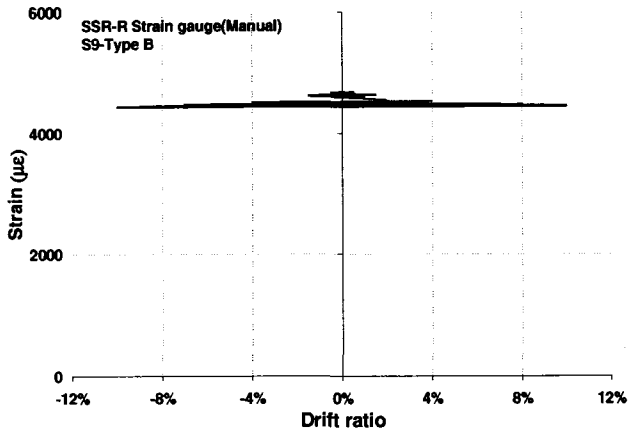

d) 9th Strand(Gauge Type B)

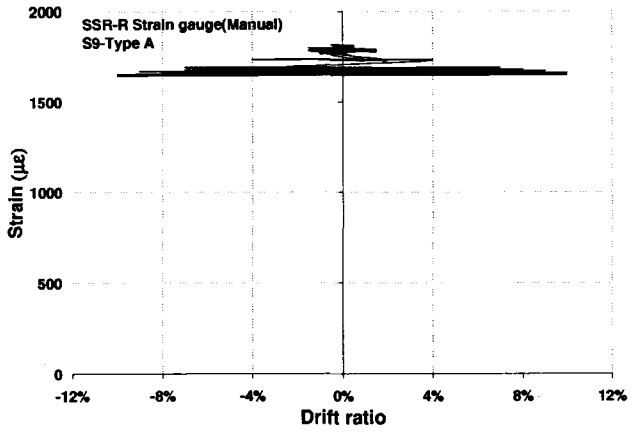

c) 9th Strand(Gauge Type A)

Figure A.22 Prestressing strand strains for column SSR-R (Continued)

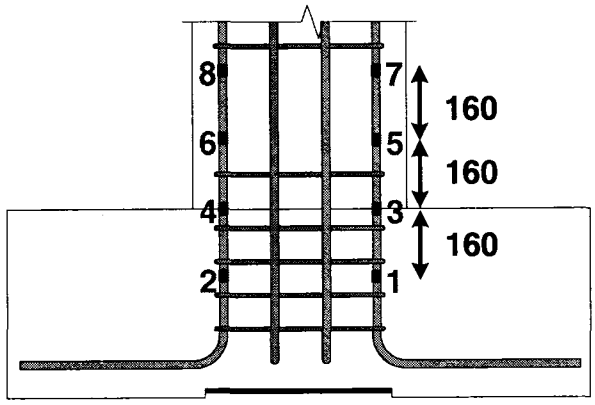

a) Strain gauge location on longitudinal bars

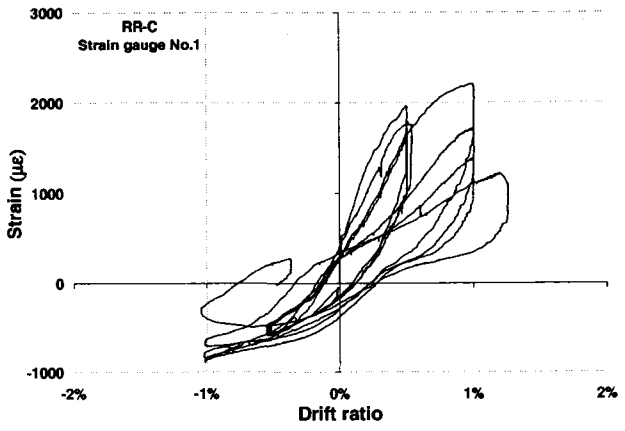

b) Strain gauge No.1

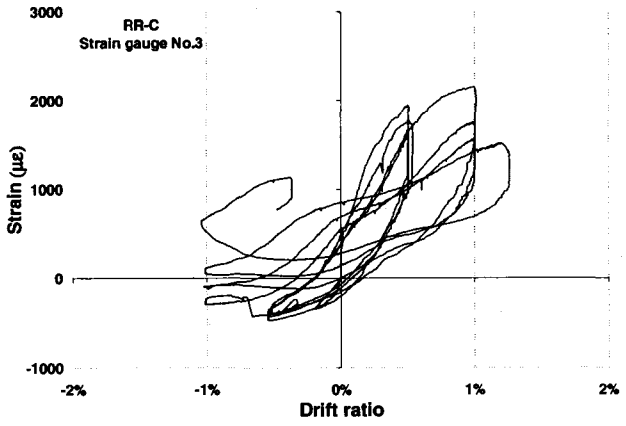

c) Strain gauge No.3

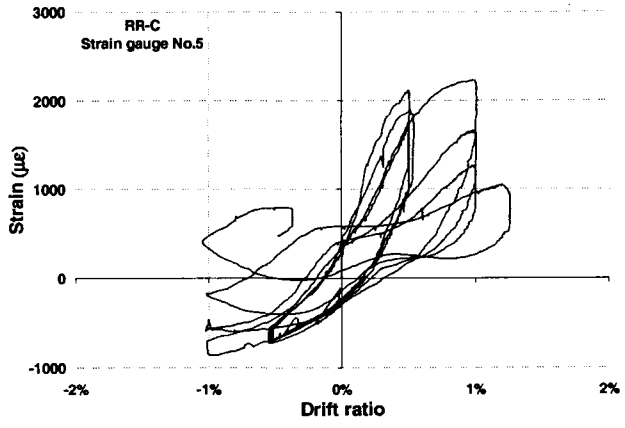

d) Strain gauge No.5

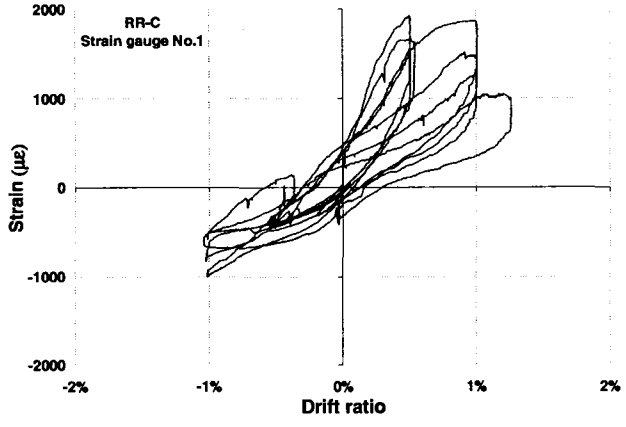

e) Strain gauge No.7

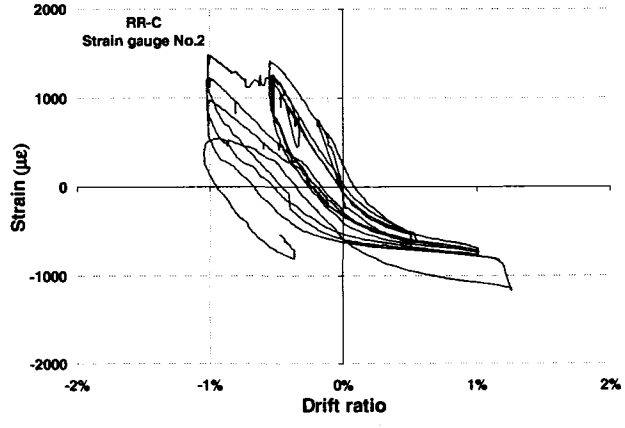

f) Strain gauge No.2

Figure A.23 Longitudinal reinforcement steel strains for column RR-C

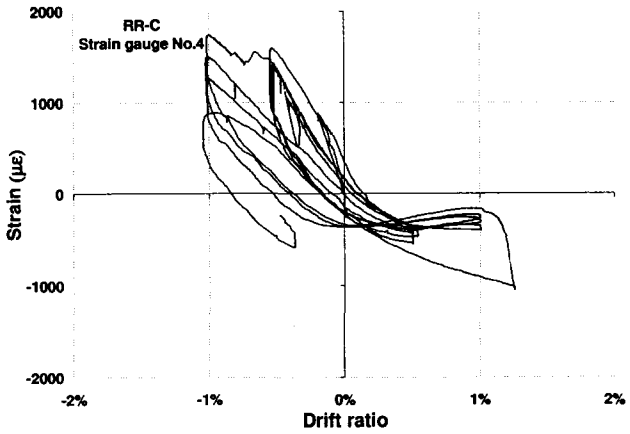

g) Strain gauge No.4

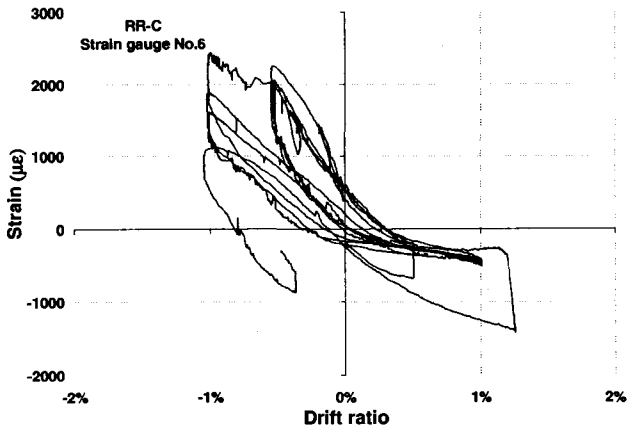

h) Strain gauge No.6

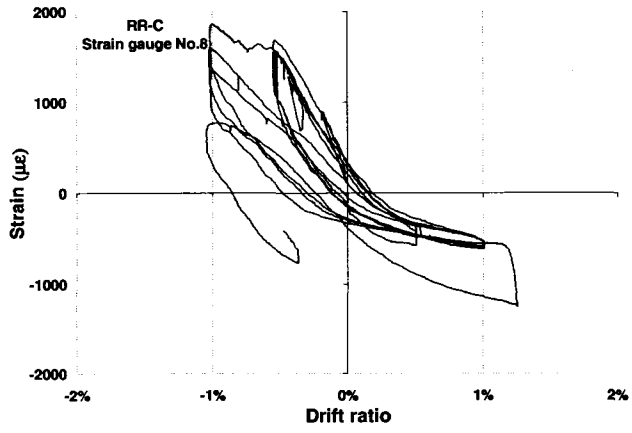

i) Strain gauge No.8

Figure A.23 Longitudinal reinforcement steel strains for column RR-C (Continued)

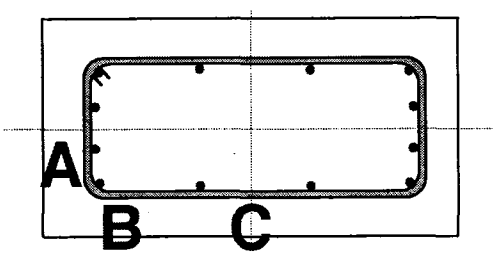

a) Strain gauge location on the 2nd hoop

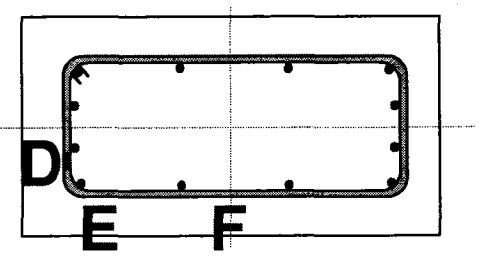

b) Strain gauge location on the 3rd hoop

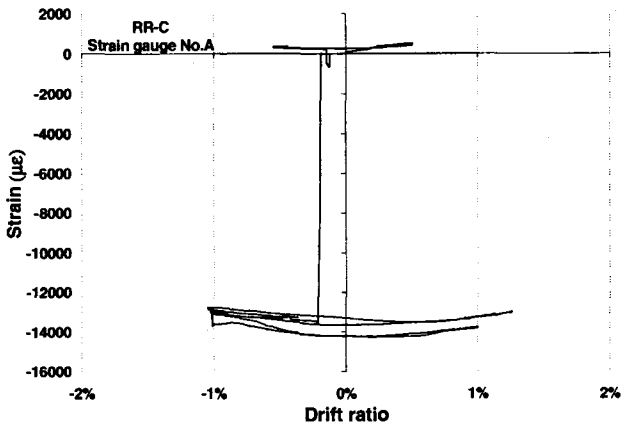

c) Strain gauge No.A

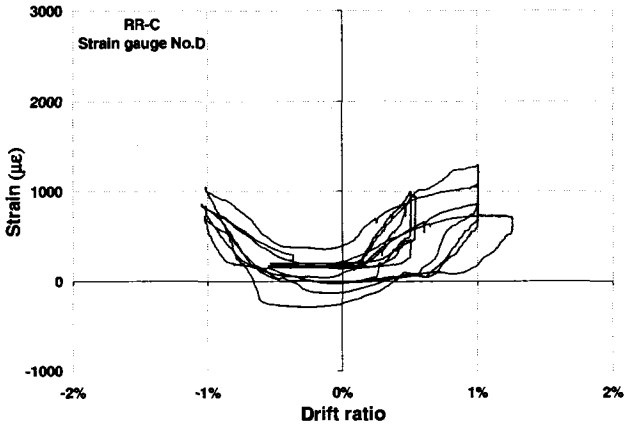

d) Strain gauge No.D

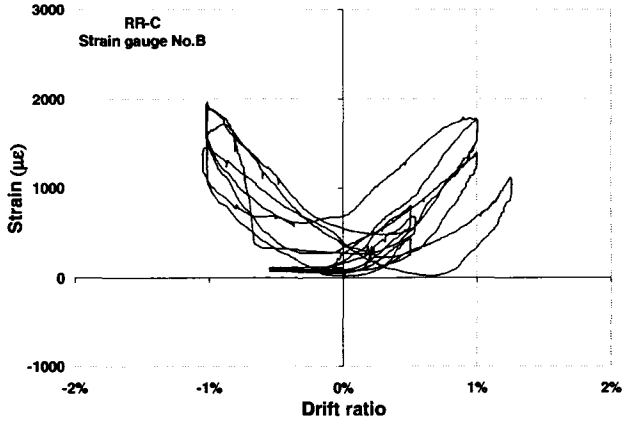

e) Strain gauge No.B

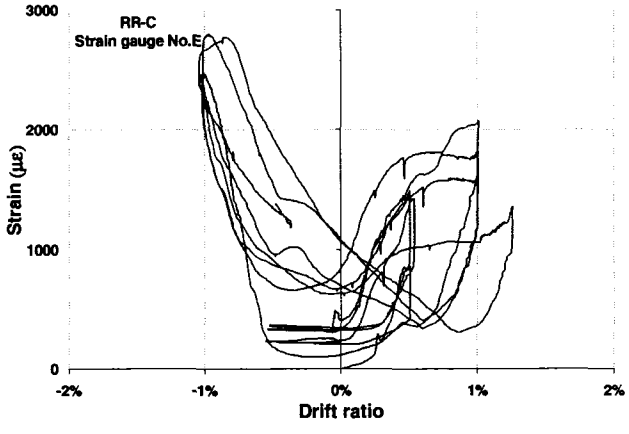

f) Strain gauge No.E

Figure A.24 Transverse reinforcement steel strains for column RR-C

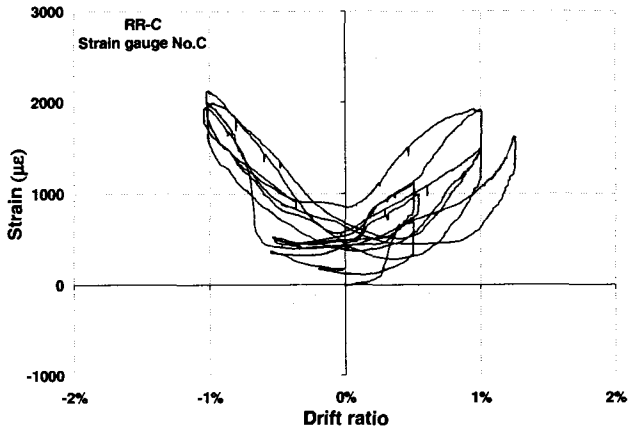

g) Strain gauge No. C

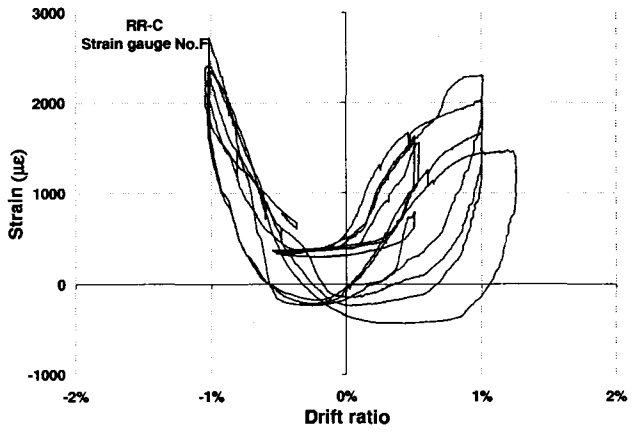

h) Strain gauge No. F

Figure A.24 Transverse reinforcement steel strains for column RR-C (Continued)

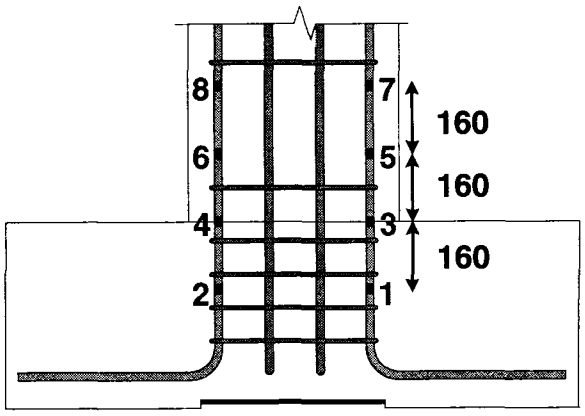

a) Strain gauge location on longitudinal bars

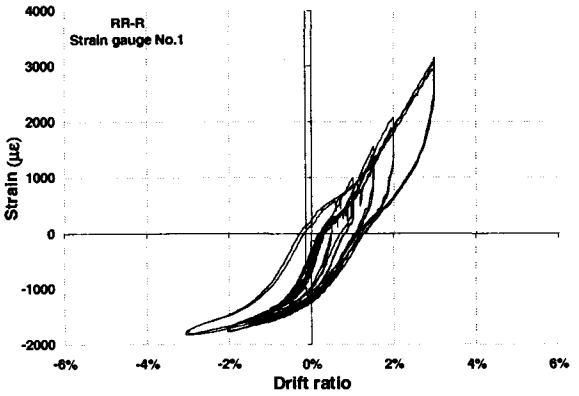

b) Strain gauge No.1

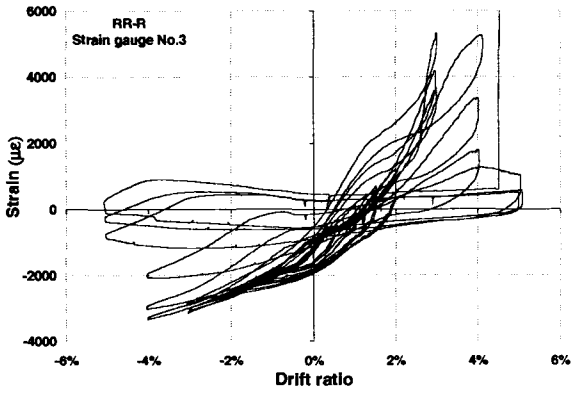

c) Strain gauge No.3

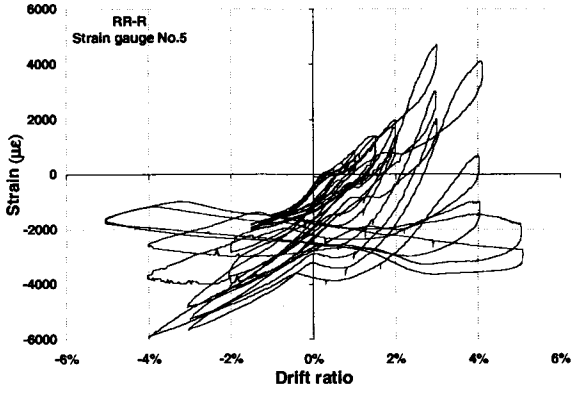

d) Strain gauge No.5

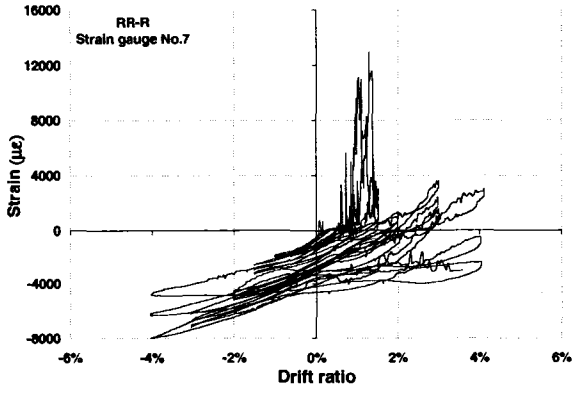

e) Strain gauge No.7

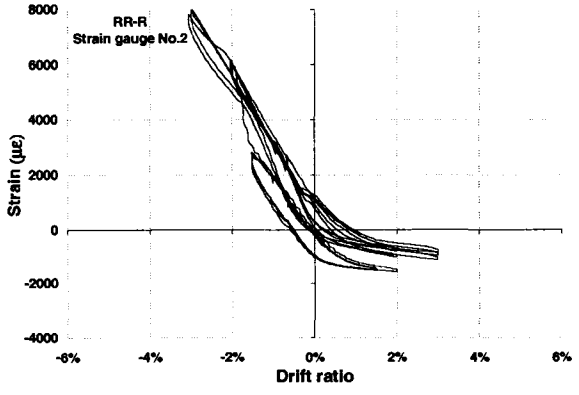

f) Strain gauge No.2

Figure A.25 Longitudinal reinforcement steel strains for column RR-R

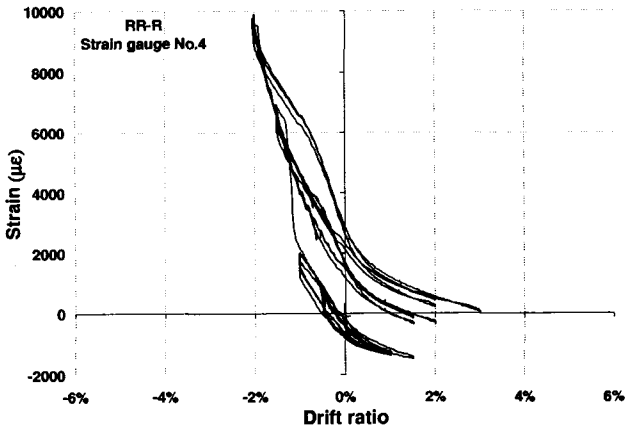

g) Strain gauge No.4

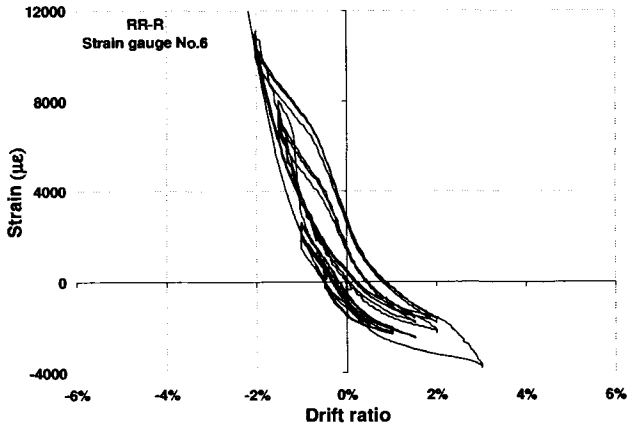

h) Strain gauge No.6

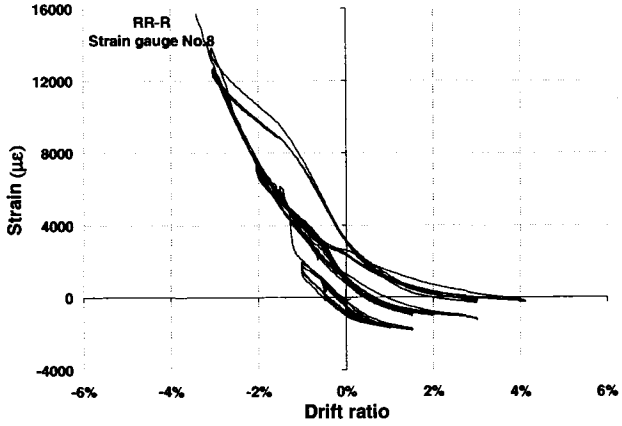

i) Strain gauge No.8

Figure A.25 Longitudinal reinforcement steel strains for column RR-R (Continued)

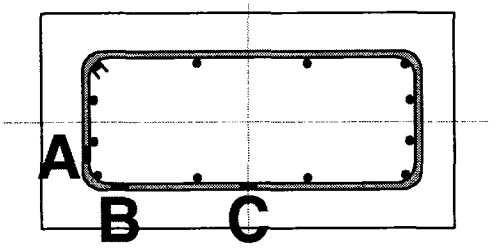

a) Strain gauge location on the 2nd hoop

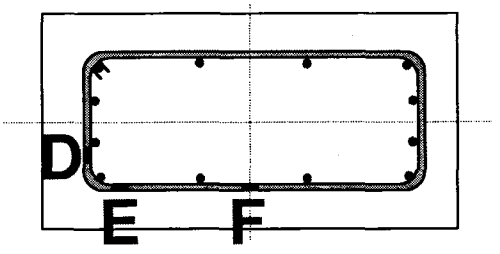

b) Strain gauge location on the 3rd hoop

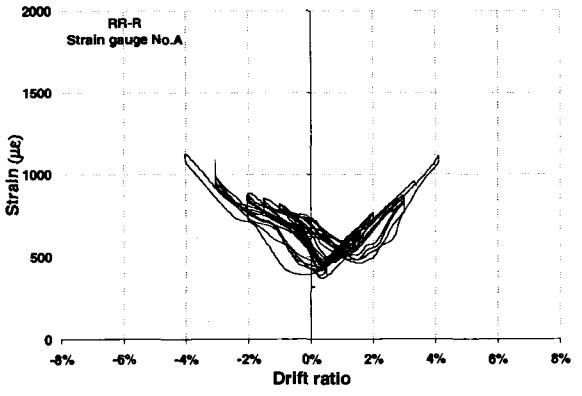

c) Strain gauge No. A

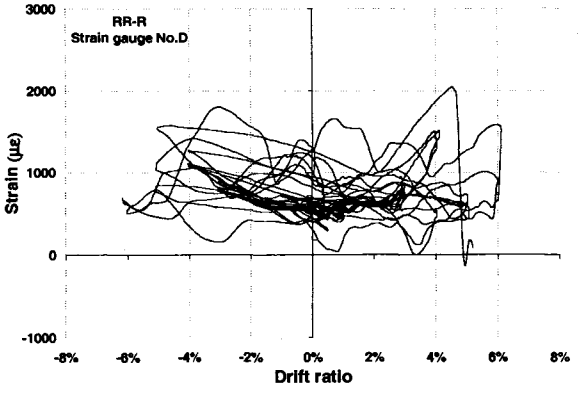

d) Strain gauge No. D

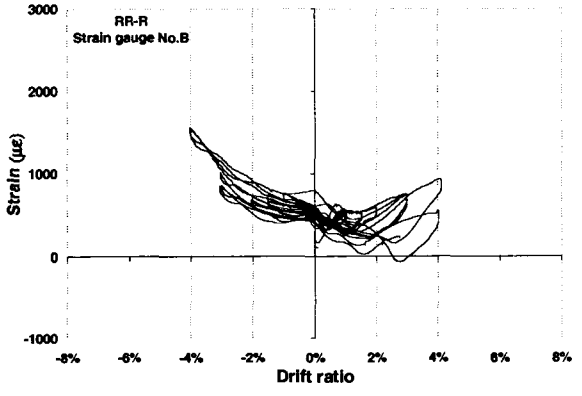

e) Strain gauge No. B

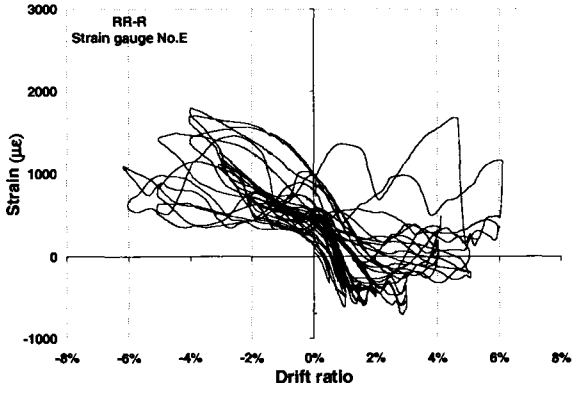

f) Strain gauge No. E

Figure A.26 Transverse reinforcement steel strains for column RR-R

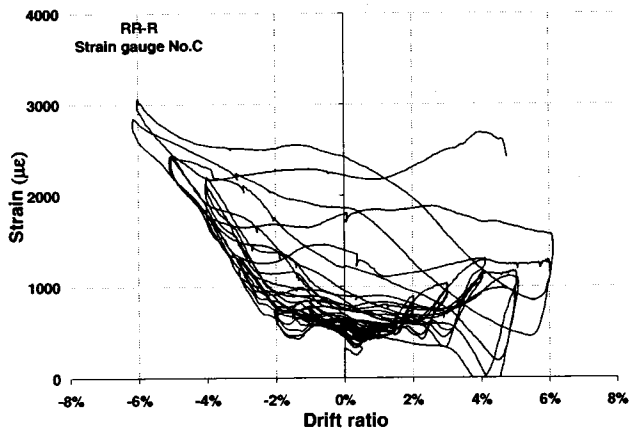

g) Strain gauge No. C

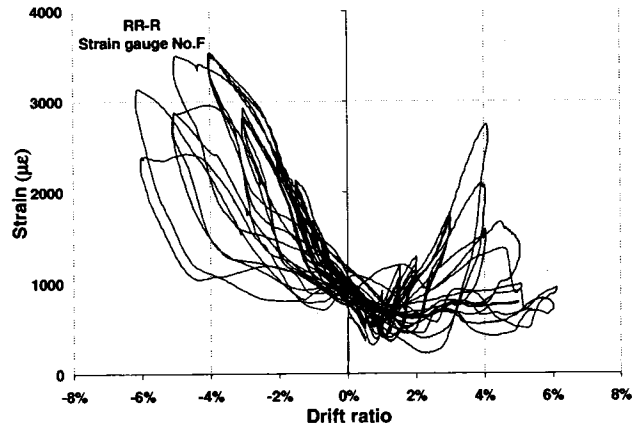

h) Strain gauge No. F

Figure A.26 Transverse reinforcement steel strains for column RR-R (Continued)

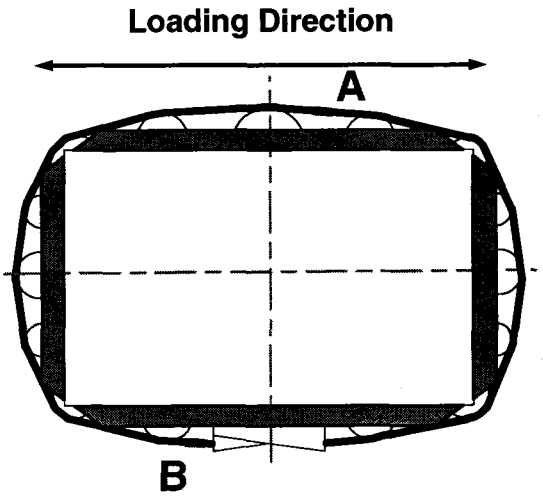

a) Strain gauge location on prestressing strands

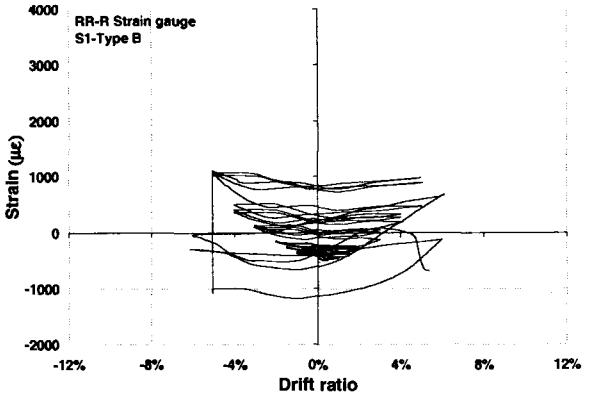

b) 1st Strand(Gauge Type B)

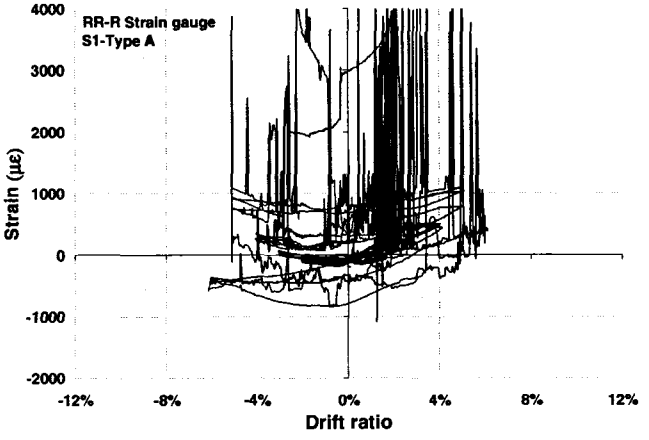

c) 1st Strand(Gauge Type A)

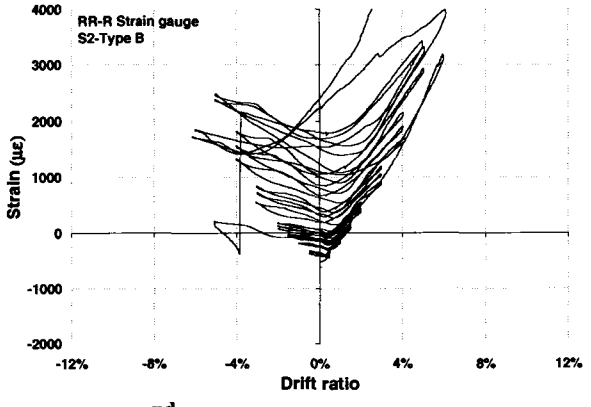

d) 2nd Strand(Gauge Type B)

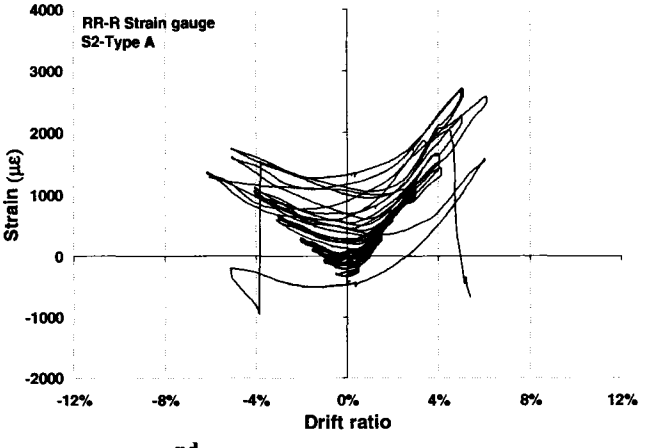

e) 2nd Strand(Gauge Type A)

Figure A.27 Prestressing strand strains for column RR-R

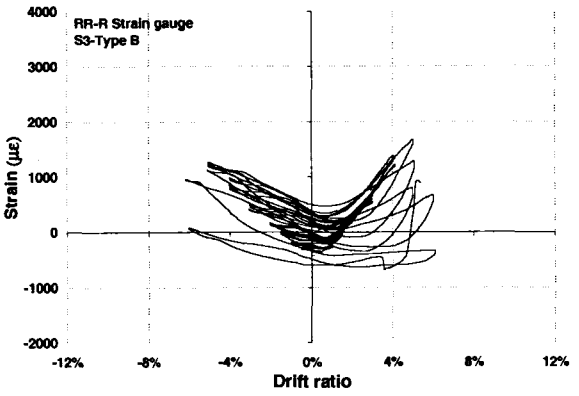

f) 3rd Strand(Gauge Type B)

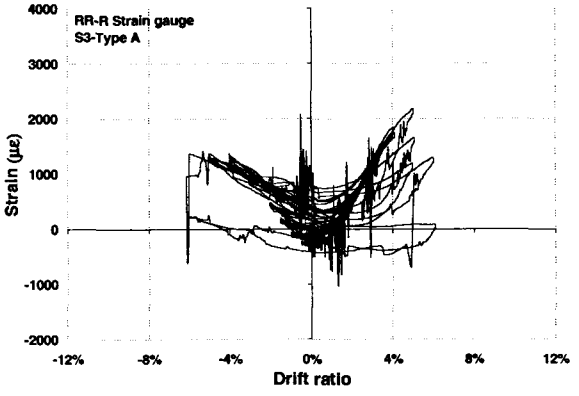

g) 3rd Strand(Gauge Type A)

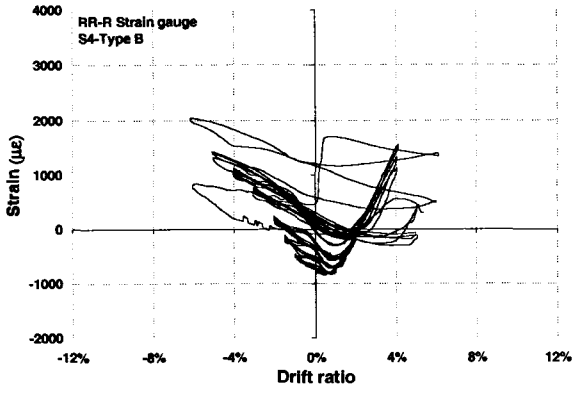

h) 4th Strand(Gauge Type B)

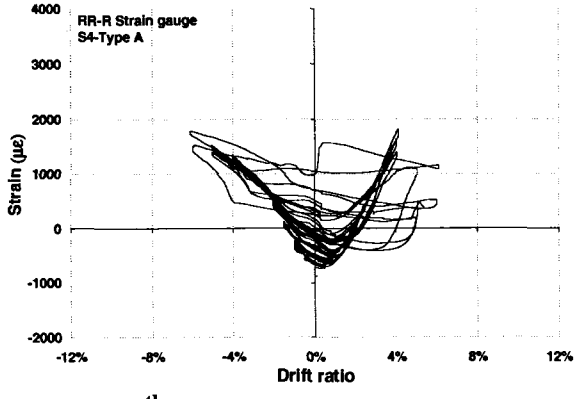

i) 4th Strand(Gauge Type A)

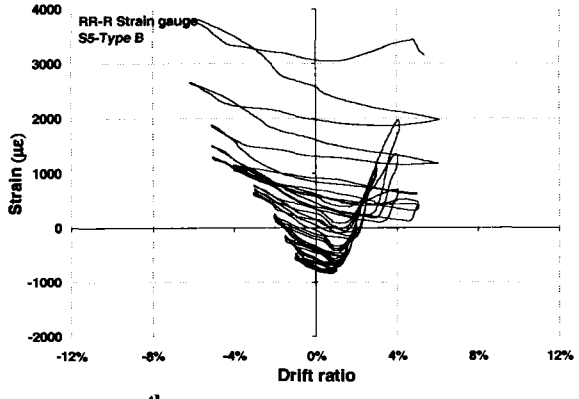

j) 5th Strand(Gauge Type B)

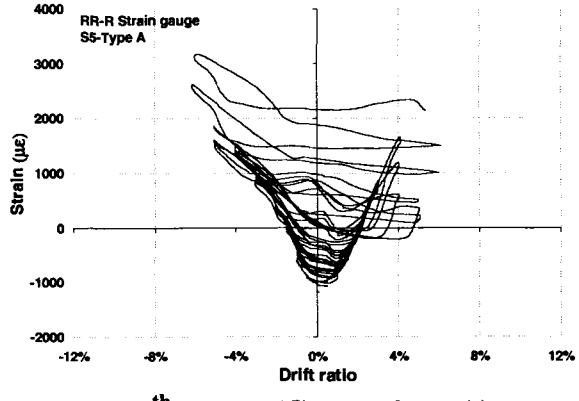

k) 5th Strand(Gauge Type A)

Figure A.27 Prestressing strand strains for column RR-R (Continued)

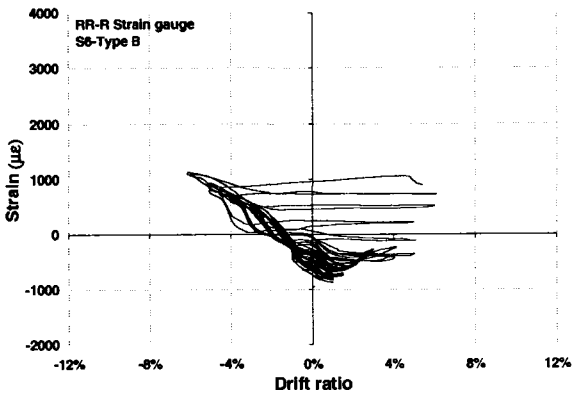

l) 6th Strand(Gauge Type B)

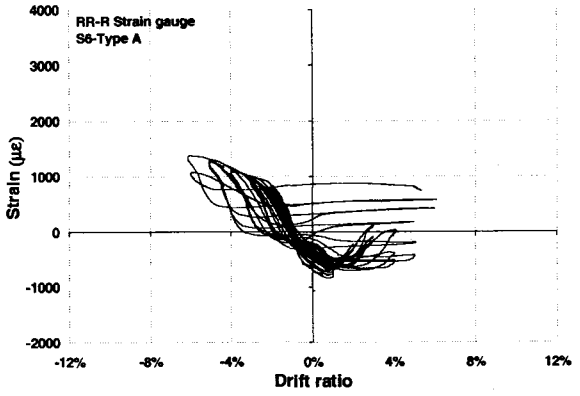

m) 6th Strand(Gauge Type A)

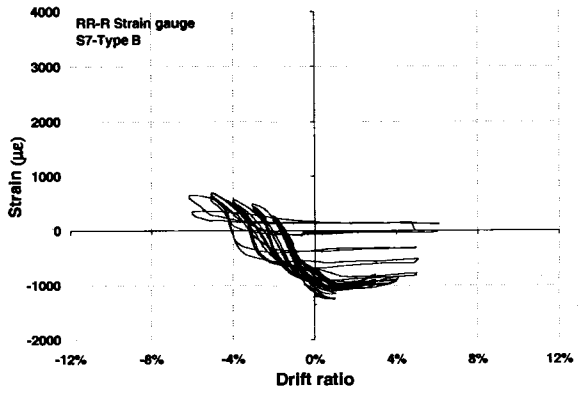

n) 7th Strand(Gauge Type B)

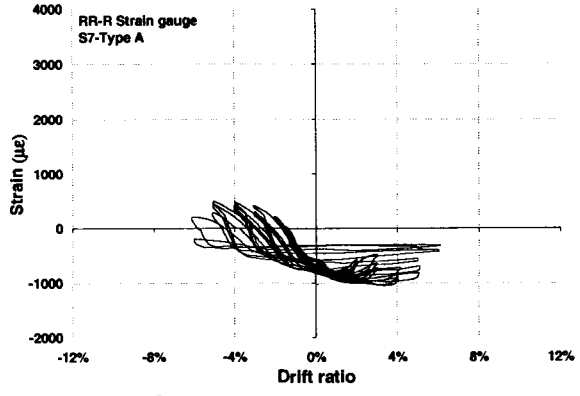

o) 7th Strand(Gauge Type A)

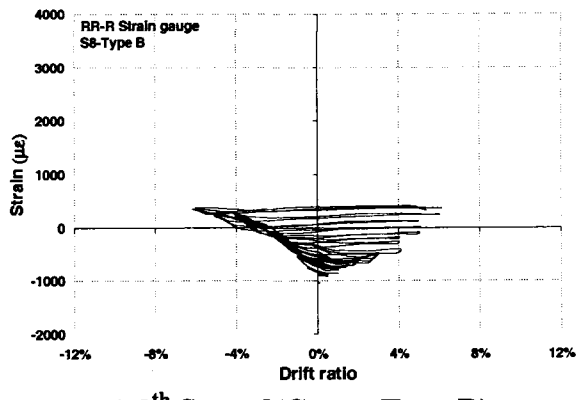

p) 8th Strand(Gauge Type B)

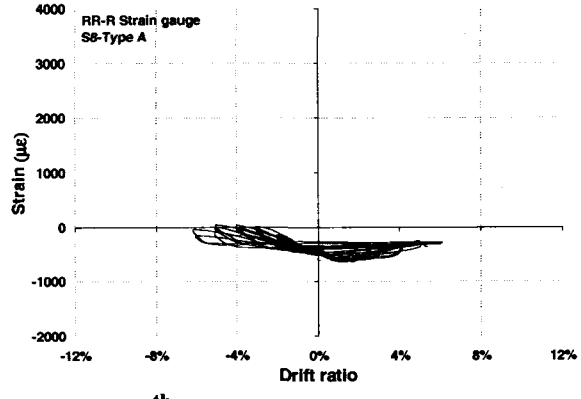

q) 8th Strand(Gauge Type A)

Figure A.27 Prestressing strand strains for column RR-R (Continued)